Thesis

Universality and Information Flow in Turbulence

Department of Physics, Kyoto University

Tomohiro Tanogami

January 16, 2023

Abstract

Turbulence appears ubiquitously, often inevitably, in natural environments, engineering applications, and everyday life. It still remains a major challenge for science, despite its importance to many other research fields. Turbulence is characterized by cascade transfer, where inviscid conserved quantities such as energy are conservatively transferred from large to small scales. Cascade transfer can be regarded as a nonequilibrium cooperative phenomenon that emerges from strong interference of fluctuations between disparate space-time scales. This transfer phenomenon is widely observed in various systems, not limited to ordinary fluids, and underlies the universality in those systems. In this thesis, we investigate such universal aspects of cascade transfer from the viewpoint of statistical physics.

In Part I, we aim to establish the concept of "universality class" for cascade transfer. As a first step toward this end, we explore novel types of cascade phenomena by considering (i) fluid quite different from ordinary fluid, (ii) ordinary fluid under extreme conditions, and (iii) a simple model different from a fluid model:

(i) We investigate the similarity and difference between quantum and classical turbulence. By using a phenomenological argument based on the Onsager "ideal turbulence" theory, we show that the compressibility effects can induce a novel energy cascade, which we call *quantum stress cascade*, at scales smaller than the mean intervortex distance.

(ii) We explore a novel type of energy cascade by focusing on supercritical turbulence near a gas-liquid critical point. We find that it exhibits a novel type of energy cascade, which we call *van der Waals cascade*, at "microscopic length scales" smaller than the correlation length of equilibrium density fluctuations. Interestingly, the mechanism of this novel cascade is analogous to that of the quantum stress cascade in quantum turbulence.

(iii) We propose a simple model representing one universality class for cascade transfer without paying much attention to its relevance to real systems. The constructed model can be regarded as a modified XY model where the amplitude fluctuates. We show that an inverse energy cascade with a non-Kolmogorov energy spectrum emerges from spatially local interactions. Interestingly, the behavior of this model is similar to that observed in spin turbulence and atmospheric turbulence.

In Part II, we aim to elucidate the nature of information flow associated with cascade transfer in ordinary fluid turbulence. Specifically, we investigate how information flows in the shell model with thermal noise from an information-thermodynamic viewpoint. We find that information of turbulent fluctuations flows from large to small scales along with the energy cascade. Furthermore, our numerical simulations suggest that transferring information from large to small scales involves enormous thermodynamic costs.

Publication List

This thesis is based on the following five papers:

1. Tomohiro Tanogami and Ryo Araki, "Information-Thermodynamic Bound on Information Flow in Turbulent Cascade", arXiv:2206.11163.

2. Tomohiro Tanogami and Shin-ichi Sasa, "XY model for cascade transfer", Physical Review Research **4**, L022015 (2022).

3. Tomohiro Tanogami, "Reply to "Comment on 'Theoretical analysis of quantum turbulence using the Onsager ideal turbulence theory' "", Physical Review E **105**, 027102 (2022).

4. Tomohiro Tanogami and Shin-ichi Sasa, "Van der Waals cascade in supercritical turbulence near a critical point", Physical Review Research **3**, L032027 (2021).

5. Tomohiro Tanogami, "Theoretical analysis of quantum turbulence using the Onsager ideal turbulence theory", Physical Review E **103**, 023106 (2021).

The following two papers are not included in the thesis:

6. Tomohiro Tanogami, "Violation of the second fluctuation-dissipation relation and entropy production in nonequilibrium medium", Journal of Statistical Physics **187**, 25 (2022).

7. Tomohiro Tanogami, "Linear stability analysis of self-gravitating granular gas", arXiv:1903.01674.

Contents

Chapter 1

Introduction

Our world is filled with various types of fluid flows. Most of these flows exhibit extremely complicated behavior, described as *turbulence*.[1] Turbulence appears ubiquitously, often inevitably, in natural environments, engineering applications, and everyday life. Despite its importance to many other research fields, turbulence remains a major challenge and is sometimes even referred to as "graveyard of theories" [2].

In a nutshell, turbulence is intricate and unpredictable fluid motion caused by interference of fluctuations between disparate space-time scales. Fluid flow patterns can be classified by using the Reynolds number $\mathrm{Re} := UL/\nu$, where U and L denote a characteristic velocity and length scale of the flow, and ν denotes the kinematic viscosity. A fluid flow becomes turbulent when Re is sufficiently large. In particular, turbulence that emerges in the limit $\mathrm{Re} \to \infty$ is called *fully developed turbulence*. Throughout this thesis, "turbulence" shall mean "fully developed turbulence" unless otherwise stated.

Although turbulence appears to be hopelessly complicated, the great efforts of scientists have revealed that some universal aspects are hidden in the disordered fluid motion. For example, the energy spectrum exhibits a universal power law called the *Kolmogorov spectrum* over a wide range of scales, independent of the details of the flow under consideration. Such remarkable universality is believed to be induced by *energy cascade* process,[2] where the energy is transferred conservatively from large to small scales. While the energy cascade can be described intuitively as the successive generation of smaller vortices by the stretching of larger vortices, the existence of such a well-ordered unidirectional transport phenomenon in disordered fluid flow is nontrivial and mysterious. Along with the energy cascade, turbulent fluctuations also exhibit quite nontrivial and universal behavior called *intermittency*, which is the central enigma of turbulence. In this thesis, we focus on these universal aspects of turbulent cascade.

In the following few sections, we provide a more detailed overview of three-dimensional fluid turbulence, focusing on the incompressible case where the mass density of a fluid is constant. For more exhaustive and pedagogical reviews, see, e.g., [4–10]. We begin by presenting three key experimental observations in the next section. In Section 1.2, we introduce the Navier–Stokes equation, which can be regarded as the "standard model" of

[1] The word "turbulence" derives from the Latin *turbulentia* and has been used to mean "trouble" or "crowds." In the context of hydrodynamics, "turbulence" seems to have been used for the first time in 1887 by Lord Kelvin [1]. The main researchers of the time, including Reynolds, Rayleigh, and Boussinesq, did not use the term "turbulence" but instead used "sinuous motion," "irregular motion," "eddy agitation," "sinuous path," etc.

[2] In the context of turbulence, it seems that the term *cascade* was used for the first time by Onsager in his note to Lin [3].

fluid turbulence. In Section 1.3, we review one of the few exact and nontrivial results in fluid turbulence, called *Kolmogorov's 4/5-law*. Then, in Section 1.4, we describe the main aim of this thesis and summarize the main contribution.

1.1 Experimental observation

In this section, we describe three important observations from experiments and numerical simulations of turbulence. Let $\boldsymbol{v}(\boldsymbol{x}, t)$ be the velocity field of the fluid at position $\boldsymbol{x}$ and time t, which can be measured, e.g., by using hot wire anemometers, PIV (Particle Image Velocimetry), PTV (Particle Tracking Velocimetry), and LDV (Laser Doppler Velocimetry). Similarly, let ν be the kinematic viscosity, which is a material constant different for each system. Throughout this thesis, we often suppress argument t to simplify the notation. Hereafter, the bracket $\langle\cdot\rangle$ denotes some suitable average such as ensemble, spatial, or time average. The first observation concerns the energy dissipation. Let ε be the kinetic energy dissipation rate defined by

$$\varepsilon := \nu\langle|\nabla \boldsymbol{v}|^2\rangle. \tag{1.1}$$

Dissipative anomaly

In the inviscid limit $\nu \to 0$, ε does not vanish:

$$\varepsilon_* = \liminf_{\nu\to 0} \varepsilon > 0. \tag{1.2}$$

There are many experimental and numerical results that are consistent with this remarkable phenomenon [11–17]. At first glance, this behavior is counter-intuitive because the energy dissipation rate is proportional to the viscosity ν. In order to achieve a non-vanishing limit of dissipation, $\langle|\nabla \boldsymbol{v}|^2\rangle$ must diverge. This observation is at the heart of the Onsager "ideal turbulence" theory [3, 18], which will be described in Chapter 2. Since most turbulence theories are based on this experimental fact, it is often called the "zeroth law" of turbulence.

The second key observation concerns the *second-order longitudinal structure function* $\langle(\delta v_\parallel(\boldsymbol{\ell}; \boldsymbol{x}))^2\rangle$, where

$$\delta v_\parallel(\boldsymbol{\ell}; \boldsymbol{x}) := \delta \boldsymbol{v}(\boldsymbol{\ell}; \boldsymbol{x}) \cdot \frac{\boldsymbol{\ell}}{\ell} \tag{1.3}$$

with

$$\delta \boldsymbol{v}(\boldsymbol{\ell}; \boldsymbol{x}) := \boldsymbol{v}(\boldsymbol{x} + \boldsymbol{\ell}) - \boldsymbol{v}(\boldsymbol{x}) \tag{1.4}$$

denotes the longitudinal velocity increment. Let L be the energy injection scale or *integral scale*, which is the characteristic length scale for the generation of turbulence. Similarly, let $\eta := \nu^{3/4}\varepsilon^{-1/4}$ be the *Kolmogorov dissipation scale*, where the viscous effects become relevant. As Re increases, the dissipation scale η becomes much smaller than the injection scale L, and we can take the intermediate asymptotic limit $\eta \ll \ell \ll L$, which is called the *inertial range*. For atmospheric boundary layer turbulence, for instance, these length scales are typically $L \sim 100\text{m}$ and $\eta \sim 1\text{mm}$ with $\text{Re} \sim 10^7$ and $\nu \sim 0.1\text{cm}^2/\text{s}$ [19, 20].

Two-thirds law

In the inertial range $\eta \ll \ell \ll L$, the second-order longitudinal structure function exhibits the following power law:

$$\langle (\delta v_{\parallel}(\boldsymbol{\ell}; \boldsymbol{x}))^2 \rangle = C_2 \varepsilon^{2/3} \ell^{2/3}, \tag{1.5}$$

where $C_2 = 2.0 \pm 0.4$ is a dimensionless constant, which may not be universal.
This two-thirds law is equivalent to the five-thirds law for the energy spectrum, which is called the *Kolmogorov spectrum*:

$$E(k) = C_K \varepsilon^{2/3} k^{-5/3} \qquad \text{for} \quad k_f \ll k \ll k_\nu, \tag{1.6}$$

where $k_f := L^{-1}$ and $k_\nu := \eta^{-1}$.

The energy spectrum satisfies the relation $\frac{1}{2}\langle |\boldsymbol{v}|^2 \rangle = \int_0^\infty dk E(k)$ and can be interpreted as the mean kinetic energy per unit mass at scale k. We note that the Kolmogorov spectrum can be obtained by a simple dimensional analysis. Indeed, if we suppose that $E(k)$ depends only on ε and k in the inertial range, then we obtain $E(k) \sim \varepsilon^{2/3} k^{-5/3}$. Historically, (1.5) was derived by Kolmogorov from his 4/5-law by assuming self-similarity of the velocity field at a time when there were no convincing experimental data to suggest the two-thirds law [21].[3]

We now consider the higher-order longitudinal structure function $\langle (\delta v_{\parallel}(\boldsymbol{\ell}; \boldsymbol{x}))^p \rangle$ $(p \geq 2)$. If we assume self-similarity of the velocity field

$$\delta \boldsymbol{v}(\lambda \boldsymbol{\ell}; \boldsymbol{x}) \overset{d}{=} \lambda^h \delta \boldsymbol{v}(\boldsymbol{\ell}; \boldsymbol{x}), \tag{1.7}$$

i.e., $\delta \boldsymbol{v}(\lambda \boldsymbol{\ell}; \boldsymbol{x})$ and $\lambda^h \delta \boldsymbol{v}(\boldsymbol{\ell}; \boldsymbol{x})$ have the same statistical property for a unique scaling exponent $\lambda \in \mathbb{R}_+$ for all $\boldsymbol{x} \in \Omega$ and $\boldsymbol{\ell}$ in the inertial range, the two-thirds law implies that $h = 1/3$. Therefore, we expect that

$$\langle (\delta v_{\parallel}(\boldsymbol{\ell}; \boldsymbol{x}))^p \rangle = C_p \varepsilon^{p/3} \ell^{p/3} \qquad \text{for} \quad \eta \ll \ell \ll L \tag{1.8}$$

with a dimensionless constant C_p.[4] This scaling is called *K41 scaling*, since it was obtained in Kolmogorov's 1941 paper [21, 22]. Interestingly, many experiments and numerical simulations suggest that (1.8) is questionable especially when $p \geq 4$. The breakdown of self-similarity is called *intermittency*.

Intermittency

In the inertial range $\eta \ll \ell \ll L$, the p-th order longitudinal structure function displays the power-law behavior

$$\langle (\delta v_{\parallel}(\boldsymbol{\ell}; \boldsymbol{x}))^p \rangle \propto \ell^{\zeta_p} \tag{1.9}$$

with the exponent ζ_p that is not exactly $p/3$.

[3] He also derived (1.5) by assuming universality of small-scale statistical properties [22]. This universality assumption is questionable, as first pointed out by Landau [5, 23]. It should also be noted that the Kolmogorov spectrum was independently discovered by Obukhov [24,25], Onsager [26], von Weizsäcker [27], and Heisenberg [28].

[4] Even if C_2 is universal, there is no guarantee that C_p for $p \neq 2$ is universal. At present, only C_3 is found to be universal.

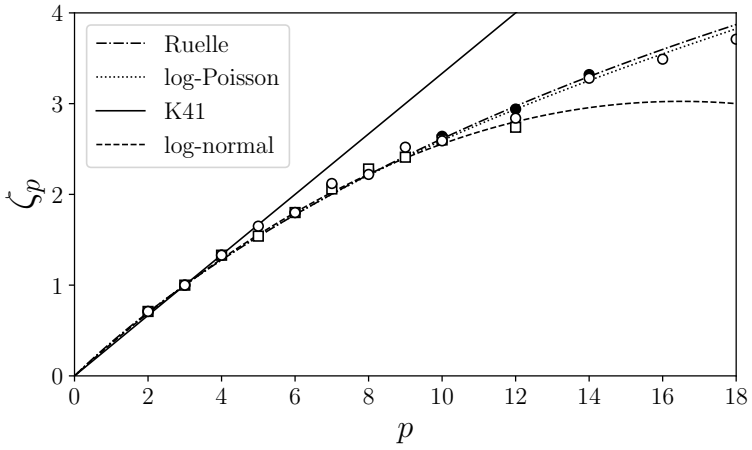

Fig. 1.1: p-dependence of the exponent ζ_p. Black circles, white squares, and white circles denote experimental data from [29]. Solid line denotes $\zeta_p = p/3$. Dashed line denotes the prediction of the log-normal model: $\zeta_p = p/3 + \mu(3p - p^2)/18$ with $\mu = 0.2$ [30,31]. Dotted line denotes the prediction of the log-Poisson model: $\zeta_p = p/9 + 2 - 2(2/3)^{p/3}$ [32–34]. Dash-dotted line denotes the prediction of the Ruelle model: $\zeta_p = p/3 - \ln\Gamma(p/3+1)/\ln\kappa$ with $\kappa = 22$ [35–37].

Figure 1.1 shows experimental data from [29]. The solid, dashed, dotted, and dash-dotted lines denote the theoretical prediction based on various models. It clearly shows the breakdown of self-similarity. The scaling exponent ζ_p is believed to be universal.[5] By introducing the anomalous dimension $\delta\zeta_p := \zeta_p - p/3$, (1.9) can be expressed as

$$\langle (\delta v_\parallel(\boldsymbol{\ell}; \boldsymbol{x}))^p \rangle = C_p \varepsilon^{p/3} \ell^{p/3} \left(\frac{\ell}{L}\right)^{\delta\zeta_p}. \tag{1.11}$$

From this expression, we see that deviations from K41 scaling require that the structure functions explicitly depend on the injection scale L. In other words, the small-scale turbulent fluctuations "remember" the number of "cascade steps" $\log_2(L/\ell)$ [10]. Intuitively, intermittency corresponds to the occurrence of clumps of intense turbulent fluctuations in a relatively quiescent background.

1.2 "Standard model" of turbulence

To understand these remarkable and mysterious behaviors of fluid turbulence, we need some phenomenological model. While there can be a variety of such models,[6] it is believed that incompressible fluid turbulence can be described by the Navier–Stokes equation:

$$\partial_t \boldsymbol{v} + \boldsymbol{v} \cdot \nabla \boldsymbol{v} = -\nabla p + \nu \nabla^2 \boldsymbol{v}. \tag{1.12}$$

This is a nonlinear and nonlocal equation that governs the time evolution of the velocity field $\boldsymbol{v}(\boldsymbol{x}, t)$ with $\nabla \cdot \boldsymbol{v} = 0$. Here, $p(\boldsymbol{x}, t)$ denotes the pressure divided by the constant

[5] A more precise definition of the scaling exponent ζ_p is as follows [5, 10]:

$$\zeta_p := \liminf_{\ell \to 0} \frac{\ln\langle (\delta v_\parallel(\boldsymbol{\ell}; \boldsymbol{x}))^p \rangle}{\ln(\ell/L)}. \tag{1.10}$$

[6] "*Nature gives physicists phenomena, not equations*" [38].

mass density of a fluid $\rho(\boldsymbol{x}, t) = \rho$. Although the existence and uniqueness of the solution of the Navier–Stokes equation are still unknown,[7] this model probably contains all of the turbulence [5]. The Navier–Stokes equation can be derived from the Boltzmann equation (for dilute gases) [40], lattice gas models [41], and even Hamiltonian particle systems [42]. For later convenience, here we describe the inviscid conservation laws of the Navier–Stokes equation. We suppose that a fluid is confined in a cube $\Omega = [0, L_\Omega]^3$ with periodic boundary conditions. Let $\langle\cdot\rangle_\Omega := \int_\Omega d^3\boldsymbol{x} \cdot / |\Omega|$ be the spatial average.

- **Inviscid conservation law of energy.**
  The mean kinetic energy per unit mass $\langle|\boldsymbol{v}|^2\rangle_\Omega/2$ obeys the following balance equation:[8]

$$\frac{d}{dt}\left\langle \frac{1}{2}|\boldsymbol{v}|^2 \right\rangle_\Omega = -\nu\langle|\nabla\boldsymbol{v}|^2\rangle_\Omega. \tag{1.13}$$

  Note that $\langle|\nabla\boldsymbol{v}|^2\rangle_\Omega$ can be rewritten as $\langle|\boldsymbol{\omega}|^2\rangle_\Omega$, which is called mean *enstrophy*.[9]

- **Inviscid conservation law of helicity.**
  The mean *helicity* $\langle\boldsymbol{v}\cdot\boldsymbol{\omega}\rangle_\Omega/2$ obeys the following balance equation:

$$\frac{d}{dt}\left\langle \frac{1}{2}\boldsymbol{v}\cdot\boldsymbol{\omega} \right\rangle_\Omega = -\nu\langle\boldsymbol{\omega}\cdot\nabla\times\boldsymbol{\omega}\rangle_\Omega, \tag{1.14}$$

  where $\boldsymbol{\omega} := \nabla\times\boldsymbol{v}$ denotes the vorticity field.

In two-dimensional flow, there is an additional inviscid conservation law:

- **Inviscid conservation law of enstrophy (in two-dimensional flow).**
  The mean enstrophy $\langle|\boldsymbol{\omega}|^2\rangle_\Omega/2$ obeys the following balance equation:

$$\frac{d}{dt}\left\langle \frac{1}{2}|\boldsymbol{\omega}|^2 \right\rangle_\Omega = -\nu\langle|\nabla\times\boldsymbol{\omega}|^2\rangle_\Omega. \tag{1.15}$$

In the inviscid limit $\nu \to 0$, the energy and helicity (and enstrophy in two-dimensional flow) become conserved quantities if the velocity field is sufficiently smooth. Therefore, we call such quantities *inviscid conserved quantities*. In deriving these inviscid conservation laws, we have assumed that the velocity and pressure fields are sufficiently smooth. While we conjecture that this assumption is valid for finite positive viscosity, it may breakdown for the solutions of the Euler equations, as first conjectured by Onsager [3, 18]. We finally note that the nonlinear term in the Navier–Stokes equation does not contribute to the balance equations for inviscid conserved quantities. As we will see in the next section, the nonlinear term redistributes the inviscid conserved quantities over a wide range of scales.

1.3 Milestone: Kolmogorov's 4/5-law

At present, there is no satisfactory theory that can derive the empirical laws presented in Section 1.1 based on the Navier–Stokes equation. Still, for the third-order longitudinal

[7] This is one of the million-dollar prize problems: https://www.claymath.org/millennium-problems/navier-stokes-equation. Its mathematical status is summarized in [39].

[8] The words "mean" and "per unit mass" are often omitted.

[9] Only the quantity $\nu|\nabla\boldsymbol{v}(\boldsymbol{x}, t)|^2$ deserves to be called the *local energy dissipation*, because it is possible that there is no energy dissipation although $|\boldsymbol{\omega}(\boldsymbol{x}, t)|^2$ is finite.

structure function $\langle(\delta v_\parallel(\boldsymbol{\ell};\boldsymbol{x}))^3\rangle$, an exact relation can be derived. This exact relation was first derived by Kolmogorov, and it is called *Kolmogorov's 4/5-law* [21].

Kolmogorov's 4/5-law

By assuming homogeneity, isotropy, and dissipative anomaly, the third-order longitudinal structure function for $\ell \ll L$ takes the following form in the inviscid limit $\nu \to 0$:

$$\langle(\delta v_\parallel(\boldsymbol{\ell};\boldsymbol{x}))^3\rangle = -\frac{4}{5}\varepsilon\ell. \tag{1.16}$$

Here, homogeneity means that $\delta\boldsymbol{v}(\boldsymbol{\ell};\boldsymbol{x}+\boldsymbol{r}) \overset{d}{=} \delta\boldsymbol{v}(\boldsymbol{\ell};\boldsymbol{x})$ for all $\boldsymbol{x} \in \Omega$ and $\boldsymbol{r}, \boldsymbol{\ell}$ small compared to L. Similarly, isotropy means that $\mathsf{R}\delta\boldsymbol{v}(\mathsf{R}^{-1}\boldsymbol{\ell};\boldsymbol{x}) \overset{d}{=} \delta\boldsymbol{v}(\boldsymbol{\ell};\boldsymbol{x})$ for all $\boldsymbol{x} \in \Omega$, $\mathsf{R} \in \mathrm{SO}(3)$, and $\boldsymbol{\ell}$ small compared to L. The 4/5-law is one of the few exact and nontrivial results in fully developed fluid turbulence. We note that the two-thirds law can be derived from the 4/5-law if we assume self-similarity. The important point here is that the dimensionless constant $C_3 = -4/5$ does not depend on the details of the flow under consideration. That is, Kolmogorov's 4/5-law is a universal relation, which is valid for all types of flow that satisfies the assumptions imposed in deriving it. There is compelling experimental and numerical support for this law [43–45].

Below, we provide an outline of the proof. To this end, we first show that kinetic energy is transferred conservatively from large to small scales in three-dimensional fluid turbulence. We will see that this energy cascade is crucial in deriving the 4/5-law and underlies the universality.

Energy cascade. We consider the Navier–Stokes equation with the external force that acts at large scales $\sim L = k_f^{-1}$:

$$\partial_t\boldsymbol{v} + \boldsymbol{v}\cdot\nabla\boldsymbol{v} = -\nabla p + \nu\nabla^2\boldsymbol{v} + \boldsymbol{f}. \tag{1.17}$$

To investigate the energy transfer across scales, we introduce the low-pass filtering operator

$$\mathcal{P}_K^< : \boldsymbol{a}(\boldsymbol{x}) \mapsto \boldsymbol{a}_K^<(\boldsymbol{x}), \tag{1.18}$$

which sets to zero all Fourier components of any field $\boldsymbol{a}$ with wavenumber larger than K:

$$\boldsymbol{a}_K^<(\boldsymbol{x}) := \sum_{|\boldsymbol{k}|\le K} \hat{\boldsymbol{a}}_{\boldsymbol{k}} e^{i\boldsymbol{k}\cdot\boldsymbol{x}}, \tag{1.19}$$

where $\hat{\boldsymbol{a}}_{\boldsymbol{k}} = \int_\Omega d^3\boldsymbol{x}\boldsymbol{a}(\boldsymbol{x})e^{-i\boldsymbol{k}\cdot\boldsymbol{x}}$ is the Fourier coefficient with wavevector $\boldsymbol{k} \in (2\pi/L_\Omega)\mathbb{Z}^3$. Note that $\mathcal{P}_K^<$ is a projection operator, $\mathcal{P}_K^< = \mathcal{P}_K^< \circ \mathcal{P}_K^<$, and commutes with ∇. By applying $\mathcal{P}_K^<$ to the Navier–Stokes equation, we obtain the time evolution equation for the large-scale energy $\langle|\boldsymbol{v}_K^<|^2\rangle/2$:

$$\partial_t\left\langle\frac{1}{2}|\boldsymbol{v}_K^<|^2\right\rangle = -\Pi_K - \nu\sum_{|\boldsymbol{k}|\le K} k^2\langle|\hat{\boldsymbol{v}}_{\boldsymbol{k}}|^2\rangle + \sum_{|\boldsymbol{k}|\le K}\langle\hat{\boldsymbol{f}}_{\boldsymbol{k}}\cdot\hat{\boldsymbol{v}}_{-\boldsymbol{k}}\rangle. \tag{1.20}$$

Here, Π_K denotes the scale-to-scale energy flux through wavenumber K:

$$\Pi_K := -\langle\nabla\boldsymbol{v}_K^< : \left(\mathcal{P}_K^<[\boldsymbol{v}\boldsymbol{v}] - \boldsymbol{v}_K^<\boldsymbol{v}_K^<\right)\rangle. \tag{1.21}$$

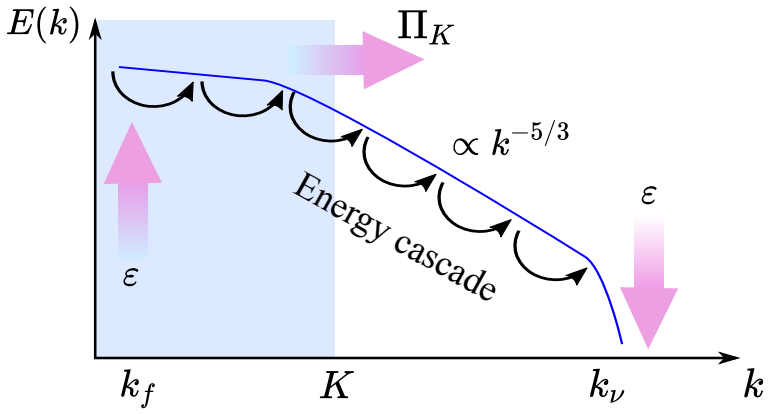

Fig. 1.2: Schematic of energy cascade. The kinetic energy in the shaded region corresponds to the large-scale energy $\langle|\boldsymbol{v}_K^<|^2\rangle/2$.

From this expression, we can see that Π_K represents the nonlinear interference between large and small scales. The second term on the right-hand side of (1.20) denotes the viscous dissipation, and the last term denotes the energy injection due to the external force. We note that if we take the limit $K \to \infty$ for fixed ν, we recover the energy balance equation:

$$\frac{d}{dt}\left\langle \frac{1}{2}|\boldsymbol{v}|^2 \right\rangle = -\nu\langle|\nabla \boldsymbol{v}|^2\rangle + \langle \boldsymbol{f}\cdot\boldsymbol{v}\rangle. \tag{1.22}$$

Now, we take the inviscid limit $\nu \to 0$ (i.e., $k_\nu = \eta^{-1} \to \infty$) for fixed K in (1.20). Then, we find that

$$\begin{aligned}\nu \sum_{|\boldsymbol{k}|\le K} k^2\langle|\hat{\boldsymbol{v}}_{\boldsymbol{k}}|^2\rangle &\le \nu K^2\langle|\boldsymbol{v}_K^<|^2\rangle \\ &\le \nu K^2\langle|\boldsymbol{v}|^2\rangle \to 0.\end{aligned} \tag{1.23}$$

Next, we take the limit $K \to \infty$ with fixed k_f. Since $\boldsymbol{f}$ acts only at large scales $\sim L = k_f^{-1}$, we obtain

$$\sum_{|\boldsymbol{k}|\le K} \langle \hat{\boldsymbol{f}}_{\boldsymbol{k}}\cdot\hat{\boldsymbol{v}}_{-\boldsymbol{k}}\rangle \to \langle \boldsymbol{f}\cdot\boldsymbol{v}\rangle. \tag{1.24}$$

By assuming the dissipative anomaly $\varepsilon := \nu\langle|\nabla\boldsymbol{v}|^2\rangle > 0$ in the inviscid limit, we have $\langle \boldsymbol{f}\cdot\boldsymbol{v}\rangle = \varepsilon$ in the steady state. Therefore, we obtain

$$\lim_{K\to\infty}\lim_{\nu\to 0}\Pi_K = \varepsilon. \tag{1.25}$$

This relation states that the scale-to-scale energy flux is independent of K in the inertial range $k_f \ll K \ll k_\nu$. In other words, the kinetic energy is transferred conservatively from large to small scales (Fig. 1.2). This is the energy cascade phenomenon and governs the energy distribution in the k-space. Since this phenomenon was intuitively described by Richardson as the successive generation of smaller vortices by the stretching of larger vortices, the energy cascade in ordinary fluid turbulence is also called the *Richardson cascade*.

Outline of the proof of Kolmogorov's 4/5-law. We prove the 4/5-law in the steady state regime, although it is valid even in freely decaying turbulence. Our starting point is the relation (1.25). We use the fact that Π_K can be expressed in terms of the third-order longitudinal structure function if we assume homogeneity and isotropy:

$$\Pi_K = -\frac{1}{6\pi}\int_0^\infty d\ell \frac{\sin(K\ell)}{\ell}(1+\ell\partial_\ell)(3+\ell\partial_\ell)(5+\ell\partial_\ell)\frac{\langle(\delta v_\parallel(\boldsymbol{\ell};\boldsymbol{x}))^3\rangle}{\ell}. \tag{1.26}$$

For the derivation of this expression, see, e.g., [5]. By substituting this expression into (1.25) and changing variable from ℓ to $x = K\ell$, we obtain

$$-\lim_{K\to\infty}\lim_{\nu\to 0}\int_0^\infty dx \frac{\sin x}{x} F\left(\frac{x}{K}\right) = \varepsilon, \tag{1.27}$$

where we have introduced

$$F(\ell) := (1+\ell\partial_\ell)(3+\ell\partial_\ell)(5+\ell\partial_\ell)\frac{\langle(\delta v_\parallel(\boldsymbol{\ell};\boldsymbol{x}))^3\rangle}{6\pi\ell}. \tag{1.28}$$

By noting that $\int_0^\infty dx \sin x/x = \pi/2$, we obtain the following differential equation for small ℓ:

$$F(\ell) = -\frac{2}{\pi}\varepsilon. \tag{1.29}$$

By solving this equation, we obtain

$$\frac{\langle(\delta v_\parallel(\boldsymbol{\ell};\boldsymbol{x}))^3\rangle}{\ell} = -\frac{4}{5}\varepsilon + A\ell^{-1} + B\ell^{-3} + C\ell^{-5}, \tag{1.30}$$

where A, B, and C are constants. Therefore, the only solution that $\langle(\delta v_\parallel(\boldsymbol{\ell};\boldsymbol{x}))^3\rangle \to 0$ as $\ell \to 0$ is[10]

$$\lim_{\ell\to 0}\lim_{\nu\to 0}\frac{\langle(\delta v_\parallel(\boldsymbol{\ell};\boldsymbol{x}))^3\rangle}{\ell} = -\frac{4}{5}\varepsilon. \tag{1.31}$$

Remark 1: dimensional analysis. Here, we remark that dimensional analysis provides results consistent with Kolmogorov's 4/5-law. Let v_ℓ be the characteristic velocity associated with the length scale $\ell \ll L$, which is defined, for instance, as $\langle(\delta v_\parallel(\boldsymbol{\ell};\boldsymbol{x}))^2\rangle^{1/2}$. Similarly, we denote by $v_L \sim v_{\rm rms} := \langle|\boldsymbol{v}|^2\rangle^{1/2}$ the characteristic velocity at the injection scale L. Then, the characteristic time scale for an eddy of size $\sim \ell$ to be stretched into smaller eddies reads

$$\tau_\ell \sim \frac{\ell}{v_\ell}. \tag{1.32}$$

This time scale is called *eddy turnover time* or *circulation time* associated with the length scale ℓ. In particular, τ_L is called the *large-eddy turnover time*. Now, let Π_ℓ be the energy flux from scales $\sim \ell$ to smaller scales, which may be defined as Π_K in (1.21) with $K \sim \ell^{-1}$. By using v_ℓ and τ_ℓ, we estimate Π_ℓ as

$$\Pi_\ell \sim \frac{v_\ell^2}{\tau_\ell} \sim \frac{v_\ell^3}{\ell}. \tag{1.33}$$

[10] We note that the condition $\langle(\delta v_\parallel(\boldsymbol{\ell};\boldsymbol{x}))^3\rangle \to 0$ as $\ell \to 0$ is an assumption, since the limit $\nu \to 0$ is taken before the limit $\ell \to 0$.

We now assume the dissipative anomaly. Then, in the inertial range $\eta \ll \ell \ll L$, where there is neither external energy injection nor viscous dissipation, the energy flux should be independent of ℓ and equal to the energy dissipation rate:

$$\Pi_\ell \sim \varepsilon. \tag{1.34}$$

From (1.33) and (1.34), we obtain

$$v_\ell \sim \varepsilon^{1/3}\ell^{1/3}. \tag{1.35}$$

This estimation states that the velocity field is scale-invariant with exponent $h = 1/3$, which is consistent with Kolmogorov's 4/5-law. Furthermore, by substituting this expression into (1.32), we find that

$$\tau_\ell \sim \varepsilon^{-1/3}\ell^{2/3}. \tag{1.36}$$

Thus, the small-scale eddies evolve faster, or in other words, the cascade is accelerated as ℓ decreases. By extrapolating the estimation (1.35) to the injection scale L, we can obtain Taylor's estimation of the energy dissipation $\varepsilon \sim v_L^3/L$ [46]. We remark that the Kolmogorov dissipation scale η can also be obtained by comparing the eddy turnover time τ_ℓ with the characteristic time scale for viscous dissipation $\tau_\ell^{\mathrm{vis}} := \ell^2/\nu$:

$$\begin{aligned} &\tau_\eta \sim \tau_\eta^{\mathrm{vis}} \\ \therefore \quad &\eta \sim \nu^{3/4}\varepsilon^{-1/4} \sim \mathrm{Re}^{-3/4}L. \end{aligned} \tag{1.37}$$

In the atmospheric boundary layer turbulence, the large-eddy turnover time can be estimated as $\tau_L \sim 1\mathrm{min}$. Therefore, the cascade may reach from $L \sim 100\mathrm{m}$ to $\eta \sim 1\mathrm{mm}$ within a few minutes.

Remark 2: cascade and universality. One important property about energy cascade not mentioned above is scale locality. Energy cascade is scale-local if only modes near a given scale mainly contribute to the energy transfer at that scale. It is believed that the universality of small-scale turbulent fluctuations is due to this scale-local cascade process [5, 10]. In other words, small-scale turbulent fluctuations "forget" the details of large scales because of the chaotic nature of the stepwise cascade process.

1.4 Overview of this thesis

So far, we have reviewed some of the most notable experimental observations and theoretical achievements on fully developed fluid turbulence. In particular, we have seen that turbulence exhibits rich universal behaviors despite its seemingly extremely complicated flow patterns. Importantly, energy cascade lies at the core of this remarkable universality of small-scale turbulent fluctuations. In this thesis, we investigate the universal aspect of energy cascade from the viewpoint of statistical physics. Below, we describe the main purpose of this thesis and summarize the main contribution.

Part I: Toward establishing the concept of "universality class" for cascade transfer

It is important to note that *cascade transfer* phenomenon is not limited to kinetic energy, but is also possible for other inviscid conserved quantities, such as enstrophy and helicity.

Remarkably, such cascade transfer phenomena are widely observed in various systems, including quantum fluids, elastic bodies, and spin systems [47–59]. For example, it is known that *quantum turbulence*, which is explained below, exhibits the Kolmogorov spectrum at scales larger than the mean intervortex distance, although the governing equation is different from the Navier–Stokes equation [47–51]. Thus, cascade transfer phenomena are ubiquitous and underlie the universality observed in various systems. This fact motivates us to systematically classify various cascade phenomena by establishing the concept of a "universality class," as in equilibrium critical phenomena. As a first step toward this end, we explore novel types of cascade phenomena by considering (i) fluid quite different from ordinary fluid, (ii) ordinary fluid under extreme conditions, and (iii) a simple model different from a fluid model. Specifically, (i) we investigate the similarity and difference between quantum and classical turbulence [60, 61], (ii) explore a novel type of energy cascade by focusing on supercritical turbulence [62], and (iii) construct a simple model where energy cascade emerges from spatially local interaction [63]. Below, we provide a brief summary of these three works.

(i) Quantum turbulence

Quantum fluids, such as superfluid helium and atomic Bose-Einstein condensates, also exhibit complicated and unpredictable fluid motion, which is called *quantum turbulence* [47–51]. We focus on *pure quantum turbulence*, where the temperature is sufficiently low so that the viscous normal fluid density is negligible compared to the inviscid superfluid density. Different from ordinary fluids, the vorticity in quantum fluids is quantized [18, 64]. Many experiments and numerical simulations suggest that at scales larger than the mean intervortex distance ℓ_i, quantum turbulence exhibits the Richardson cascade with the Kolmogorov spectrum, while at scales smaller than ℓ_i, a novel energy cascade specific to quantum turbulence emerges. This novel energy cascade is believed to be induced by the interaction of Kelvin waves of different wave numbers on a single quantum vortex, and is called *Kelvin-wave cascade*. While the nature of the Kelvin-wave cascade has been intensively investigated over recent decades, the effects of compressibility on the novel cascade remain to be elucidated. Because the superfluid density changes significantly in the vicinity of quantum vortices, the compressibility effects can induce a nontrivial impact on the energy cascade.

In Chapter 3, we aim to reveal the compressibility effects on the energy cascade. To this end, we theoretically analyze the Gross-Pitaevskii equation by taking a phenomenological approach based on the Onsager "ideal turbulence" theory. We show that the compressibility effects can induce a novel energy cascade, which we call *quantum stress cascade*, at scales smaller than ℓ_i. We conjecture that the incompressible part of this quantum stress cascade corresponds to the conventional Kelvin-wave cascade.

(ii) Van der Waals turbulence

In ordinary fluid turbulence, the Kolmogorov dissipation scale η is overwhelmingly larger than the microscopic length scales such as the molecular mean free path λ_{mfp} [5], and thus the cascade never reaches microscopic length scales. However, if we consider the strong turbulent regime of a supercritical fluid near a gas-liquid critical point, where the correlation length of equilibrium density fluctuations ξ reaches a macroscopic order of magnitude, the cascade possibly reaches "microscopic length scales" smaller than ξ. Then, we ask how the Richardson cascade is modified by density fluctuations at scales smaller

than ξ.

In Chapter 4, we answer this question by investigating hydrodynamic equations called the *Navier–Stokes–Korteweg equation*. This equation includes the stress due to the density fluctuations determined by the van der Waals theory. By using a similar argument developed in Chapter 3, we show that supercritical turbulence near a critical point exhibits a novel type of energy cascade, which we call *van der Waals cascade*, at "microscopic length scales" smaller than ξ. Interestingly, the mechanism of this novel cascade is analogous to that of the quantum stress cascade in quantum turbulence. In other words, pure quantum turbulence and this *van der Waals turbulence* may belong to the same "universality class."

(iii) Simple XY model for cascade transfer

Since we are interested only in the universal aspect of cascade transfer, it is sufficient to investigate the simplest model that describes it. Simple models have provided phenomenological perspectives on various phenomena such as critical phenomena [65], phase separation [38,66], directed percolation [67], surface growth [68,69], and flocking [70]. Here, we aim to construct a simple model representing one universality class for cascade transfer without paying much attention to its relevance to real systems. In doing so, we regard cascade transfer as a cooperative phenomenon and ask how it emerges from spatially local interactions.

In Chapter 5, we propose such a simple model that represents a different "universality class" from ordinary fluid turbulence. The constructed model can be regarded as a modified XY model where the amplitude fluctuates. We show that an inverse energy cascade with a non-Kolmogorov energy spectrum $E(k) \propto k^{-3}$ emerges from spatially local interactions. Interestingly, the behavior of this model is similar to that observed in *spin turbulence* and *atmospheric turbulence*.

Part II: Information flow in turbulence

At the end of Section 1.3, we mentioned a common intuitive picture of the origin of universality that small-scale turbulent fluctuations "forget" the details of large scales because of the chaotic nature of the stepwise cascade process. Somewhat contrary to this picture, it is known that, along with the energy cascade, fluctuations of small-scale quantities (e.g., the energy dissipation rate) follow those of large-scale quantities (e.g., the energy injection rate) with a time delay that corresponds to the large-eddy turnover time [71–73]. Moreover, the energy cascade induces chaos synchronization of small-scale motions, where small-scale velocity field is slaved to the chaotic dynamics of large-scale velocity field [74–78]. These phenomena suggest that information of large-scale turbulent fluctuations is transferred to small scales.

In Chapter 7, we aim to elucidate the nature of information flow in ordinary fluid turbulence from an information-thermodynamic viewpoint [79]. To this end, we employ the framework of fluctuating hydrodynamics to explicitly take thermal fluctuations into account. Specifically, we use the shell model with thermal noise, which is a simplified caricature of the fluctuating Navier–Stokes equation. Information thermodynamics is essentially stochastic thermodynamics for subsystems [80, 81] and provides constraints that are consistent with thermodynamics on the exchange of information between subsystems. This approach not only enables us to obtain fundamental constraints on information flow, but also allows comparative studies with other information processing systems.

We show that information of large-scale eddies is transferred to small scales along with the energy cascade. The information transfer rate is characterized by the large-eddy turnover time. Furthermore, we numerically show that the information-thermodynamic efficiency is extremely low compared to other information processing systems such as Maxwell's demon. This result implies that transferring information from large to small scales involves enormous thermodynamic costs, indicating the poor performance of turbulence as an information processing system.

1.4.1 Organization of the thesis

The remainder of this thesis is organized as follows (see also Fig. 1.3).

Part I consists of Chapters 2, 3, 4, and 5:

- In Chapter 2, we briefly review the Onsager "ideal turbulence" theory, which can be regarded as a central pillar of our understanding of fluid turbulence. The Onsager theory provides exact results consistent with various experimental facts and rich phenomenological perspectives, which will be used in Chapter 3 and 4.
- In Chapter 3, we investigate the similarity and difference between quantum and classical turbulence. Specifically, by taking a phenomenological approach based on the Onsager "ideal turbulence" theory, we show that the compressibility effects can induce a novel energy cascade, which we call quantum stress cascade. This chapter is based on [T. Tanogami, Phys. Rev. E **103**, 023106 (2021)] and [T. Tanogami, Phys. Rev. E **105**, 027102 (2022)].
- In Chapter 4, we explore a novel type of energy cascade by focusing on supercritical turbulence near a gas-liquid critical point. We show that supercritical turbulence near a critical point exhibits a novel type of energy cascade, which we call van der Waals cascade. This chapter is based on [T. Tanogami and S.-i. Sasa, Phys. Rev. Research **3**, L032027 (2021)].
- In Chapter 5, we construct a simple model representing one universality class for cascade transfer without paying much attention to its relevance to real systems. We show that an inverse energy cascade with a non-Kolmogorov energy spectrum emerges from spatially local interactions. This chapter is based on [T. Tanogami and S.-i. Sasa, Phys. Rev. Research **4**, L022015 (2022)].

Part II consists of Chapters 6 and 7:

- In Chapter 6, we introduce several information-theoretic quantities and briefly review stochastic thermodynamics and information thermodynamics, which will be used in Chapter 7.
- In Chapter 7, we investigate the nature of information flow in ordinary fluid turbulence from an information-thermodynamic viewpoint. We show that information of turbulent fluctuations flows from large to small scales along with the energy cascade. This chapter is based on [T. Tanogami and R. Araki, arXiv:2206.11163].

Finally, in Chapter 8, we conclude this thesis with some future perspectives.

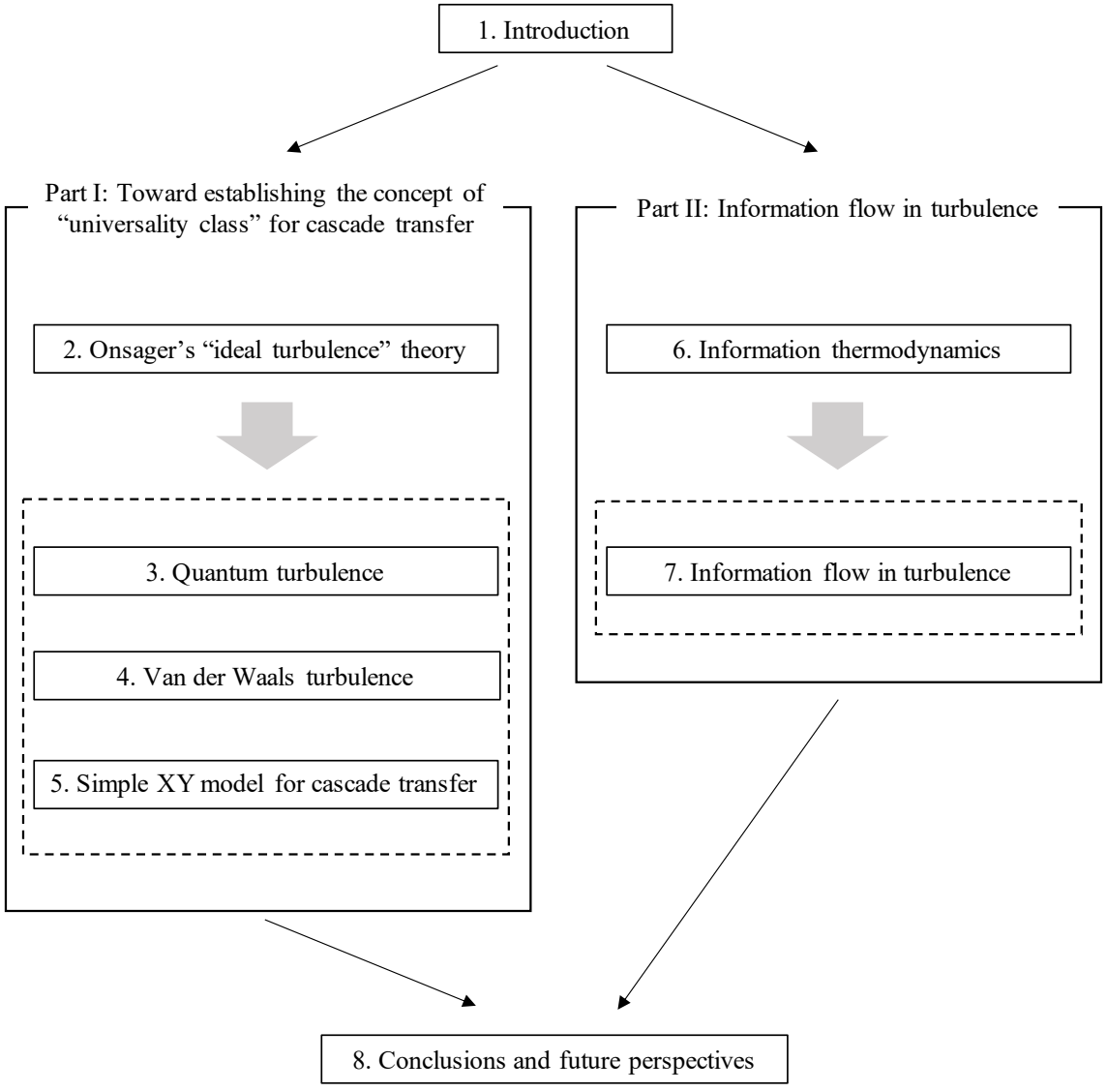

Fig. 1.3: Organization of the thesis.

Part I

Toward establishing the concept of "universality class" for cascade transfer

Chapter 2

Onsager's "ideal turbulence" theory

In this chapter, we briefly review the Onsager "ideal turbulence" theory [3, 10, 18, 82]. In the previous chapter, we have seen that dissipative anomaly is one of the most crucial experimental facts in three-dimensional fluid turbulence. This phenomenon implies that the velocity field does not remain differentiable in the inviscid limit and that the core of turbulence can be described by "non-differentiable solutions," or in modern terms, *weak solutions*, of the Euler equation. This observation is at the heart of the Onsager "ideal turbulence" theory. The Onsager theory has been extended to various turbulent phenomena, such as two-dimensional enstrophy cascade [83, 84], three-dimensional helicity cascade [85, 86], magnetohydrodynamic turbulence [87–89], compressible turbulence [90–95], collisionless plasma turbulence [96], and relativistic fluid turbulence [97]. Although the Onsager theory involves sophisticated mathematical concepts such as weak solutions, it also provides a phenomenological perspective on the relation between cascades and the singularity of the velocity field. Such a phenomenological perspective provides a basis for the argument in Chapter 3 and 4.

This chapter is organized as follows. In the next section, we explain the so-called Onsager's conjecture. In Section 2.2, we briefly explain the outline of the proof of the first part of the conjecture. Some mathematical concepts and results introduced in this section will be used in Chapter 3 and 4. In Section 2.3, we provide a brief introduction to the ideas behind the proof of the second part of the conjecture. Concluding remarks are provided in Section 2.4.

2.1 The Onsager conjecture

At the end of his 1949 paper [18], Onsager provided the following remark, which is now called the "Onsager conjecture":[1]

> "It is of some interest to note that in principle, turbulent dissipation as described could take place just as readily without the final assistance by viscosity. In the absence of viscosity, the standard proof of the conservation of energy does not apply, because the velocity field does not remain differentiable! In fact it is possible to show that the velocity field in such "ideal" turbulence cannot obey any LIPSCHITZ condition of the form
>
> $$|\boldsymbol{v}(\boldsymbol{r}' + \boldsymbol{r}) - \boldsymbol{v}(\boldsymbol{r}')| < (\text{const.})r^n,$$

[1] Onsager was aware of Taylor's estimation of the energy dissipation $\varepsilon \sim v_{\text{rms}}^3/L$ [46] and of Dryden's experiments suggesting the existence of dissipative anomaly [11].

> for any order n greater than 1/3; otherwise the energy is conserved. Of course, under the circumstances, the ordinary formulation of the laws of motion in terms of differential equations becomes inadequate and must be replaced by a more general description; for example, the formulation (15) in terms of FOURIER series will do. The detailed conservation of energy (17) does not imply conservation of the total energy if the number of steps in the cascade is infinite, as expected, and the double sum of $Q(\boldsymbol{k}, \boldsymbol{k}')$ converges only conditionally."

This remark can be summarized in the following two statements:

Onsager conjecture

Let $\boldsymbol{v}$ be a (generalized) solution of the Euler equation with Hölder exponent h:

$$|\boldsymbol{v}(\boldsymbol{x}+\boldsymbol{r}) - \boldsymbol{v}(\boldsymbol{x})| \leq Cr^h, \qquad \forall \boldsymbol{r}, \boldsymbol{x},$$

where C is a constant independent of $\boldsymbol{r}, \boldsymbol{x}$.

1. If $h > 1/3$, then energy is conserved.
2. For $h < 1/3$, there are solutions that dissipates energy.

Historically, the Onsager conjecture seems to have been nearly forgotten for a long time until rediscovered by Eyink [3, 98].[2] In [98], a result close to the first part of the Onsager conjecture was proved in terms of *weak solutions*, which can be regarded as the modern concept corresponding to "general description" in Onsager's remark. Shortly thereafter, Constantin *et al.* found a proof of the first conjecture and even obtained a sharper result based on *Besov spaces* [100]. In later work, Duchon and Robert provided another similar proof for the first conjecture by using the so-called *point-splitting regularization* and established the connection between the Onsager conjecture and the Kolmogorov 4/5-law [101]. Remarkably, Onsager had obtained results similar to those of Duchon and Robert in his unpublished notes (see pp. 14-18 of [https://ntnu.tind.io/record/121183] for his handwritten notes and [3] for a historical review).

The second part of the conjecture was almost certainly not proved by Onsager and has a long history. The first related result was provided by Scheffer [102] and Shnirelman [103], although they were not motivated by the Onsager conjecture. They constructed a nontrivial weak Euler solution with compact support in space and time, which is hard to interpret physically. The essential idea toward settling the second conjecture was proposed by De Lellis and Székelyhidi Jr [104–107]. Remarkably, their idea is closely connected with the Nash–Kuiper theorem [108–110] and Gromov's homotopy principle (or h-principle) [111, 112]. Based on their program, the second conjecture was finally proved by Isett [113] and Buckmaster *et al.* [114].

Below, we provide a brief sketch of the proof of the Onsager conjecture. We mainly focus on the first part of the conjecture, because some mathematical concepts and arguments in the proof provide a basis for the phenomenological approach used in Chapter 3 and 4.

[2] Even in the review article on turbulence by J. von Neumann in 1949 [99], Onsager's remark is not mentioned. In this article, Neumann reviews, e.g., the K41 theory, Heisenberg's theory, and the Burgers equation, and emphasizes the importance of numerical simulations in turbulence research.

2.2 On the first part of the conjecture

Here, we sketch the proof of the first part of the Onsager conjecture following Constantin *et al.* [100]. Before we proceed to the sketch of the proof, we first introduce some mathematical concepts.

2.2.1 Some mathematical concepts

Here, we introduce some mathematical concepts and useful results without proof. The emphasis is on relevance to physics rather than mathematical rigor. For more mathematically rigorous definitions and proofs, see, e.g., [115–117].

L^p-norm

To prove the first part of the Onsager conjecture, we need to measure the "size" of the energy flux. Therefore, we introduce the L^p-norm: for any measurable function $f : \Omega \to \mathbb{R}$, L^p-norm of f is defined by[3]

$$\|f\|_p := \begin{cases} \left(\dfrac{1}{|\Omega|} \displaystyle\int_\Omega |f(\boldsymbol{x})|^p d^3\boldsymbol{x} \right)^{1/p} = \langle |f|^p \rangle_\Omega^{1/p} & \text{if} \quad 1 \le p < \infty, \\ \|f\|_\infty := \operatorname{ess\,sup}_\Omega |f| & \text{if} \quad p = \infty. \end{cases} \tag{2.1}$$

The set of all measurable functions $f : \Omega \to \mathbb{R}$ such that $\|f\|_p < \infty$ is called L^p space, denoted by $L^p(\Omega)$.[4] For a vector $\boldsymbol{a} : \Omega \to \mathbb{R}^m$, we define $\|\boldsymbol{a}\|_p := \||\boldsymbol{a}|\|_p$ with $|\boldsymbol{a}| := \sqrt{a_1^2 + a_2^2 + \cdots + a_m^2}$. For a matrix $\mathsf{A} = (a_{ij})$, we define its L^p-norm $\|\mathsf{A}\|_p = \||\mathsf{A}|\|_p$ via the Frobenius norm $|\mathsf{A}| := \sqrt{\sum_i \sum_j |a_{ij}|^2}$.

(Generalized) Hölder inequality

Suppose $p, q, r \in [1, \infty]$ satisfy $1/p + 1/q = 1/r$ and $f \in L^p(\Omega)$ and $g \in L^q(\Omega)$. Then, $fg \in L^r(\Omega)$ and

$$\|fg\|_r \le \|f\|_p \|g\|_q. \tag{2.2}$$

Minkowski inequality

Suppose $p \in [1, \infty]$ and $f, g \in L^p(\Omega)$. Then, $f + g \in L^p(\Omega)$ and

$$\|f + g\|_p \le \|f\|_p + \|g\|_p. \tag{2.3}$$

From the Hölder inequality, we note that $\|f\|_p \le \|f\|_q$ for $p \le q$.

[3] Here, we employed the definition where the integral is normalized by $|\Omega|$ so that the absolute structure function can be expressed as $\langle |\delta \boldsymbol{v}(\boldsymbol{r}; \boldsymbol{x})|^p \rangle_\Omega = \|\delta \boldsymbol{v}(\boldsymbol{r}; \cdot)\|_p^p$.

[4] Strictly speaking, $L^p(\Omega)$ is not a space of functions, but of equivalence classes. That is, we identify two functions if they are equal almost everywhere.

Besov regularity

Next, we introduce the Besov regularity, which is a "L^p-version" of Hölder continuity [90, 118, 119]. A function $\boldsymbol{a} \in L^p(\Omega)$ $(p \in [1,\infty])$ with

$$\|\delta \boldsymbol{a}(\boldsymbol{r};\cdot)\|_p \le C r^{\sigma_p} \tag{2.4}$$

is called *Besov regular* with pth-order Besov exponent σ_p.[5] Note that Besov regularity of $p=\infty$ corresponds to uniform Hölder continuity:

$$|\delta \boldsymbol{a}(\boldsymbol{r};\boldsymbol{x})| \le C r^{\sigma_\infty}, \qquad \forall \boldsymbol{x} \in \Omega. \tag{2.6}$$

In the context of turbulence, note that $\|\delta \boldsymbol{v}(\boldsymbol{r};\cdot)\|_p$ is essentially the traditional absolute structure function $\langle |\delta \boldsymbol{v}(\boldsymbol{r};\boldsymbol{x})|^p \rangle_\Omega = \|\delta \boldsymbol{v}(\boldsymbol{r};\cdot)\|_p^p$:

$$\langle |\delta \boldsymbol{v}(\boldsymbol{r};\boldsymbol{x})|^p \rangle_\Omega \sim v_{\mathrm{rms}}^p \left(\frac{r}{L}\right)^{\zeta_p} \quad \text{for} \quad r \ll L, \tag{2.7}$$

where the symbol $\sim$ means that

$$\zeta_p = \liminf_{r\to 0} \frac{\ln \langle |\delta \boldsymbol{v}(\boldsymbol{r};\boldsymbol{x})|^p \rangle_\Omega}{\ln(r/L)}. \tag{2.8}$$

Therefore, if σ_p is the maximal Besov exponent of order p for the velocity field, i.e.,[6]

$$\sigma_p = \liminf_{r\to 0} \frac{\ln \|\delta \boldsymbol{v}(\boldsymbol{r};\cdot)\|_p}{\ln(r/L)}, \tag{2.11}$$

then $\sigma_p = \zeta_p/p$ [10].

Mollification

We now introduce mollification or coarse-graining procedure. Let $G_\ell(\boldsymbol{r}) := \ell^{-3} G(\boldsymbol{r}/\ell)$ be the Friedrichs mollifier with $\ell > 0$, where $G \in C_0^\infty(\Omega)$ satisfies

$$G(\boldsymbol{r}) \ge 0, \tag{2.12}$$

$$G(\boldsymbol{r}) = 0 \qquad \text{for} \quad r \ge 1, \tag{2.13}$$

$$\int_\Omega d^3\boldsymbol{r} G(\boldsymbol{r}) = 1. \tag{2.14}$$

[5] More precisely, the Besov space $B_p^{\sigma_p,\infty}(\Omega)$ comprises measurable functions $f : \Omega \to \mathbb{R}$ such that the following Besov norm is finite:

$$\|f\|_{B_p^{\sigma_p,\infty}(\Omega)} := \|f\|_p + \sup_{\boldsymbol{r}} \frac{\|\delta f(\boldsymbol{r};\cdot)\|_p}{r^{\sigma_p}}. \tag{2.5}$$

[6] In other words, for every $\epsilon > 0$, there exists a $\delta > 0$ such that whenever $\ell < \delta$, we have

$$\sigma_p - \epsilon \le \inf_{r<\ell} \frac{\ln \|\delta \boldsymbol{v}(\boldsymbol{r};\cdot)\|_p}{\ln(r/L)} \le \sigma_p + \epsilon. \tag{2.9}$$

By noting that $\ln(r/L) < 0$, this implies that

$$\exists r < \ell, \quad \|\delta \boldsymbol{v}(\boldsymbol{r};\cdot)\|_p \ge C \left(\frac{r}{L}\right)^{\sigma_p+\epsilon} \quad \text{and} \quad \forall r < \ell, \quad \|\delta \boldsymbol{v}(\boldsymbol{r};\cdot)\|_p \le C \left(\frac{r}{L}\right)^{\sigma_p-\epsilon}. \tag{2.10}$$

That is, $\boldsymbol{v} \in B_p^{\sigma,\infty}(\Omega)$ for any $\sigma < \sigma_p$, while $\boldsymbol{v} \notin B_p^{\sigma,\infty}(\Omega)$ for any $\sigma > \sigma_p$.

For convenience, we also assume isotropy: $G(\boldsymbol{r}) = G(r)$ with $r := |\boldsymbol{r}|$. For any locally integrable function $\boldsymbol{a}(\boldsymbol{x})$,[7] we define a coarse-grained field at length-scale $\ell > 0$ as

$$\bar{\boldsymbol{a}}_\ell(\boldsymbol{x}) := \int_\Omega d^3\boldsymbol{r} G_\ell(\boldsymbol{r}) \boldsymbol{a}(\boldsymbol{x}+\boldsymbol{r}). \tag{2.15}$$

Note that the coarse-grained field $\bar{\boldsymbol{a}}_\ell$ is a smooth function because of the smoothness of the mollifier. We remark that if $f \in L^p(\Omega)$ for $1 \le p < \infty$, then $\bar{f}_\ell \in L^p(\Omega)$ with

$$\|\bar{f}_\ell\|_p \le \|f\|_p, \tag{2.16}$$

and $\bar{f}_\ell \to f$ in $L^p(\Omega)$ as $\ell \to 0$:

$$\lim_{\ell \to 0} \|\bar{f}_\ell - f\|_p = 0. \tag{2.17}$$

Weak solution

We introduce a *weak solution* (also called *distributional* or *generalized solution*) of the Euler equation through the coarse-graining procedure. We consider the incompressible Euler equation:

$$\partial_t \boldsymbol{v} + \boldsymbol{v} \cdot \nabla \boldsymbol{v} = -\nabla p, \tag{2.18}$$
$$\nabla \cdot \boldsymbol{v} = 0. \tag{2.19}$$

For simplicity, we assume that the solution is differentiable in time and do not consider external forces. Because the coarse-graining operation commutes with space and time derivatives, coarse-graining of (2.18) and (2.19) reads

$$\partial_t \bar{\boldsymbol{v}}_\ell + \nabla \cdot [\bar{\boldsymbol{v}}_\ell \bar{\boldsymbol{v}}_\ell + \bar{\tau}_\ell(\boldsymbol{v}, \boldsymbol{v})] = -\nabla \bar{p}_\ell, \tag{2.20}$$
$$\nabla \cdot \bar{\boldsymbol{v}}_\ell = 0, \tag{2.21}$$

where we have introduced the small-scale stress tensor

$$\bar{\tau}_\ell(\boldsymbol{v}, \boldsymbol{v}) := \overline{(\boldsymbol{v}\boldsymbol{v})}_\ell - \bar{\boldsymbol{v}}_\ell \bar{\boldsymbol{v}}_\ell. \tag{2.22}$$

Note that the coarse-grained equation is not closed in terms of the coarse-grained fields $\bar{\boldsymbol{v}}_\ell$ and $\bar{p}_\ell$ due to the existence of the small-scale stress tensor $\bar{\tau}_\ell$.

We say that $\boldsymbol{v}$ is a weak solution of the Euler equation (2.18) and (2.19) if it satisfies the coarse-grained equation (2.20) and (2.21) for all $\ell > 0$. Note that this definition of weak solution is equivalent to the conventional definition based on distributions [92]. We remark that weak solutions are not unique in general. That is, there can be more than one solution even for the same initial data.

2.2.2 Sketch of the proof

We assume that $\boldsymbol{v}$ is a weak solution of the Euler equation that satisfies the Besov regularity

$$\|\delta \boldsymbol{v}(\boldsymbol{r}; \cdot)\|_p \sim v_{\mathrm{rms}} \left(\frac{r}{L}\right)^{\sigma_p} \quad \text{for} \quad r \ll L \tag{2.23}$$

[7] *Locally integrable* means that f is integrable for every compact set $K \subset \Omega$, and the set of locally integrable functions is denoted by $L^1_{\mathrm{loc}}(\Omega)$. For $p \in [1, \infty]$, there is a inclusion $L^p(\Omega) \subset L^1_{\mathrm{loc}}(\Omega)$.

with the Besov exponent $\sigma_p \in (0,1]$ for some $p \geq 3$. Our starting point is the coarse-grained Euler equation (2.20) and (2.21). We define the large-scale kinetic energy density per mass as $|\bar{\boldsymbol{v}}_\ell|^2/2$. From (2.20), we obtain the large-scale kinetic energy balance equation:

$$\partial_t \left(\frac{1}{2} |\bar{\boldsymbol{v}}_\ell|^2 \right) + \nabla \cdot \boldsymbol{J}_\ell = -\Pi_\ell, \tag{2.24}$$

where

$$\boldsymbol{J}_\ell := \left(\frac{1}{2} |\bar{\boldsymbol{v}}_\ell|^2 + \bar{p}_\ell \right) \bar{\boldsymbol{v}}_\ell + \bar{\boldsymbol{v}}_\ell \cdot \bar{\tau}_\ell(\boldsymbol{v}, \boldsymbol{v}) \tag{2.25}$$

denotes the spatial transport of large-scale kinetic energy, and

$$\Pi_\ell := -\nabla \bar{\boldsymbol{v}}_\ell : \bar{\tau}_\ell(\boldsymbol{v}, \boldsymbol{v}) \tag{2.26}$$

denotes the scale-to-scale energy flux called *deformation work* [4], which represents work done by the large-scale strain $\nabla \bar{\boldsymbol{v}}_\ell$ against the small-scale stress $\bar{\tau}_\ell(\boldsymbol{v}, \boldsymbol{v})$.[8] We note that for smooth solutions, we obtain $\Pi_\ell \to 0$ as $\ell \to 0$.

A key observation in the proof is that Π_ℓ can be expressed in terms of velocity-increments $\delta \boldsymbol{v}(\boldsymbol{r}; \boldsymbol{x}) = \boldsymbol{v}(\boldsymbol{x} + \boldsymbol{r}) - \boldsymbol{v}(\boldsymbol{x})$. Indeed, the large-scale strain $\nabla \bar{\boldsymbol{v}}_\ell$ and the small-scale stress $\bar{\tau}_\ell(\boldsymbol{v}, \boldsymbol{v})$ can be expressed as

$$\nabla \bar{\boldsymbol{v}}_\ell = -\frac{1}{\ell} \int_\Omega d^3\boldsymbol{r} (\nabla G)_\ell(\boldsymbol{r}) \delta \boldsymbol{v}(\boldsymbol{r}; \boldsymbol{x}), \tag{2.28}$$

$$\bar{\tau}_\ell(\boldsymbol{v}, \boldsymbol{v}) = \int_\Omega d^3\boldsymbol{r} G_\ell(\boldsymbol{r}) \delta \boldsymbol{v}(\boldsymbol{r}; \boldsymbol{x}) \delta \boldsymbol{v}(\boldsymbol{r}; \boldsymbol{x}) - \int_\Omega d^3\boldsymbol{r} G_\ell(\boldsymbol{r}) \delta \boldsymbol{v}(\boldsymbol{r}; \boldsymbol{x}) \int_\Omega d^3\boldsymbol{r} G_\ell(\boldsymbol{r}) \delta \boldsymbol{v}(\boldsymbol{r}; \boldsymbol{x}), \tag{2.29}$$

where we have used $\int_\Omega d^3\boldsymbol{r} \nabla G(\boldsymbol{r}) = \boldsymbol{0}$ in (2.28). Based on this observation, we now evaluate the scale dependence of the deformation work by using L^p-norm. We first note that, by using the Cauchy-Schwarz and Hölder inequality,

$$\begin{aligned} \|\Pi_\ell\|_{p/3} &= \|\nabla \bar{\boldsymbol{v}}_\ell : \bar{\tau}_\ell(\boldsymbol{v}, \boldsymbol{v})\|_{p/3} \\ &\leq \|\nabla \bar{\boldsymbol{v}}_\ell\|_p \|\bar{\tau}_\ell(\boldsymbol{v}, \boldsymbol{v})\|_{p/2}. \end{aligned} \tag{2.30}$$

For the large-scale strain $\nabla \bar{\boldsymbol{v}}_\ell$, we can evaluate its scale dependence as follows:

$$\begin{aligned} \|\nabla \bar{\boldsymbol{v}}_\ell\|_p &= \left\| \frac{1}{\ell} \int_\Omega d^3\boldsymbol{r} (\nabla G)_\ell(\boldsymbol{r}) \delta \boldsymbol{v}(\boldsymbol{r}; \cdot) \right\|_p \\ &\leq \frac{1}{\ell} \int_\Omega d^3\boldsymbol{r} |(\nabla G)_\ell(\boldsymbol{r})| \|\delta \boldsymbol{v}(\boldsymbol{r}; \cdot)\|_p \\ &\leq \frac{C}{\ell} \|\delta \boldsymbol{v}(\ell)\|_p, \end{aligned} \tag{2.31}$$

[8] Note that the deformation work is a spatially local version of the spectral energy flux Π_K introduced in Section 1.3. Indeed, by using isotropy of $G(\boldsymbol{r})$, we can show that the two fluxes are related by [82]

$$\langle \Pi_\ell \rangle_\Omega = \int_0^\infty dk P_\ell(k) \Pi_K. \tag{2.27}$$

Here, $P_\ell(k) := -d_k |\hat{G}(k\ell)|^2$ satisfies $\int_0^\infty dk P_\ell(k) = 1$ and $P_\ell(k) \geq 0$ for standard mollifier, where $\hat{G}(k)$ is the Fourier transform of $G(\boldsymbol{r})$.

where $C := \int_\Omega d^3\boldsymbol{\rho}|\nabla G(\boldsymbol{\rho})|$, and $\|\delta\boldsymbol{v}(\ell)\|_p := \sup_{|\boldsymbol{r}|<\ell}\|\delta\boldsymbol{v}(\boldsymbol{r};\cdot)\|_p$. Therefore, we find that

$$\|\nabla\bar{\boldsymbol{v}}_\ell\|_p = O\left(\frac{\|\delta\boldsymbol{v}(\ell)\|_p}{\ell}\right). \tag{2.32}$$

Similarly, by using the Minkowski and Hölder inequalities, the scale dependence of the small-scale stress $\bar{\tau}_\ell(\boldsymbol{v},\boldsymbol{v})$ can be evaluated as

$$\begin{aligned}\|\bar{\tau}_\ell(\boldsymbol{v},\boldsymbol{v})\|_{p/2} &\le \left\|\int_\Omega d^3\boldsymbol{r}G_\ell(\boldsymbol{r})\delta\boldsymbol{v}(\boldsymbol{r};\cdot)\delta\boldsymbol{v}(\boldsymbol{r};\cdot)\right\|_{p/2} + \left\|\int_\Omega d^3\boldsymbol{r}G_\ell(\boldsymbol{r})\delta\boldsymbol{v}(\boldsymbol{r};\cdot)\right\|_p^2 \\ &\le \int_\Omega d^3\boldsymbol{r}G_\ell(\boldsymbol{r})\|\delta\boldsymbol{v}(\boldsymbol{r};\cdot)\|_p^2 + \left(\int_\Omega d^3\boldsymbol{r}G_\ell(\boldsymbol{r})\|\delta\boldsymbol{v}(\boldsymbol{r};\cdot)\|_p\right)^2 \\ &\le 2\|\delta\boldsymbol{v}(\ell)\|_p^2,\end{aligned} \tag{2.33}$$

and thus

$$\|\bar{\tau}_\ell(\boldsymbol{v},\boldsymbol{v})\|_{p/2} = O(\|\delta\boldsymbol{v}(\ell)\|_p^2), \quad p \ge 2. \tag{2.34}$$

By combining (2.32) and (2.34), we obtain a rigorous upper bound for the deformation work:

$$\|\Pi_\ell\|_{p/3} = O\left(\frac{\|\delta\boldsymbol{v}(\ell)\|_p^3}{\ell}\right), \quad p \ge 3. \tag{2.35}$$

From the Besov regularity assumption, we finally obtain

$$\|\Pi_\ell\|_{p/3} = O\left(\ell^{3\sigma_p-1}\right), \quad p \ge 3. \tag{2.36}$$

Note that

$$\begin{aligned}|\langle\Pi_\ell\rangle_\Omega| &\le \langle|\Pi_\ell|\rangle_\Omega \\ &\le \|\Pi_\ell\|_r \quad \text{for} \quad r \ge 1,\end{aligned} \tag{2.37}$$

where we have used the Hölder inequality in the second line. Then, (2.36) implies that $\langle\Pi_\ell\rangle_\Omega \to 0$, i.e., $\partial_t\langle|\bar{\boldsymbol{v}}_\ell|^2\rangle_\Omega/2 \to 0$ as $\ell \to 0$ if $\sigma_p > 1/3$ for some $p \ge 3$. In other words, dissipative anomaly requires a singular velocity field with $\sigma_p \le 1/3$ for any $p \ge 3$. Interestingly, in terms of the scaling exponent ζ_p for the absolute structure function, defined by (2.7), this result implies that $\zeta_p \le p/3$ for any $p \ge 3$, which is consistent with intermittency.

2.2.3 Remark: dissipative anomaly and Kolmogorov's 4/5-law

We can further derive the local energy balance equation in the sense of distributions by taking the limit $\ell \to 0$ in the large-scale kinetic energy balance equation (2.24):

$$\partial_t\left(\frac{1}{2}|\boldsymbol{v}|^2\right) + \nabla\cdot\left[\left(\frac{1}{2}|\boldsymbol{v}|^2 + p\right)\boldsymbol{v}\right] = -D(\boldsymbol{v}), \tag{2.38}$$

where $D(\boldsymbol{v}) = \lim_{\ell\to 0}\Pi_\ell$, which is independent of the choice of $G(\boldsymbol{r})$ [101]. $D(\boldsymbol{v})$ represents a possible dissipation or production of energy caused by the lack of smoothness in the

velocity field $\boldsymbol{v}$. The result (2.36) implies that $D(\boldsymbol{v}) = 0$ if $\sigma_p > 1/3$ for some $p \geq 3$.[9] Note that if $\zeta_p \leq p/3$ for any $p \geq 3$, $D(\boldsymbol{v})$ need not be zero and can be both positive and negative, reflecting the time-reversal symmetry of the Euler equation. In particular, for weak solutions of the Euler equation obtained in the inviscid limit of Navier–Stokes solutions, it is true that $D(\boldsymbol{v}) \geq 0$. More specifically, if a sequence of Navier–Stokes solutions $\boldsymbol{v}^\nu$ converges $\boldsymbol{v}^\nu \to \boldsymbol{v}$ as $\nu \to 0$ in L^3-norm, i.e., $\lim_{\nu\to 0} \|\boldsymbol{v}^\nu - \boldsymbol{v}\|_3 = 0$, then $\boldsymbol{v}$ is a weak solution of the Euler equation and satisfies the local energy balance equation (2.38) with the following relation [101]:[10][11]

$$D(\boldsymbol{v}) = \lim_{\nu\to 0} \nu |\nabla \boldsymbol{v}^\nu|^2 \geq 0. \tag{2.41}$$

This relation implies that the Euler equation has a mechanism for energy dissipation without the aid of viscosity, as pointed out by Onsager.

From the relation (2.41), we can further derive a generalization of Kolmogorov's 4/5-law [101]. To see this, we first note that there is an alternative expression for $D(\boldsymbol{v})$:

$$D(\boldsymbol{v}) = \lim_{\ell\to 0} \frac{1}{4\ell} \int_\Omega d^3\boldsymbol{r} (\nabla G)_\ell(\boldsymbol{r}) \cdot \delta\boldsymbol{v}(\boldsymbol{r};\boldsymbol{x}) |\delta\boldsymbol{v}(\boldsymbol{r};\boldsymbol{x})|^2. \tag{2.42}$$

In fact, by introducing a *point-splitting regularization* of the kinetic energy density as $\boldsymbol{v}\cdot\bar{\boldsymbol{v}}_\ell/2$, we have[12]

$$\partial_t \left(\frac{1}{2}\boldsymbol{v}\cdot\bar{\boldsymbol{v}}_\ell\right) + \nabla\cdot\left[\left(\frac{1}{2}\boldsymbol{v}\cdot\bar{\boldsymbol{v}}_\ell\right)\boldsymbol{v} + \frac{1}{2}(\bar{p}_\ell\boldsymbol{v} + p\bar{\boldsymbol{v}}_\ell) + \frac{1}{2}\left(\overline{(|\boldsymbol{v}|^2\boldsymbol{v})}_\ell - \overline{(|\boldsymbol{v}|^2)}_\ell\boldsymbol{v}\right)\right] = -D_\ell(\boldsymbol{v}), \tag{2.43}$$

where

$$D_\ell(\boldsymbol{v}) := \frac{1}{4\ell} \int_\Omega d^3\boldsymbol{r} (\nabla G)_\ell(\boldsymbol{r}) \cdot \delta\boldsymbol{v}(\boldsymbol{r};\boldsymbol{x}) |\delta\boldsymbol{v}(\boldsymbol{r};\boldsymbol{x})|^2. \tag{2.44}$$

Because the left-hand side of (2.43) converges to the left hand-side of (2.38) in the sense of distributions if $\boldsymbol{v} \in L^3$, $\lim_{\ell\to 0} D_\ell(\boldsymbol{v})$ corresponds to $D(\boldsymbol{v})$. Thus, the relation (2.41) can be rewritten as

$$\lim_{\ell\to 0} \frac{1}{4\ell} \int_\Omega d^3\boldsymbol{r} (\nabla G)_\ell(\boldsymbol{r}) \cdot \delta\boldsymbol{v}(\boldsymbol{r};\boldsymbol{x}) |\delta\boldsymbol{v}(\boldsymbol{r};\boldsymbol{x})|^2 = \hat{\varepsilon} \tag{2.45}$$

---

[9] In fact, since for every test function $\varphi \in C_0^\infty(\Omega)$,

$$|\langle \varphi \Pi_\ell \rangle_\Omega| \leq \|\varphi\|_\infty \|\Pi_\ell\|_r \tag{2.39}$$

for $r \geq 1$, we find that $\lim_{\ell\to 0} |\langle \varphi\Pi_\ell\rangle_\Omega| = 0$ if $\sigma_p > 1/3$ for some $p \geq 3$. Thus, Π_ℓ converges to zero in the sense of distributions.

[10] More precisely, $D(\boldsymbol{v})$ is a nonnegative distribution: for every test function $\varphi \in C_0^\infty(\Omega)$, $\langle \varphi D(\boldsymbol{v})\rangle_\Omega \geq 0$.

[11] Here, we have assumed that there are no singularities in the Navier–Stokes solutions at any small, but finite, viscosity. If there exists the Navier–Stokes singularities, then (2.41) is modified as follows [101]:

$$D(\boldsymbol{v}) = \lim_{\nu\to 0} \left(\nu|\nabla\boldsymbol{v}^\nu|^2 + D(\boldsymbol{v}^\nu)\right) \geq 0 \tag{2.40}$$

in the sense of distributions.

[12] This relation appears in p. 14 of Onsager's unpublished note [https://ntnu.tind.io/record/121183] in a space-integrated form (see also [3]).

with $\hat{\varepsilon} := \lim_{\nu\to 0} \nu|\nabla \boldsymbol{v}^\nu|^2$. By using isotropy of $G(\boldsymbol{r})$ and introducing the angular average $\langle\cdot\rangle_{\rm ang} := (4\pi)^{-1}\int_{S^2}\cdot d\omega(\hat{\boldsymbol{r}})$, where $d\omega$ denotes the measure on solid angles, we obtain

$$\begin{aligned}\hat{\varepsilon} &= \lim_{\ell\to 0}\frac{1}{4\ell}4\pi\int r^2 dr (G')_\ell(r)\langle \delta v_\parallel(\boldsymbol{r};\boldsymbol{x})|\delta\boldsymbol{v}(\boldsymbol{r};\boldsymbol{x})|^2\rangle_{\rm ang}\\ &= \lim_{\ell\to 0}\pi\int \rho^3 d\rho G'(\rho)\left.\frac{\langle \delta v_\parallel(\boldsymbol{r};\boldsymbol{x})|\delta\boldsymbol{v}(\boldsymbol{r};\boldsymbol{x})|^2\rangle_{\rm ang}}{r}\right|_{r=\ell\rho}\\ &= -\frac{3}{4}\lim_{r\to 0}\frac{\langle \delta v_\parallel(\boldsymbol{r};\boldsymbol{x})|\delta\boldsymbol{v}(\boldsymbol{r};\boldsymbol{x})|^2\rangle_{\rm ang}}{r},\end{aligned} \tag{2.46}$$

where we have used $\delta v_\parallel(\boldsymbol{r};\boldsymbol{x}) := \delta\boldsymbol{v}(\boldsymbol{r};\boldsymbol{x})\cdot\hat{\boldsymbol{r}}$ and $4\pi\int\rho^2 d\rho G(\rho) = 1$. Thus, we conclude that

$$\lim_{r\to 0}\frac{\langle \delta v_\parallel(\boldsymbol{r};\boldsymbol{x})|\delta\boldsymbol{v}(\boldsymbol{r};\boldsymbol{x})|^2\rangle_{\rm ang}}{r} = -\frac{4}{3}\hat{\varepsilon}. \tag{2.47}$$

By introducing $\delta\boldsymbol{v}_\perp := \delta\boldsymbol{v} - \delta v_\parallel\hat{\boldsymbol{r}}$ that satisfies $\hat{\boldsymbol{r}}\cdot\delta\boldsymbol{v}_\perp = 0$, we can further show that [120]

$$\lim_{r\to 0}\frac{\langle \big(\delta v_\parallel(\boldsymbol{r};\boldsymbol{x})\big)^3\rangle_{\rm ang}}{r} = -\frac{4}{5}\hat{\varepsilon}. \tag{2.48}$$

Interestingly, while the original Kolmogorov's 4/5-law requires averaging over ensembles assuming homogeneity and isotropy, this form of the 4/5-law is valid for individual realizations.

2.3 On the second part of the conjecture

The proof of the second part of the conjecture is based on Gromov's *convex integration*, which is a deep mathematical work originating in the Nash–Kuiper theorem and Gromov's h-principle. Here, we shall not go into details of the proof, but only provide a brief introduction to the ideas behind it. For more detailed reviews on the second part of the Onsager conjecture, see, e.g., [10, 121, 122].[13]

The Nash–Kuiper theorem concerns the isometric embedding of Riemannian manifolds, a classical problem in differential geometry [108–110]:

Nash–Kuiper theorem

Let (M, g) be an m-dimensional Riemannian manifold, and let $\bar{\boldsymbol{u}} : M \to \mathbb{R}^n$ be a C^∞ short embedding into Euclidean space $\mathbb{R}^n$ with $n \geq m+1$. Then, for arbitrary $\epsilon > 0$, there exists a C^1 isometric embedding $\boldsymbol{u} : M \to \mathbb{R}^n$ with $|\bar{\boldsymbol{u}}(x) - \boldsymbol{u}(x)| < \epsilon$ for any $x \in M$.

[13] See also

https://abelprize.no/abel-prize-laureates/2015

https://hevea-project.fr/ENIndexHevea.html

for an introductory review of the Nash–Kuiper theorem and convex integration. For more technical review of the convex integration, see, e.g., the textbook [123] or Borrelli's lecture notes at

http://math.univ-lyon1.fr/homes-www/borrelli/Recherche.html

Here, *short embedding* means that $\bar{\boldsymbol{u}}$ decreases length of curves on M:

$$\partial_i \bar{\boldsymbol{u}} \cdot \partial_j \bar{\boldsymbol{u}} \leq g_{ij}, \tag{2.49}$$

while *isometric embedding* means that $\boldsymbol{u}$ preserves the length:

$$\partial_i \boldsymbol{u} \cdot \partial_j \boldsymbol{u} = g_{ij}. \tag{2.50}$$

Let us consider embedding the square flat torus in three-dimensional space $\mathbb{R}^3$, for example. Without stretching the square, it seems impossible to represent it in $\mathbb{R}^3$. In fact, Gauss's Theorema Egregium implies that curvature must be preserved by any isometric embedding. However, the Nash–Kuiper theorem states that isometric embedding of the square flat torus in three-dimensional space is possible if the embedding belongs to the class C^1. Remarkably, this theorem further states that there are infinitely many such isometric embeddings, although the system (2.50) is overdetermined for $m \geq 3$ and $n = m + 1$.

While Nash and Kuiper's proof relies on intricate construction, Gromov proposed a more systematic and general construction method, called convex integration, by extracting the underlying concept of Nash and Kuiper's result: the h-principle [111, 112]. Simply put, the convex integration technique enables us to systematically construct sequences of short embeddings converging toward isometric embeddings. That is, starting from a short embedding, we iteratively add a highly oscillatory correction, called *corrugations*, to lengthen distances in various directions to reduce the metric error. The algorithmic nature of the convex integration technique led to the visualization of an isometrically embedded square flat torus in three-dimensional space [124] (for an introductory review, see https://hevea-project.fr/ENIndexHevea.html).

De Lellis and Székelyhidi Jr realized that there is an unexpected and deep mathematical analogy between C^1 isometric embedding and weak solutions of the Euler equation [104–107]. The analog of a short embedding $\bar{\boldsymbol{u}} : M \to \mathbb{R}^n$ for the Euler equation is a smooth *subsolution* $\bar{\boldsymbol{v}}$ that satisfies

$$\partial_t \bar{\boldsymbol{v}} + \nabla \cdot [\bar{\boldsymbol{v}}\bar{\boldsymbol{v}} + \bar{\tau}] = -\nabla \bar{p}, \tag{2.51}$$

$$\nabla \cdot \bar{\boldsymbol{v}} = 0, \tag{2.52}$$

where $\bar{\tau}$ is a symmetric positive-definite tensor. The equation (2.51) has the same form as the coarse-grained Euler equation (2.20). That is, the error term $\bar{\tau}$ in (2.51) corresponds to a small-scale stress tensor $\bar{\tau}_\ell(\boldsymbol{v}, \boldsymbol{v}) := \overline{(\boldsymbol{v}\boldsymbol{v})}_\ell - \bar{\boldsymbol{v}}_\ell \bar{\boldsymbol{v}}_\ell$ in (2.20). In the context of the Nash–Kuiper theorem, $\bar{\tau} \geq 0$ is a precise analogue of (2.49). By using the convex integration technique, the second part of the Onsager conjecture was finally proved by Isett [113] and Buckmaster *et al.* [114]:

Theorem 1.1 of [114]

Let $e : [0, T] \to \mathbb{R}^+$ be any strictly positive smooth function. For any $h \in (0, 1/3)$, there exists a weak solution $\boldsymbol{v} \in C^h(\mathbb{T}^3 \times [0, T])$ of the Euler equation such that

$$\int_{\mathbb{T}^3} d^3\boldsymbol{x} \frac{1}{2} |\boldsymbol{v}(\boldsymbol{x}, t)|^2 = e(t). \tag{2.53}$$

Note that $e(t)$ can be any function strictly decreasing in time. Thus, this theorem states that there is a weak Euler solution with Hölder regularity $h < 1/3$ that dissipates kinetic

energy.[14] Such a dissipative weak Euler solution is constructed by the convex integration procedure as follows. For some specified smooth subsolution $\bar{\boldsymbol{v}}_n$ with $\bar{\tau}_n$ that satisfies

$$\partial_t \bar{\boldsymbol{v}}_n + \nabla \cdot [\bar{\boldsymbol{v}}_n \bar{\boldsymbol{v}}_n + \bar{\tau}_n] = -\nabla \bar{p}_n, \tag{2.54}$$

$$\nabla \cdot \bar{\boldsymbol{v}}_n = 0, \tag{2.55}$$

we add small-scale modes $\boldsymbol{W}_{n+1}$ to the velocity field so that $\bar{\boldsymbol{v}}_{n+1} = \bar{\boldsymbol{v}}_n + \boldsymbol{W}_{n+1}$ is again a subsolution with $|\bar{\tau}_{n+1}| \ll |\bar{\tau}_n|$. By iterating this procedure, we have $\bar{\tau}_n \to 0$ and $\bar{\boldsymbol{v}}_n \to \boldsymbol{v}$, which is a weak solution of the Euler equation.

2.4 Concluding remarks

Many experiments and numerical simulations suggest the validity of Onsager's prediction that the velocity field in "ideal turbulence" must be singular with the Hölder exponent $h \le 1/3$. For example, the multifractal dimension spectrum of Hölder singularities $D(h) = \inf_p\{ph + (3 - \zeta_p)\}$ has been obtained with the most probable exponent $h_* \simeq 1/3$ [125,126]. The Besov regularity of the velocity field with $\sigma_p \le 1/3$ for any $p \ge 3$ has also been well-established through the measurement of the structure functions [29, 43, 44, 127, 128]. Thus, the Onsager theory provides exact results consistent with various experimental facts. While the concept of weak solutions seems irrelevant and even pathological for many other phenomena, the consistency of the Onsager theory and experiments suggests that the mathematical framework of weak solutions is suitable for describing fluid turbulence.

There remain many interesting open questions concerning the Onsager theory. For example, it is not known whether the constructed dissipative weak Euler solution exhibits intermittency. It seems also interesting research direction to investigate what behavior of fluid motion and microscopic molecular dynamics corresponds to the dissipative weak solutions.

[14] In their construction, it is impossible to construct a weak Euler solution with Hölder regularity $h = 1/3$.

Chapter 3

Quantum turbulence

As emphasized in Chapter 1, cascade transfer of inviscid conserved quantities with universal scaling of turbulent fields is a ubiquitous phenomenon. In this chapter, we focus on such turbulent behavior observed in quantum fluids, such as superfluid helium and atomic Bose-Einstein condensates (BECs) [47–51]. Specifically, we consider *pure quantum turbulence*, where the temperature is sufficiently low so that the viscous normal fluid density is negligible compared to the inviscid superfluid density. Quantum fluids differ significantly from ordinary classical fluids in that vorticity is quantized, as first pointed out by Onsager and Feynman [18, 64]. Despite this difference, many experiments and numerical simulations suggest that at scales larger than the mean intervortex distance ℓ_i, the Richardson cascade with the Kolmogorov spectrum emerges, as in ordinary classical turbulence [129–133]. Because of this similarity, pure quantum turbulence is sometimes referred to as the "prototype" or "skeleton" of turbulence [131, 132, 134].

At scales smaller than ℓ_i, however, a novel energy cascade emerges that has never been observed in classical turbulence. This novel energy cascade is believed to be induced by the interaction of Kelvin waves of different wave numbers on a single quantum vortex and is called *Kelvin-wave cascade*. The nature of the Kelvin-wave cascade has been intensively investigated, and the associated energy spectral exponent is predicted to be, e.g., $-7/5$ [135], $-5/3$ [136], or -1 [137–139]. Because these previous studies are based on the vortex filament model [140], the effects of compressibility on the Kelvin-wave cascade remain to be elucidated [134]. The compressibility effect is particularly important in quantum turbulence in atomic BECs, for which various experimental techniques have been developed in recent years. Note that the superfluid density changes significantly in the vicinity of quantum vortices. Therefore, the compressibility effects can induce a nontrivial impact on the energy cascade, at least for scales smaller than ℓ_i.

In this chapter, we aim to reveal the compressibility effects on the energy cascade in three-dimensional pure quantum turbulence. To this end, we theoretically analyze the Gross-Pitaevskii (GP) equation, which can describe quantum turbulence in atomic BECs, by taking a phenomenological approach based on the Onsager "ideal turbulence" theory. Specifically, we use the fact that the GP equation can be mapped to the *quantum Euler equation* via the Madelung transformation, which has a form similar to that of the ordinary compressible Euler equation. Although the Onsager theory involves sophisticated mathematical concepts such as weak solutions, it also provides a phenomenological perspective on the relation between cascades and the singularity of the velocity field. In particular, we can exploit recent developments that extend the Onsager theory to classical compressible turbulence [90–95].

We show that the compressibility effects can induce a novel energy cascade, which we call *quantum stress cascade*, at scales smaller than ℓ_i. In doing so, we derive the quantum counterpart of Kolmogorov's 4/5-law. We conjecture that the incompressible part of this quantum stress cascade corresponds to the conventional Kelvin-wave cascade.

This chapter is organized as follows. In the next section, we explain the setup and introduce the quantum Euler equations. Its basic properties are described in Section 3.2. In particular, we investigate the local energy balance and the characteristic length scales of this system. In Section 3.3, by coarse-graining turbulent fields, we show that there are three types of scale-to-scale energy fluxes. In Section 3.4, we describe our main results. We derive these results in Section 3.5. Concluding remarks are provided in Section 3.6.

3.1 Setup

We consider a superfluid system of weakly interacting bosons of mass m, confined in a cube $\Omega = [0, L_\Omega]^3$ with periodic boundary conditions. Let $\Psi(\boldsymbol{x}, t)$ be the condensate wave function. The time evolution of $\Psi(\boldsymbol{x}, t)$ is described by the following GP equation:

$$i\hbar \frac{\partial}{\partial t}\Psi(\boldsymbol{x}, t) = \left[-\frac{\hbar^2}{2m}\nabla^2 + V_{\rm ext} + g|\Psi|^2\right]\Psi(\boldsymbol{x}, t). \tag{3.1}$$

Here, $g > 0$ denotes a constant that represents the strength of the interaction between bosons, and $V_{\rm ext}(\boldsymbol{x}, t)$ expresses both the trapping potential and external stirring, e.g., rotation along distinct axes [141]. Note that our analysis can be applied for both decaying and forced turbulence. By applying the Madelung transformation $\Psi = \sqrt{n}\exp(i\theta)$ [142, 143], which relates Ψ to the superfluid mass density $\rho = mn$ and velocity $\boldsymbol{v} = (\hbar/m)\nabla\theta$, the GP equation (3.1) can be mapped to the *quantum Euler equations*:[1]

$$\partial_t \rho + \nabla \cdot (\rho \boldsymbol{v}) = 0, \tag{3.3}$$

$$\partial_t(\rho \boldsymbol{v}) + \nabla \cdot (\rho \boldsymbol{v}\boldsymbol{v} + p\boldsymbol{I} - \boldsymbol{\Sigma}) = \boldsymbol{f}, \tag{3.4}$$

where $p := g\rho^2/(2m^2)$, $\boldsymbol{f}$ denotes the external force due to $V_{\rm ext}$, which acts at large scales $\sim L$, and $\boldsymbol{\Sigma}$ denotes the *quantum stress*, which is also called *quantum pressure*:

$$\boldsymbol{\Sigma} := \frac{\hbar^2}{4m^2}\Delta\rho\boldsymbol{I} - \frac{\hbar^2}{m^2}\nabla\sqrt{\rho}\nabla\sqrt{\rho}, \tag{3.5}$$

[1] Note that the quantum Euler equations can describe the motion of the vortex lines. In other words, the solutions of the quantum Euler equations contain the solutions of the GP equation with quantum vortices as a proper subset [61]. To see this, let $\{\rho_\Psi(\cdot, t), \boldsymbol{v}_\Psi(\cdot, t)\}$ be the superfluid mass density and velocity fields at time t obtained from the condensate's complex wave function $\Psi(\cdot, t)$ that satisfies the GP equation via the Madelung transformation:

$$\Psi(\boldsymbol{x}, t) = \sqrt{\frac{\rho_\Psi(\boldsymbol{x}, t)}{m}}\exp(i\theta(\boldsymbol{x}, t)) \tag{3.2}$$

with $\boldsymbol{v}_\Psi = (\hbar/m)\nabla\theta$, where m denotes the boson mass. Note that $\{\rho_\Psi(\cdot, t), \boldsymbol{v}_\Psi(\cdot, t)\}$ satisfies the following properties: (i) on the nodal lines where superfluid is absent, i.e., $\{\boldsymbol{x}|\rho_\Psi(\boldsymbol{x}, t) = 0\}$, the superfluid velocity $\boldsymbol{v}_\Psi$ is *obviously* not defined, and (ii) for any closed loop C that does not pass through the nodal lines, the circulation $\Gamma_C := \oint_C \boldsymbol{v}_\Psi(\boldsymbol{r}, t) \cdot d\boldsymbol{r}$ is an integer multiple of $2\pi\hbar/m$ because of the single-valuedness of Ψ. Conversely, the single-valued function $\Psi(\cdot, t)$ is uniquely recovered from $\{\rho_\Psi(\cdot, t), \boldsymbol{v}_\Psi(\cdot, t)\}$ up to an overall phase factor because of the quantization condition for Γ_C [144]. Because these properties hold at any time t, there is one-to-one correspondence between Ψ and $\{\rho_\Psi, \boldsymbol{v}_\Psi\}$ up to an overall phase factor. Of course, in general, a function $\tilde{\Psi}$ constructed from the solutions of the quantum Euler equations $\{\rho, \boldsymbol{v}\}$ becomes a multivalued function because $\boldsymbol{v}$ does not necessarily satisfy the quantization condition. Thus, the solutions of the quantum Euler equations contain the solutions of the GP equation as a proper subset [61, 144].

where $\boldsymbol{I}$ is the unit tensor. Note that the quantum Euler equations (3.3) and (3.4) become identical to the ordinary compressible Euler equations if $\boldsymbol{\Sigma} \to 0$, which is achieved in the classical limit $\hbar \to 0$. The important point here is that the quantum stress $\nabla \cdot \boldsymbol{\Sigma}$ becomes relevant in the vicinity of quantum vortices because it contains higher-order spatial derivatives. Note that because the density changes are significant even outside the vortex cores [145–147], we cannot ignore the quantum stress even in that region in general.

3.2 Basic properties

3.2.1 Quantum vortex

One of the most striking properties of quantum fluids is the fact that vorticity is quantized. We first note that the superfluid velocity $\boldsymbol{v}$ is not defined on the nodal lines where superfluid is absent, i.e., $\{\boldsymbol{x}|\rho(\boldsymbol{x},t)=0\}$. For any closed loop C that does not pass through the nodal lines, the circulation $\Gamma_C := \oint_C \boldsymbol{v}(\boldsymbol{r},t)\cdot d\boldsymbol{r}$ is an integer multiple of the quantum circulation $\kappa := 2\pi\hbar/m$ because of the single-valuedness of Ψ:

$$\Gamma_C := \oint_C \boldsymbol{v}(\boldsymbol{r},t)\cdot d\boldsymbol{r} = n\kappa \qquad (n\in\mathbb{Z}). \tag{3.6}$$

3.2.2 Energy balance

The total energy E of this system can be decomposed into three parts, the kinetic energy $\int d^3\boldsymbol{x}\rho|\boldsymbol{v}|^2/2$, interaction energy $\int d^3\boldsymbol{x}p$, and *quantum energy* $\int d^3\boldsymbol{x}\hbar^2|\nabla\sqrt{\rho}|^2/2m^2$ [129, 130]:

$$E = \int_\Omega d^3\boldsymbol{x}\left[\frac{1}{2}\rho|\boldsymbol{v}|^2 + p + \frac{\hbar^2}{2m^2}|\nabla\sqrt{\rho}|^2\right]. \tag{3.7}$$

The local energy balance equation is given by[2]

$$\partial_t\left(\frac{1}{2}\rho|\boldsymbol{v}|^2 + p + \frac{\hbar^2}{2m^2}|\nabla\sqrt{\rho}|^2\right) + \nabla\cdot\left\{\left[\left(\frac{1}{2}\rho|\boldsymbol{v}|^2 + p + \frac{\hbar^2}{2m^2}|\nabla\sqrt{\rho}|^2\right)\boldsymbol{I} + p\boldsymbol{I} - \boldsymbol{\Sigma}\right]\cdot\boldsymbol{v} + \frac{\hbar^2}{4m^2}(\nabla\rho)\nabla\cdot\boldsymbol{v}\right\} = \boldsymbol{v}\cdot\boldsymbol{f}. \tag{3.8}$$

The evolution equation for the kinetic energy density is given by

$$\partial_t\left(\frac{1}{2}\rho|\boldsymbol{v}|^2\right) + \nabla\cdot\left[\left(\frac{1}{2}\rho|\boldsymbol{v}|^2 + p\right)\boldsymbol{v} - \boldsymbol{\Sigma}\cdot\boldsymbol{v}\right] = p\nabla\cdot\boldsymbol{v} - \boldsymbol{\Sigma}:\nabla\boldsymbol{v} + \boldsymbol{v}\cdot\boldsymbol{f}. \tag{3.9}$$

By combining (3.8) and (3.9), we can also derive the evolution equation for the sum of the interaction and quantum energy densities:

$$\partial_t\left(p + \frac{\hbar^2}{2m^2}|\nabla\sqrt{\rho}|^2\right) + \nabla\cdot\left[\left(p + \frac{\hbar^2}{2m^2}|\nabla\sqrt{\rho}|^2\right)\boldsymbol{v} + \frac{\hbar^2}{4m^2}(\nabla\rho)\nabla\cdot\boldsymbol{v}\right] = -p\nabla\cdot\boldsymbol{v} + \boldsymbol{\Sigma}:\nabla\boldsymbol{v}. \tag{3.10}$$

Note that, even with no external force, the total kinetic energy is not conserved because of the effect of the first two terms on the right-hand side of (3.9). The first term (with

[2] We note that the energy current term $\hbar^2(\nabla\rho)\nabla\cdot\boldsymbol{v}/4m^2$ appearing in (3.8) and (3.10) does not exist in ordinary hydrodynamics. This term corresponds to *interstitial working* in the Navier–Stokes–Korteweg equations [148, 149] (see also Chapter 4).

minus sign) $-p\nabla\cdot\boldsymbol{v}$ is known as *pressure-dilatation*, which represents conversion of kinetic energy into interaction or quantum energy and vice versa. From numerical simulations for classical compressible turbulence [150], we conjecture that the pressure-dilatation converts kinetic energy into interaction or quantum energy on average. The existence of the second term $\boldsymbol{\Sigma}:\nabla\boldsymbol{v}$ is specific to quantum turbulence. Because the form of this term is similar to that of pressure-dilatation, we refer to it as *quantum-stress–strain*. It also represents the conversion of kinetic energy into interaction or quantum energy and vice versa.

3.2.3 Characteristic length scales

The existence of quantum vortices leads to several characteristic length scales specific to quantum turbulence. One of the most important length scales is the mean intervortex distance $\ell_i := L_D^{-1/2}$, where L_D denotes the vortex line density, i.e., the total length of vortex lines per unit volume. In terms of the critical velocity for the amplification of the remnant vortices v_c,[3] the mean intervortex distance can be estimated as [152][4]

$$\ell_i \sim \kappa/v_c. \tag{3.11}$$

In addition to the mean intervortex distance, there is another characteristic length scale associated with quantum vortices: the vortex core radius, or *healing length* $\xi \sim \hbar/\sqrt{2mg\rho_0}$, where $\rho_0 := \langle\rho\rangle_\Omega$ denotes the average superfluid mass density. In a typical fully developed quantum turbulence, $\xi \sim 10^{-10}$m in ^{4}He (10^{-8}m in ^{3}He-B), $\ell_i \sim 10^{-5}$m, and $L \sim 10^{-2}$m [50]. Note that these scales are not widely separated in atomic BECs.

We remark that the mean intervortex distance can also be interpreted as the characteristic length scale where the quantum stress $\boldsymbol{\Sigma}$ becomes comparable to the momentum flux $\rho\boldsymbol{v}\boldsymbol{v}$. Indeed, if we use v_c and ρ_0 as the characteristic velocity and density, respectively, and denote by ℓ_c the crossover length scale, we obtain

$$\begin{aligned}
&\rho\boldsymbol{v}\boldsymbol{v} \sim \boldsymbol{\Sigma}\\
&\rho_0 v_c^2 \sim \kappa^2\rho_0/\ell_c^2\\
&\therefore \ell_c \sim \kappa/v_c \sim \ell_i.
\end{aligned} \tag{3.12}$$

This observation implies the possibility of the quantum stress cascade, induced by the quantum stress $\boldsymbol{\Sigma}$, at scales $\ll \ell_i$.

We now introduce other important characteristic length scales by considering the kinetic energy balance (3.9). Recall that there are energy sink or source terms on the right-hand side of (3.9): the pressure-dilatation $-p\nabla\cdot\boldsymbol{v}$ and the quantum-stress–strain $\boldsymbol{\Sigma}:\nabla\boldsymbol{v}$. Recent numerical simulations [150,154] suggest that there is a characteristic length scale ℓ_{large} such that the contribution to the global pressure-dilatation $\langle -p\nabla\cdot\boldsymbol{v}\rangle_\Omega$ from scales $\gg \ell_{\mathrm{large}}$ is dominant, whereas the contribution from scales $\ll \ell_{\mathrm{large}}$ is negligible. The length scale ℓ_{large} is defined, for instance, as follows:

$$\ell_{\mathrm{large}} := \frac{\sum_k k^{-1}E^{(p)}(k)}{\sum_k E^{(p)}(k)}, \tag{3.13}$$

[3] Several experimental studies suggest that $v_c \sim 1$mm/s to 200mm/s [47,49,151]. Note that this critical velocity characterizes the amplification of remnant vortices rather than the intrinsic nucleation of vortices, which is characterized by the Landau critical velocity ~ 50m/s.

[4] In terms of the quantum circulation κ and the effective energy injection rate $\varepsilon_{\mathrm{eff}}$, which will be defined in Section 3.4, the critical velocity may be estimated as $v_c \sim (\kappa\varepsilon_{\mathrm{eff}})^{1/4}$ [153]. Correspondingly, the mean intervortex distance can be estimated as $\ell_i \sim (\kappa^3/\varepsilon_{\mathrm{eff}})^{1/4}$, which is also called the *quantum length scale* [153].

where $E^{(p)}(k)$ denotes the pressure-dilatation co-spectrum:

$$E^{(p)}(k) := -\frac{1}{\Delta k} \sum_{k-\Delta k/2<|\boldsymbol{k}|<k+\Delta k/2} \hat{p}(\boldsymbol{k})\widehat{\nabla\cdot\boldsymbol{v}}(-\boldsymbol{k}) \tag{3.14}$$

with $\Delta k := 2\pi/L_\Omega$. Similarly, because both the quantum stress $\boldsymbol{\Sigma}$ and strain $\nabla\boldsymbol{v}$ change rapidly in space, there may be a characteristic length scale $\ell_{\rm small}$ such that the contribution to the global quantum-stress–strain $\langle -\boldsymbol{\Sigma} : \nabla\boldsymbol{v}\rangle_\Omega$ from scales $\gg \ell_{\rm small}$ is negligible, whereas the contribution from scales $\ll \ell_{\rm small}$ is dominant. We define $\ell_{\rm small}$ as

$$\ell_{\rm small} := \frac{\sum_k k^{-1}E^{(\Sigma)}(k)}{\sum_k E^{(\Sigma)}(k)}, \tag{3.15}$$

where $E^{(\Sigma)}(k)$ denotes the quantum-stress–strain co-spectrum:

$$E^{(\Sigma)}(k) := \frac{1}{\Delta k} \sum_{k-\Delta k/2<|\boldsymbol{k}|<k+\Delta k/2} \hat{\boldsymbol{\Sigma}}(\boldsymbol{k}) : \widehat{\nabla\boldsymbol{v}}(-\boldsymbol{k}). \tag{3.16}$$

In the following, we assume the existence of the intermediate asymptotic limit $\xi \lesssim \ell_{\rm small} \ll \ell \ll \ell_i$ and $\ell_i \ll \ell \ll \ell_{\rm large} \lesssim L$ for fully developed quantum turbulence. The validity of this assumption will be discussed in Section 3.5.

3.3 Scale-to-scale energy fluxes

3.3.1 Coarse-graining

We investigate energy transfer across scales by using coarse-graining procedure introduced in the previous chapter. For any locally integrable function $\boldsymbol{a}(\boldsymbol{x})$, we define a coarse-grained field at length scale $\ell > 0$ as

$$\bar{\boldsymbol{a}}_\ell(\boldsymbol{x}) := \int_\Omega d^3\boldsymbol{r} G_\ell(\boldsymbol{r})\boldsymbol{a}(\boldsymbol{x}+\boldsymbol{r}). \tag{3.17}$$

Here, $G_\ell(\boldsymbol{r}) := \ell^{-3}G(\boldsymbol{r}/\ell)$ is the Friedrichs mollifier, where $G : \Omega \to [0,\infty)$ is a smooth symmetric function supported in the open unit ball with $\int_\Omega G = 1$. In the following, we always assume that $\ell \gg \xi$ because we are interested only in scales $\gg \xi$.

Because the coarse-graining operation commutes with space and time derivatives, coarse-graining of (3.3) and (3.4) gives

$$\partial_t\bar{\rho}_\ell + \nabla\cdot\overline{(\rho\boldsymbol{v})}_\ell = 0, \tag{3.18}$$

$$\partial_t\overline{(\rho\boldsymbol{v})}_\ell + \nabla\cdot\overline{(\rho\boldsymbol{v}\boldsymbol{v})}_\ell = -\nabla\bar{p}_\ell + \nabla\cdot\bar{\boldsymbol{\Sigma}}_\ell + \bar{\boldsymbol{f}}_\ell. \tag{3.19}$$

Note that the coarse-grained equations (3.20) and (3.21) are not closed in terms of large-scale fields $\bar{\rho}_\ell$, $\bar{\boldsymbol{v}}_\ell$, $\bar{p}_\ell$, $\bar{\boldsymbol{\Sigma}}_\ell$, and $\bar{\boldsymbol{f}}_\ell$. This point becomes more explicit by introducing the density-weighted Favre average $\tilde{\boldsymbol{a}}_\ell := \overline{(\rho\boldsymbol{a})}_\ell/\bar{\rho}_\ell$ [155]:

$$\partial_t\bar{\rho}_\ell + \nabla\cdot(\bar{\rho}_\ell\tilde{\boldsymbol{v}}_\ell) = 0, \tag{3.20}$$

$$\bar{\rho}_\ell(\partial_t + \tilde{\boldsymbol{v}}_\ell\cdot\nabla)\tilde{\boldsymbol{v}}_\ell + \nabla\cdot(\bar{\rho}_\ell\tilde{\tau}_\ell(\boldsymbol{v},\boldsymbol{v})) = -\nabla\bar{p}_\ell + \nabla\cdot\bar{\boldsymbol{\Sigma}}_\ell + \bar{\boldsymbol{f}}_\ell, \tag{3.21}$$

where $\tilde{\tau}_\ell(\boldsymbol{v},\boldsymbol{v}) := \widetilde{(\boldsymbol{v}\boldsymbol{v})}_\ell - \tilde{\boldsymbol{v}}_\ell\tilde{\boldsymbol{v}}_\ell$. Note that there appears an additional cumulant term $\nabla\cdot(\bar{\rho}_\ell\tilde{\tau}_\ell(\boldsymbol{v},\boldsymbol{v}))$ on the left-hand side of (3.21). This cumulant term depends on the small-scale ($<\ell$) velocity field and can be regarded as the source of the energy cascade, as described below.

3.3.2 Large-scale energy balance

We derive the large-scale energy balance equation and show that there are three types of scale-to-scale energy fluxes in quantum turbulence. Here, the large-scale kinetic energy density is defined as $\bar{\rho}_\ell|\tilde{\boldsymbol{v}}_\ell|^2/2$ and satisfies the inequality [91]

$$\int_\Omega d^3\boldsymbol{x}\frac{1}{2}\bar{\rho}_\ell|\tilde{\boldsymbol{v}}_\ell|^2 \le \int_\Omega d^3\boldsymbol{x}\frac{1}{2}\rho|\boldsymbol{v}|^2. \tag{3.22}$$

From the coarse-grained equations (3.20) and (3.21), we can obtain the large-scale kinetic energy balance equation,

$$\partial_t\left(\frac{1}{2}\bar{\rho}_\ell|\tilde{\boldsymbol{v}}_\ell|^2\right) + \nabla\cdot\boldsymbol{J}_\ell = \bar{p}_\ell\nabla\cdot\bar{\boldsymbol{v}}_\ell - \bar{\boldsymbol{\Sigma}}_\ell : \nabla\bar{\boldsymbol{v}}_\ell - Q_\ell^{\mathrm{flux}} + \varepsilon_\ell^{\mathrm{in}}. \tag{3.23}$$

Here, $\boldsymbol{J}_\ell$ represents the spatial transport of large-scale kinetic energy, which does not contribute to the transfer of kinetic energy across scales:

$$\boldsymbol{J}_\ell := \left(\frac{1}{2}\bar{\rho}_\ell|\tilde{\boldsymbol{v}}_\ell|^2 + \bar{p}_\ell\right)\tilde{\boldsymbol{v}}_\ell + \bar{\rho}_\ell\tilde{\boldsymbol{v}}_\ell\cdot\tilde{\tau}_\ell(\boldsymbol{v},\boldsymbol{v}) - \frac{\bar{p}_\ell}{\bar{\rho}_\ell}\bar{\tau}_\ell(\rho,\boldsymbol{v}) - \bar{\boldsymbol{\Sigma}}_\ell\cdot\tilde{\boldsymbol{v}}_\ell + \frac{\bar{\boldsymbol{\Sigma}}_\ell}{\bar{\rho}_\ell}\cdot\bar{\tau}_\ell(\rho,\boldsymbol{v}), \tag{3.24}$$

where $\bar{\tau}_\ell(\rho,\boldsymbol{v}) := \overline{(\rho\boldsymbol{v})}_\ell - \bar{\rho}_\ell\bar{\boldsymbol{v}}_\ell$, and $\varepsilon_\ell^{\mathrm{in}}$ denotes the energy injection rate due to external stirring at scale ℓ:

$$\varepsilon_\ell^{\mathrm{in}} := \tilde{\boldsymbol{v}}_\ell\cdot\bar{\boldsymbol{f}}_\ell. \tag{3.25}$$

The first two terms on the right-hand side of (3.23), $-\bar{p}_\ell\nabla\cdot\bar{\boldsymbol{v}}_\ell$ and $\bar{\boldsymbol{\Sigma}}_\ell : \nabla\bar{\boldsymbol{v}}_\ell$, can be interpreted as the large-scale pressure-dilatation and quantum-stress–strain, respectively. Note that these two terms are closed in terms of the large-scale fields $\bar{\boldsymbol{v}}_\ell$, $\bar{p}_\ell$, and $\bar{\boldsymbol{\Sigma}}_\ell$. Therefore, they only contribute to the conversion of the large-scale kinetic energy into interaction and quantum energies, and vice versa.

The third term on the right-hand side of (3.23), Q_ℓ^{flux}, can be decomposed into three parts:

$$Q_\ell^{\mathrm{flux}} = \Pi_\ell + \Lambda_\ell^{(p)} + \Lambda_\ell^{(\Sigma)}. \tag{3.26}$$

The first term Π_ℓ is called *deformation work* [4], which corresponds to the energy flux of the Richardson cascade:

$$\Pi_\ell := -\bar{\rho}_\ell\nabla\tilde{\boldsymbol{v}}_\ell : \tilde{\tau}_\ell(\boldsymbol{v},\boldsymbol{v}). \tag{3.27}$$

The deformation work represents work done by the large-scale strain $\nabla\tilde{\boldsymbol{v}}_\ell$ against the small-scale stress $\bar{\rho}_\ell\tilde{\tau}_\ell(\boldsymbol{v},\boldsymbol{v})$. The second term $\Lambda_\ell^{(p)}$ is called *baropycnal work* [93, 95, 156], which represents work done by the large-scale pressure gradient force $-\nabla\bar{p}_\ell/\bar{\rho}_\ell$ against the small-scale mass flux $\bar{\tau}_\ell(\rho,\boldsymbol{v})$:

$$\Lambda_\ell^{(p)} := \frac{1}{\bar{\rho}_\ell}\nabla\bar{p}_\ell\cdot\bar{\tau}_\ell(\rho,\boldsymbol{v}). \tag{3.28}$$

While the deformation work and the baropycnal work also exist in classical compressible turbulence, the existence of the third term $\Lambda_\ell^{(\Sigma)}$ is specific to quantum turbulence:

$$\Lambda_\ell^{(\Sigma)} := -\frac{1}{\bar{\rho}_\ell}\nabla\cdot\bar{\boldsymbol{\Sigma}}_\ell\cdot\bar{\tau}_\ell(\rho,\boldsymbol{v}). \tag{3.29}$$

Because this term has a form similar to that of the baropycnal work, we call it *quantum baropycnal work*. The quantum baropycnal work represents work done by the large-scale

force $\nabla \cdot \bar{\boldsymbol{\Sigma}}_\ell / \bar{\rho}_\ell$ against the small-scale mass flux $\bar{\tau}_\ell(\rho, \boldsymbol{v})$. Importantly, in the large-scale kinetic energy balance equation (3.23), only these three terms are capable of the direct transfer of kinetic energy across scales because each of the three terms has a form "large-scale ($> \ell$) quantity $\times$ small-scale ($< \ell$) quantity," whereas the other terms on the right-hand side of (3.23) do not.[5] Thus, Q_ℓ^{flux} can be interpreted as the total scale-to-scale kinetic energy flux.

3.4 Main result

The first main result concerns the most fundamental property of the energy cascade: the total scale-to-scale energy flux $\langle Q_\ell^{\mathrm{flux}} \rangle_\Omega$ becomes scale-independent in the "inertial range" $\ell_{\mathrm{small}} \ll \ell \ll \ell_{\mathrm{large}}$:

$$\langle Q_\ell^{\mathrm{flux}} \rangle_\Omega \simeq \varepsilon_{\mathrm{eff}}, \tag{3.30}$$

where $\varepsilon_{\mathrm{eff}} := \langle p \nabla \cdot \boldsymbol{v} \rangle_\Omega + \langle \boldsymbol{v} \cdot \boldsymbol{f} \rangle_\Omega$ denotes the effective energy injection rate, which is scale-independent. We emphasize that, because Q_ℓ^{flux} can be expressed in terms of field increments $\delta \boldsymbol{v}(\boldsymbol{r}; \boldsymbol{x})$ and $\delta \rho(\boldsymbol{r}; \boldsymbol{x})$, the relation (3.30) plays the same role as Kolmogorov's 4/5-law [21].

The second main result is the prediction of the *quantum stress cascade*. Specifically, in the range of $\ell_i \ll \ell \ll \ell_{\mathrm{large}}$, the Richardson cascade, induced by the momentum flux, becomes dominant, whereas in the range of $\ell_{\mathrm{small}} \ll \ell \ll \ell_i$, the quantum stress cascade, induced by quantum stress, develops:

$$\langle \Lambda_\ell^{(\Sigma)} \rangle_\Omega \ll \langle \Pi_\ell \rangle_\Omega \simeq \varepsilon_{\mathrm{eff}} \quad \text{for} \quad \ell_i \ll \ell \ll \ell_{\mathrm{large}}, \tag{3.31}$$

$$\langle \Pi_\ell \rangle_\Omega \ll \langle \Lambda_\ell^{(\Sigma)} \rangle_\Omega \simeq \varepsilon_{\mathrm{eff}} \quad \text{for} \quad \ell_{\mathrm{small}} \ll \ell \ll \ell_i. \tag{3.32}$$

Correspondingly, the velocity power spectrum is estimated to exhibit the power-law $\propto k^{-5/3}$ for $\ell_{\mathrm{large}}^{-1} \ll k \ll \ell_i^{-1}$ and $\propto k^{-3}$ for $\ell_i^{-1} \ll k \ll \ell_{\mathrm{small}}^{-1}$ (see Fig. 3.1).[6]

3.4.1 Interpretation of the result

From the above result, we conjecture the following energy transfer scenario (see also Fig. 3.1):

1. At large scales ($\sim L$), kinetic energy is injected due to external force.
2. In the scale range larger than ℓ_{large}, part of the injected kinetic energy is transferred to smaller scales because of the effect of deformation work, while some part of the kinetic energy is converted into interaction and quantum energies through the pressure-dilatation effect.
3. In the inertial range $\ell_{\mathrm{small}} \ll \ell \ll \ell_{\mathrm{large}}$, the following two-step cascade process emerges:

[5] We note that these three terms are all Galilean invariant. While we can also define, for instance, the deformation work as $\tilde{v}_j \partial_i (\bar{\rho} \tilde{\tau}_\ell(v_i, v_j))$ ($i \in \{1, 2, 3\}$), which differs from (3.27) by the total gradient $\partial_j (\bar{\rho}_\ell \tilde{v}_i \tilde{\tau}_\ell(v_i, v_j))$, this quantity is not Galilean invariant. That is, the amount of energy transferred from large to small scales at point $\boldsymbol{x}$ in the flow would depend on the velocity of the observer. As pointed out by Eyink [157], Galilean invariance is necessary for the scale locality of the energy cascade. Note that non-Galilean-invariant terms in (3.23) do not contribute to the energy transfer across scales.

[6] The k^{-3} scaling at small scales seems to be consistent with experimental observations for grid turbulence in ^{3}He-B [153, 158].

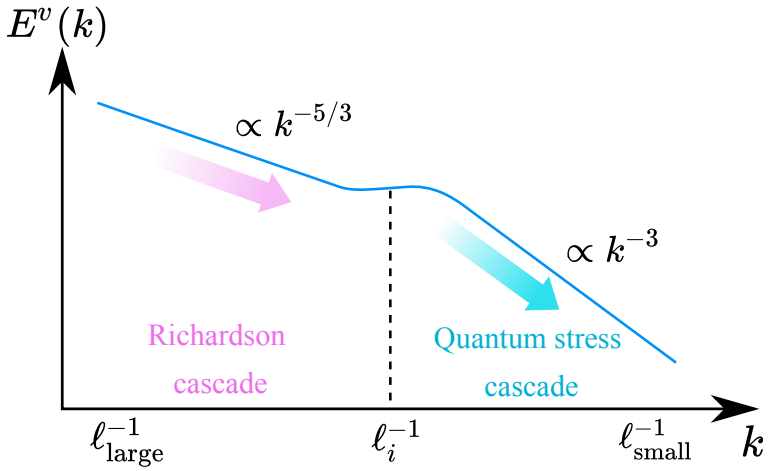

Fig. 3.1: Schematic of the predicted velocity power spectrum $E^v(k)$ in the inertial range $\ell_{\rm large}^{-1} \ll k \ll \ell_{\rm small}^{-1}$.

(a) In the scale range $\ell_i \ll \ell \ll \ell_{\rm large}$, the Richardson cascade, induced by deformation work, becomes dominant. Intuitively, this is because quantum vortices form a tangled structure that effectively behaves like classical eddies.

(b) At scales smaller than the mean intervortex distance ℓ_i, the effect of the quantum stress due to quantum vortices becomes significant. Therefore, the Richardson cascade is no longer dominant, and the quantum stress cascade, induced by quantum baropycnal work, develops.

4. In the scale range smaller than $\ell_{\rm small}$, part of the kinetic energy transferred by the two-step cascade is converted into interaction and quantum energies through the quantum-stress–strain effect, while some part of the kinetic energy is converted into compressible excitations through vortex reconnections and Kelvin-waves [159, 160]. The kinetic energy may also dissipate due to the interaction between the condensate and the excitations [161].[7]

3.4.2 Remark

Here, we remark on several assumptions imposed in deriving the main result. In deriving the second main result, we have assumed that the velocity field satisfies the Besov regularity, introduced in the previous chapter:

$$\|\delta \boldsymbol{v}(\boldsymbol{r};\cdot)\|_p \sim v_{\rm rms}\left(\frac{r}{L}\right)^{\sigma_p} \quad \text{for} \quad r \ll L, \tag{3.33}$$

with the Besov exponent $\sigma_p \in (0,1]$ for $p \in [1,\infty]$. We note that $\|\delta \boldsymbol{v}(\boldsymbol{r};\cdot)\|_p$ is essentially the traditional absolute structure function. According to recent experiments on quantum turbulence [162], the condition (3.33) is expected to hold up to $p = 6$ at least in the scale range $\ell_i \ll \ell \ll \ell_{\rm large}$.

[7] While there is no viscous dissipation in pure quantum turbulence, dissipation of the condensate can be induced by the interaction between the condensate and the excitations [161]. If we add such a dissipation term in the GP equation, which acts at small scales $\lesssim \xi$ at a low temperature, the system can reach a steady state where the mean kinetic energy is constant [131].

In addition, we have imposed the following conditions for the density field:

$$\|\delta\rho(\boldsymbol{r};\cdot)\|_p = O\left(r/L\right) \quad \text{for} \quad r \ll L, \tag{3.34}$$

$$\|1/\bar{\rho}_\ell\|_\infty \leq M \quad \text{for} \quad \ell \gg \xi, \tag{3.35}$$

where M is a ℓ-independent positive constant. The requirements (3.34) are reasonable because the energy density of the system (3.7) contains the density gradient term $\propto |\nabla\rho|^2$. Note that the condition (3.35) is not strong enough to prohibit the existence of the nodal lines $\{\boldsymbol{x} \in \Omega | \rho(\boldsymbol{x}) = 0\}$ where the quantized vortices exists.

3.5 Derivation of the main result

In this section, we derive the main result. First, we investigate the scale dependence of the scale-to-scale energy fluxes. Then, we derive the first and second main results.

3.5.1 Scale dependence of the energy fluxes

Here, we investigate the scale dependence of deformation work, baropycnal work, and quantum baropycnal work, by using arguments similar to those used in the Onsager "ideal turbulence" theory.

Deformation work

We first investigate the scale dependence of the deformation work $\Pi_\ell = -\bar{\rho}_\ell \nabla\tilde{\boldsymbol{v}}_\ell : \tilde{\tau}_\ell(\boldsymbol{v},\boldsymbol{v})$ by expressing it in terms of the increments $\delta\boldsymbol{v}(\boldsymbol{r};\boldsymbol{x})$ and $\delta\rho(\boldsymbol{r};\boldsymbol{x})$. By using the Cauchy-Schwarz and Hölder inequalities, we obtain

$$\begin{aligned}\|\Pi_\ell\|_{p/3} &= \|\bar{\rho}_\ell \nabla\tilde{\boldsymbol{v}}_\ell : \tilde{\tau}_\ell(\boldsymbol{v},\boldsymbol{v})\|_{p/3} \\ &\leq \|\rho\|_\infty \|\nabla\tilde{\boldsymbol{v}}_\ell\|_p \|\tilde{\tau}_\ell(\boldsymbol{v},\boldsymbol{v})\|_{p/2}.\end{aligned} \tag{3.36}$$

First, we investigate the scale dependence of the large-scale strain $\nabla\tilde{\boldsymbol{v}}_\ell$. Because $\tilde{\boldsymbol{v}}_\ell$ can be rewritten as

$$\tilde{\boldsymbol{v}}_\ell = \bar{\boldsymbol{v}}_\ell + \frac{\bar{\tau}_\ell(\rho,\boldsymbol{v})}{\bar{\rho}_\ell}, \tag{3.37}$$

the large-scale strain can be expressed as

$$\nabla\tilde{\boldsymbol{v}}_\ell = \nabla\bar{\boldsymbol{v}}_\ell + \frac{1}{\bar{\rho}_\ell}\nabla\bar{\tau}_\ell(\rho,\boldsymbol{v}) - \frac{\bar{\tau}_\ell(\rho,\boldsymbol{v})}{\bar{\rho}_\ell^2}\nabla\bar{\rho}_\ell. \tag{3.38}$$

Therefore, from the Minkowski inequality, it follows that

$$\|\nabla\tilde{\boldsymbol{v}}_\ell\|_p \leq \|\nabla\bar{\boldsymbol{v}}_\ell\|_p + \left\|\frac{1}{\bar{\rho}_\ell}\nabla\bar{\tau}_\ell(\rho,\boldsymbol{v})\right\|_p + \left\|\frac{\bar{\tau}_\ell(\rho,\boldsymbol{v})}{\bar{\rho}_\ell^2}\nabla\bar{\rho}_\ell\right\|_p. \tag{3.39}$$

Note that for any locally integrable function $\boldsymbol{a}(\boldsymbol{x})$,

$$\nabla\bar{\boldsymbol{a}}_\ell(\boldsymbol{x}) = -\frac{1}{\ell}\int_\Omega d^3\boldsymbol{r}(\nabla G)_\ell(\boldsymbol{r})\delta\boldsymbol{a}(\boldsymbol{r};\boldsymbol{x}), \tag{3.40}$$

because $\int d^3\boldsymbol{r}\nabla G(\boldsymbol{r}) = \boldsymbol{0}$. Hence, we obtain

$$\begin{aligned}\|\nabla\bar{\boldsymbol{a}}_\ell\|_p &= \left\|\frac{1}{\ell}\int_\Omega d^3\boldsymbol{r}(\nabla G)_\ell(\boldsymbol{r})\delta\boldsymbol{a}(\boldsymbol{r};\cdot)\right\|_p \\ &\le \frac{1}{\ell}\int_\Omega d^3\boldsymbol{r}|(\nabla G)_\ell(\boldsymbol{r})|\|\delta\boldsymbol{a}(\boldsymbol{r};\cdot)\|_p \\ &\le \frac{(\text{const})}{\ell}\|\delta\boldsymbol{a}(\ell)\|_p, \end{aligned} \tag{3.41}$$

where $\|\delta\boldsymbol{a}(\ell)\|_p := \sup_{|\boldsymbol{r}|<\ell}\|\delta\boldsymbol{a}(\boldsymbol{r};\cdot)\|_p$, and thus we find that

$$\|\nabla\bar{\boldsymbol{v}}_\ell\|_p = O\left(\frac{\|\delta\boldsymbol{v}(\ell)\|_p}{\ell}\right). \tag{3.42}$$

To evaluate the second and last terms of (3.39), we use the assumption (3.35) and Propositions (3.79) and (3.80) in Appendix 3.7.1. Then, we obtain

$$\begin{aligned}\left\|\frac{1}{\bar{\rho}_\ell}\nabla\bar{\tau}_\ell(\rho,\boldsymbol{v})\right\|_p &\le \frac{(\text{const})}{\ell}\|1/\bar{\rho}_\ell\|_\infty\|\delta\rho(\ell)\|_\infty\|\delta\boldsymbol{v}(\ell)\|_p \\ &\le \frac{(\text{const})}{\ell}M\|\rho\|_\infty\|\delta\boldsymbol{v}(\ell)\|_p, \end{aligned} \tag{3.43}$$

and

$$\begin{aligned}\left\|\frac{\bar{\tau}_\ell(\rho,\boldsymbol{v})}{\bar{\rho}_\ell^2}\nabla\bar{\rho}_\ell\right\|_p &\le M^2\|\nabla\bar{\rho}_\ell\|_\infty\|\bar{\tau}_\ell(\rho,\boldsymbol{v})\|_p \\ &\le \frac{(\text{const})}{\ell}M^2\|\delta\rho(\ell)\|_\infty^2\|\delta\boldsymbol{v}(\ell)\|_p \\ &\le (\text{const})M^2\|\rho\|_\infty^2\frac{\|\delta\boldsymbol{v}(\ell)\|_p}{\ell}. \end{aligned} \tag{3.44}$$

Thus, combining the results (3.42), (3.43), and (3.44), we obtain

$$\begin{aligned}\|\nabla\tilde{\boldsymbol{v}}_\ell\|_p &= \frac{\|\delta\boldsymbol{v}(\ell)\|_p}{\ell}\Big(O(1)+O(M\|\rho\|_\infty)+O(M^2\|\rho\|_\infty^2)\Big) \\ &= O\left(\frac{\|\delta\boldsymbol{v}(\ell)\|_p}{\ell}\right). \end{aligned} \tag{3.45}$$

We now evaluate the scale dependence of the small-scale stress $\tilde{\tau}_\ell(\boldsymbol{v},\boldsymbol{v})$. By using the relation

$$\tilde{\tau}_\ell(\boldsymbol{v},\boldsymbol{v}) = \bar{\tau}_\ell(\boldsymbol{v},\boldsymbol{v}) + \frac{1}{\bar{\rho}_\ell}\bar{\tau}_\ell(\rho,\boldsymbol{v},\boldsymbol{v}) - \frac{1}{\bar{\rho}_\ell^2}\bar{\tau}_\ell(\rho,\boldsymbol{v})\bar{\tau}_\ell(\rho,\boldsymbol{v}) \tag{3.46}$$

and the Minkowski inequality, we obtain

$$\|\tilde{\tau}_\ell(\boldsymbol{v},\boldsymbol{v})\|_{p/2} \le \|\bar{\tau}_\ell(\boldsymbol{v},\boldsymbol{v})\|_{p/2} + \left\|\frac{1}{\bar{\rho}_\ell}\bar{\tau}_\ell(\rho,\boldsymbol{v},\boldsymbol{v})\right\|_{p/2} + \left\|\frac{1}{\bar{\rho}_\ell^2}\bar{\tau}_\ell(\rho,\boldsymbol{v})\bar{\tau}_\ell(\rho,\boldsymbol{v})\right\|_{p/2}. \tag{3.47}$$

Subsequently, by using the assumption (3.35) and Proposition (3.79) in Appendix 3.7.1, one obtains

$$\begin{aligned}\|\tilde{\tau}_\ell(\boldsymbol{v},\boldsymbol{v})\|_{p/2} &= \|\delta\boldsymbol{v}(\ell)\|_p^2\Big(O(1)+O(M\|\rho\|_\infty)+O(M^2\|\rho\|_\infty^2)\Big) \\ &= O\left(\|\delta\boldsymbol{v}(\ell)\|_p^2\right), \quad p\ge 2. \end{aligned} \tag{3.48}$$

By combining (3.36), (3.45), (3.48), and the assumptions (3.33), we finally obtain

$$\begin{aligned}\|\Pi_\ell\|_{p/3} &= \|\bar{\rho}_\ell \nabla \tilde{\boldsymbol{v}}_\ell : \tilde{\tau}_\ell(\boldsymbol{v},\boldsymbol{v})\|_{p/3} \\ &= O\left(\frac{\|\delta \boldsymbol{v}(\ell)\|_p^3}{\ell}\right) \\ &= O\left(\left(\frac{\ell}{L}\right)^{3\sigma_p - 1}\right), \quad p \geq 3, \end{aligned} \tag{3.49}$$

as a rigorous upper bound. This implies that if $\sigma_p > 1/3$ for some $p \geq 3$, then the mean deformation work goes to zero $\langle \Pi_\ell \rangle_\Omega \to 0$, because $|\langle \Pi_\ell \rangle_\Omega| \leq \langle |\Pi_\ell| \rangle_\Omega \leq \|\Pi_\ell\|_{p/3}$ for $p \geq 3$. Note that the upper bound of (3.49) becomes independent of ℓ when $\sigma_p = 1/3$.

Baropycnal work

We next evaluate the scale dependence of the baropycnal work $\Lambda_\ell^{(p)} = (1/\bar{\rho}_\ell)\nabla \bar{p}_\ell \cdot \bar{\tau}_\ell(\rho, \boldsymbol{v})$. By using the assumption (3.35) and Cauchy-Schwarz and Hölder inequalities, we obtain

$$\begin{aligned}\|\Lambda_\ell^{(p)}\|_{p/3} &= \|(1/\bar{\rho}_\ell)\nabla \bar{p}_\ell \cdot \bar{\tau}_\ell(\rho, \boldsymbol{v})\|_{p/3} \\ &\leq M \|\nabla \bar{p}_\ell\|_p \|\bar{\tau}_\ell(\rho, \boldsymbol{v})\|_{p/2}. \end{aligned} \tag{3.50}$$

For $\|\nabla \bar{p}_\ell\|_p$, from the inequality (3.41),

$$\begin{aligned}\|\nabla \bar{p}_\ell\|_p &\leq \frac{(\text{const})}{\ell} \|\delta p(\ell)\|_p \\ &= O\left(\frac{\|\delta \rho(\ell)\|_p}{\ell}\right), \end{aligned} \tag{3.51}$$

where we have used $\|\delta p(\ell)\|_p = O(\|\delta \rho(\ell)\|_p)$, which follows from the definition of $p := g\rho^2/(2m^2)$ and the mean value theorem. For $\|\bar{\tau}_\ell(\rho, \boldsymbol{v})\|_{p/2}$, by using Proposition (3.79) in Appendix 3.7.1, we obtain

$$\|\bar{\tau}_\ell(\rho, \boldsymbol{v})\|_{p/2} = O(\|\delta \rho(\ell)\|_p \|\delta \boldsymbol{v}(\ell)\|_p). \tag{3.52}$$

From the assumptions (3.33) and (3.34), we thus obtain

$$\begin{aligned}\|\Lambda_\ell^{(p)}\|_{p/3} &= \|(1/\bar{\rho}_\ell)\nabla \bar{p}_\ell \cdot \bar{\tau}_\ell(\rho, \boldsymbol{v})\|_{p/3} \\ &= O\left(\frac{1}{\ell}\|\delta \rho(\ell)\|_p \|\delta \rho(\ell)\|_p \|\delta \boldsymbol{v}(\ell)\|_p\right) \\ &= O\left(\left(\frac{\ell}{L}\right)^{\sigma_p + 1}\right), \quad p \geq 3. \end{aligned} \tag{3.53}$$

This result implies that the mean baropycnal work goes to zero $\langle \Lambda_\ell^{(p)} \rangle_\Omega \to 0$ as $\ell/L \to 0$. Therefore, baropycnal work does not contribute to the energy transfer across scales.[8]

[8] In classical compressible turbulence, the baropycnal work can contribute to energy transfer [93,95,156]. If the assumption (3.34) is violated, the baropycnal work can induce energy transfer across scales even in quantum turbulence, at least in the large scale $\ell_i \ll \ell \ll \ell_{\text{large}}$.

Quantum baropycnal work

Now, we investigate the scale dependence of the quantum baropycnal work $\Lambda_\ell^{(\Sigma)} = -(1/\bar{\rho}_\ell)\nabla\cdot\bar{\boldsymbol{\Sigma}}_\ell\cdot\bar{\tau}_\ell(\rho,\boldsymbol{v})$. From the assumption (3.35) and the Cauchy-Schwarz and Hölder inequalities, we obtain

$$\begin{aligned}\|\Lambda_\ell^{(\Sigma)}\|_{p/3} &= \big\|(1/\bar{\rho}_\ell)\nabla\cdot\bar{\boldsymbol{\Sigma}}_\ell\cdot\bar{\tau}_\ell(\rho,\boldsymbol{v})\big\|_{p/3}\\ &\le M\|\nabla\cdot\bar{\boldsymbol{\Sigma}}_\ell\|_p\|\bar{\tau}_\ell(\rho,\boldsymbol{v})\|_{p/2}.\end{aligned}\tag{3.54}$$

For $\|\nabla\cdot\bar{\boldsymbol{\Sigma}}_\ell\|_p$, by using the Minkowski inequality and the inequality (3.41), one obtains

$$\begin{aligned}\|\nabla\cdot\bar{\boldsymbol{\Sigma}}_\ell\|_p &\le \left\|\frac{\hbar^2}{4m^2}\nabla\Delta\bar{\rho}_\ell\right\|_p + \left\|\frac{\hbar^2}{m^2}\nabla\cdot\overline{(\nabla\sqrt{\rho}\nabla\sqrt{\rho})}_\ell\right\|_p\\ &\le \frac{(\text{const})}{\ell^3}\|\delta\rho(\ell)\|_p + \frac{(\text{const})}{\ell}\|\nabla\rho\|_\infty^2.\end{aligned}\tag{3.55}$$

Here, we have implicitly assumed that $\|\nabla\rho\|_\infty < \infty$, which is reasonable by considering the fact that the energy density of the system includes the gradient term $\propto|\nabla\rho|^2$. From (3.52), (3.54), (3.55), and the assumptions (3.33), (3.34), and (3.35), we thus obtain

$$\begin{aligned}\|\Lambda_\ell^{(\Sigma)}\|_{p/3} &= \big\|(1/\bar{\rho}_\ell)\nabla\cdot\bar{\boldsymbol{\Sigma}}_\ell\cdot\bar{\tau}_\ell(\rho,\boldsymbol{v})\big\|_{p/3}\\ &= O\left(\frac{1}{\ell^3}\|\delta\rho(\ell)\|_p^2\|\delta\boldsymbol{v}(\ell)\|_p\right) + O\left(\frac{1}{\ell}\|\delta\rho(\ell)\|_p\|\delta\boldsymbol{v}(\ell)\|_p\right)\\ &= O\left(\left(\frac{\ell}{L}\right)^{\sigma_p-1}\right) + O\left(\left(\frac{\ell}{L}\right)^{\sigma_p}\right)\\ &= O\left(\left(\frac{\ell}{L}\right)^{\sigma_p-1}\right), \quad p\ge 3.\end{aligned}\tag{3.56}$$

Note that, for any $\sigma_p\in(0,1]$, we cannot conclude that the quantum baropycnal work goes to zero as $\ell/L\to 0$. In other words, unlike deformation work, quantum baropycnal work can contribute to the transfer of kinetic energy across scales regardless of the regularity of the velocity field. The scale-independent upper bound is obtained when $\sigma_p = 1$.

3.5.2 Derivation of the first main result

We derive the first main result in the steady state regime for simplicity, although it is valid even in freely decaying turbulence. In the steady state, spatial averaging of (3.23) reads

$$\langle Q_\ell^{\text{flux}}\rangle_\Omega = \langle\bar{p}_\ell\nabla\cdot\bar{\boldsymbol{v}}_\ell\rangle_\Omega - \langle\bar{\boldsymbol{\Sigma}}_\ell : \nabla\bar{\boldsymbol{v}}_\ell\rangle_\Omega + \langle\varepsilon_\ell^{\text{in}}\rangle_\Omega.\tag{3.57}$$

As mentioned in Section 3.2.3, the pressure-dilatation is assumed to be significant at large scales $\gg\ell_{\text{large}}$. That is, the large-scale pressure-dilatation can be approximated as $-\langle\bar{p}_\ell\nabla\cdot\bar{\boldsymbol{v}}_\ell\rangle_\Omega \simeq -\langle p\nabla\cdot\boldsymbol{v}\rangle_\Omega$ for $\ell\ll\ell_{\text{large}}$. Similarly, because the contribution to $\langle\boldsymbol{\Sigma} : \nabla\boldsymbol{v}\rangle_\Omega$ from large scales $\gg\ell_{\text{small}}$ is assumed to be negligible, the large-scale quantum-stress–strain becomes $\langle\bar{\boldsymbol{\Sigma}}_\ell : \nabla\bar{\boldsymbol{v}}_\ell\rangle_\Omega \simeq 0$ for $\ell\gg\ell_{\text{small}}$. Finally, because the external force $\boldsymbol{f}$ acts at large scales $\sim L$, the coarse-grained energy injection can be approximated as $\langle\varepsilon_\ell^{\text{in}}\rangle_\Omega := \langle\tilde{\boldsymbol{v}}_\ell\cdot\bar{\boldsymbol{f}}_\ell\rangle_\Omega \simeq \langle\boldsymbol{v}\cdot\boldsymbol{f}\rangle_\Omega$ for $\ell\ll L$ [10, 95]. Thus, we conclude that

$$\langle Q_\ell^{\text{flux}}\rangle_\Omega \simeq \langle p\nabla\cdot\boldsymbol{v}\rangle_\Omega + \langle\boldsymbol{v}\cdot\boldsymbol{f}\rangle_\Omega =: \varepsilon_{\text{eff}},\tag{3.58}$$

in the "inertial range" $\ell_{\rm small} \ll \ell \ll \ell_{\rm large}$.

Here, we remark on the existence of the intermediate scale range $\ell_{\rm small} \ll \ell \ll \ell_{\rm large}$. In the above derivation, we have assumed that $-\langle \bar{p}_\ell \nabla \cdot \bar{\boldsymbol{v}}_\ell \rangle_\Omega \simeq -\langle p \nabla \cdot \boldsymbol{v} \rangle_\Omega$ for $\ell \ll \ell_{\rm large}$. In other words, we have assumed that the pressure-dilatation co-spectrum satisfies $E^{(p)}(k) = O(k^{-\alpha})$ with $\alpha > 1$, as in classical compressible turbulence [93, 94, 150, 154]. This assumption is based on the decorrelation effects between the large-scale pressure $\bar{p}_\ell$, which mainly acts at large scales, and $\nabla \cdot \bar{\boldsymbol{v}}_\ell$, which becomes significant at small scales as $\|\nabla \cdot \bar{\boldsymbol{v}}_\ell\|_p = O(\|\delta \boldsymbol{v}(\ell)\|_p/\ell)$ [93, 94]. For the large-scale quantum-stress–strain, on the other hand, such decorrelation effects are not expected because both $\bar{\boldsymbol{\Sigma}}_\ell$ and $\nabla \bar{\boldsymbol{v}}_\ell$ change rapidly in space. By combining the similar argument as in (3.55) and (3.42), its scale-dependence can be evaluated as follows:

$$\begin{aligned} \|\bar{\boldsymbol{\Sigma}}_\ell : \nabla \bar{\boldsymbol{v}}_\ell\|_{p/2} &\le \|\bar{\boldsymbol{\Sigma}}_\ell\|_p \|\nabla \bar{\boldsymbol{v}}_\ell\|_p \\ &= O\left(\left(\frac{\ell}{L} \right)^{\sigma_p - 2} \right), \quad p \ge 2. \end{aligned} \tag{3.59}$$

Thus, there possibly exists a characteristic length scale $\ell_{\rm small} \ll \ell_{\rm large}$ such that $\langle \bar{\boldsymbol{\Sigma}}_\ell : \nabla \bar{\boldsymbol{v}}_\ell \rangle_\Omega \simeq 0$ for $\ell \gg \ell_{\rm small}$.

3.5.3 Derivation of the second main result

We first note that the contribution to the energy transfer from the baropycnal work $\Lambda_\ell^{(p)}$ can be ignored because it converges to zero as $\ell/L \to 0$, as shown in (3.53). Therefore, the first main result (3.58) can be further approximated as

$$\langle \Pi_\ell \rangle_\Omega + \langle \Lambda_\ell^{(\Sigma)} \rangle_\Omega \simeq \varepsilon_{\rm eff}. \tag{3.60}$$

From (3.49) and (3.56), it immediately follows that the upper bounds of the mean deformation work $\langle \Pi_\ell \rangle_\Omega$ and mean quantum baropycnal work $\langle \Lambda_\ell^{(\Sigma)} \rangle_\Omega$ have different ℓ dependences. In particular, the upper bound of $\langle \Pi_\ell \rangle_\Omega$ becomes scale independent when $\sigma_3 = 1/3$, whereas that of $\langle \Lambda_\ell^{(\Sigma)} \rangle_\Omega$ behaves as $O(\ell^{-2/3})$:

$$\langle \Pi_\ell \rangle_\Omega \le \|\Pi_\ell\|_1 = O(1), \tag{3.61}$$

$$\langle \Lambda_\ell^{(\Sigma)} \rangle_\Omega \le \|\Lambda_\ell^{(\Sigma)}\|_1 = O\left(\left(\frac{\ell}{L} \right)^{-2/3} \right), \tag{3.62}$$

When $\sigma_3 = 1$, on the other hand, the upper bound of $\langle \Lambda_\ell^{(\Sigma)} \rangle_\Omega$ becomes constant, whereas that of $\langle \Pi_\ell \rangle_\Omega$ behaves as $O(\ell^2)$:

$$\langle \Pi_\ell \rangle_\Omega \le \|\Pi_\ell\|_1 = O\left(\left(\frac{\ell}{L} \right)^{2} \right), \tag{3.63}$$

$$\langle \Lambda_\ell^{(\Sigma)} \rangle_\Omega \le \|\Lambda_\ell^{(\Sigma)}\|_1 = O(1). \tag{3.64}$$

The above observation and the first main result implies that there exists a characteristic length scale λ such that deformation work is dominant in $\lambda \ll \ell \ll \ell_{\rm large}$, while quantum baropycnal work becomes dominant in $\ell_{\rm small} \ll \ell \ll \lambda$ (see Fig. 3.2):

$$\langle \Lambda_\ell^{(\Sigma)} \rangle_\Omega \ll \langle \Pi_\ell \rangle_\Omega = O(1) \quad \text{for} \quad \lambda \ll \ell \ll \ell_{\rm large}, \tag{3.65}$$

$$\langle \Pi_\ell \rangle_\Omega \ll \langle \Lambda_\ell^{(\Sigma)} \rangle_\Omega = O(1) \quad \text{for} \quad \ell_{\rm small} \ll \ell \ll \lambda. \tag{3.66}$$

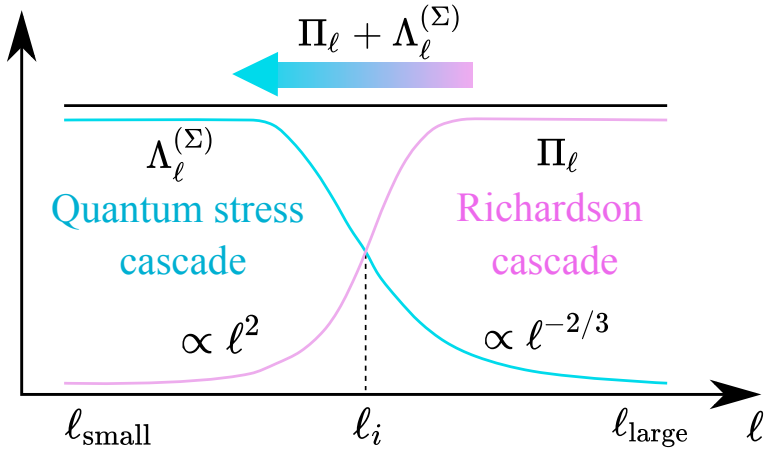

Fig. 3.2: Scale dependence of the scale-to-scale kinetic energy fluxes. The solid lines indicate the upper bounds of the energy fluxes, and the arrow indicates the direction of energy transfer.

The crossover scale λ can be estimated, for instance, as follows. If we use the critical velocity v_c and the average mass density $\rho_0 = \langle\rho\rangle_\Omega$ as the characteristic velocity and density, the deformation work (3.27) and quantum baropycnal work (3.29) can be evaluated as

$$\Lambda_\ell^{(\Sigma)} \sim \kappa^2 \ell^{-3} \rho_0 v_c \tag{3.67}$$

with the quantum circulation $\kappa = h/m$, and

$$\Pi_\ell \sim \rho_0 \ell^{-1} v_c^3. \tag{3.68}$$

Then, the balance condition $\Pi_\lambda \sim \Lambda_\lambda^{(\Sigma)}$ leads to $\lambda \sim \kappa/v_c \sim \ell_i$. Thus, in the range of $\ell_i \ll \ell \ll \ell_{\rm large}$, the Richardson cascade, induced by the deformation work, becomes dominant, whereas in the range of $\ell_{\rm small} \ll \ell \ll \ell_i$, the quantum stress cascade, induced by quantum baropycnal work, develops.

We now consider the pth-order (absolute) structure function for the velocity field:

$$S_p^v(\ell) := \langle |\delta \boldsymbol{v}(\ell)|^p \rangle_\Omega = \|\delta \boldsymbol{v}(\ell)\|_p^p \tag{3.69}$$

with assumed scaling exponent ζ_p:

$$S_p^v(\ell) \sim C_p v_{\rm rms}^p \left(\frac{\ell}{L}\right)^{\zeta_p} \quad \text{for} \quad \ell \ll L, \tag{3.70}$$

where C_p is a dimensionless constant. Using the Hölder inequality, it can be shown that ζ_p is a concave function of $p \in [0, \infty)$ [5, 10]. From this property, it immediately follows that $\sigma_p = \zeta_p/p$ is a non-increasing function of p [10]. Note that the second-order structure function $S_2^v(\ell) \propto \ell^{\zeta_2}$ is related to the velocity spectrum $E^v(k) \propto k^{-\zeta_2 - 1}$.

Because $\sigma_3 = 1/3$ in $\ell_i \ll \ell \ll \ell_{\rm large}$ and σ_p is a non-increasing function of p, it follows that $\sigma_2 \geq 1/3$ in this scale range. Hence, we can write $\zeta_2 = 2\sigma_2 \equiv 2/3 + \mu/9$, where μ is a positive constant. This additional constant μ formally corresponds to the so-called *intermittency exponent* [5]. Therefore, the velocity power spectrum exhibits the following asymptotic behavior:

$$E^v(k) \sim C_{\rm large} k^{-5/3-\mu/9} \quad \text{for} \quad \ell_{\rm large}^{-1} \ll k \ll \ell_i^{-1}, \tag{3.71}$$

where C_{large} is a positive constant.

In $\ell_{\mathrm{small}} \ll \ell \ll \ell_i$, where the quantum stress cascade becomes dominant, we have found that $\sigma_3 = 1$. Because σ_p is a non-increasing function of p, it follows that $\sigma_2 = 1$. This result implies that the velocity power spectrum exhibits the following asymptotic behavior:

$$E^v(k) \sim C_{\mathrm{small}} k^{-3} \quad \text{for} \quad \ell_i^{-1} \ll k \ll \ell_{\mathrm{small}}^{-1}, \tag{3.72}$$

where C_{small} is a positive constant.

3.6 Concluding remarks

In this chapter, we have investigated the compressibility effects on energy transfer across scales in three-dimensional pure quantum turbulence described by the GP equation. We first derived the quantum counterpart of Kolmogorov's 4/5-law. Then, we have shown that a novel energy cascade, which we call quantum stress cascade, emerges due to the quantum stress at scales $\ll \ell_i$ by using a phenomenological argument based on the Onsager "ideal turbulence" theory. Below, we provide some remarks on our results.

Kelvin-wave cascade and quantum stress cascade

We first consider the relation between the Kelvin-wave cascade and the quantum stress cascade. If the Kelvin-wave cascade exists, there must be the corresponding scale-to-scale energy flux other than the deformation work Π_ℓ. In the large-scale kinetic energy balance equation (3.23), such energy flux specific to the quantum case is only the quantum baropycnal work $\Lambda_\ell^{(\Sigma)}$, which induces the quantum stress cascade. From this observation, we conjecture that the incompressible part of the quantum baropycnal work $\Lambda_\ell^{(\Sigma)}$ corresponds to the energy flux of the Kelvin-wave cascade.

Scale locality of energy cascade

Scale locality is one of the most crucial aspects of the energy cascade because it is considered to underlie universality in the inertial range. An energy cascade is scale-local if only modes near a given scale mainly contribute to the energy transfer at that scale. While we can show that the Richardson cascade in quantum turbulence is scale local, the quantum stress cascade is only *ultraviolet local* and does not satisfy the sufficient condition to be *infrared local* (see Appendix 3.7.2). Thus, the contributions of large-scale velocity increments could be non-negligible and could contribute to quantum baropycnal work. Note that this situation is similar to the enstrophy cascade in two-dimensional incompressible turbulence [157, 163, 164].

Optimality of the upper bound on quantum baropycnal work

We note that k^{-3} spectrum for the quantum stress cascade can become shallower due to *depletion of nonlinearity* [5]. The depletion of nonlinearity is a phenomenon that the nonlinear effect is "reduced" because of cancellations due to wave oscillations [96] or *dynamical alignment* [165, 166]. In our case, Kelvin-wave oscillations could lead to cancellations in the quantum baropycnal work, making the upper bound (3.56) no longer optimal.

We can also obtain a tighter bound on the quantum baropycnal work by further assuming the Besov regularity of the density gradient field $\nabla\rho$:

$$\|\delta(\nabla\rho)(\boldsymbol{r};\cdot)\|_p = O((r/L)^{\sigma_p^{\nabla\rho}}) \quad \text{for} \quad r \ll L, \tag{3.73}$$

with $\sigma_p^{\nabla\rho} \in (0,1]$. In this case, the upper bound of the quantum baropycnal work can be evaluated as

$$\|\Lambda_\ell^{(\Sigma)}\|_{p/3} = O\left(\left(\frac{\ell}{L}\right)^{\sigma_p+\sigma_p^{\nabla\rho}-1}\right), \quad p \geq 3, \tag{3.74}$$

and the velocity power spectrum can be estimated as $E^v(k) \propto k^{-3+2\sigma_2^{\nabla\rho}}$ for $\ell_i^{-1} \ll k \ll \ell_{\rm small}^{-1}$. Thus, the spectral exponent associated with the quantum stress cascade possibly depends on the scaling exponent for the density field.

Besov regularity of the velocity field

Although the Besov regularity for the velocity field is expected to hold up to $p = 6$ at least in the scale range $\ell_i \ll \ell \ll \ell_{\rm large}$ according to recent experiments [162], the validity is still not verified at small scales $\ell_{\rm small} \ll \ell \ll \ell_i$. To avoid this subtle problem, we can instead use the density-weighted velocity $\boldsymbol{w} := \sqrt{\rho}\boldsymbol{v}$. Specifically, we assume the Besov regularity of the density-weighted velocity $\boldsymbol{w}$:

$$\|\delta\boldsymbol{w}(\boldsymbol{r};\cdot)\|_p \sim w_{\rm rms}\left(\frac{r}{L}\right)^{\sigma_p} \quad \text{for} \quad r \ll L \tag{3.75}$$

with the Besov exponent $\sigma_p \in (0,1]$ for $p \in [1,\infty]$. Note that the validity of this condition is partially verified in several numerical simulations [145, 167–169]. Even for this case, we can predict the two-step cascade scenario, where the quantum stress cascade follows the Richardson cascade, as shown in Appendix 3.7.3.

3.7 Appendix

3.7.1 Cumulant estimation

In this section, we present some useful results concerning the cumulant estimation obtained by Drivas and Eyink [92]. We consider coarse-graining of functions $f_i \in L^\infty(\Omega), i = 1,2,3,\cdots$. Because $L^\infty(\Omega) \subset L^p(\Omega)$ for $p \geq 1$, $f_i \in L^p(\Omega)$.

Coarse-graining cumulants $\{\bar{\tau}_\ell(f_1,f_2,\cdots,f_n)\}_n$ are defined iteratively in n by $\bar{\tau}_\ell(f) := \bar{f}_\ell$ and

$$\overline{(f_1 f_2 \cdots f_n)}_\ell = \sum_P \prod_{p=1}^{|P|} \bar{\tau}_\ell\left(f_{i_1^{(p)}},\cdots,f_{i_{n_p}^{(p)}}\right), \tag{3.76}$$

where the sum is over all the partitions P of the set $\{1,2,\cdots,n\}$ into $|P|$ disjoint subsets $\{i_1^{(p)},\cdots,i_{n_p}^{(p)}\}$, $p = 1,\cdots,|P|$. For example, when $n = 2$,

$$\overline{(fg)}_\ell = \bar{f}_\ell\bar{g}_\ell + \bar{\tau}_\ell(f,g). \tag{3.77}$$

Lemma 1 of [92]

For $n > 1$, the coarse-graining cumulants are related to the cumulants of increment $\delta f(\boldsymbol{r};\boldsymbol{x}) := f(\boldsymbol{x}+\boldsymbol{r}) - f(\boldsymbol{x})$ as follows:

$$\bar{\tau}_\ell(f_1, f_2, \cdots, f_n) = \langle \delta f_1, \cdots, \delta f_n \rangle_\ell^c, \tag{3.78}$$

where $\langle\cdot\rangle_\ell$ denotes the average over displacement vector $\boldsymbol{r}$ with density $G_\ell(\boldsymbol{r})$ and superscript c indicates the cumulant with respect to this average.

From the above lemma, the propositions below immediately follow:

Proposition 3 of [92] (Cumulant estimates)

For $p \in [1, \infty]$ and $n > 1$,

$$\|\bar{\tau}_\ell(f_1, f_2, \cdots, f_n)\|_p = O\left(\prod_{i=1}^n \|\delta f_i(\ell)\|_{p_i}\right) \quad \text{with} \quad \frac{1}{p} = \sum_{i=1}^n \frac{1}{p_i}, \tag{3.79}$$

where $\|\delta f(\ell)\|_p := \sup_{|\boldsymbol{r}|<\ell} \|\delta f(\boldsymbol{r};\cdot)\|_p$.

Proposition 4 of [92] (Cumulant-derivative estimates)

For $n > 1$ and $\partial_k = \partial/\partial x_k$, $k = 1, 2, \cdots, d$,

$$\|\partial_{k_1} \cdots \partial_{k_m} \bar{\tau}_\ell(f_1, f_2, \cdots, f_n)\|_p = O\left(\ell^{-m} \prod_{i=1}^n \|\delta f_i(\ell)\|_{p_i}\right) \quad \text{with} \quad \frac{1}{p} = \sum_{i=1}^n \frac{1}{p_i}. \tag{3.80}$$

3.7.2 Scale locality of quantum baropycnal work

In proving the scale locality of the quantum baropycnal work $\Lambda_\ell^{(\Sigma)} = -(1/\bar{\rho}_\ell)\nabla\cdot\bar{\boldsymbol{\Sigma}}_\ell\cdot\bar{\tau}_\ell(\rho, \boldsymbol{v})$, it is not necessary to consider $\nabla\sqrt{\rho}\nabla\sqrt{\rho}$ in the quantum stress because its contribution to the energy flux vanishes as $\ell/L \to 0$ (see Section 3.5.1). Therefore, it is sufficient to prove the scale locality of

$$Z_\ell(\rho, \rho, \rho, \boldsymbol{v}) := -(\hbar^2/4m^2\bar{\rho}_\ell)\nabla\Delta\bar{\rho}_\ell \cdot \bar{\tau}_\ell(\rho, \boldsymbol{v}), \tag{3.81}$$

where the first density argument corresponds to the factor $1/\bar{\rho}_\ell$, and the second to the factor $\nabla\Delta\bar{\rho}_\ell$. Following Eyink [157], we describe the energy flux $Z_\ell(\rho, \rho, \rho, \boldsymbol{v})$ as *ultraviolet local* if $\langle Z_\ell(\rho'_\delta, \rho'_\delta, \rho'_\delta, \boldsymbol{v}'_\delta)\rangle_\Omega$ decays as fast as $(\delta/\ell)^\alpha$, for $\alpha > 0$, whenever $\delta \ll \ell$. Here, $\boldsymbol{a}'_\ell$ denotes a small-scale field defined by

$$\boldsymbol{a}'_\ell(\boldsymbol{x}) := \boldsymbol{a}(\boldsymbol{x}) - \bar{\boldsymbol{a}}_\ell(\boldsymbol{x}). \tag{3.82}$$

Similarly, we describe the energy flux $Z_\ell(\rho, \rho, \rho, \boldsymbol{v})$ as *infrared local* if $\langle Z_\ell(\rho, \rho, \rho, \bar{\boldsymbol{v}}_\Delta)\rangle_\Omega$ decays as fast as $(\Delta/\ell)^{-\alpha}$, for $\alpha > 0$, whenever $\Delta \gg \ell$. As observed by Aluie [93, 94], in defining the infrared locality of the energy flux, the condition of negligible contribution of the large-scale density field to the flux is not necessary.

Ultraviolet locality

It is obvious that $1/\bar{\rho}_\ell$ has a vanishing contribution from small scales $\delta \ll \ell$ because its Fourier amplitudes decay faster than any power n of wavenumber k^{-n} as $k \to \infty$ as a direct consequence of the Riemann-Lebesgue lemma. For the remaining three arguments, using the assumptions (3.33), (3.34), and (3.35) and the Hölder inequality, we obtain

$$\begin{aligned}
\|Z_\ell(\rho, \rho'_\delta, \rho'_\delta, \boldsymbol{v}'_\delta)\|_{p/3} &= \left\|(\hbar^2/4m^2\bar{\rho}_\ell)\nabla\Delta\overline{(\rho'_\delta)}_\ell \cdot \bar{\tau}_\ell(\rho'_\delta, \boldsymbol{v}'_\delta)\right\|_{p/3} \\
&\le (\text{const})\left(\frac{1}{\ell^3}\int_\Omega d^3\boldsymbol{r}|(\nabla\Delta G)_\ell(\boldsymbol{r})|\|\rho'_\delta\|_p\right)\|\bar{\tau}_\ell(\rho'_\delta, \boldsymbol{v}'_\delta)\|_{p/2} \\
&\le (\text{const})\frac{1}{\ell^3}\|\rho'_\delta\|_p\|\rho'_\delta\|_p\|\boldsymbol{v}'_\delta\|_p \\
&= O\left(\left(\frac{\delta}{\ell}\right)^{\sigma_p+2}\right), \quad p \ge 3.
\end{aligned} \tag{3.83}$$

Here, we have used the fact that

$$\begin{aligned}
\|\boldsymbol{a}'_\delta\|_p &\le \int_\Omega d^3\boldsymbol{r}G_\delta(\boldsymbol{r})\|\delta\boldsymbol{a}(\boldsymbol{r};\cdot)\|_p \\
&\le \|\delta\boldsymbol{a}(\delta)\|_p.
\end{aligned} \tag{3.84}$$

Therefore, Z_ℓ is ultraviolet local.

Infrared locality

Using the assumptions (3.33), (3.34), and (3.35) and the Hölder inequality, we obtain

$$\begin{aligned}
\|Z_\ell(\rho, \rho, \rho, \bar{\boldsymbol{v}}_\Delta)\|_{p/3} &= \left\|(\hbar^2/4m^2\bar{\rho}_\ell)\nabla\Delta\bar{\rho}_\ell \cdot \bar{\tau}_\ell(\rho, \bar{\boldsymbol{v}}_\Delta))\right\|_{p/3} \\
&\le (\text{const})\frac{1}{\ell^3}\|\delta\rho(\ell)\|_p\|\delta\rho(\ell)\|_p\|\delta\bar{\boldsymbol{v}}_\Delta(\ell)\|_p \\
&= O\left(\left(\frac{\Delta}{\ell}\right)^{\sigma_p-1}\right), \quad p \ge 3.
\end{aligned} \tag{3.85}$$

Here, we have used the following evaluation [157]:

$$\begin{aligned}
\|\delta\bar{\boldsymbol{v}}_\Delta(\ell)\|_p &\le \sup_{|\boldsymbol{\rho}|<\ell}\left\|\int_\Omega d^3\boldsymbol{r}G_\Delta(\boldsymbol{r})\left(\boldsymbol{v}(\boldsymbol{x}+\boldsymbol{\rho}+\boldsymbol{r}) - \boldsymbol{v}(\boldsymbol{x}+\boldsymbol{r})\right)\right\|_p \\
&= \sup_{|\boldsymbol{\rho}|<\ell}\left\|\int_\Omega d^3\boldsymbol{r}\left(G_\Delta(\boldsymbol{r}-\boldsymbol{\rho}) - G_\Delta(\boldsymbol{r})\right)\boldsymbol{v}(\boldsymbol{x}+\boldsymbol{r})\right\|_p \\
&= \sup_{|\boldsymbol{\rho}|<\ell}\left\|\frac{1}{\Delta}\int_0^1 d\theta\int_\Omega d^3\boldsymbol{r}\boldsymbol{\rho}\cdot(\nabla G)_\Delta(\boldsymbol{r}-\theta\boldsymbol{\rho})\delta\boldsymbol{v}(\boldsymbol{r};\boldsymbol{x})\right\|_p \\
&\le \frac{\ell}{\Delta}\int_0^1 d\theta\int_\Omega d^3\boldsymbol{r}|(\nabla G)_\Delta(\boldsymbol{r})|\|\delta\boldsymbol{v}(\Delta)\|_p \\
&= O\left(\left(\frac{\Delta}{\ell}\right)^{\sigma_p-1}\right).
\end{aligned} \tag{3.86}$$

Therefore, in the scale range $\ell_{\rm small} \ll \ell \ll \Delta \ll \ell_i$,

$$\begin{aligned}\langle Z_\ell(\rho,\rho,\rho,\bar{\boldsymbol{v}}_\Delta)\rangle_\Omega &\le \|Z_\ell(\rho,\rho,\rho,\bar{\boldsymbol{v}}_\Delta)\|_1 \\ &= O(1) \quad \text{for} \quad \ell \ll \Delta,\end{aligned} \tag{3.87}$$

because $\sigma_3 = 1$ in this range. Thus, Z_ℓ does not satisfy the sufficient condition to be infrared local.

3.7.3 More sophisticated analysis using the density-weighted velocity

Here, we provide the details of the more sophisticated analysis using the density-weighted velocity. Let $\boldsymbol{w} := \sqrt{\rho}\boldsymbol{v}$ be the density-weighted velocity. The quantum Euler equations can be rewritten in terms of this quantity as

$$\partial_t \rho + \nabla\cdot(\sqrt{\rho}\boldsymbol{w}) = 0, \tag{3.88}$$

$$\partial_t(\sqrt{\rho}\boldsymbol{w}) + \nabla\cdot(\boldsymbol{w}\boldsymbol{w}) = -\nabla p + \nabla\cdot\boldsymbol{\Sigma} + \boldsymbol{f}. \tag{3.89}$$

Coarse-graining of (3.88) and (3.89) gives

$$\partial_t \bar{\rho}_\ell + \nabla\cdot\overline{(\sqrt{\rho}\boldsymbol{w})}_\ell = 0, \tag{3.90}$$

$$\partial_t\overline{(\sqrt{\rho}\boldsymbol{w})}_\ell + \nabla\cdot\overline{(\boldsymbol{w}\boldsymbol{w})}_\ell = -\nabla\bar{p}_\ell + \nabla\cdot\bar{\boldsymbol{\Sigma}}_\ell + \bar{\boldsymbol{f}}_\ell. \tag{3.91}$$

We introduce the following density-weighted coarse-grained variable $\widehat{\boldsymbol{w}}_\ell$ to obtain a simple physical interpretation:

$$\widehat{\boldsymbol{w}}_\ell := \frac{\overline{(\sqrt{\rho}\boldsymbol{w})}_\ell}{\sqrt{\bar{\rho}_\ell}}. \tag{3.92}$$

Note that $\widehat{\boldsymbol{w}}_\ell$ is different from the density-weighted average $\overline{(\sqrt{\rho}\boldsymbol{w})}_\ell/\overline{\sqrt{\rho}}_\ell$. In fact, because $\sqrt{\rho}$ is a concave function of ρ, we find that $\overline{\sqrt{\rho}}_\ell \le \sqrt{\bar{\rho}_\ell}$. We can rewrite (3.90) and (3.91) in terms of $\widehat{\boldsymbol{w}}_\ell$ as

$$\partial_t \bar{\rho}_\ell + \nabla\cdot\left(\sqrt{\bar{\rho}_\ell}\widehat{\boldsymbol{w}}_\ell\right) = 0, \tag{3.93}$$

$$\partial_t\left(\sqrt{\bar{\rho}_\ell}\widehat{\boldsymbol{w}}_\ell\right) + \nabla\cdot\overline{(\boldsymbol{w}\boldsymbol{w})}_\ell = -\nabla\bar{p}_\ell + \nabla\cdot\bar{\boldsymbol{\Sigma}}_\ell + \bar{\boldsymbol{f}}_\ell. \tag{3.94}$$

We now consider the large-scale kinetic energy balance. We first not that, since $|\boldsymbol{v}|^2$ is a convex function of $\boldsymbol{v}$, the following inequality holds:

$$\frac{1}{2}|\widehat{\boldsymbol{w}}_\ell|^2 = \frac{1}{2}\bar{\rho}_\ell\left|\frac{\overline{(\rho\boldsymbol{v})}_\ell}{\bar{\rho}_\ell}\right|^2 \le \frac{1}{2}\bar{\rho}_\ell\frac{\overline{(\rho|\boldsymbol{v}|^2)}_\ell}{\bar{\rho}_\ell} = \frac{1}{2}\overline{(\rho|\boldsymbol{v}|^2)}_\ell. \tag{3.95}$$

Therefore, the integral over space of $|\widehat{\boldsymbol{w}}_\ell|^2/2$ is less than the total kinetic energy:

$$\int_\Omega d^3\boldsymbol{x}\frac{1}{2}|\widehat{\boldsymbol{w}}_\ell|^2 \le \int_\Omega d^3\boldsymbol{x}\frac{1}{2}\rho|\boldsymbol{v}|^2, \tag{3.96}$$

and thus $|\widehat{\boldsymbol{w}}_\ell|^2/2$ represents the large-scale kinetic energy as in the one based on the Favre averaging [60,91]. From (3.93) and (3.94), we obtain the large-scale kinetic energy balance:

$$\partial_t\frac{1}{2}|\widehat{\boldsymbol{w}}_\ell|^2 + \nabla\cdot\boldsymbol{J}_\ell = \bar{p}_\ell\nabla\cdot\frac{\overline{\sqrt{\rho}}_\ell\bar{\boldsymbol{w}}_\ell}{\bar{\rho}_\ell} - \bar{\boldsymbol{\Sigma}}_\ell : \nabla\frac{\overline{\sqrt{\rho}}_\ell\bar{\boldsymbol{w}}_\ell}{\bar{\rho}_\ell} + \varepsilon_\ell^{\rm in} - Q_\ell^{\rm flux} - \nabla\frac{\widehat{\boldsymbol{w}}_\ell}{\sqrt{\bar{\rho}_\ell}} : (\widehat{\boldsymbol{w}}_\ell\widehat{\boldsymbol{w}}_\ell - \bar{\boldsymbol{w}}_\ell\bar{\boldsymbol{w}}_\ell). \tag{3.97}$$

Here, $\varepsilon_\ell^{\rm in} := \widehat{\boldsymbol{w}}_\ell \cdot \bar{\boldsymbol{f}}_\ell/\sqrt{\bar{\rho}_\ell}$ denotes the energy injection rate due to external stirring at scale ℓ and $\boldsymbol{J}_\ell$ represents the spatial transport of large-scale kinetic energy:

$$\boldsymbol{J}_\ell := \frac{1}{2}|\widehat{\boldsymbol{w}}_\ell|^2 \frac{\widehat{\boldsymbol{w}}_\ell}{\sqrt{\bar{\rho}_\ell}} + \bar{p}_\ell \frac{\overline{\sqrt{\rho}_\ell \boldsymbol{w}_\ell}}{\bar{\rho}_\ell} - \bar{\boldsymbol{\Sigma}}_\ell \cdot \frac{\overline{\sqrt{\rho}_\ell \boldsymbol{w}_\ell}}{\bar{\rho}_\ell} + \frac{\widehat{\boldsymbol{w}}_\ell}{\sqrt{\bar{\rho}_\ell}} \cdot \bar{\tau}_\ell(\boldsymbol{w}, \boldsymbol{w}) - \frac{\widehat{\boldsymbol{w}}_\ell}{\sqrt{\bar{\rho}_\ell}} \cdot (\widehat{\boldsymbol{w}}_\ell \widehat{\boldsymbol{w}}_\ell - \bar{\boldsymbol{w}}_\ell \bar{\boldsymbol{w}}_\ell)\,, \tag{3.98}$$

where $\bar{\tau}_\ell(f, g) := \overline{(fg)}_\ell - \bar{f}_\ell \bar{g}_\ell$. The first two terms on the right-hand side of (3.97) are the large-scale pressure-dilatation and quantum-stress–strain. The last term on the right-hand side of (3.97), which does not exist in (3.23), arises due to the introduction of the density-weighted variable $\widehat{\boldsymbol{w}}_\ell$. Since this term contains $\widehat{\boldsymbol{w}}_\ell \widehat{\boldsymbol{w}}_\ell - \bar{\boldsymbol{w}}_\ell \bar{\boldsymbol{w}}_\ell$, we expect that its contribution to the energy balance is small relative to the other terms. The term $Q_\ell^{\rm flux}$ represents the scale-to-scale kinetic energy flux:

$$Q_\ell^{\rm flux} := \Pi_\ell + \Lambda_\ell^{(p)} + \Lambda_\ell^{(\Sigma)}. \tag{3.99}$$

Here, Π_ℓ is the deformation work,

$$\Pi_\ell := -\nabla \frac{\widehat{\boldsymbol{w}}_\ell}{\sqrt{\bar{\rho}_\ell}} : \bar{\tau}_\ell(\boldsymbol{w}, \boldsymbol{w}), \tag{3.100}$$

$\Lambda_\ell^{(p)}$ is the baropycnal work,

$$\Lambda_\ell^{(p)} := \frac{1}{\bar{\rho}_\ell} \nabla \bar{p}_\ell \cdot \bar{\tau}_\ell(\sqrt{\rho}, \boldsymbol{w}), \tag{3.101}$$

and $\Lambda_\ell^{(\Sigma)}$ is the quantum baropycnal work,

$$\Lambda_\ell^{(\Sigma)} := -\frac{1}{\bar{\rho}_\ell} \nabla \cdot \bar{\boldsymbol{\Sigma}}_\ell \cdot \bar{\tau}_\ell(\sqrt{\rho}, \boldsymbol{w}). \tag{3.102}$$

Note that only these three terms are capable of the direct transfer of kinetic energy across scales because each of the three terms has a form "large-scale ($> \ell$) quantity $\times$ small-scale ($< \ell$) quantity," whereas the other terms on the right-hand side of (3.97) do not. We remark that these energy fluxes are not Galilean invariant unlike those defined in [60]. Therefore, they can be scale local only if spatially or ensemble averaged [170].

Instead of assuming the Besov regularity of the velocity field $\boldsymbol{v}$, we here assume the Besov regularity of the density-weighted velocity $\boldsymbol{w}$:

$$\|\delta \boldsymbol{w}(\boldsymbol{r}; \cdot)\|_p \sim w_{\rm rms} \left(\frac{r}{L}\right)^{\sigma_p} \quad \text{for} \quad r \ll L \tag{3.103}$$

with the Besov exponent $\sigma_p \in (0, 1]$ for $p \in [1, \infty]$. The important point here is that the validity of the Besov regularity (3.103) is well-established even at scales $\ll \ell_i$ [145,167,169]. In addition, we assume the following properties for $\sqrt{\rho}$ instead of ρ:

$$\|\delta \sqrt{\rho}(\boldsymbol{r}; \cdot)\|_p = O(r/L) \quad \text{for} \quad r \ll L, \tag{3.104}$$

$$\|1/\sqrt{\bar{\rho}_\ell}\|_\infty \le M \quad \text{for} \quad \ell \gg \xi, \tag{3.105}$$

where M is a ℓ-independent positive constant. Under these assumptions, we can derive the same results as in the main text:

$$\|\Pi_\ell\|_{p/3} = O\left(\left(\frac{\ell}{L}\right)^{3\sigma_p - 1}\right), \tag{3.106}$$

$$\|\Lambda_\ell^{(p)}\|_{p/3} = O\left(\left(\frac{\ell}{L}\right)^{\sigma_p + 1}\right), \tag{3.107}$$

$$\|\Lambda_\ell^{(\Sigma)}\|_{p/3} = O\left(\left(\frac{\ell}{L}\right)^{\sigma_p - 1}\right), \tag{3.108}$$

for $p \geq 3$. We thus find that the asymptotic behavior of the energy spectrum reads

$$E(k) \sim \begin{cases} C_{\mathrm{large}} k^{-5/3} & \text{for} \quad \ell_{\mathrm{large}}^{-1} \ll k \ll \ell_i^{-1}, \\ C_{\mathrm{small}} k^{-3} & \text{for} \quad \ell_i^{-1} \ll k \ll \ell_{\mathrm{small}}^{-1}, \end{cases} \tag{3.109}$$

where C_{large} and C_{small} are positive constants. Note that $E(k)$ denotes the standard energy spectrum, not the velocity power spectrum $E^v(k)$. We also remark that the k^{-3} spectrum for the quantum stress cascade can become shallower because of the Kelvin-wave oscillations, as mentioned in Section 3.6.

Chapter 4

Van der Waals turbulence

We begin this chapter by considering whether the Richardson cascade can reach the microscopic length scales in ordinary fluid turbulence. Within the K41 theory, we can show that the Kolmogorov dissipation scale $\eta := \nu^{3/4}\varepsilon^{-1/4}$ is overwhelmingly larger than the microscopic length scales such as the molecular mean free path $\lambda_{\rm mfp}$ [5]. Indeed, by estimating the injection scale as $L \sim v_{\rm rms}^3/\varepsilon \sim {\rm Re}^{3/4}\eta$ and by denoting c_s the sound velocity, we find that

$$\begin{aligned}\frac{\eta}{\lambda_{\rm mfp}} &\sim \frac{\eta}{L}\frac{Lv_{\rm rms}}{\lambda_{\rm mfp}c_s}\frac{c_s}{v_{\rm rms}} \\ &\sim {\rm Re}^{1/4}{\rm Ma}^{-1} \gg 1, \end{aligned} \tag{4.1}$$

where ${\rm Ma} = v_{\rm rms}/c_s$ denotes the Mach number. Thus, the Richardson cascade never reaches the microscopic length scales in ordinary fluid turbulence.

In the vicinity of a gas-liquid critical point, however, it is not obvious whether the Richardson cascade is truncated at the Kolmogorov dissipation scale because the correlation length of equilibrium density fluctuations ξ reaches a macroscopic order of magnitude [171, 172]. We here consider the strong turbulent regime of a supercritical fluid near a critical point where ξ is much larger than the Kolmogorov dissipation scale. Even for such strong turbulence, ξ still provides a length scale at which the stress induced by density fluctuations is comparable to the momentum flux. In this case, density fluctuations are driven by turbulence, so that the equilibrium critical fluctuations are destroyed. We then ask how the Richardson cascade is modified by density fluctuations in the turbulence near a critical point. Although turbulence in supercritical fluids has been studied over the past few decades, previous studies have focused on cases where the Kolmogorov dissipation scale is larger than ξ [173–176].

We answer the above question by studying hydrodynamic equations including density fluctuations. Specifically, we include a density gradient contribution to the entropy functional to describe the effects of density fluctuations. Such a formulation that takes into account gradient contributions was originally proposed in the pioneering work of van der Waals [177], who introduced a gradient term in the Helmholtz free energy density to describe a gas-liquid interface, and the formulation has been widely used in statistical physics since the publication of seminal papers by Ginzbrug and Landau for type-I superconductors [178] and by Cahn and Hilliard for binary alloys [179]. Following the van der Waals theory, Korteweg proposed hydrodynamic equations that contain the *van der Waals stress* (vdW stress), arising from the density gradient [148, 180], and Onuki generalized the theory by including the gradient contribution to both entropy and energy functionals [181, 182].

In this study, we analyze the model using a phenomenological approach based on the Onsager "ideal turbulence" theory [3, 18, 82], as in Chapter 3. We show that supercritical turbulence near a critical point exhibits the Richardson cascade and novel type of cascade which we call *van der Waals cascade*, induced by the vdW stress.

This chapter is organized as follows. In the next section, we explain the setup. In Section 4.2, we investigate characteristic length scale of the system. In Section 4.3, by coarse-graining turbulent fields, we show that there are three types of scale-to-scale energy fluxes. In Section 4.4, we describe our main results. We consider the experimental conditions required to observe van der Waals cascade in Section 4.5. We derive the main results in Section 4.6. Concluding remarks are provided in Section 4.7.

4.1 Setup

Let ρ be the mass density, $\boldsymbol{v}$ be the fluid velocity, and u be the internal energy density. For simplicity, we assume that a fluid is confined in a cube $\Omega = [0, L_\Omega]^3$ with periodic boundary conditions. We further assume that there is no vacuum region; i.e., $\rho(\boldsymbol{x}, t) > 0$ for all $\boldsymbol{x} \in \Omega$ and time t. Following the van der Waals theory, we include a gradient contribution to the entropy functional to describe enhanced density fluctuations near a critical point [177, 181–183]:[1]

$$\mathcal{S}([u],[\rho]) = \int_\Omega d^3\boldsymbol{x} \left(s(u,\rho) + \frac{c(\rho)}{2}|\nabla\rho|^2 \right), \tag{4.2}$$

where $([u],[\rho]) := (u(\boldsymbol{x}),\rho(\boldsymbol{x}))_{\boldsymbol{x}\in\Omega}$, $s(u,\rho)$ denotes the entropy density, and $c(\rho) \le 0$ is the capillary coefficient. In the following discussion, we consider the case in which the capillary coefficient is a sufficiently smooth function of ρ; e.g., $c(\rho) = \text{const}$ [182]. Through thermodynamic relations, the temperature $T(u,\rho)$ and pressure tensor $\boldsymbol{P}$ are determined from (4.2):

$$\boldsymbol{P} = p\boldsymbol{I} + \boldsymbol{\Sigma}, \tag{4.3}$$

where $p(u,\rho)$ denotes the pressure defined by $s(u,\rho)$, $\boldsymbol{I}$ is the unit tensor, and $\boldsymbol{\Sigma}$ is the *vdW stress tensor*, which arises from the gradient contribution and is defined as

$$\boldsymbol{\Sigma} := \left(Tc\rho\Delta\rho + \frac{1}{2}Tc'\rho|\nabla\rho|^2 + \frac{1}{2}Tc|\nabla\rho|^2 \right)\boldsymbol{I} - Tc\nabla\rho\nabla\rho. \tag{4.4}$$

For the derivation, see Appendix 4.8.1. The time evolution of the densities of mass ρ, momentum $\rho\boldsymbol{v}$, and total energy $\rho|\boldsymbol{v}|^2/2 + u$ is then governed by the *Navier–Stokes–Korteweg equations* [149, 184]:[2]

$$\partial_t\rho + \nabla\cdot(\rho\boldsymbol{v}) = 0, \tag{4.5}$$

$$\partial_t(\rho\boldsymbol{v}) + \nabla\cdot(\rho\boldsymbol{v}\boldsymbol{v} + \boldsymbol{P} + \boldsymbol{\sigma}) = \boldsymbol{f}, \tag{4.6}$$

$$\partial_t\left(u + \frac{1}{2}\rho|\boldsymbol{v}|^2\right) + \nabla\cdot\left\{\left[\left(u + \frac{1}{2}\rho|\boldsymbol{v}|^2\right)\boldsymbol{I} + \boldsymbol{P} + \boldsymbol{\sigma}\right]\cdot\boldsymbol{v} - \lambda\nabla T\right\} = \boldsymbol{v}\cdot\boldsymbol{f}, \tag{4.7}$$

[1] Here, we have assumed that there is no gradient contribution to the internal energy [182].
[2] For the Euler-Korteweg equations, an Onsager-type theorem was obtained in [185].

where $\boldsymbol{f}$ denotes an external force acting at large scales $\sim L$, λ is the thermal conductivity, and $\boldsymbol{\sigma}$ is the viscous stress tensor of the form

$$\sigma_{ij} = -\mu\left(\partial_i v_j + \partial_j v_i - \frac{2}{3}\delta_{ij}\nabla\cdot\boldsymbol{v}\right) - \zeta\delta_{ij}\nabla\cdot\boldsymbol{v}. \tag{4.8}$$

Here μ and ζ are the shear and bulk viscosity coefficients, respectively. We assume that the viscous effect is sufficiently weak for the Kolmogorov dissipation scale η to be sufficiently smaller than any other length scales.

In the following, (4.5)-(4.7) are applied even to scales smaller than the equilibrium correlation length. Strictly speaking, dynamics at such scales should be described within the framework of fluctuating hydrodynamics [23,186,187]. In a turbulent regime, however, the equilibrium correlation may be cut off, and the noise terms may be irrelevant for energy transfer. We therefore assume that (4.5)-(4.7) are sufficient for our phenomenological argument.

4.2 Characteristic length scales

Owing to the effect of the gradient contribution, several characteristic length scales that are not relevant in ordinary fluid turbulence become important. Let $\rho_0 := \langle\rho\rangle_\Omega$, $c_0 := c(\rho_0)$, and $T_0 := \langle T\rangle_\Omega$ be the typical density, capillary coefficient, and temperature, respectively. In addition, let $v_0 := (\rho_0 K_{T_0})^{-1/2}$ be a velocity characterized by the isothermal compressibility $K_{T_0} := \rho_0^{-1}\partial\rho(T_0,p)/\partial p$, which is zero at a critical point. One of the most crucial length scales is the correlation length of equilibrium density fluctuations

$$\xi = \frac{\sqrt{T_0|c_0|\rho_0}}{v_0}, \tag{4.9}$$

which is expressed by the capillary coefficient $c(\rho)$ and parameters in the entropy density $s(u,\rho)$ (for the derivation, see Appendix 4.8.2). The important point here is that even for strong turbulence, ξ still provides a characteristic length scale at which the vdW stress $\boldsymbol{\Sigma}$ and momentum flux $\rho\boldsymbol{v}\boldsymbol{v}$ are comparable. Let ℓ_c be such a length scale. Using an estimation that $\rho\boldsymbol{v}\boldsymbol{v}\sim\rho_0 v_0^2$ and $\boldsymbol{\Sigma}\sim T_0|c_0|\rho_0^2/\ell_c^2$, we obtain

$$\ell_c \sim \xi. \tag{4.10}$$

Note that $\boldsymbol{\Sigma}$ can be significant at small scales because it contains higher-order spatial derivatives. Therefore, at scales $\gg \ell_c$, the effect of the vdW stress is small compared with the momentum flux, whereas at scales $\ll \ell_c$, the vdW stress becomes relevant. This observation implies the possibility of the van der Waals cascade, induced by the vdW stress, at scales $\ll \ell_c$.

We now introduce other important characteristic length scales by noting the local kinetic energy balance equation

$$\partial_t\left(\frac{1}{2}\rho|\boldsymbol{v}|^2\right) + \nabla\cdot\left[\left(\frac{1}{2}\rho|\boldsymbol{v}|^2\boldsymbol{I} + \boldsymbol{P} + \boldsymbol{\sigma}\right)\cdot\boldsymbol{v}\right] = p\nabla\cdot\boldsymbol{v} + \boldsymbol{\Sigma}:\nabla\boldsymbol{v} + \boldsymbol{\sigma}:\nabla\boldsymbol{v} + \boldsymbol{v}\cdot\boldsymbol{f}. \tag{4.11}$$

The first term (with minus sign) on the right-hand side of (4.11), $-p\nabla\cdot\boldsymbol{v}$, is the pressure-dilatation, which represents the conversion of kinetic energy into internal energy and vice versa. As mentioned in Chapter 3, recent numerical simulations on ordinary compressible

turbulence [150, 154] suggest that there is a characteristic length scale ℓ_{large} such that the contribution to the global pressure-dilatation $\langle -p\nabla\cdot\boldsymbol{v}\rangle_\Omega$ from scales $\gg \ell_{\mathrm{large}}$ is dominant, whereas the contribution from scales $\ll \ell_{\mathrm{large}}$ is negligible. The length scale ℓ_{large} is defined, for instance, as follows:

$$\ell_{\mathrm{large}} := \frac{\sum_k k^{-1}E^{(p)}(k)}{\sum_k E^{(p)}(k)}, \tag{4.12}$$

where $E^{(p)}(k)$ denotes the pressure-dilatation co-spectrum:

$$E^{(p)}(k) := -\frac{1}{\Delta k}\sum_{k-\Delta k/2<|\boldsymbol{k}|<k+\Delta k/2} \hat{p}(\boldsymbol{k})\widehat{\nabla\cdot\boldsymbol{v}}(-\boldsymbol{k}) \tag{4.13}$$

with $\Delta k := 2\pi/L_\Omega$. The second term (with minus sign) on the right-hand side of (4.11), $-\boldsymbol{\Sigma}:\nabla\boldsymbol{v}$, which we call the *vdW-stress–strain*, arises because of the gradient contribution. It also represents the conversion between kinetic and internal energy. Because both the vdW stress $\boldsymbol{\Sigma}$ and strain $\nabla\boldsymbol{v}$ change rapidly in space, there may be a characteristic length scale ℓ_{small} such that the contribution to the global vdW-stress–strain $\langle -\boldsymbol{\Sigma}:\nabla\boldsymbol{v}\rangle_\Omega$ from scales $\gg \ell_{\mathrm{small}}$ is negligible, whereas the contribution from scales $\ll \ell_{\mathrm{small}}$ is dominant. We define ℓ_{small} as

$$\ell_{\mathrm{small}} := \frac{\sum_k k^{-1}E^{(\Sigma)}(k)}{\sum_k E^{(\Sigma)}(k)}, \tag{4.14}$$

where $E^{(\Sigma)}(k)$ denotes the vdW-stress–strain co-spectrum:

$$E^{(\Sigma)}(k) := -\frac{1}{\Delta k}\sum_{k-\Delta k/2<|\boldsymbol{k}|<k+\Delta k/2} \hat{\boldsymbol{\Sigma}}(\boldsymbol{k}):\widehat{\nabla\boldsymbol{v}}(-\boldsymbol{k}). \tag{4.15}$$

In the following, we assume the existence of the intermediate asymptotic limit $\ell_{\mathrm{small}} \ll \ell \ll \ell_c$ and $\ell_c \ll \ell \ll \ell_{\mathrm{large}} \lesssim L$. The validity of this assumption will be discussed in Section 4.6.

4.3 Scale-to-scale energy fluxes

We investigate energy transfer across scales by coarse-graining turbulent fields, as in the previous chapter. For any locally integrable function $\boldsymbol{a}(\boldsymbol{x})$, we define a coarse-grained field at length scale ℓ as

$$\bar{\boldsymbol{a}}_\ell(\boldsymbol{x}) := \int_\Omega d^3\boldsymbol{r}\, G_\ell(\boldsymbol{r})\boldsymbol{a}(\boldsymbol{x}+\boldsymbol{r}). \tag{4.16}$$

Here, $G_\ell(\boldsymbol{r}) := \ell^{-3}G(\boldsymbol{r}/\ell)$ is the Friedrichs mollifier, where $G:\Omega\to[0,\infty)$ is a smooth symmetric function supported in the open unit ball with $\int_\Omega G = 1$. By coarse-graining (4.5) and (4.6), we can obtain the large-scale kinetic energy balance equation

$$\partial_t\left(\frac{1}{2}\bar{\rho}_\ell|\tilde{\boldsymbol{v}}_\ell|^2\right) + \nabla\cdot\boldsymbol{J}_\ell = \bar{p}_\ell\nabla\cdot\bar{\boldsymbol{v}}_\ell + \bar{\boldsymbol{\Sigma}}_\ell:\nabla\bar{\boldsymbol{v}}_\ell - Q_\ell^{\mathrm{flux}} - D_\ell + \varepsilon_\ell^{\mathrm{in}}, \tag{4.17}$$

where we have introduced the density-weighted coarse-grained velocity $\tilde{\boldsymbol{v}}_\ell := \overline{(\rho\boldsymbol{v})}_\ell/\bar{\rho}_\ell$ to reduce the number of additional cumulant terms and to obtain a simple physical interpretation. Here, $\varepsilon_\ell^{\mathrm{in}} := \tilde{\boldsymbol{v}}_\ell\cdot\bar{\boldsymbol{f}}_\ell$ denotes the energy injection rate due to external stirring at scale ℓ, $D_\ell := -\nabla\tilde{\boldsymbol{v}}_\ell : \bar{\boldsymbol{\sigma}}_\ell$ denotes the viscous dissipation acting at scale ℓ, and $\boldsymbol{J}_\ell$

represents the spatial transport of large-scale kinetic energy, which does not contribute to the energy transfer across scales. The first two terms on the right-hand side of (4.17), $-\bar{p}_\ell \nabla \cdot \bar{\boldsymbol{v}}_\ell$ and $-\bar{\boldsymbol{\Sigma}}_\ell : \nabla \bar{\boldsymbol{v}}_\ell$, are the large-scale pressure-dilatation and vdW-stress–strain, respectively. Note that these two terms are closed in terms of the large-scale fields $\bar{\boldsymbol{v}}_\ell$, $\bar{p}_\ell$, and $\bar{\boldsymbol{\Sigma}}_\ell$. Therefore, they contribute only to the conversion of the large-scale kinetic energy into internal energy and vice versa. The third term on the right-hand side of (4.17) denotes the total scale-to-scale kinetic energy flux:

$$Q_\ell^{\mathrm{flux}} := \Pi_\ell + \Lambda_\ell^{(p)} + \Lambda_\ell^{(\Sigma)}. \tag{4.18}$$

Here, the first term Π_ℓ denotes the deformation work, which corresponds to the energy flux of the Richardson cascade:

$$\Pi_\ell := -\bar{\rho}_\ell \nabla \tilde{\boldsymbol{v}}_\ell : \tilde{\tau}_\ell(\boldsymbol{v}, \boldsymbol{v}), \tag{4.19}$$

where $\tilde{\tau}_\ell(\boldsymbol{v}, \boldsymbol{v}) := \widetilde{(\boldsymbol{v}\boldsymbol{v})}_\ell - \tilde{\boldsymbol{v}}_\ell \tilde{\boldsymbol{v}}_\ell$. The deformation work represents the work done by the large-scale strain $\nabla \tilde{\boldsymbol{v}}_\ell$ against the small-scale stress $\bar{\rho}_\ell \tilde{\tau}_\ell(\boldsymbol{v}, \boldsymbol{v})$. The second term $\Lambda_\ell^{(p)}$ denotes the baropycnal work defined by

$$\Lambda_\ell^{(p)} := \frac{1}{\bar{\rho}_\ell} \nabla \bar{p}_\ell \cdot \bar{\tau}_\ell(\rho, \boldsymbol{v}), \tag{4.20}$$

where $\bar{\tau}_\ell(\rho, \boldsymbol{v}) := \overline{(\rho \boldsymbol{v})}_\ell - \bar{\rho}_\ell \bar{\boldsymbol{v}}_\ell$, and it represents the work done by the large-scale pressure gradient force $-\nabla \bar{p}_\ell / \bar{\rho}_\ell$ against the small-scale mass flux $\bar{\tau}_\ell(\rho, \boldsymbol{v})$. While Π_ℓ and $\Lambda_\ell^{(p)}$ also exist in ordinary compressible turbulence, the existence of the third term $\Lambda_\ell^{(\Sigma)}$ is specific to a fluid near a gas-liquid critical point. Because this term arises due to the gradient contribution, we call it *capillary work*. The capillary work has a form similar to that of baropycnal work,

$$\Lambda_\ell^{(\Sigma)} := \frac{1}{\bar{\rho}_\ell} \nabla \cdot \bar{\boldsymbol{\Sigma}}_\ell \cdot \bar{\tau}_\ell(\rho, \boldsymbol{v}), \tag{4.21}$$

and represents the work done by the large-scale force $\nabla \cdot \bar{\boldsymbol{\Sigma}}_\ell / \bar{\rho}_\ell$ against the small-scale mass flux $\bar{\tau}_\ell(\rho, \boldsymbol{v})$. Note that in (4.17), only these three terms are capable of the direct transfer of kinetic energy across scales because each of the three terms has a form "large-scale ($> \ell$) quantity $\times$ small-scale ($< \ell$) quantity," whereas the other terms on the right-hand side of (4.17) do not.

4.4 Main result

The first main result concerns the most fundamental property of the energy cascade: the total scale-to-scale energy flux $\langle Q_\ell^{\mathrm{flux}} \rangle_\Omega$ becomes scale-independent in the "inertial range" $\ell_{\mathrm{small}} \ll \ell \ll \ell_{\mathrm{large}}$:

$$\langle Q_\ell^{\mathrm{flux}} \rangle_\Omega \simeq \varepsilon_{\mathrm{eff}}, \tag{4.22}$$

where $\varepsilon_{\mathrm{eff}} := \langle p \nabla \cdot \boldsymbol{v} \rangle_\Omega + \langle \boldsymbol{v} \cdot \boldsymbol{f} \rangle_\Omega$ denotes the effective energy injection rate, which is scale-independent. We emphasize that, because Q_ℓ^{flux} can be expressed in terms of field increments $\delta \boldsymbol{v}(\boldsymbol{r}; \boldsymbol{x})$ and $\delta \rho(\boldsymbol{r}; \boldsymbol{x})$, the relation (4.22) plays the same role as Kolmogorov's 4/5-law [21].

The second main result is the prediction of the van der Waals cascade. In the range of $\ell_c \ll \ell \ll \ell_{\mathrm{large}}$, the Richardson cascade, induced by the momentum flux, becomes

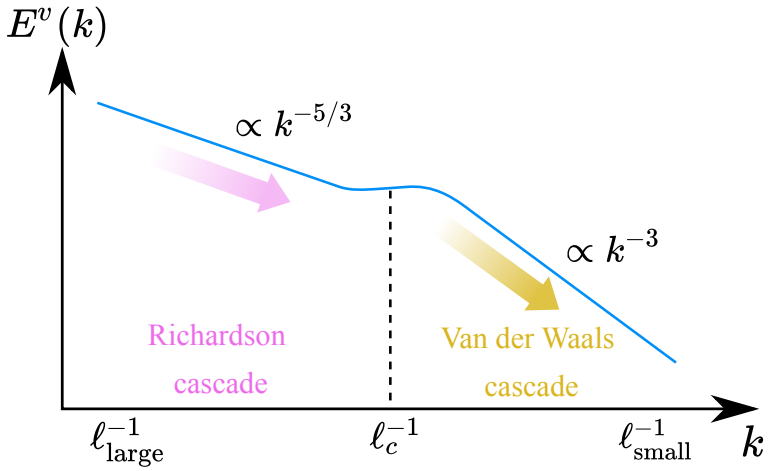

Fig. 4.1: Velocity power spectrum $E^v(k)$ in the inertial range $\ell_{\rm large}^{-1} \ll k \ll \ell_{\rm small}^{-1}$.

dominant, whereas in the range of $\ell_{\rm small} \ll \ell \ll \ell_c$, the van der Waals cascade, induced by vdW stress, develops:

$$\begin{aligned} \langle \Lambda_\ell^{(\Sigma)} \rangle_\Omega \ll \langle \Pi_\ell \rangle_\Omega \simeq \varepsilon_{\rm eff} \quad &\text{for} \quad \ell_c \ll \ell \ll \ell_{\rm large}, \\ \langle \Pi_\ell \rangle_\Omega \ll \langle \Lambda_\ell^{(\Sigma)} \rangle_\Omega \simeq \varepsilon_{\rm eff} \quad &\text{for} \quad \ell_{\rm small} \ll \ell \ll \ell_c. \end{aligned} \tag{4.23}$$

Correspondingly, the velocity power spectrum is estimated to exhibit the power-law $\propto k^{-5/3}$ for $\ell_{\rm large}^{-1} \ll k \ll \ell_c^{-1}$ and $\propto k^{-3}$ for $\ell_c^{-1} \ll k \ll \ell_{\rm small}^{-1}$ (see Fig. 4.1).

4.4.1 Interpretation of the result

The above result can be interpreted in terms of the following energy transfer scenario (see Fig. 4.1):

1. At large scales ($\sim L$), kinetic energy is injected due to external force.

2. In the scale range larger than $\ell_{\rm large}$, part of the injected kinetic energy is transferred to smaller scales because of the effect of deformation work, while part of the kinetic energy is converted into internal energy through the pressure-dilatation effect.

3. In the inertial range $\ell_{\rm small} \ll \ell \ll \ell_{\rm large}$, the following two-step cascade process emerges:

   (a) In the scale range $\ell_c \ll \ell \ll \ell_{\rm large}$, the Richardson cascade, induced by deformation work, becomes dominant.

   (b) At scales smaller than the crossover length ℓ_c, the effect of the vdW stress due to enhanced density fluctuations becomes significant. Therefore, the Richardson cascade is no longer dominant, and the van der Waals cascade, induced by capillary work, develops.

4. In the scale range smaller than $\ell_{\rm small}$, the kinetic energy transferred by the two-step cascade is dissipated due to the viscous effects.

4.4.2 Remark

Here, we remark on several assumptions imposed in deriving the main result. In deriving the second main result, we have assumed that the velocity field satisfies the Besov regularity in the inviscid limit:

$$\|\delta \boldsymbol{v}(\boldsymbol{r};\cdot)\|_p \sim v_{\rm rms}\left(\frac{r}{L}\right)^{\sigma_p} \quad \text{for} \quad r \ll L, \tag{4.24}$$

with the Besov exponent $\sigma_p \in (0,1]$ for $p \in [1,\infty]$.

In addition, we have imposed the following conditions for the density and pressure field:

$$\|\delta\rho(\boldsymbol{r};\cdot)\|_p = O\left(\frac{r}{L}\right), \tag{4.25}$$

$$\|\delta p(\boldsymbol{r};\cdot)\|_p = O\left(\left(\frac{r}{L}\right)^{\sigma_p^p}\right), \tag{4.26}$$

where $\sigma_p^p \in (0,1]$. The requirement (4.25) is reasonable because the entropy functional of the system (4.2) includes the density gradient term $\propto |\nabla\rho|^2$. For ordinary compressible turbulence, the Besov regularity of these turbulent fields is well-established through experiments and numerical simulations [94, 188–190].

4.5 Suggested experiments

We consider the experimental conditions required for observing the van der Waals cascade. In the study of critical phenomena, CO_2 has been widely used because its critical state occurs under readily realized experimental conditions ($T_c = 304.13$ K, $p_c = 7.3773$ MPa, $\rho_c = 0.4678$ g cm^{-3}) [191, 192]. In this case, the shear viscosity μ takes a value around 3.5×10^{-4} g cm^{-1} s^{-1} [176, 191, 193]. We first estimate the Kolmogorov dissipation scale η, which can be estimated in terms of μ, ρ_c, L, and $v_{\rm rms} := \sqrt{\langle|\boldsymbol{v}|^2\rangle_\Omega}$ as

$$\eta \sim \left(\frac{\mu}{\rho_c v_{\rm rms} L}\right)^{3/4} L. \tag{4.27}$$

If we achieve a quite strong turbulent regime, in which Re $\sim 10^7$ (e.g., $v_{\rm rms} \sim 10$ m/s and $L \sim 0.1$ m), the Kolmogorov dissipation scale is $\sim 10^3$ Å. Therefore, if one can reach the vicinity of the critical point such that the correlation length is at least $\sim 10^4$ Å, it may be possible to verify our predictions by measuring the velocity field using hot-wire anemometry or laser Doppler velocimetry. To achieve a correlation length of that magnitude, we must control the system with an accuracy of at least $T - T_c \sim 10^{-4}$ K because $\xi \simeq \xi_0 \varepsilon^{-\nu}$, where $\xi_0 = 1.5$ Å, $\varepsilon := (T - T_c)/T_c$, and $\nu = 0.630$ [191, 193].

4.6 Derivation of the main result

In this section, we derive the main result. First, we investigate the scale dependence of the scale-to-scale energy fluxes. Then, we derive the first and second main results.

4.6.1 Scale dependence of the energy fluxes

Here, we investigate the scale dependence of deformation work, baropycnal work, and capillary work, by using arguments similar to those used in the Onsager "ideal turbulence" theory.

Deformation work

The scale dependence of the deformation work $\Pi_\ell = -\bar{\rho}_\ell \nabla \tilde{\boldsymbol{v}}_\ell : \tilde{\tau}_\ell(\boldsymbol{v}, \boldsymbol{v})$ is completely the same as in pure quantum turbulence (Section 3.5.1). The result reads

$$\|\Pi_\ell\|_{p/3} = O\left(\left(\frac{\ell}{L}\right)^{3\sigma_p - 1}\right), \quad p \geq 3. \tag{4.28}$$

Baropycnal work

We next evaluate the scale dependence of the baropycnal work $\Lambda_\ell^{(p)} = (1/\bar{\rho}_\ell)\nabla \bar{p}_\ell \cdot \bar{\tau}_\ell(\rho, \boldsymbol{v})$. By using the Cauchy-Schwarz and Hölder inequalities, we obtain

$$\begin{aligned} \|\Lambda_\ell^{(p)}\|_{p/3} &= \|(1/\bar{\rho}_\ell)\nabla \bar{p}_\ell \cdot \bar{\tau}_\ell(\rho, \boldsymbol{v})\|_{p/3} \\ &\leq \|1/\bar{\rho}_\ell\|_\infty \|\nabla \bar{p}_\ell\|_p \|\bar{\tau}_\ell(\rho, \boldsymbol{v})\|_{p/2}. \end{aligned} \tag{4.29}$$

The second factor $\|\nabla \bar{p}_\ell\|_p$ can be evaluated as (see (3.41) of Section 3.5.1)

$$\|\nabla \bar{p}_\ell\|_p = O\left(\frac{\|\delta p(\ell)\|_p}{\ell}\right). \tag{4.30}$$

For $\|\bar{\tau}_\ell(\rho, \boldsymbol{v})\|_{p/2}$, by using Proposition (3.79) in Appendix 3.7.1, we obtain

$$\|\bar{\tau}_\ell(\rho, \boldsymbol{v})\|_{p/2} = O(\|\delta\rho(\ell)\|_p \|\delta \boldsymbol{v}(\ell)\|_p). \tag{4.31}$$

Then, from the Besov regularity (4.24), (4.25), and (4.26), we obtain

$$\begin{aligned} \|\Lambda_\ell^{(p)}\|_{p/3} &= \|(1/\bar{\rho}_\ell)\nabla \bar{p}_\ell \cdot \bar{\tau}_\ell(\rho, \boldsymbol{v})\|_{p/3} \\ &= O\left(\frac{1}{\ell}\|\delta p(\ell)\|_p \|\delta\rho(\ell)\|_p \|\delta \boldsymbol{v}(\ell)\|_p\right) \\ &= O\left(\left(\frac{\ell}{L}\right)^{\sigma_p + \sigma_p^p}\right), \quad p \geq 3. \end{aligned} \tag{4.32}$$

This result implies that the mean baropycnal work goes to zero $\langle \Lambda_\ell^{(p)} \rangle_\Omega \to 0$ as $\ell/L \to 0$. Therefore, the baropycnal work does not contribute to the energy transfer across scales.[3]

Capillary work

Finally, we investigate the scale dependence of the capillary work, $\Lambda_\ell^{(\Sigma)} = (1/\bar{\rho}_\ell)\nabla \cdot \bar{\boldsymbol{\Sigma}}_\ell \cdot \bar{\tau}_\ell(\rho, \boldsymbol{v})$. From the Cauchy-Schwarz and Hölder inequalities, we obtain

$$\begin{aligned} \|\Lambda_\ell^{(\Sigma)}\|_{p/3} &= \left\|(1/\bar{\rho}_\ell)\nabla \cdot \bar{\boldsymbol{\Sigma}}_\ell \cdot \bar{\tau}_\ell(\rho, \boldsymbol{v})\right\|_{p/3} \\ &\leq \|1/\bar{\rho}_\ell\|_\infty \left(\|\nabla \overline{(Tc\rho\Delta\rho)}_\ell\|_p + \|\nabla \cdot \bar{\boldsymbol{\Xi}}_\ell\|_p\right) \|\bar{\tau}_\ell(\rho, \boldsymbol{v})\|_{p/2} \end{aligned} \tag{4.33}$$

where we have introduced $\boldsymbol{\Xi}$ as

$$\boldsymbol{\Xi} := \left(\frac{1}{2}Tc'\rho|\nabla\rho|^2 + \frac{1}{2}Tc|\nabla\rho|^2\right)\boldsymbol{I} - Tc\nabla\rho\nabla\rho. \tag{4.34}$$

[3] In ordinary compressible turbulence, the baropycnal work can contribute to energy transfer [93, 95, 156]. If the assumption (4.25) is violated, the baropycnal work can induce energy transfer across scales even in this case, at least in the large scale $\ell_c \ll \ell \ll \ell_{\text{large}}$.

We now evaluate $\|\nabla\overline{(Tc\rho\Delta\rho)}_\ell\|_p$ and $\|\nabla\cdot\bar{\boldsymbol{\Xi}}_\ell\|$. By noting that

$$\begin{aligned}\nabla\overline{(Tc\rho\Delta\rho)}_\ell &= -\frac{1}{\ell}\int_\Omega d^3\boldsymbol{r}(\nabla G)_\ell(\boldsymbol{r})(Tc\rho\Delta\rho)(\boldsymbol{x}+\boldsymbol{r})\\ &= \frac{1}{\ell^2}\int_\Omega d^3\boldsymbol{r}(\nabla\nabla G)_\ell(\boldsymbol{r})\cdot(Tc\rho\nabla\rho)(\boldsymbol{x}+\boldsymbol{r})\\ &\quad+\frac{1}{\ell}\int_\Omega d^3\boldsymbol{r}(\nabla G)_\ell(\boldsymbol{r})(\nabla(Tc\rho)\cdot\nabla\rho)(\boldsymbol{x}+\boldsymbol{r}),\end{aligned} \tag{4.35}$$

we obtain

$$\begin{aligned}\|\nabla\overline{(Tc\rho\Delta\rho)}_\ell\|_p &\le \frac{1}{\ell^2}\int_\Omega d^3\boldsymbol{r}|(\nabla\nabla G)_\ell(\boldsymbol{r})|\|Tc\rho\nabla\rho\|_p+\frac{1}{\ell}\int_\Omega d^3\boldsymbol{r}|(\nabla G)_\ell(\boldsymbol{r})|\|\nabla(Tc\rho)\cdot\nabla\rho\|_p\\ &= O\left(\ell^{-2}\right).\end{aligned} \tag{4.36}$$

Similarly, $\|\nabla\cdot\bar{\boldsymbol{\Xi}}_\ell\|$ can be evaluated as

$$\begin{aligned}\|\nabla\cdot\bar{\boldsymbol{\Xi}}_\ell\|_p &\le \frac{1}{\ell}\int_\Omega d^3\boldsymbol{r}|(\nabla G)_\ell(\boldsymbol{r})|\|\boldsymbol{\Xi}\|_p\\ &= O\left(\ell^{-1}\right).\end{aligned} \tag{4.37}$$

By combining (4.33), (4.36), (4.37), and the conditions (4.24) and (4.25), we obtain

$$\begin{aligned}\|\Lambda_\ell^{(\Sigma)}\|_{p/3} &= \|(1/\bar\rho_\ell)\nabla\cdot\bar{\boldsymbol{\Sigma}}_\ell\cdot\bar\tau_\ell(\rho,\boldsymbol{v})\|_{p/3}\\ &= O\left(\left(\frac{\ell}{L}\right)^{\sigma_p-1}\right),\quad p\ge 3.\end{aligned} \tag{4.38}$$

Note that, for any $\sigma_p\in(0,1]$, we cannot conclude that the capillary work goes to zero as $\ell/L\to 0$. In other words, unlike deformation work, capillary work can contribute to the transfer of kinetic energy across scales regardless of the regularity of the velocity field. The scale-independent upper bound is obtained when $\sigma_p=1$.

4.6.2 Derivation of the first main result

We derive the first main result in the steady state regime for simplicity, although it is valid even in freely decaying turbulence. In the steady state, the spatial averaging of (4.17) gives

$$\langle Q_\ell^{\mathrm{flux}}\rangle_\Omega = \langle\bar p_\ell\nabla\cdot\bar{\boldsymbol{v}}_\ell\rangle_\Omega+\langle\bar{\boldsymbol{\Sigma}}_\ell:\nabla\bar{\boldsymbol{v}}_\ell\rangle_\Omega-\langle D_\ell\rangle_\Omega+\langle\varepsilon_\ell^{\mathrm{in}}\rangle_\Omega. \tag{4.39}$$

As mentioned in Section 4.2, the pressure-dilatation is assumed to be significant at large scales $\gg\ell_{\mathrm{large}}$. That is, the large-scale pressure-dilatation can be approximated as $-\langle\bar p_\ell\nabla\cdot\bar{\boldsymbol{v}}_\ell\rangle_\Omega\simeq-\langle p\nabla\cdot\boldsymbol{v}\rangle_\Omega$ for $\ell\ll\ell_{\mathrm{large}}$. Similarly, because the contribution to $-\langle\boldsymbol{\Sigma}:\nabla\boldsymbol{v}\rangle_\Omega$ from large scales $\gg\ell_{\mathrm{small}}$ is assumed to be negligible, the large-scale vdW-stress–strain becomes $-\langle\bar{\boldsymbol{\Sigma}}_\ell:\nabla\bar{\boldsymbol{v}}_\ell\rangle_\Omega\simeq 0$ for $\ell\gg\ell_{\mathrm{small}}$. Finally, because the Kolmogorov dissipation scale is assumed to be sufficiently smaller than other length scales and the external force $\boldsymbol{f}$ acts at large scales $\sim L$, the viscous dissipation $\langle\bar D_\ell\rangle_\Omega$ and the energy injection can be approximated as $\langle\bar D_\ell\rangle_\Omega\simeq 0$ and $\langle\varepsilon_\ell^{\mathrm{in}}\rangle_\Omega:=\langle\tilde{\boldsymbol{v}}_\ell\cdot\bar{\boldsymbol{f}}_\ell\rangle_\Omega\simeq\langle\boldsymbol{v}\cdot\boldsymbol{f}\rangle_\Omega$ for $\ell_{\mathrm{small}}\ll\ell\ll\ell_{\mathrm{large}}$ [10,95]. Thus, in the intermediate scale range $\ell_{\mathrm{small}}\ll\ell\ll\ell_{\mathrm{large}}$, (4.39) becomes

$$\langle Q_\ell^{\mathrm{flux}}\rangle_\Omega\simeq\langle p\nabla\cdot\boldsymbol{v}\rangle_\Omega+\langle\boldsymbol{v}\cdot\boldsymbol{f}\rangle_\Omega=:\varepsilon_{\mathrm{eff}}. \tag{4.40}$$

Here, we remark on the existence of the intermediate scale range $\ell_{\rm small} \ll \ell \ll \ell_{\rm large}$. In the above derivation, we have assumed that $-\langle \bar{p}_\ell \nabla \cdot \bar{\boldsymbol{v}}_\ell \rangle_\Omega \simeq -\langle p \nabla \cdot \boldsymbol{v} \rangle_\Omega$ for $\ell \ll \ell_{\rm large}$. In other words, we have assumed that the pressure-dilatation co-spectrum satisfies $E^{(p)}(k) = O(k^{-\alpha})$ with $\alpha > 1$, as in ordinary compressible turbulence [93,94,150,154]. This assumption is based on the decorrelation effects between the large-scale pressure $\bar{p}_\ell$, which mainly acts at large scales, and $\nabla \cdot \bar{\boldsymbol{v}}_\ell$, which becomes significant at small scales as $\|\nabla \cdot \bar{\boldsymbol{v}}_\ell\|_p = O(\|\delta \boldsymbol{v}(\ell)\|_p/\ell)$ [93,94]. For the large-scale vdW-stress–strain, on the other hand, such decorrelation effects are not expected because both $\bar{\boldsymbol{\Sigma}}_\ell$ and $\nabla \bar{\boldsymbol{v}}_\ell$ change rapidly in space. From the similar argument as in (4.38), its scale-dependence can be evaluated as follows:

$$\begin{aligned} \|\bar{\boldsymbol{\Sigma}}_\ell : \nabla \bar{\boldsymbol{v}}_\ell\|_{p/2} &\le \|\bar{\boldsymbol{\Sigma}}_\ell\|_p \|\nabla \bar{\boldsymbol{v}}_\ell\|_p \\ &= O\left(\left(\frac{\ell}{L} \right)^{\sigma_p - 2} \right), \quad p \ge 2. \end{aligned} \tag{4.41}$$

Thus, there possibly exists a characteristic length scale $\ell_{\rm small} \ll \ell_{\rm large}$ such that $\langle \bar{\boldsymbol{\Sigma}}_\ell : \nabla \bar{\boldsymbol{v}}_\ell \rangle_\Omega \simeq 0$ for $\ell \gg \ell_{\rm small}$.

4.6.3 Derivation of the second main result

We first note that the contribution to the energy transfer from the baropycnal work $\Lambda_\ell^{(p)}$ can be ignored because it converges to zero as $\ell/L \to 0$, as shown in (4.32). Therefore, the first main result (4.22) can be further approximated as

$$\langle \Pi_\ell \rangle_\Omega + \langle \Lambda_\ell^{(\Sigma)} \rangle_\Omega \simeq \varepsilon_{\rm eff}. \tag{4.42}$$

From (4.28) and (4.38), it immediately follows that the upper bounds of the mean deformation work $\langle \Pi_\ell \rangle_\Omega$ and mean capillary work $\langle \Lambda_\ell^{(\Sigma)} \rangle_\Omega$ have different ℓ dependences. In particular, the upper bound of $\langle \Pi_\ell \rangle_\Omega$ becomes scale independent when $\sigma_3 = 1/3$, whereas that of $\langle \Lambda_\ell^{(\Sigma)} \rangle_\Omega$ behaves as $O(\ell^{-2/3})$:

$$\langle \Pi_\ell \rangle_\Omega \le \|\Pi_\ell\|_1 = O(1), \tag{4.43}$$

$$\langle \Lambda_\ell^{(\Sigma)} \rangle_\Omega \le \|\Lambda_\ell^{(\Sigma)}\|_1 = O\left(\left(\frac{\ell}{L} \right)^{-2/3} \right), \tag{4.44}$$

When $\sigma_3 = 1$, on the other hand, the upper bound of $\langle \Lambda_\ell^{(\Sigma)} \rangle_\Omega$ becomes constant, whereas that of $\langle \Pi_\ell \rangle_\Omega$ behaves as $O(\ell^2)$:

$$\langle \Pi_\ell \rangle_\Omega \le \|\Pi_\ell\|_1 = O\left(\left(\frac{\ell}{L} \right)^{2} \right), \tag{4.45}$$

$$\langle \Lambda_\ell^{(\Sigma)} \rangle_\Omega \le \|\Lambda_\ell^{(\Sigma)}\|_1 = O(1). \tag{4.46}$$

The above observation and the first main result implies that there exists a characteristic length scale λ such that deformation work is dominant in $\lambda \ll \ell \ll \ell_{\rm large}$, while capillary work becomes dominant in $\ell_{\rm small} \ll \ell \ll \lambda$ (see Fig. 4.2):

$$\langle \Lambda_\ell^{(\Sigma)} \rangle_\Omega \ll \langle \Pi_\ell \rangle_\Omega = O(1) \quad \text{for} \quad \lambda \ll \ell \ll \ell_{\rm large}, \tag{4.47}$$

$$\langle \Pi_\ell \rangle_\Omega \ll \langle \Lambda_\ell^{(\Sigma)} \rangle_\Omega = O(1) \quad \text{for} \quad \ell_{\rm small} \ll \ell \ll \lambda. \tag{4.48}$$

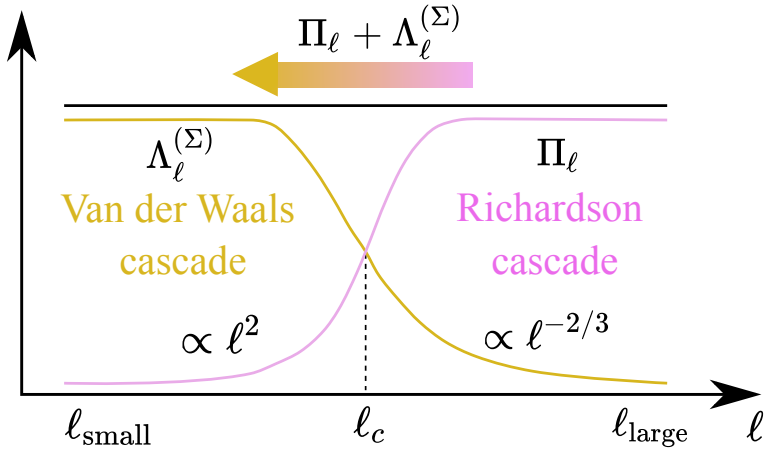

Fig. 4.2: Scale dependence of the scale-to-scale kinetic energy fluxes. The solid lines indicate the upper bounds of the energy fluxes, and the arrow indicates the direction of energy transfer.

The crossover scale λ can be estimated, for instance, as follows. If we use $v_0 := (\rho_0 K_{T_0})^{-1/2}$ and $\rho_0 = \langle\rho\rangle_\Omega$ as the characteristic velocity and density, the deformation work (4.19) and capillary work (4.21) can be evaluated as

$$\Lambda_\ell^{(\Sigma)} \sim \lambda^{-3} T_0 |c_0| \rho_0^2 v_0 \tag{4.49}$$

and

$$\Pi_\ell \sim \rho_0 \ell^{-1} v_0^3. \tag{4.50}$$

Then, the balance condition $\Pi_\lambda \sim \Lambda_\lambda^{(\Sigma)}$ leads to $\lambda \sim \sqrt{T_0|c_0|\rho_0}/v_0$. Thus, in the range of $\ell_c \ll \ell \ll \ell_{\rm large}$, the Richardson cascade, induced by the deformation work, becomes dominant, whereas in the range of $\ell_{\rm small} \ll \ell \ll \ell_c$, the van der Waals cascade, induced by capillary work, develops. From the same argument as in Section 3.5.3, we can estimate the velocity power spectrum as $E^v(k) \propto k^{-5/3}$ for $\ell_{\rm large}^{-1} \ll k \ll \ell_c^{-1}$ and $E^v(k) \propto k^{-3}$ for $\ell_c^{-1} \ll k \ll \ell_{\rm small}^{-1}$.

4.7 Concluding remarks

In summary, we have shown that supercritical turbulence near a critical point can exhibit a novel type of cascade, which we call van der Waals cascade, at scales smaller than the correlation length of equilibrium density fluctuations ξ. This *van der Waals turbulence* is distinct from other known ordinary fluid turbulence in that its cascade reaches the "microscopic length scales" smaller than ξ. Thus, the problem addressed here could lead to an understanding not only of turbulence but also of the relation between the macroscopic and microscopic descriptions of nature. We therefore hope that experiments will be conducted to verify our predictions. Below, we provide some remarks on our results.

Similarity to pure quantum turbulence

Interestingly, the behavior of the van der Waals turbulence is quite similar to those of pure quantum turbulence described in Chapter 3. Indeed, if we replace $c(\rho)$ and T with A/ρ and $-\hbar^2/(4m^2A)$ with some constant A, respectively, the van der Waals stress formally corresponds to the quantum stress. Thus, the mechanisms of the quantum stress cascade

and the van der Waals cascade are essentially the same. Therefore, our results provide an interesting perspective on quantum turbulence, which will help illuminate the role of quantized vortices and Kelvin waves in the energy cascade.

Scale locality of van der Waals cascade

As in pure quantum turbulence, the van der Waals cascade is only ultraviolet local and does not satisfy the sufficient condition to be infrared local (for the scale locality in pure quantum turbulence, see Appendix 3.7.2). Thus, the contributions of large-scale velocity increments could be non-negligible and could contribute to capillary work.

Optimality of the upper bound on capillary work

We note that k^{-3} spectrum for the van der Waals cascade can become shallower due to depletion of nonlinearity [5] or additional assumption on the Besov regularity. For example, we can obtain a tighter bound on the capillary work by further assuming the Besov regularity of the density gradient field $\nabla\rho$:

$$\|\delta(\nabla\rho)(\boldsymbol{r};\cdot)\|_p = O((r/L)^{\sigma_p^{\nabla\rho}}) \quad \text{for} \quad r \ll L, \tag{4.51}$$

with $\sigma_p^{\nabla\rho} \in (0,1]$. In this case, the upper bound of the capillary work can be evaluated as

$$\|\Lambda_\ell^{(\Sigma)}\|_{p/3} = O\left(\left(\frac{\ell}{L}\right)^{\sigma_p+\sigma_p^{\nabla\rho}-1}\right), \quad p \geq 3, \tag{4.52}$$

and the velocity power spectrum can be estimated as $E^v(k) \propto k^{-3+2\sigma_2^{\nabla\rho}}$ for $\ell_c^{-1} \ll k \ll \ell_{\text{small}}^{-1}$. Thus, the spectral exponent associated with the van der Waals cascade possibly depends on the scaling exponent for the density field.

4.8 Appendix

4.8.1 Derivation of the pressure tensor

Here, we derive the pressure tensor ((4.3) and (4.4) in the main text). The equilibrium value of $([u],[\rho]) = (u(\boldsymbol{x}),\rho(\boldsymbol{x}))_{\boldsymbol{x}\in\Omega}$ in the isolated system enclosed by adiabatic walls, denoted as $(u_*(\boldsymbol{x}),\rho_*(\boldsymbol{x}))$, is determined as the maximizer of the entropy functional,

$$\mathcal{S}([u],[\rho]) = \int_\Omega d^3\boldsymbol{x}\left(s(u,\rho) + \frac{c(\rho)}{2}|\nabla\rho|^2\right) \tag{4.53}$$

with the conservation law,

$$\int_\Omega d^3\boldsymbol{x}\rho(\boldsymbol{x})/m = N, \tag{4.54}$$

$$\int_\Omega d^3\boldsymbol{x}u(\boldsymbol{x}) = E, \tag{4.55}$$

where E and N are constants. The variational equation reads

$$\frac{1}{T(u_*,\rho_*)} = \lambda_1, \tag{4.56}$$

$$-\frac{\mu(u_*,\rho_*)}{T(u_*,\rho_*)}+\frac{c'(\rho_*)}{2}|\nabla\rho_*|^2-\nabla\cdot(c(\rho_*)\nabla\rho_*)=\lambda_2, \tag{4.57}$$

where λ_1 and λ_2 are Lagrange multipliers that are physically connected to the equilibrium values of temperature and chemical potential as $\lambda_1 = 1/T^{\mathrm{eq}}$ and $\lambda_2 = -\mu^{\mathrm{eq}}/T^{\mathrm{eq}}$, respectively.

We define

$$\tilde{\mu} := \mu(u,\rho) - T(u,\rho)\left(\frac{c'(\rho)}{2}|\nabla\rho|^2 - \nabla\cdot(c(\rho)\nabla\rho)\right), \tag{4.58}$$

such that the equilibrium condition is given by $\nabla\tilde{\mu} = \mathbf{0}$. We then determine $\tilde{p}$, such that $\nabla\cdot\tilde{p} = \mathbf{0}$ in equilibrium and $\tilde{p} = p(u,\rho)$ when the gradient terms are ignored. To this end, we use a relation,

$$\nabla(p/T) = -u\nabla(1/T) + \rho\nabla(\mu/T), \tag{4.59}$$

which is derived from

$$p = \mu\rho - u + Ts, \tag{4.60}$$

$$\nabla s = \frac{1}{T}\nabla u - \frac{\mu}{T}\nabla\rho. \tag{4.61}$$

We first rewrite the second term on the right-hand side of (4.59) in terms of the generalized chemical potential, $\tilde{\mu}$, as

$$\begin{aligned}\rho\nabla(\mu/T) &= \rho\nabla(\tilde{\mu}/T) - \rho\nabla((\tilde{\mu}-\mu)/T)\\ &= \rho\nabla(\tilde{\mu}/T) - \nabla(\rho(\tilde{\mu}-\mu)/T) + \nabla\cdot\left(-\frac{c}{2}|\nabla\rho|^2\boldsymbol{I} + c\nabla\rho\nabla\rho\right)\\ &= \rho\nabla(\tilde{\mu}/T) - \nabla\cdot\left(\rho c\Delta\rho\boldsymbol{I} + \frac{1}{2}\rho c'|\nabla\rho|^2\boldsymbol{I} + \frac{1}{2}c|\nabla\rho|^2\boldsymbol{I} - c\nabla\rho\nabla\rho\right).\end{aligned} \tag{4.62}$$

Here, we used the relation,

$$(\tilde{\mu}-\mu)/T = -\frac{1}{2}c'|\nabla\rho|^2 + \nabla\cdot(c\nabla\rho), \tag{4.63}$$

which follows from the definition of $\tilde{\mu}$ (4.58). By substituting this result into (4.59), we obtain

$$\nabla(\tilde{p}/T) = -u\nabla(1/T) + \rho\nabla(\tilde{\mu}/T) \tag{4.64}$$

with

$$\tilde{p} = \left(p + T\rho c\Delta\rho + \frac{1}{2}T\rho c'|\nabla\rho|^2 + \frac{1}{2}Tc|\nabla\rho|^2\right)\boldsymbol{I} - Tc\nabla\rho\nabla\rho. \tag{4.65}$$

The equilibrium condition, $\nabla T = \mathbf{0}$ and $\nabla\tilde{\mu} = \mathbf{0}$, leads to $\nabla\cdot\tilde{p} = \mathbf{0}$. In addition, it is evident that $\tilde{p} = p\boldsymbol{I}$ when the density gradient is ignored. In the main text, we used the notation $\boldsymbol{P} = \tilde{p}$ to emphasize that $\tilde{p}$ is a second-order tensor and defined the van der Waals stress $\boldsymbol{\Sigma}$ as

$$\begin{aligned}\boldsymbol{\Sigma} &:= \boldsymbol{P} - p\boldsymbol{I}\\ &= \left(Tc\rho\Delta\rho + \frac{1}{2}Tc'\rho|\nabla\rho|^2 + \frac{1}{2}Tc|\nabla\rho|^2\right)\boldsymbol{I} - Tc\nabla\rho\nabla\rho.\end{aligned} \tag{4.66}$$

4.8.2 Correlation length of equilibrium density fluctuations

In this section, we derive the correlation length of equilibrium density fluctuations and thus confirm that the correlation length is determined by the capillary coefficient and parameters in the entropy density. To this end, we introduce the Helmholtz free energy functional,

$$\mathcal{F}(T,[\rho]) := \int_\Omega d^3\boldsymbol{x}\left(f(T,\rho) - \frac{1}{2}Tc(\rho)|\nabla\rho|^2\right), \tag{4.67}$$

where $f := u - Ts$. Assuming small, slowly varying deviations in density, we consider the expansion of f in terms of the local deviation, $\delta\rho(\boldsymbol{x}) := \rho(\boldsymbol{x}) - \rho_0$, as follows:

$$f(T,\rho) = f(T,\rho_0) + \mu(T,\rho_0)\delta\rho + \frac{1}{2}\frac{1}{\rho_0^2 K_T}(\delta\rho)^2 + \cdots, \tag{4.68}$$

where K_T is the isothermal compressibility, given by

$$K_T := \frac{1}{\rho}\left.\frac{\partial\rho(T,p)}{\partial p}\right|_{\rho=\rho_0}. \tag{4.69}$$

Substituting (4.68) into (4.67), we obtain

$$\begin{aligned}\mathcal{F}(T,[\rho]) &\simeq \int_\Omega d^3\boldsymbol{x}\left(f(T,\rho_0) + \frac{1}{2}\frac{1}{\rho_0^2 K_T}(\delta\rho)^2 - \frac{1}{2}Tc_0|\nabla\rho|^2\right)\\ &= \int_\Omega d^3\boldsymbol{x} f(T,\rho_0) + \delta\mathcal{F}(T,[\rho]),\end{aligned} \tag{4.70}$$

where

$$\delta\mathcal{F}(T,[\rho]) := \int_\Omega d^3\boldsymbol{x}\left(\frac{1}{2}\frac{1}{\rho_0^2 K_T}(\delta\rho)^2 - \frac{1}{2}Tc_0|\nabla\rho|^2\right). \tag{4.71}$$

Here, the first power of $\delta\rho$ has been dropped considering the conservation of particles, and $c(\rho)$ is replaced by $c_0 := c(\rho_0)$ because the difference $c(\rho) - c_0$ is a higher-order contribution.

Introducing the Fourier transform of the density deviation,

$$\delta\hat{\rho}(\boldsymbol{k}) = \frac{1}{V}\int_\Omega d^3\boldsymbol{x} e^{-i\boldsymbol{k}\cdot\boldsymbol{x}}\delta\rho(\boldsymbol{x}), \tag{4.72}$$

where $V := L_\Omega^3$ and $\boldsymbol{k} \in (2\pi/L_\Omega)\mathbb{Z}$, (4.71) becomes

$$\delta\mathcal{F}(T,[\rho]) = \frac{1}{2}V\sum_{\boldsymbol{k}}\left(\frac{1}{\rho_0^2 K_T} - Tc_0k^2\right)|\delta\hat{\rho}(\boldsymbol{k})|^2, \tag{4.73}$$

and $k := |\boldsymbol{k}|$. According to fluctuation theory in equilibrium statistical mechanics, $\delta F(T,[\rho])$ plays a role of an effective Hamiltonian describing density fluctuations of the system with temperature T. That is, the density correlation function takes the Ornstein-Zernike form [194], as follows:

$$\begin{aligned}\langle|\delta\hat{\rho}(\boldsymbol{k})|^2\rangle_\Omega &= \frac{\int\left(\prod_{\boldsymbol{q}} d\delta\hat{\rho}(\boldsymbol{q})\right)|\delta\hat{\rho}(\boldsymbol{k})|^2\exp\left(-\frac{V}{2k_\mathrm{B}T}\sum_{\boldsymbol{q}}\left(\frac{1}{\rho_0^2K_T} - Tc_0q^2\right)|\delta\hat{\rho}(\boldsymbol{q})|^2\right)}{\int\left(\prod_{\boldsymbol{q}} d\delta\hat{\rho}(\boldsymbol{q})\right)\exp\left(-\frac{V}{2k_\mathrm{B}T}\sum_{\boldsymbol{q}}\left(\frac{1}{\rho_0^2K_T} - Tc_0q^2\right)|\delta\hat{\rho}(\boldsymbol{q})|^2\right)}\\ &= \frac{k_\mathrm{B}T}{V}\frac{1}{(\rho_0^2K_T)^{-1} - Tc_0k^2}\\ &= \frac{k_\mathrm{B}}{V|c_0|}\frac{1}{\xi^{-2}+k^2} \quad \text{for} \quad \boldsymbol{k}\neq\boldsymbol{0}.\end{aligned} \tag{4.74}$$

Here, ξ is the correlation length of density fluctuations

$$\begin{aligned}\xi &:= \sqrt{T|c_0|\rho_0^2 K_T} \\ &= \frac{\sqrt{T|c_0|\rho_0}}{v_0},\end{aligned} \tag{4.75}$$

where we introduce a velocity characterized by the isothermal compressibility, as follows:

$$v_0 := \frac{1}{\sqrt{\rho_0 K_T}}. \tag{4.76}$$

As an example, we consider a van der Waals fluid for which the equation of state is given as follows:

$$p(T,\rho) = \frac{k_{\rm B}T}{m}\frac{\rho}{1-b\rho} - a\rho^2, \tag{4.77}$$

where m denotes the mass of a particle; the heat capacity per unit volume is given by

$$c_V(T,\rho) = \eta k_{\rm B}\rho, \tag{4.78}$$

where a, b, and η are constants. In this case, the entropy density is given by

$$s(u,\rho) = \frac{k_{\rm B}}{m}\rho \ln\frac{1-b\rho}{\rho/m} + \eta k_{\rm B}\rho \ln\frac{u+a\rho^2}{\rho/m} + c\rho, \tag{4.79}$$

where c is a constant. The critical density, temperature, and pressure are expressed as

$$\rho_c = \frac{1}{3b}, \quad T_c = \frac{8am}{27bk_{\rm B}}, \quad p_c = \frac{a}{27b^2}, \tag{4.80}$$

respectively. If $\rho_0 = \rho_c$, the isothermal compressibility can be expressed as

$$K_T = \frac{1}{6p_c}\frac{T_c}{T-T_c}. \tag{4.81}$$

From (4.75), (4.79), (4.80), and (4.81), it is straightforward to confirm that the correlation length ξ is determined by the capillary coefficient $c(\rho)$ and the parameters in the entropy density $s(u,\rho)$.

Chapter 5

Simple XY model for cascade transfer

Many phenomena in nature can be regarded as cooperative phenomena in the sense that they emerge from interactions between many components. Even if such interactions are complicated, the resulting cooperative phenomena can be universal regardless of the details of the interactions, allowing for phenomenological understanding. Therefore, if we are interested only in the universal aspect of such a phenomenon, it is sufficient to investigate the simplest model that describes it. Simple models have provided phenomenological perspectives on various phenomena such as critical phenomena [65], phase separation [38, 66], directed percolation [67], surface growth [68, 69], and flocking [70].

Cascade transfer can also be regarded as a nonequilibrium cooperative phenomenon, where inviscid conserved quantities are conservatively transferred across scales due to extremely complicated nonlinear interactions. Remarkably, cascade transfer is also observed even in systems different from fluids, including elastic bodies and spin systems [52–59]. Thus, cascade transfer phenomena are ubiquitous and underlie the universality in various systems. This fact motivates us to systematically classify various cascade phenomena by establishing the concept of a "universality class," as in equilibrium critical phenomena. As a first step toward this end, we have explored novel types of cascade transfer in quantum fluid and supercritical fluid near a critical point in Chapters 3 and 4.

In this chapter, we explore novel cascade phenomena by constructing a simple model representing one universality class for cascade transfer without paying much attention to its relevance to real systems. In constructing the model, we focus on how cascade transfer emerges from spatially local interactions, noting that most existing cascade models have nonlocal interactions [5, 195–197].

The constructed model is a modified XY model with amplitude fluctuations, in which the spin is regarded as the "velocity" of a turbulent field in d dimensions. We show that the model exhibits an inverse "energy" cascade, and we calculate the functional form of the velocity correlation function, which corresponds to the non-Kolmogorov energy spectrum $\propto k^{-3}$. This behavior is quite different from ordinary fluid turbulence even in two dimensions, where the inverse energy cascade inevitably accompanies the enstrophy cascade and the Kolmogorov spectrum.

This chapter is organized as follows. In the next section, we consider the minimum elements required for cascade transfer. In Section 5.2, we introduce our model. Then, its basic properties are described in Section 5.3. The main results are presented in Section 5.4. In Section 5.5, we numerically illustrate these results. The derivation of the main results

are explained in Section 5.6. Concluding remarks are provided in Section 5.7.

5.1 Insights into the cascade transfer

Let us consider the minimum elements required for cascade transfer to occur. Obviously, nonlinearity is indispensable because the essence of cascade transfer is strong inevitable interference between widely separated length scales. Furthermore, this nonlinearity must conserve "energy" if there is neither injection nor dissipation.[1] To ensure the existence of the "inertial range," the injection and dissipation must act at large (small) and small (large) scales, respectively. Thus, the minimum elements required for the "energy" cascade to occur are (i) nonlinearity that conserves "energy"; (ii) injection at large (small) scales; and (iii) dissipation at small (large) scales.

We now construct a simple model for cascade transfer by specifying these three elements. Respecting the ease of the intuitive interpretation of the nonlinear interaction, we consider the two-component "velocity" vector $\boldsymbol{v}_i$ at each site i on a two-dimensional square lattice. In the case shown in Figs. 5.1(a) and 5.1(b), the "energy" $\langle|\boldsymbol{v}_i|^2\rangle/2$ is localized at small and large scales, respectively. For the model to evolve from the state

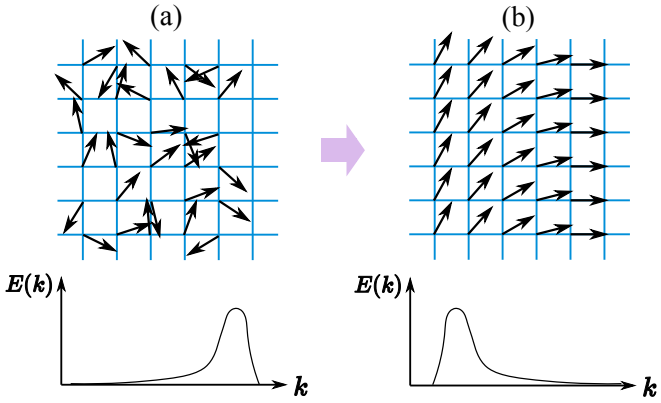

Fig. 5.1: Schematic illustration of the idea of constructing a simple model. The arrow on each site represents the "velocity" of a turbulent field. Bottom panels show the corresponding energy spectrum.

shown in Fig. 5.1(a) to that shown in Fig. 5.1(b) while conserving energy, "ferromagnetic interactions" may be suitable nonlinearity. Because this nonlinear interaction may induce an inverse energy cascade, where the energy is transferred from small to large scales, we must incorporate into the model injection and dissipation terms that act at small and large scales, respectively. To this end, it may be suitable for the ease of analysis to choose a random force that is white in space and time and a friction dissipation.

5.2 Model

Let $\boldsymbol{v}_i(t) := (v_i^1(t), v_i^2(t)) \in \mathbb{R}^2$ be the "velocity" at site i of a d-dimensional hypercubic lattice. For simplicity, we consider a hypercubic lattice with N^d vertices and lattice constant a and impose periodic boundary conditions. The collection of the nearest neighboring sites of i is denoted B_i. The time evolution of v_i^a, $a \in \{1, 2\}$, is given by the following Langevin

[1] Here, we do not consider the case where the nonlinear term itself dissipates energy.

equation:

$$\partial_t v_i^a = \lambda \sum_{j \in B_i} \mathsf{R}^{ab}(\boldsymbol{v}_i) v_j^b - \gamma v_i^a + \sqrt{\varepsilon}\xi_i^a, \tag{5.1}$$

where $\mathsf{R}^{ab}(\boldsymbol{v}_i)$ represents the projection in the direction perpendicular to $\boldsymbol{v}_i$:

$$\mathsf{R}^{ab}(\boldsymbol{v}_i) := \delta^{ab} - \frac{v_i^a v_i^b}{|\boldsymbol{v}_i|^2}. \tag{5.2}$$

Here, $\lambda > 0$ is a coupling constant, $\gamma \geq 0$ is a friction coefficient, and $\varepsilon > 0$ represents the strength of the random force, which is the zero-mean white Gaussian noise that satisfies

$$\langle \xi_i^a(t) \xi_j^b(t') \rangle = \delta^{ab} \delta_{ij} \delta(t - t'), \tag{5.3}$$

and $|\boldsymbol{v}_i|^2 := v_i^c v_i^c$. Here and hereafter, we employ the summation convention for a, b, c that repeated indices in one term are summed over $\{1, 2\}$. A snapshot of the steady-state velocity profile of the model for the case $d = 2$ is shown in Fig. 5.2. Below, we mainly consider the case of $d = 2$, but the extension to any d is straightforward.

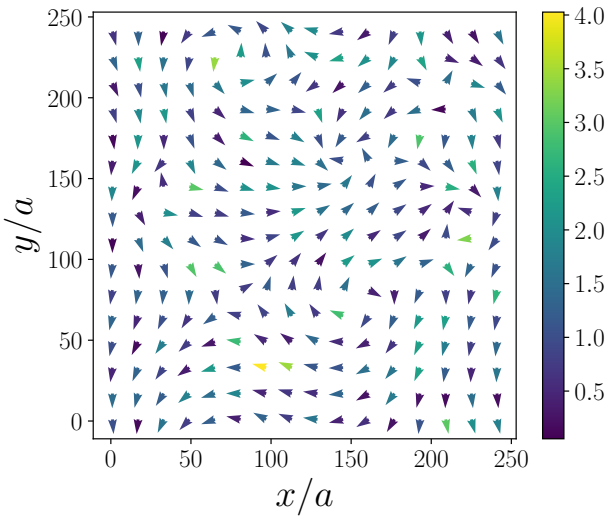

Fig. 5.2: Snapshot of the steady-state velocity profile of the model with $T = \lambda = 1$ and $\gamma = 0.001$. The color bar denotes the magnitude of the velocity vector $|\boldsymbol{v}_i|$.

5.3 Basic properties

Let $|\boldsymbol{v}_i|^2/2$ be the "energy" at site i. A crucial property of the nonlinear term of the model (5.1) is that the term does not contribute to the energy exchange:

$$v_i^a \left(\lambda \sum_{j \in B_i} \mathsf{R}^{ab}(\boldsymbol{v}_i) v_j^b \right) = 0. \tag{5.4}$$

Therefore, the time evolution of $|\boldsymbol{v}_i|^2/2$ is governed only by the dissipation rate $\gamma|\boldsymbol{v}_i|^2$ and injection rate $\sqrt{\varepsilon} v_i^c \circ \xi_i^c$:

$$\partial_t \frac{1}{2} |\boldsymbol{v}_i|^2 = -\gamma |\boldsymbol{v}_i|^2 + \sqrt{\varepsilon} v_i^c \circ \xi_i^c, \tag{5.5}$$

where the symbol $\circ$ denotes multiplication in the sense of Stratonovich [198] (see also Appendix 6.4 of Chapter 6). Thus, if there is neither injection nor dissipation (i.e., $\varepsilon = \gamma = 0$), the energy at site i, $|\boldsymbol{v}_i|^2/2$, is conserved without any averaging. If $\varepsilon > 0$ and $\gamma > 0$, it follows that $\langle |\boldsymbol{v}_i|^2 \rangle = 2T$ in the steady-state, where we have introduced the "temperature" as $T := \varepsilon/2\gamma$.

It becomes easier to understand the behavior of the model by introducing the amplitude A_i and the phase θ_i as $\boldsymbol{v}_i = A_i(\cos\theta_i, \sin\theta_i)$. In terms of A_i and θ_i, (5.1) can be expressed as (see Appendix 5.8.1)

$$\partial_t A_i = -\gamma A_i + \frac{\varepsilon}{2A_i} + \sqrt{\varepsilon}\xi_i^A, \tag{5.6}$$

$$A_i \partial_t \theta_i = -\lambda \sum_{j \in B_i} A_j \sin(\theta_i - \theta_j) + \sqrt{\varepsilon}\xi_i^\theta. \tag{5.7}$$

Here, $\xi_i^A := \xi_i^1 \cos\theta_i + \xi_i^2 \sin\theta_i$ and $\xi_i^\theta := -\xi_i^1 \sin\theta_i + \xi_i^2 \cos\theta_i$, where the multiplication is interpreted in the Ito sense [198] (see also Appendix 6.4 of Chapter 6). Note that (5.7) has the form of the random-bond XY model with asymmetric coupling. If A_i is frozen uniformly in space, the system exhibits the Kosterlitz-Thouless transition [199–201]. Therefore, we can say that this model is a modified XY model with amplitude (energy) fluctuations. We emphasize that, in contrast with the standard XY model, the detailed balance is broken in our model due to the amplitude fluctuations (see Appendix 5.8.2). The absence of the detailed balance is necessary for the cascade transfer to occur in the steady-state.

In the following, we use the property that the energy dissipation and injection act at large and small scales, respectively. Let $K_i \equiv \ell_i^{-1}$ be the energy injection scale. Since the injection due to the noise ξ_i^a acts with uniform strength on each Fourier mode, K_i can be defined, for instance, as

$$K_i := \frac{2\pi}{L}\frac{1}{N^d} \sum_{n_1=-N/2+1}^{N/2} \cdots \sum_{n_d=-N/2+1}^{N/2} \sqrt{n_1^2 + \cdots + n_d^2}, \tag{5.8}$$

where $L := Na$. The energy injection due to the "thermal noise" mainly acts at scales $\ll \ell_i$. Similarly, let $K_\gamma \equiv \ell_\gamma^{-1}$ be the dissipation scale. This scale may depend on the friction coefficient γ and dissipation rate $\gamma\langle |\boldsymbol{v}_i|^2 \rangle = \varepsilon$. Therefore, K_γ is defined as $K_\gamma := \gamma^{3/2}\varepsilon^{-1/2}$ [202–204]. We thus expect that the dissipation is dominant at scales $\gg \ell_\gamma$. Note that $K_\gamma \to 0$ as $\gamma \to 0$.

5.4 Main result

Let $\Pi(k)$ be the scale-to-scale energy flux, which represents the energy transfer from scales $> k^{-1}$ to scales $< k^{-1}$. (The precise definition is given below.) In the steady-state, $\Pi(k)$ becomes scale independent in the "inertial range" $K_\gamma \ll k \ll K_i$:

$$\Pi(k) \simeq -\varepsilon < 0. \tag{5.9}$$

Since $\Pi(k)$ is negative, (5.9) states that the model exhibits an inverse energy cascade; i.e., the energy is transferred conservatively and continuously from small to large scales. Correspondingly, the equal-time correlation function $C(\boldsymbol{\ell}) := \langle v_i^c v_l^c \rangle$, where $\boldsymbol{\ell} := \boldsymbol{r}_i - \boldsymbol{r}_l$ and $\boldsymbol{r}_i$ denotes the position of site i, follows a power law:

$$C(\boldsymbol{\ell}) \sim \frac{1}{16}(\lambda a^2)^{-1}\varepsilon\ell^2 \quad \text{for} \quad \ell_i \ll \ell \ll \ell_\gamma. \tag{5.10}$$

From (5.10), the one-dimensional energy spectrum $E^{(1D)}(k)$ reads

$$E^{(1D)}(k) \sim C(\lambda a^2)^{-1}\varepsilon k^{-3} \quad \text{for} \quad K_\gamma \ll k \ll K_i, \tag{5.11}$$

where C is a positive dimensionless constant.

5.5 Numerical simulation

We here present the results of numerical simulation for the case $d = 2$ (see Appendix 5.8.3 for three-dimensional case). Time integration is performed using the simplest discretization method with $\Delta t = 0.01$. The initial value of v_i^a is set as $v_i^a(0) = \sqrt{\varepsilon}\Delta W_i^a$, where $\{\Delta W_i^a\}$ denote the independent Wiener processes with variance Δt. The parameter values are chosen as $\lambda = 1$, $\varepsilon = 0.002$, and $\gamma = 0.001$, so that $T = 1$. The system size is fixed as $N = 1024$ with $a = 1$. In this case, the injection and dissipation scales are estimated as $K_i a \simeq 2.41$ and $K_\gamma a \simeq 1 \times 10^{-3}$, respectively. Note that K_i does not increase but approaches a constant value as N increases.

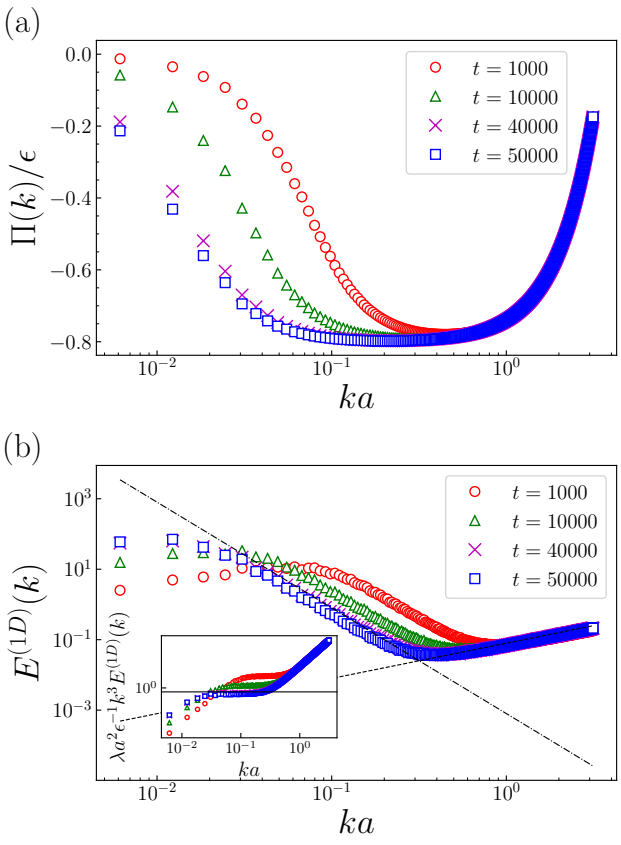

Fig. 5.3: Scale dependence of (a) the scale-to-scale energy flux $\Pi(k)/\varepsilon$ and (b) the energy spectrum $E^{(1D)}(k)$ with $T = \lambda = 1$ and $\gamma = 0.001$ at different times. The dash-dotted and dotted lines represent the power-laws $\propto k^{-3}$ and $\propto k$, respectively. The inset shows the compensated energy spectrum $\lambda a^2\varepsilon^{-1}k^3E^{(1D)}(k)$, where the solid line represents $C = 1/2$.

Figure 5.3(a) shows the scale dependence of the scale-to-scale energy flux $\Pi(k)$ at different times. As expected from the result (5.9), $\Pi(k)$ is negative and scale independent in the inertial range $K_\gamma \ll k \ll K_i$. The magnitude of $\Pi(k)$ in the inertial range is on

the order of ε, i.e., $\Pi(k)/\varepsilon \simeq -1$, which is consistent with (5.9). Furthermore, the scale range over which $\Pi(k)$ is nearly constant extends to larger scales as time increases. This result also supports that the energy is continuously transferred from small to large scales. In Fig. 5.3(b), we plot the one-dimensional energy spectrum $E^{(1D)}(k)$ for the same times as in Fig. 5.3(a). In the inertial range, $E^{(1D)}(k)$ follows the power law $\propto k^{-3}$, which is consistent with the theoretical prediction (5.11). At scales smaller than the injection scale K_i, $E^{(1D)}(k)$ is proportional to k. This result implies that the "equipartition of energy" is realized for small scales $\gtrsim K_i$. We can also confirm the existence of the inverse energy cascade by noting that the spectrum extends to larger scales as time passes. Note that the range over which $\Pi(k)$ is flat does not exactly correspond to the range over which $E^{(1D)}(k) \propto k^{-3}$. This discrepancy is similar to that observed in ordinary fluid turbulence [16].

5.6 Derivation of the main result

Let $\hat{v}^a_{\boldsymbol{k}}$ be the discrete Fourier transform of v^a_i with $\boldsymbol{k} := 2\pi \boldsymbol{n}/L$, where $n^1, n^2 \in \{-N/2+1, \cdots, 0, 1, \cdots, N/2\}$. We define the low-pass filtering operator by

$$\mathcal{P}^{<K} : \boldsymbol{v}_i \mapsto \boldsymbol{v}_i^{<K} := \sum_{|\boldsymbol{k}|<K} \hat{\boldsymbol{v}}_{\boldsymbol{k}} e^{i\boldsymbol{k}\cdot\boldsymbol{r}_i}, \tag{5.12}$$

where $\sum_{|\boldsymbol{k}|<K}$ denotes the sum over all possible $\boldsymbol{k}$ that satisfy $|\boldsymbol{k}| < K$. This operator sets to zero all Fourier components with a wavenumber larger than K. By applying this operator to both sides of (5.1) and taking the average, we obtain the low-pass filtered energy balance equation:

$$\partial_t \frac{1}{2}\langle |\boldsymbol{v}_i^{<K}|^2 \rangle = -\Pi(K) - \gamma \langle |\boldsymbol{v}_i^{<K}|^2 \rangle + \sqrt{\varepsilon}\langle \boldsymbol{v}_i^{<K} \circ \boldsymbol{\xi}_i^{<K} \rangle, \tag{5.13}$$

where

$$\Pi(K) := -\lambda \left\langle \boldsymbol{v}_i^{<K} \cdot \mathcal{P}^{<K} \left[\sum_{j \in B_i} \mathsf{R}(v_i) \cdot \boldsymbol{v}_j \right] \right\rangle \tag{5.14}$$

denotes the scale-to-scale energy flux. Note that only $\Pi(K)$ includes the contribution from the Fourier modes with $|\boldsymbol{k}| \geq K$ because of the nonlinear interaction. The dissipation mainly acts at scales $\gg \ell_\gamma$, and it follows that $\gamma\langle |\boldsymbol{v}_i^{<K}|^2 \rangle \simeq \gamma \langle |\boldsymbol{v}_i^{<K_\gamma}|^2 \rangle \simeq \gamma \langle |\boldsymbol{v}_i|^2 \rangle$ for $K_\gamma \ll K$. Similarly, because the injection mainly acts at scales $\ll \ell_i$, $\langle \boldsymbol{v}_i^{<K} \circ \boldsymbol{\xi}_i^{<K} \rangle \simeq 0$ for $K \ll K_i$. Therefore, in the steady-state, we obtain

$$\begin{aligned} \Pi(K) &= -\gamma \langle |\boldsymbol{v}_i^{<K}|^2 \rangle + \sqrt{\varepsilon}\langle \boldsymbol{v}_i^{<K} \circ \boldsymbol{\xi}_i^{<K} \rangle \\ &\simeq -\gamma \langle |\boldsymbol{v}_i|^2 \rangle \\ &= -\varepsilon < 0 \quad \text{for} \quad K_\gamma \ll K \ll K_i. \end{aligned} \tag{5.15}$$

The model thus exhibits the inverse energy cascade; i.e., the energy is transferred conservatively from small to large scales in the "inertial range" $K_\gamma \ll K \ll K_i$. Note that the above argument is essentially the same as that for the two-dimensional fluid turbulence [202–205].

We now determine the functional form of the energy spectrum. To this end, we express the energy flux in terms of the velocity correlation function as in the derivation of the

Kolmogorov 4/5-law (see Section 1.3). We first note that $\Pi(K)$ can be rewritten as

$$\begin{aligned}\Pi(K) &= -\,\partial_t \frac{1}{2}\langle|\boldsymbol{v}_i^{<K}|^2\rangle\Big|_{\mathrm{NL}} \\ &= -\sum_{|\boldsymbol{k}|<K}\frac{1}{N^2}\sum_{\boldsymbol{r}_j-\boldsymbol{r}_l} e^{-i\boldsymbol{k}\cdot(\boldsymbol{r}_j-\boldsymbol{r}_l)}\,\partial_t\frac{1}{2}\langle v_j^c v_l^c\rangle\Big|_{\mathrm{NL}},\end{aligned} \tag{5.16}$$

where $\partial_t\cdot|_{\mathrm{NL}}$ denotes the time evolution due to the nonlinear term. By taking the continuum limit, (5.16) can be expressed as

$$\begin{aligned}\Pi(K) &= -\int_{|\boldsymbol{k}|<K}\frac{d^2\boldsymbol{k}}{(2\pi)^2}\int d^2\boldsymbol{\ell}e^{-i\boldsymbol{k}\cdot\boldsymbol{\ell}}\varepsilon(\ell) \\ &= -\int_0^\infty K d\ell J_1(K\ell)\varepsilon(\ell).\end{aligned} \tag{5.17}$$

Here, J_1 is the Bessel function of the first kind and we have assumed the homogeneity $\varepsilon(\boldsymbol{\ell}) := \partial_t\langle v^c(\boldsymbol{\ell})v^c(\boldsymbol{0})\rangle/2|_{\mathrm{NL}} = \partial_t\langle v^c(\boldsymbol{r}_j)v^c(\boldsymbol{r}_l)\rangle/2|_{\mathrm{NL}}$ and isotropy $\varepsilon(\boldsymbol{\ell}) = \varepsilon(\ell)$ with $\boldsymbol{\ell} := \boldsymbol{r}_j - \boldsymbol{r}_l$. We now substitute (5.17) into the relation (5.15) to find

$$\int_0^\infty dx J_1(x)\varepsilon\left(\frac{x}{K}\right) \simeq \varepsilon \quad \text{for} \quad K_\gamma \ll K \ll K_i. \tag{5.18}$$

By taking first the limit $\gamma \to 0$ ($K_\gamma \to 0$) and then the limit $K \to 0$, we obtain, for large ℓ, [5]

$$\varepsilon(\ell) \simeq \varepsilon, \tag{5.19}$$

where we have used the identity $\int_0^\infty dx J_1(x) = 1$. A simple expression for $\varepsilon(\ell)$ can be obtained by noting that $\boldsymbol{v}_i$ tends to align with $\langle\langle\boldsymbol{v}_i\rangle\rangle := \sum_{j\in B_i}\boldsymbol{v}_j/4$ because of the nonlinearity of the model. In other words, for the angle α_i between $\hat{\boldsymbol{v}}_i := \boldsymbol{v}_i/|\boldsymbol{v}_i|$ and $\langle\langle\boldsymbol{v}_i\rangle\rangle/|\langle\langle\boldsymbol{v}_i\rangle\rangle|$, we conjecture that $\alpha_i \ll 1$ in the steady-state. Therefore, by assuming that each angle between $\hat{\boldsymbol{v}}_i$ and its nearest neighbor $\hat{\boldsymbol{v}}_j$ is on the order of $\alpha_i \ll 1$, we find that

$$\begin{aligned}\mathsf{R}^{ab}(\boldsymbol{v}_i)\langle\langle v_i^b\rangle\rangle &= \langle\langle v_i^a\rangle\rangle - \hat{v}_i^a|\langle\langle\boldsymbol{v}_i\rangle\rangle|\cos\alpha_i \\ &\simeq \langle\langle v_i^a\rangle\rangle - \hat{v}_i^a|\langle\langle\boldsymbol{v}_i\rangle\rangle| \\ &\simeq \langle\langle v_i^a\rangle\rangle - v_i^a + \hat{v}_i^a\left(A_i - \langle\langle A_i\rangle\rangle\right).\end{aligned} \tag{5.20}$$

Since $\{A_i\}$ are independent and identically distributed random variables, we obtain from (5.20) that

$$\begin{aligned}\partial_t\,\frac{1}{2}\langle v_j^c v_l^c\rangle\Big|_{\mathrm{NL}} &= 2\lambda\left[\left\langle v_l^a\mathsf{R}^{ac}(\boldsymbol{v}_j)\langle\langle v_j^c\rangle\rangle\right\rangle + \left\langle v_j^a\mathsf{R}^{ac}(\boldsymbol{v}_l)\langle\langle v_l^c\rangle\rangle\right\rangle\right] \\ &\simeq 2\lambda\left[\left\langle v_l^c\left[\langle\langle v_j^c\rangle\rangle - v_j^c\right]\right\rangle + \left\langle v_j^c\left[\langle\langle v_l^c\rangle\rangle - v_l^c\right]\right\rangle\right],\end{aligned} \tag{5.21}$$

for $|\boldsymbol{r}_j - \boldsymbol{r}_l| > a$. Note that $\langle\langle\cdot\rangle\rangle - \cdot$ is the discrete Laplacian. Therefore, $\varepsilon(\ell)$ in (5.19) can be expressed in terms of $C(\ell) := \langle v^c(\boldsymbol{r}_j)v^c(\boldsymbol{r}_l)\rangle$:

$$4\lambda a^2\left(\frac{\partial^2}{\partial\ell^2} + \frac{1}{\ell}\frac{\partial}{\partial\ell}\right)C(\ell) \simeq \varepsilon. \tag{5.22}$$

It follows from this equation that

$$C(\ell) \sim \frac{1}{16}(\lambda a^2)^{-1}\varepsilon\ell^2 \quad \text{for} \quad \ell_i \ll \ell \ll \ell_\gamma. \tag{5.23}$$

Correspondingly, the asymptotic behavior of the one-dimensional energy spectrum $E^{(1D)}(k)$ in the inertial range reads

$$E^{(1D)}(k) \sim C(\lambda a^2)^{-1}\varepsilon k^{-3} \quad \text{for} \quad K_\gamma \ll k \ll K_i, \tag{5.24}$$

where C is a dimensionless positive constant.

5.7 Concluding remarks

One of the fundamental properties of cascades that we have not discussed here is scale locality [157, 170, 206]. From the fact that the energy flux and spectrum gradually extend to larger scales as time passes (see Fig. 5.3), it seems that the inverse cascade is scale-local. However, a numerical study of scale locality implies that it is not scale-local (see Appendix 5.8.4), although there remains a problem of how to define the scale locality. A more detailed study on the scale locality should be carried out in the future.

Interestingly, the behavior of the energy spectrum $E^{(1D)}(k) \propto k^{-3}$ at large scales is also observed in atmospheric turbulence. In the upper troposphere and lower stratosphere, $E^{(1D)}(k) \propto k^{-5/3}$ at scales between 10 and 500 km while $E^{(1D)}(k) \propto k^{-3}$ at scales between 500 and 3000 km [205, 207–212]. We also note that turbulent behavior similar to that of our model is found in so-called spin turbulence [54–59] and Fibonacci turbulence [213]. It would thus be interesting to investigate the relationship between these systems and our model.

In conclusion, we constructed a modified XY model in which cascade transfer emerges. Because this inverse cascade induces the non-Kolmogorov spectrum $E^{(1D)}(k) \propto k^{-3}$, it represents a different universality class from ordinary fluid turbulence. We thus hope that our model triggers further investigation of cascade transfer in various systems such as condensed matter, active matter, and other statistical mechanical systems.

5.8 Appendix

5.8.1 Derivation of (5.6) and (5.7)

The model (5.1) is mathematically the following stochastic differential equation (for stochastic differential equation, see Appendix 6.4 of Chapter 6):

$$dv_i^a = \lambda \sum_{j \in B_i} \mathsf{R}^{ab}(\boldsymbol{v}_i) v_j^b dt - \gamma v_i^a dt + \sqrt{\varepsilon} dW_i^a, \tag{5.25}$$

where W_i^a denotes the independent Wiener process. We set $\boldsymbol{v}_i = A_i(\cos\theta_i, \sin\theta_i)$ and $a_i := \ln A_i$, so that

$$a_i + i\theta_i = \ln(v_i^1 + iv_i^2). \tag{5.26}$$

By using the Ito calculus [198], we obtain

$$\begin{aligned}
d(a_i + i\theta_i) &= \frac{d(v_i^1 + iv_i^2)}{v_i^1 + iv_i^2} - \frac{[d(v_i^1 + iv_i^2)]^2}{2(v_i^1 + iv_i^2)^2} \\
&= \frac{\lambda}{v_i^1 + iv_i^2}\left(\sum_{j\in B_i} \mathsf{R}^{1b}(\boldsymbol{v}_i)v_j^b + i\sum_{j\in B_i} \mathsf{R}^{2b}(\boldsymbol{v}_i)v_j^b\right)dt - \gamma dt + \frac{\sqrt{\varepsilon}}{v_i^1 + iv_i^2}(dW_i^1 + idW_i^2) \\
&\quad - \frac{\varepsilon}{2(v_i^1 + iv_i^2)^2}(dW_i^1 + idW_i^2)^2 \\
&= \lambda e^{-a_i - i\theta_i}\sum_{j\in B_i}\big[(1-\cos^2\theta_i)A_j\cos\theta_j - \cos\theta_i\sin\theta_i A_j\sin\theta_j \\
&\quad -i\cos\theta_i\sin\theta_i A_j\cos\theta_j + i(1-\sin^2\theta_i)A_j\sin\theta_j\big]\,dt \\
&\quad - \gamma dt + \sqrt{\varepsilon}e^{-a_i - i\theta_i}(dW_i^1 + idW_i^2)
\end{aligned} \tag{5.27}$$

By taking the real and imaginary parts, we obtain

$$da_i = -\gamma dt + \sqrt{\varepsilon}e^{-a_i}dW_i^A, \tag{5.28}$$

$$d\theta_i = e^{-a_i}\left[-\lambda\sum_{j\in B_i} A_j\sin(\theta_i - \theta_j)dt + \sqrt{\varepsilon}dW_i^\theta\right], \tag{5.29}$$

where $dW_i^A := \cos\theta_i dW_i^1 + \sin\theta_i dW_i^2$ and $dW_i^\theta = -\sin\theta_i dW_i^1 + \cos\theta_i dW_i^2$. Therefore,

$$\begin{aligned}
dA_i &= A_i da_i + \frac{1}{2}A_i(da_i)^2 \\
&= -\gamma A_i dt + \frac{\varepsilon}{2A_i}dt + \sqrt{\varepsilon}dW_i^A,
\end{aligned} \tag{5.30}$$

$$A_i d\theta_i = -\lambda\sum_{j\in B_i} A_j\sin(\theta_i - \theta_j)dt + \sqrt{\varepsilon}dW_i^\theta. \tag{5.31}$$

5.8.2 Violation of detailed balance

The Fokker-Planck equation corresponding the model (5.1) reads

$$\partial_t P_t(\{v_i^a\}) = -\sum_i \frac{\partial}{\partial v_i^a}\left(\lambda\sum_{j\in B_i}\mathsf{R}^{ab}(\boldsymbol{v}_i)v_j^b - \gamma v_i^a - \frac{\varepsilon}{2}\frac{\partial}{\partial v_i^a}\right)P_t(\{v_i^a\}), \tag{5.32}$$

where $P_t(\{v_i^a\})$ denotes the probability density of finding $\{v_i^a\}$ at time t. Note that, regardless of whether the "velocity" variables $\{v_i^a\}$ are even or odd under time reversal, the drift term is irreversible. Therefore, the necessary and sufficient condition for the system to have a stationary distribution that satisfies detailed balance is [198]

$$\begin{aligned}
\frac{\partial}{\partial v_i^a}\ln P_{\rm ss}(\{v_i^a\}) &= \frac{2}{\varepsilon}\left[\lambda\sum_{j\in B_i}\mathsf{R}^{ab}(\boldsymbol{v}_i)v_j^b - \gamma v_i^a\right] \\
&=: Z_i^a(\{v_i^a\}),
\end{aligned} \tag{5.33}$$

which expresses the vanishing of the probability current. However, this condition cannot be satisfied because

$$\frac{\partial Z_i^a}{\partial v_j^b} \neq \frac{\partial Z_j^b}{\partial v_i^a} \quad \text{for} \quad j \in B_i, \tag{5.34}$$

in general. In fact,

$$\frac{\partial Z_i^a}{\partial v_j^b} = \frac{2\lambda}{\varepsilon}\left(\delta^{ab} - \frac{v_i^a v_i^b}{|\boldsymbol{v}_i|^2}\right), \tag{5.35}$$

whereas

$$\frac{\partial Z_j^b}{\partial v_i^a} = \frac{2\lambda}{\varepsilon}\left(\delta^{ab} - \frac{v_j^a v_j^b}{|\boldsymbol{v}_j|^2}\right). \tag{5.36}$$

5.8.3 Three-dimensional case

In this section, we present the numerical result for the three-dimensional case with two-component velocity $\boldsymbol{v}_i$. Even for this case, we can derive the inverse energy cascade with k^{-3} spectrum: for $K_\gamma \ll k \ll K_i$,

$$\Pi(k) \simeq -\varepsilon \tag{5.37}$$

and

$$E^{(1D)}(k) \sim C(\lambda a^2)^{-1}\varepsilon k^{-3}, \tag{5.38}$$

where C is a positive dimensionless constant. In Fig. 5.4, we plot the scale dependence of the energy flux $\Pi(k)$ and spectrum $E^{(1D)}(k)$. The parameter values and the system size are chosen as $\lambda = 1$, $\varepsilon = 0.002$, $\gamma = 0.001$, and $N = 128$ with $a = 1$. In this case, the injection and dissipation scales are estimated as $K_i a \simeq 3.02$ and $K_\gamma a \simeq 1 \times 10^{-3}$. This result is consistent with the prediction (5.37) and (5.38). Note that, in this case, $E^{(1D)}(k) \propto k^2$ at small scales, whereas it is proportional to $E^{(1D)}(k) \propto k$ in the two-dimensional case. This result also implies that the "equipartition of energy" is realized for small scales.

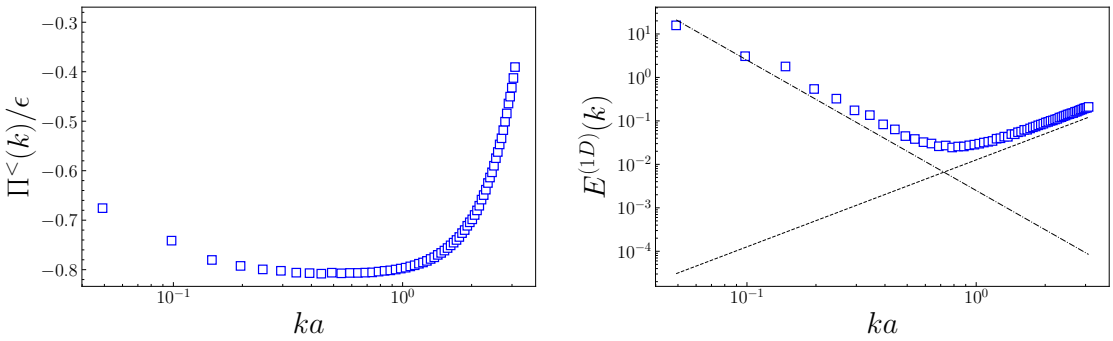

Fig. 5.4: The scale-to-scale energy flux $\Pi(k)/\varepsilon$ (left). The energy spectrum $E^{(1D)}(k)$ (right). The dash-dotted and dotted lines represent the power laws $\propto k^{-3}$ and $\propto k^2$, respectively.

5.8.4 Scale locality

In this section, we numerically investigate the scale locality of the inverse energy cascade. An energy cascade is scale-local if modes that make a significant contribution to energy transfer at each scale are limited to those in the vicinity of that scale. More precisely, we define the scale locality of the inverse energy cascade for our model as follows [157,170,206]. We first note that the scale-to-scale energy flux $\Pi(K) := -\lambda\langle \boldsymbol{v}_i^{<K} \cdot \mathcal{P}^{<K}[\sum_{j\in B_i} \mathsf{R}(\boldsymbol{v}_i)\cdot\boldsymbol{v}_j]\rangle$ has a form of "velocity" $\boldsymbol{v}_i^{<K}$ times "force" $\lambda\mathcal{P}^{<K}[\sum_{j\in B_i}\mathsf{R}(\boldsymbol{v}_i)\cdot\boldsymbol{v}_j]$. We describe the energy flux as infrared local if $|\lambda\langle \boldsymbol{v}_i^{<Q}\cdot\mathcal{P}^{<K}[\sum_{j\in B_i}\mathsf{R}(\boldsymbol{v}_i)\cdot\boldsymbol{v}_j]\rangle|$ and $|\lambda\langle \boldsymbol{v}_i^{<K}\cdot\mathcal{P}^{<K}[\sum_{j\in B_i}\mathsf{R}(\boldsymbol{v}_i^{<Q})\cdot$

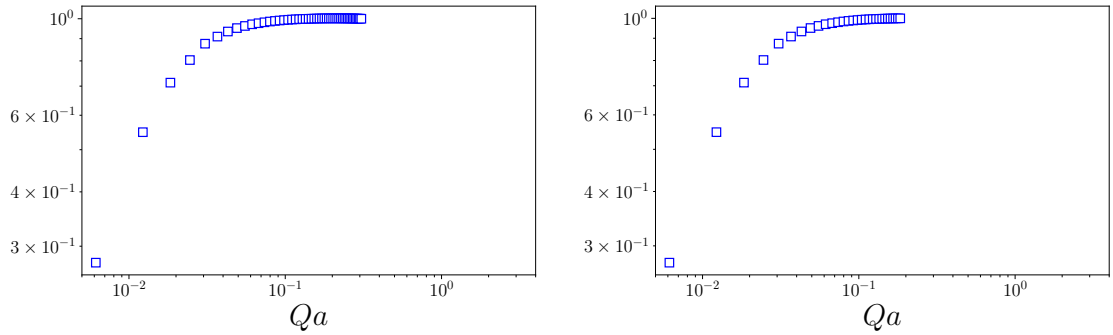

Fig. 5.5: Q-dependence of $|\lambda\langle \boldsymbol{v}_i^{<Q}\cdot\mathcal{P}^{<K}[\sum_{j\in B_i}\mathsf{R}(\boldsymbol{v}_i)\cdot\boldsymbol{v}_j]\rangle/\Pi(K)|$ for $Ka\simeq 0.31$ (left) and $Ka\simeq 0.18$ (right).

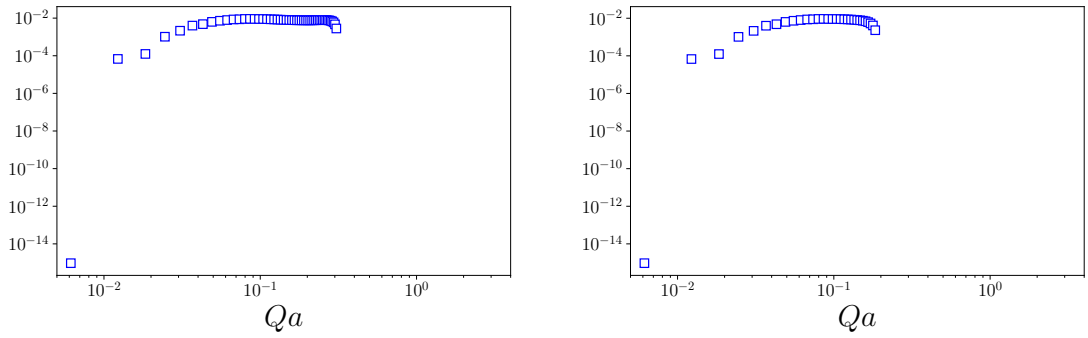

Fig. 5.6: Q-dependence of $|\lambda\langle \boldsymbol{v}_i^{<K}\cdot\mathcal{P}^{<K}[\sum_{j\in B_i}\mathsf{R}(\boldsymbol{v}_i^{<Q})\cdot\boldsymbol{v}_j^{<Q}]\rangle/\Pi(K)|$ for $Ka\simeq 0.31$ (left) and $Ka\simeq 0.18$ (right).

$\boldsymbol{v}_j^{<Q}]\rangle|$ gives an asymptotically negligible contribution for $Q\ll K$. That is, the energy flux satisfies the infrared locality if $|\lambda\langle \boldsymbol{v}_i^{<Q}\cdot\mathcal{P}^{<K}[\sum_{j\in B_i}\mathsf{R}(\boldsymbol{v}_i)\cdot\boldsymbol{v}_j]\rangle|$ and $|\lambda\langle \boldsymbol{v}_i^{<K}\cdot\mathcal{P}^{<K}[\sum_{j\in B_i}\mathsf{R}(\boldsymbol{v}_i^{<Q})\cdot\boldsymbol{v}_j^{<Q}]\rangle|$ decay as fast as $(Q/K)^\alpha$ with $\alpha>0$ for $Q\ll K$. Here, we have used the fact that $(\boldsymbol{v}_i^{<Q})^{<K}=\boldsymbol{v}_i^{<Q}$ for $Q\le K$. Similarly, we describe the energy flux as ultraviolet local if $|\lambda\langle \boldsymbol{v}_i^{<K}\cdot\mathcal{P}^{<K}[\sum_{j\in B_i}\mathsf{R}(\boldsymbol{v}_i^{>Q})\cdot\boldsymbol{v}_j^{>Q}]\rangle|$ decays as fast as $(Q/K)^{-\alpha}$ with $\alpha>0$ for $Q\gg K$. Here, we do not need to consider $|\lambda\langle(\boldsymbol{v}_i^{>Q})^{<K}\cdot\mathcal{P}^{<K}[\sum_{j\in B_i}\mathsf{R}(\boldsymbol{v}_i)\cdot\boldsymbol{v}_j]\rangle|$ because $(\boldsymbol{v}_i^{>Q})^{<K}=\boldsymbol{0}$ for $Q\ge K$.

We here remark that the energy flux $\Pi(K)$ in our model cannot be scale-local without averaging. That is, because $\Pi(K)$ is not Galilean invariant, a $\boldsymbol{k}=\boldsymbol{0}$ mode can directly contribute to the unaveraged energy flux if we boost the flow with a uniform velocity $\boldsymbol{U}$, i.e., $\boldsymbol{v}_i\mapsto\boldsymbol{v}_i+\boldsymbol{U}$ for all i. Note that this property is the same as the *unsubtracted flux* for fluid turbulence [170]. Even though the unaveraged flux is not scale-local, the averaged flux $\Pi(K)$ may become scale-local because of the cancellation of the large-scale contribution.

We now present the results of numerical simulation. The parameter values and system size are the same as in the main text: $\lambda=1$, $\varepsilon=0.002$, $\gamma=0.001$, and $N=1024$ with $a=1$, so that the injection and dissipation scales are estimated as $K_ia\simeq 2.41$ and $K_\gamma a\simeq 1\times10^{-3}$. We first consider the infrared locality. For the infrared locality, we

investigate the Q-dependence of the following quantities:

$$\left| \lambda \left\langle \boldsymbol{v}_i^{<Q} \cdot \mathcal{P}^{<K} \left[\sum_{j \in B_i} \mathsf{R}(\boldsymbol{v}_i) \cdot \boldsymbol{v}_j \right] \right\rangle \right|, \tag{5.39}$$

$$\left| \lambda \left\langle \boldsymbol{v}_i^{<K} \cdot \mathcal{P}^{<K} \left[\sum_{j \in B_i} \mathsf{R}(\boldsymbol{v}_i^{<Q}) \cdot \boldsymbol{v}_j^{<Q} \right] \right\rangle \right|. \tag{5.40}$$

We calculated these two quantities for $Ka \simeq 0.31$ and $Ka \simeq 0.18$ ($K = 2\pi n/Na$ with $n = 50$ and 30, respectively), which is within the inertial range: $K_\gamma \ll K \ll K_i$. Figures 5.5 and 5.6 show the Q-dependences of these quantities at $t = 50000$ normalized by $|\Pi(K)|$ with $Q < K$ for $Ka \simeq 0.31$ and $Ka \simeq 0.18$, respectively. Although both quantities decay as $Q \to 0$, they are almost flat in the inertial range $K_\gamma \ll Q < K \ll K_i$. This result implies that the inverse cascade is not strictly infrared local. In other words, the contributions to the energy flux from large-scale modes may not be ignored.

For the ultraviolet locality, we investigate the Q-dependence of the following quantity:

$$\left| \lambda \left\langle \boldsymbol{v}_i^{<K} \cdot \mathcal{P}^{<K} \left[\sum_{j \in B_i} \mathsf{R}(\boldsymbol{v}_i^{>Q}) \cdot \boldsymbol{v}_j^{>Q} \right] \right\rangle \right|. \tag{5.41}$$

The result is shown in Fig. 5.7. As in the case of the infrared locality, this quantity does not decay rapidly in the inertial range $K_\gamma \ll K < Q \ll K_i$. Therefore, small-scale modes may contribute significantly to the energy flux.

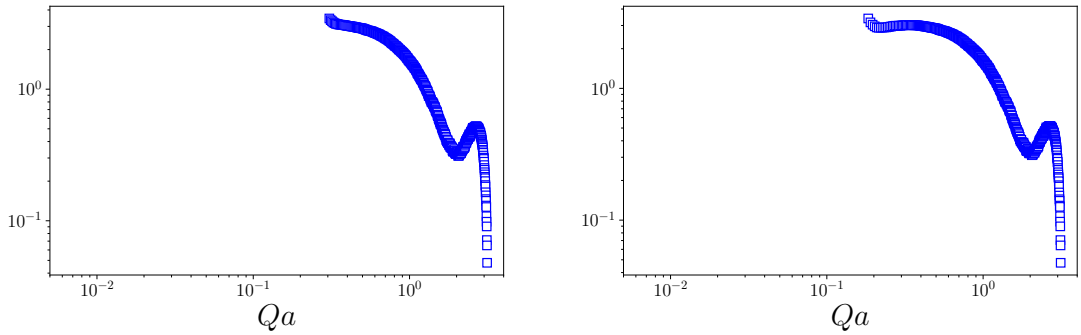

Fig. 5.7: Q-dependence of $|\lambda\langle \boldsymbol{v}_i^{<K} \cdot \mathcal{P}^{<K}[\sum_{j\in B_i} \mathsf{R}(\boldsymbol{v}_i^{>Q}) \cdot \boldsymbol{v}_j^{>Q}]\rangle/\Pi(K)|$ for $Ka \simeq 0.31$ (left) and $Ka \simeq 0.18$ (right).

Part II

Information flow in turbulence

Chapter 6

Information thermodynamics

Various phenomena observed in complicated systems such as the Earth system [214–216] and chemical reaction network [217] can be regarded as nonequilibrium cooperative phenomena that emerge from many-body interactions. To elucidate and control the dynamics behind such phenomena, it is pertinent to focus on information transfer between components constituting the system. Particularly in mesoscopic systems affected by thermal fluctuations, the nature of such information transfer can be described by information thermodynamics [79, 218]. Information thermodynamics is essentially stochastic thermodynamics for subsystems [80, 81, 219, 220] and provides constraints that are consistent with thermodynamics on the exchange of information between subsystems. Recently, it has been applied to information processing at the cellular level in biological systems [221–225] and even to deterministic chemical reaction networks [226].

In this chapter, we briefly review information thermodynamics. In the next section, we introduce several information-theoretic quantities. In Section 6.2 and 6.3, we review stochastic thermodynamics and information thermodynamics, focusing only on aspects relevant to this thesis. For more exhaustive and pedagogical reviews, see, e.g., [79–81, 219, 220].

6.1 Information-theoretic quantities

In this section, we introduce important information-theoretic quantities used in Chapter 7. While we use continuous random variables in introducing these quantities to make explicit the connection with Chapter 7, several examples are given by using discrete random variables.

Shannon entropy

Let x be a continuous random variable, and $p^X(x)$ be its probability density. The *Shannon entropy* is defined by [227]

$$S[X] := -\int dx p^X(x) \ln p^X(x). \tag{6.1}$$

The Shannon entropy $S[X]$ quantifies the randomness of the variable x. For discrete random variables, the Shannon entropy is nonnegative. We remark that the Shannon entropy is not invariant under the transformation of the variable in the continuous case.

As an example, we consider a simple case with $x \in \{0, 1\}$. We set $p^X(0) = p$ and $p^X(1) = 1 - p$ with $p \in [0, 1]$. Then, the Shannon entropy reads

$$S[X] = -p \ln p - (1 - p) \ln(1 - p). \tag{6.2}$$

As expected, it takes the maximum value $\ln 2$ for $p = 1/2$ and minimal value 0 for $p = 0$ or 1.

Mutual information

Let x and y be the two continuous random variables, and $p(x, y)$ be their joint distribution. The marginal distributions are given by $p^X(x) := \int dy p(x, y)$ and $p^Y(y) := \int dx p(x, y)$. The *mutual information* is defined by [227]

$$I[X : Y] := \int dx dy p(x, y) \ln \frac{p(x, y)}{p^X(x)p^Y(y)}. \tag{6.3}$$

Note that it is symmetric between X and Y. By introducing the conditional Shannon entropy

$$\begin{aligned} S[X|Y] &:= -\int dx dy p(x, y) \ln p(x|y) \\ &= S[X, Y] - S[Y], \end{aligned} \tag{6.4}$$

where $p(x|y) = p(x, y)/p^Y(y)$ is the conditional probability density, the mutual information can be expressed as

$$\begin{aligned} I[X : Y] &= S[X] + S[Y] - S[X, Y] \\ &= S[X] - S[X|Y] \\ &= S[Y] - S[Y|X]. \end{aligned} \tag{6.5}$$

Thus, $I[X : Y]$ quantifies how much knowing X (Y) reduces uncertainty about Y (X). In other words, the mutual information quantifies the strength of the correlation between X and Y. Indeed, it can also be expressed in terms of the Kullback-Leibler divergence $D_{\mathrm{KL}}(p\|q)$, which quantifies the "distance" between the two probability distributions p and q [227]:

$$I[X : Y] = D_{\mathrm{KL}}\left(p \| p^X p^Y\right). \tag{6.6}$$

From the nonnegativity of the Kullback-Leibler divergence, it follows that the mutual information is nonnegative $I[X : Y] \geq 0$. The equality $I[X : Y] = 0$ holds if and only if X and Y are independent $p(x.y) = p^X(x)p^Y(y)$. In fact, by applying Jensen's inequality,

$$\begin{aligned} I[X : Y] &= -\left\langle \ln \frac{p^X(x)p^Y(y)}{p(x, y)} \right\rangle_p \\ &\geq -\ln \left\langle \frac{p^X(x)p^Y(y)}{p(x, y)} \right\rangle_p \\ &= -\ln 1 = 0, \end{aligned} \tag{6.7}$$

where $\langle \cdot \rangle_p$ denotes the average with respect to $p(x, y)$.

As an example, we consider a binary symmetric channel (see Fig. 6.1). Let $x \in \{0,1\}$ be a measured random variable, and $y \in \{0,1\}$ be a measurement outcome. For simplicity, we set $p^X(0) = p^X(1) = 1/2$. We assume that the measurement error is characterized by

$$p(y=0|x=0) = p(y=1|x=1) = 1-\epsilon, \tag{6.8}$$
$$p(y=1|x=0) = p(y=0|x=1) = \epsilon, \tag{6.9}$$

where $\epsilon \in [0,1]$ is the error probability. In this case, the mutual information reads

$$I[X:Y] = \ln 2 + \epsilon \ln \epsilon + (1-\epsilon)\ln(1-\epsilon). \tag{6.10}$$

Thus, the mutual information takes the maximum value $\ln 2$ when $\epsilon = 0$ or 1, while it takes the minimal value 0 when $\epsilon = 1/2$.

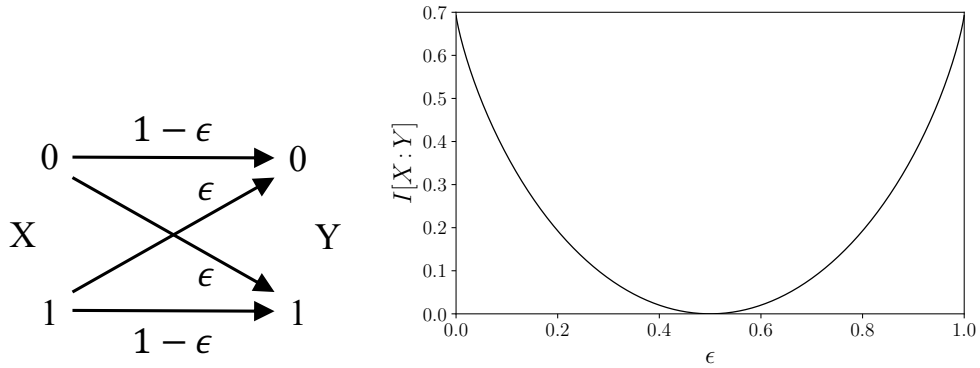

Fig. 6.1: Schematic of the binary symmetric channel (left) and the ϵ-dependence of the mutual information (right).

Learning rate (Information flow)

Here, we consider dynamical evolution of X and Y. Let x_t and y_t be continuous random variables at time t. The directional information flow from one variable to the other can be quantified by the *learning rate*, which is also called the *information flow* [221,224,228,229]. The learning rate that characterizes the rate at which X_t acquires information about Y_t is defined as

$$l^X(t) := \lim_{dt\to 0^+} \frac{I[X_{t+dt}:Y_t] - I[X_t:Y_t]}{dt}. \tag{6.11}$$

Similarly, the learning rate associated with Y is defined by

$$l^Y(t) := \lim_{dt\to 0^+} \frac{I[X_t:Y_{t+dt}] - I[X_t:Y_t]}{dt}. \tag{6.12}$$

The learning rates have a clear meaning. Suppose that $l^X(t) > 0$, for example. From the definition, the positivity of $l^X(t) > 0$ means that the dynamical evolution of X increases the mutual information. In other words, X is "learning" about Y through its dynamical evolution. Similarly, $l^X(t) < 0$ means that the dynamical evolution of X decreases the mutual information. That is, X is destroying or consuming correlation with Y through its dynamical evolution.

If these two stochastic processes x_t and y_t are Markovian and *bipartite*, i.e., if the transition probability $p(x_{t+dt}, y_{t+dt}|x_t, y_t)$ satisfies

$$p(x_{t+dt}, y_{t+dt}|x_t, y_t) = p(x_{t+dt}|x_t, y_t)p(y_{t+dt}|x_t, y_t) + O(dt^2), \tag{6.13}$$

then it follows that[1]

$$\frac{d}{dt}I[X_t : Y_t] = l^X(t) + l^Y(t). \tag{6.17}$$

Thus, the learning rates $l^X(t)$ and $l^Y(t)$ give the natural decomposition of the time derivative of the mutual information. Note that in the steady state, we have $\frac{d}{dt}I[X_t : Y_t] = 0$, and thus the two learning rates have opposite signs.

6.2 Stochastic thermodynamics

In this section, we briefly review stochastic thermodynamics, focusing only on aspects relevant to this thesis. In a nutshell, stochastic thermodynamics is a theoretical framework that extends thermodynamics to systems where thermal fluctuations are significant, such as colloidal particles and molecular motors in living cells [80, 81, 220]. Note that, in principle, stochastic thermodynamics is valid even for macroscopic systems where thermal fluctuation effects are negligible.

As an illustrative model, we here consider a colloidal particle described by an overdamped Langevin equation. Let x_t be the position of the particle at time t. The time evolution of x_t is governed by the following equation:

$$\gamma \dot{x}_t = -\partial_x U(x_t, \lambda_t) + f_t(x_t) + \sqrt{2\gamma k_{\mathrm{B}} T}\xi_t, \tag{6.18}$$

where γ denotes the friction coefficient, $U(x, \lambda)$ denotes a potential with an external control parameter λ_t, $f_t(x)$ denotes a nonconservative force. The last term on the right-hand side of (6.18) represents the thermal fluctuation due to a thermal bath at temperature T, where ξ_t is the zero-mean white Gaussian noise that satisfies $\langle \xi_t \xi_s \rangle = \delta(t - s)$. The specific form of the coefficient in front of ξ_t satisfies the fluctuation-dissipation relation (FDR) of the second kind, which expresses "balance" between the friction and fluctuation, both induced by the same equilibrium environment [230, 231].[2] We remark that the second FDR can also be derived from the *local detailed balance* condition, which requires the environment be quickly equilibrated [232–234]. Thus, this relation ensures the thermodynamic consistency of the mesoscopic model.

[1] Even if the two stochastic processes are neither bipartite nor Markovian, we still have the following relation [229]:

$$\frac{d}{dt}I[X_t : Y_t] = l^+_X(t) + l^-_Y(t) = l^-_X(t) + l^+_Y(t), \tag{6.14}$$

where $l^+_X(t)$ and $l^+_Y(t)$ are the same as (6.11) and (6.12), and $l^-_X(t)$ and $l^-_Y(t)$ are the *backward* learning rates defined by

$$l^-_X(t) := \lim_{dt\to 0^+} \frac{I[X_{t+dt} : Y_{t+dt}] - I[X_t : Y_{t+dt}]}{dt}, \tag{6.15}$$

$$l^-_Y(t) := \lim_{dt\to 0^+} \frac{I[X_{t+dt} : Y_{t+dt}] - I[X_{t+dt} : Y_t]}{dt}. \tag{6.16}$$

[2] In nonequilibrium environment, the second FDR can be violated. Even in that case, there is some restriction on the degree of the violation [231].

The corresponding Fokker-Planck equation reads

$$\partial_t p_t(x) = -\partial_x J_t(x), \tag{6.19}$$

where $J_t(x)$ denotes the probability current:

$$J_t(x) := \frac{1}{\gamma}\left[-\partial_x U(x,\lambda_t) + f_t(x)\right] p_t(x) - \frac{k_{\mathrm{B}}T}{\gamma}\partial_x p_t(x). \tag{6.20}$$

6.2.1 First law of thermodynamics

We introduce thermodynamic quantities for the above illustrative model. In stochastic thermodynamics, heat and work are introduced at the level of individual trajectories. The energy change of the overdamped system reads

$$\frac{d}{dt}U(x_t,\lambda_t) = \partial_x U(x_t,\lambda_t)\circ\dot{x}_t + \partial_\lambda U(x_t,\lambda_t)\dot{\lambda}_t, \tag{6.21}$$

where the symbol $\circ$ denotes multiplication in the sense of Stratonovich (see Appendix 6.4). We identify the increment in work applied to the system as

$$\hat{\dot{W}} = \partial_\lambda U(x_t,\lambda_t)\dot{\lambda}_t + f_t(x_t)\circ\dot{x}_t, \tag{6.22}$$

where the over-dot of W indicates that it is not a time derivative of a state function, and the hat indicates that it is a fluctuating quantity. The first and second terms arise from external control of the potential and the applied nonconservative force, respectively. By noting that $-\gamma\dot{x}_t + \sqrt{2\gamma k_{\mathrm{B}}T}\xi_t$ represents the force exerted by the environment, we then identify heat absorbed by the system as

$$\begin{aligned}\hat{\dot{Q}} &= \left[-\gamma\dot{x}_t + \sqrt{2\gamma k_{\mathrm{B}}T}\xi_t\right]\circ\dot{x}_t \\ &= -\left[-\partial_x U(x_t,\lambda_t) + f_t(x_t)\right]\circ\dot{x}_t.\end{aligned} \tag{6.23}$$

Note that $-\hat{\dot{Q}}$ can be interpreted as work done by the particle to the environment by regarding $-(-\gamma\dot{x}_t + \sqrt{2\gamma k_{\mathrm{B}}T}\xi_t)$ as the reaction force on the environment [219]. We remark that this identification of heat is consistent with the local detailed balance condition. From (6.22) and (6.23), we obtain

$$\frac{d}{dt}U(x_t,\lambda_t) = \hat{\dot{W}} + \hat{\dot{Q}}, \tag{6.24}$$

which is analogous to the first law of thermodynamics.

6.2.2 Second law of thermodynamics

We here formulate the second law of thermodynamics. The average heat dissipated into the environment is identified with an increase in entropy of the environment:

$$\dot{S}_{\mathrm{env}} = -\frac{\dot{Q}}{k_{\mathrm{B}}T}, \tag{6.25}$$

where $\dot{Q} := \langle \hat{\dot{Q}} \rangle$. Similarly, we identify the Shannon entropy $S[X_t]$ with the system entropy. Then, the sum of $d_t S[X_t]$ and $\dot{S}_{\rm env}$ is interpreted as the total entropy production rate, which is nonnegative:[3]

$$\begin{aligned}\frac{d}{dt}S[X_t] + \dot{S}_{\rm env} &= -\int dx \partial_t p_t(x) \ln p_t(x) - \int dx \partial_t p_t(x) + \frac{1}{k_{\rm B}T} \langle [-\partial_x U(x_t, \lambda_t) + f_t(x_t)] \circ \dot{x}_t \rangle \\ &= -\int dx J_t(x) \partial_x \ln p_t(x) + \frac{1}{k_{\rm B}T} \int dx \left[-\partial_x U(x, \lambda_t) + f_t(x)\right] J_t(x) \\ &= \frac{\gamma}{k_{\rm B}T} \int dx \frac{J_t^2(x)}{p_t(x)} \geq 0. \end{aligned} \tag{6.27}$$

6.3 Information thermodynamics

In this section, we briefly review information thermodynamics, again focusing only on aspects relevant to this thesis. Information thermodynamics is essentially stochastic thermodynamics for subsystems and provides constraints that are consistent with thermodynamics on the exchange of information between subsystems [79, 218].

As an illustrative model, we here consider the following coupled overdamped Langevin equations:

$$\gamma^X \dot{x}_t = -\partial_x U(x_t, y_t) + f_t^X(x_t, y_t) + \sqrt{2\gamma^X k_{\rm B}T}\xi_t^X, \tag{6.28}$$

$$\gamma^Y \dot{y}_t = -\partial_y U(x_t, y_t) + f_t^Y(x_t, y_t) + \sqrt{2\gamma^Y k_{\rm B}T}\xi_t^Y, \tag{6.29}$$

where $U(x, y)$ denotes the interaction potential, $f_t^\alpha(x, y)$ $(\alpha = X, Y)$ denotes the nonconservative force, and ξ_t^α is a zero-mean white Gaussian noise that satisfies $\langle \xi_t^\alpha \xi_{t'}^{\alpha'} \rangle = \delta_{\alpha\alpha'}\delta(t-t')$. Here, for simplicity, we have assumed that both X and Y are in contact with the same environment at temperature T with the friction coefficients γ^X and γ^Y, respectively. We have also assumed that there is no control parameter λ_t in the interaction potential. Note that since ξ_t^X and ξ_t^Y are independent, this system satisfies the bipartite property.

The corresponding Fokker-Planck equation reads

$$\partial_t p_t(x, y) = -\partial_x J_t^X(x, y) - \partial_y J_t^Y(x, y), \tag{6.30}$$

where J_t^X and J_t^Y denote the probability currents:

$$J_t^X(x, y) := \frac{1}{\gamma^X}\left[-\partial_x U(x, y) + f_t^X(x, y)\right] p_t(x, y) - \frac{k_{\rm B}T}{\gamma^X}\partial_x p_t(x, y), \tag{6.31}$$

$$J_t^Y(x, y) := \frac{1}{\gamma^Y}\left[-\partial_y U(x, y) + f_t^Y(x, y)\right] p_t(x, y) - \frac{k_{\rm B}T}{\gamma^Y}\partial_y p_t(x, y). \tag{6.32}$$

[3] In the second line, we have used the following useful relation, which holds for any nonanticipating function $g_t(x)$ [80, 198]:

$$\begin{aligned}\langle g_t(x_t) \circ \dot{x}_t \rangle &= \left\langle g_t(x_t) \left[\frac{1}{\gamma}\left(-\partial_x U(x, \lambda_t) + f_t(x)\right)\right] \right\rangle + \left\langle g_t(x_t) \cdot \sqrt{\frac{2k_{\rm B}T}{\gamma}}\xi_t \right\rangle + \left\langle \frac{k_{\rm B}T}{\gamma}\partial_x g_t(x_t) \right\rangle \\ &= \langle g_t(x_t)\nu_t(x_t) \rangle, \end{aligned} \tag{6.26}$$

where the symbol $\cdot$ denotes multiplication in the sense of Ito (see Appendix 6.4), and $\nu_t(x) := J_t(x)/p_t(x)$ denotes the *local mean velocity*.

6.3.1 First law of information thermodynamics

We here consider the first law of thermodynamics for each subsystem. We first identify increment in work applied to X as

$$\hat{W}^X = f_t^X(x_t, y_t) \circ \dot{x}_t. \tag{6.33}$$

As in the previous section, we also identify heat absorbed by X as

$$\begin{aligned}\hat{\dot{Q}}^X &= \left[-\gamma^X \dot{x}_t + \sqrt{2\gamma^X k_{\rm B}T}\xi_t^X\right] \circ \dot{x}_t \\ &= -\left[-\partial_x U(x_t, y_t) + f_t^X(x_t, y_t)\right] \circ \dot{x}_t.\end{aligned} \tag{6.34}$$

We next define work from X to Y by regarding x as an external control parameter driving Y [235, 236]:

$$\hat{W}^{X\to Y} := \partial_x U(x_t, y_t) \circ \dot{x}_t. \tag{6.35}$$

Similarly, we can define $\hat{W}^Y$, $\hat{\dot{Q}}^Y$, and $\hat{W}^{Y\to X}$. Then, the first law for each subsystem can be expressed as follows:

$$\hat{W}^{X\to Y} = \hat{W}^X + \hat{\dot{Q}}^X, \tag{6.36}$$

$$\hat{W}^{Y\to X} = \hat{W}^Y + \hat{\dot{Q}}^Y. \tag{6.37}$$

6.3.2 Second law of information thermodynamics

We here derive the second law of information thermodynamics. To this end, we first formulate the standard second law of thermodynamics for this case. As in the previous section, we identify increase in entropy of the environment as

$$\begin{aligned}\dot{S}_{\rm env} &= -\frac{\dot{Q}^X}{k_{\rm B}T} - \frac{\dot{Q}^Y}{k_{\rm B}T} \\ &=: \dot{S}_{\rm env}^X + \dot{S}_{\rm env}^Y,\end{aligned} \tag{6.38}$$

where $\dot{Q}^X := \langle\hat{\dot{Q}}^X\rangle$ and $\dot{Q}^Y := \langle\hat{\dot{Q}}^Y\rangle$. Note that there are two contributions $\dot{S}_{\rm env}^X$ and $\dot{S}_{\rm env}^Y$ to the medium entropy production. Similarly, we identify the whole system entropy with the Shannon entropy $S[X_t, Y_t]$. From the bipartite property, the time derivative of $S[X_t, Y_t]$ can be decomposed into two parts:

$$\begin{aligned}\frac{d}{dt}S[X_t, Y_t] &= -\int dxdy\partial_t p_t(x, y)\ln p_t(x, y) - \int dxdy\partial_t p_t(x, y) \\ &= -\int dxdy J_t^X(x, y)\partial_x \ln p_t(x, y) - \int dxdy J_t^Y(x, y)\partial_y \ln p_t(x, y) \\ &=: \dot{S}^X[X_t, Y_t] + \dot{S}^Y[X_t, Y_t],\end{aligned} \tag{6.39}$$

where $\dot{S}^X[X_t, Y_t]$ and $\dot{S}^Y[X_t, Y_t]$ denote the contribution to the system entropy change due to the probability current of X and Y, respectively. Then, the total entropy production

rate can be expressed as

$$\begin{aligned}\frac{d}{dt}S[X_t,Y_t]+\dot{S}_{\rm env} &= \dot{S}^X[X_t,Y_t]+\dot{S}^Y[X_t,Y_t]\\ &\quad+\frac{1}{k_{\rm B}T}\left\langle\left[-\partial_x U(x_t,y_t)+f_t^X(x_t,y_t)\right]\circ\dot{x}_t\right\rangle\\ &\quad+\frac{1}{k_{\rm B}T}\left\langle\left[-\partial_y U(x_t,y_t)+f_t^Y(x_t,y_t)\right]\circ\dot{y}_t\right\rangle\\ &= -\int dxdyJ_t^X(x,y)\partial_x\ln p_t(x,y)-\int dxdyJ_t^Y(x,y)\partial_y\ln p_t(x,y)\\ &\quad+\frac{1}{k_{\rm B}T}\int dxdy\left[-\partial_x U(x,y)+f_t^X(x,y)\right]J_t^X(x,y)\\ &\quad+\frac{1}{k_{\rm B}T}\int dxdy\left[-\partial_y U(x,y)+f_t^Y(x,y)\right]J_t^Y(x,y)\\ &= \frac{\gamma^X}{k_{\rm B}T}\int dxdy\frac{|J_t^X(x,y)|^2}{p_t(x,y)}+\frac{\gamma^Y}{k_{\rm B}T}\int dxdy\frac{|J_t^Y(x,y)|^2}{p_t(x,y)}\geq 0. \end{aligned}\tag{6.40}$$

As is clear from the above calculation, the second-law-type inequality holds even for each subsystem due to the bipartite property: e.g., for X, we obtain

$$\dot{S}^X[X_t,Y_t]+\dot{S}^X_{\rm env}=\frac{\gamma^X}{k_{\rm B}T}\int dxdy\frac{|J_t^X(x,y)|^2}{p_t(x,y)}\geq 0.\tag{6.41}$$

We note that the left-hand side of (6.41) is an example of the so-called *partial entropy production* [237]. From this relation, we can derive the second law of information thermodynamics. We first note that the learning rate $l^X(t)$ can be expressed as follows:[4]

$$\begin{aligned}l^X(t) &= \lim_{dt\to 0^+}\frac{I[X_{t+dt}:Y_t]-I[X_t:Y_t]}{dt}\\ &= \int dxdyJ_t^X(x,y)\partial_x\ln\frac{p_t(x,y)}{p_t^X(x)p_t^Y(y)}\\ &= -\int dxdyJ_t^X(x,y)\partial_x\ln p_t^X(x)+\int dxdyJ_t^X(x,y)\partial_x\ln p_t(x,y)\\ &= \frac{d}{dt}S[X_t]-\dot{S}^X[X_t,Y_t].\end{aligned}\tag{6.44}$$

[4]The second line can be obtained as follows:

$$\begin{aligned}l^X(t) &= \lim_{h\to 0^+}\frac{1}{h}\left(\int dxdy'p(x,t+h;y',t)\ln\frac{p(x,t+h;y',t)}{p_{t+h}^X(x)p_t^Y(y')}-\int dx'dy'p_t(x',y')\ln\frac{p_t(x',y')}{p_t^X(x')p_t^Y(y')}\right)\\ &= \int dxdydx'dy'\left.\frac{d}{dh}p(x,y,t+h|x',y',t)\right|_{h=0^+}p_t(x',y')\ln\frac{p_t(x,y')}{p_t^X(x)p_t^Y(y')}\\ &= \int dxdy\left(-\partial_x J_t^X(x,y)\right)\ln\frac{p_t(x,y)}{p_t^X(x)p_t^Y(y)}.\end{aligned}\tag{6.42}$$

Here, $p(x,t+h;y',t)$ denotes the two-point probability distribution with $p(x,t;y,t)=p_t(x,y)$, and $p(x,y,t+h|x',y',t)=p(x,y,t+h;x',y',t)/p_t(x',y')$ denotes the transition probability, which obeys the Fokker-Planck equation (6.30) with $p(x,y,t|x',y',t)=\delta(x-x')\delta(y-y')$. The second line of (6.44) can also be obtained by noting that the time derivative of the *stochastic mutual information* $\hat{I}_t(x_t,y_t):=\ln(p_t(x_t,y_t)/p_t^X(x_t)p_t^Y(y_t))$ reads $d_t\hat{I}_t(x_t,y_t)=\hat{l}_t^X(x_t,y_t)+\hat{l}_t^Y(x_t,y_t)$, where $\hat{l}_t^X(x_t,y_t)$ denotes the *stochastic learning rate* with $l^X(t)=\langle\hat{l}_t^X(x_t,y_t)\rangle$:

$$\hat{l}_t^X(x_t,y_t)=\dot{x}_t\circ\partial_x\ln\frac{p_t(x_t,y_t)}{p_t^X(x_t)p_t^Y(y_t)}-\frac{1}{p_t(x_t,y_t)}\partial_x J_t^X(x_t,y_t)+\frac{1}{p_t^X(x_t)}\partial_x\bar{J}_t^X(x_t),\tag{6.43}$$

where $\bar{J}_t^X(x):=\int dyJ_t^X(x,y)$.

By substituting this expression into (6.41), we obtain the second law of information thermodynamics:

$$\frac{d}{dt}S[X_t] + \dot{S}^X_{\rm env} \geq l^X(t). \tag{6.45}$$

Similarly, we can obtain

$$\frac{d}{dt}S[Y_t] + \dot{S}^Y_{\rm env} \geq l^Y(t). \tag{6.46}$$

The left-hand sides of (6.45) and (6.46) can be interpreted as the entropy production rate associated with X and Y, respectively. If X and Y are independent, then (6.45) and (6.46) corresponds to the standard second law of thermodynamics, because $l^X(t) = l^Y(t) = 0$. The appearance of the learning rate on the right-hand sides of (6.45) and (6.46) allows the negative entropy production. In other words, when the learning rate is negative, the subsystem can behave in a way that seemingly violates the second law of thermodynamics. We emphasize that even in that case, the total system satisfies the standard second law (6.40).

6.3.3 Information-thermodynamic efficiency

We here introduce the information-thermodynamic efficiency. Note that in the steady state, (6.45) and (6.46) become

$$\dot{S}^X_{\rm env} \geq l^X, \tag{6.47}$$

$$\dot{S}^Y_{\rm env} \geq l^Y, \tag{6.48}$$

with $l^X = -l^Y$. Suppose that Y acts as a sensor, or Y is "learning" about X, so that $l^Y = -l^X > 0$. In this case, we can introduce the information-thermodynamic efficiency η^Y $(0 \leq \eta^Y \leq 1)$ as

$$\eta^Y := \frac{l^Y}{\dot{S}^Y_{\rm env}}. \tag{6.49}$$

This efficiency quantifies how efficiently Y gains information about X relative to the energy dissipation. In addition, if $\dot{S}^X_{\rm env}$ is negative, then we can introduce the information-thermodynamic efficiency for X (see Fig. 6.2):

$$\eta^X := \frac{|\dot{S}^X_{\rm env}|}{|l^X|}, \tag{6.50}$$

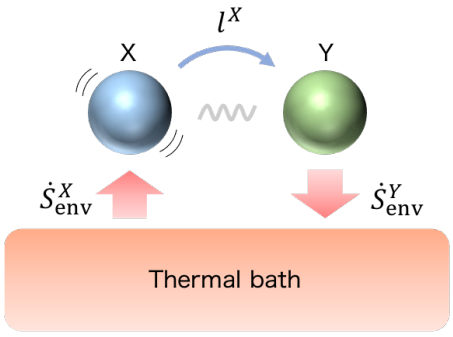

Fig. 6.2: Schematic of the case where $\dot{S}^X_{\rm env} < 0$ and $l^Y = -l^X > 0$.

which satisfies $0 \leq \eta^X \leq 1$. This efficiency quantifies how efficiently X converts information into negative entropy production.

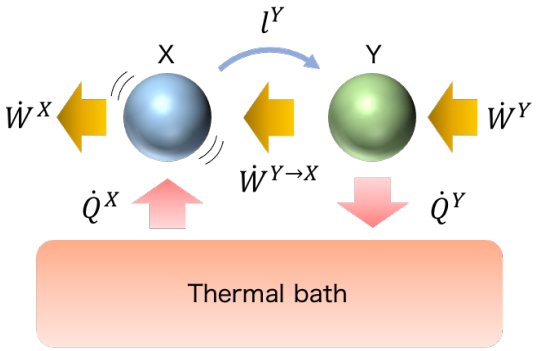

Fig. 6.3: Schematic of the case where $\dot{W}^Y > 0$ and $\dot{W}^X \leq 0$.

By using the work introduced in Section 6.3.1, we can introduce another efficiencies. In the steady state, we first note that $\dot{W}^{X\to Y} = -\dot{W}^{Y\to X}$, where $\dot{W}^{X\to Y} := \langle \hat{\dot{W}}^{X\to Y} \rangle$ and $\dot{W}^{Y\to X} := \langle \hat{\dot{W}}^{Y\to X} \rangle$. Then, the second law of information thermodynamics can be expressed in terms of $\dot{W}^X := \langle \hat{\dot{W}}^X \rangle$, $\dot{W}^Y := \langle \hat{\dot{W}}^Y \rangle$, and $\dot{W}^{X\to Y} = -\dot{W}^{Y\to X}$ as

$$\beta \dot{W}^X - \beta \dot{W}^{X\to Y} - l^X \geq 0, \tag{6.51}$$

$$\beta \dot{W}^Y - \beta \dot{W}^{Y\to X} - l^Y \geq 0, \tag{6.52}$$

where $\beta = (k_{\mathrm{B}}T)^{-1}$. Suppose that $\dot{W}^Y > 0$ and $\dot{W}^X \leq 0$ (see Fig. 6.3). In this case, Y drives X with nonnegative *transduced capacity* $-\beta \dot{W}^{X\to Y} - l^X = \beta \dot{W}^{Y\to X} + l^Y \geq 0$ [238], and we can introduce the following efficiency ($0 \leq \tilde{\eta}^X \leq 1$ and $0 \leq \tilde{\eta}^Y \leq 1$):

$$\tilde{\eta}^X := \frac{|\beta \dot{W}^X|}{|\beta \dot{W}^{X\to Y} + l^X|}, \tag{6.53}$$

$$\tilde{\eta}^Y := \frac{\beta \dot{W}^{Y\to X} + l^Y}{\beta \dot{W}^Y}. \tag{6.54}$$

Here, $\tilde{\eta}^X$ quantifies how efficiently X converts transduced capacity into output work. Similarly, $\tilde{\eta}^Y$ quantifies how efficiently Y converts applied work into transduced capacity.

6.3.4 Example

As an example, we consider the following coupled overdamped Langevin equations [239]:

$$\dot{s}_t = -\omega^S s_t + \omega^{SX} x_t + \sqrt{2D^S}\xi_t^S, \tag{6.55}$$

$$\dot{x}_t = \omega^{XS} s_t - \omega^X x_t + \sqrt{2D^X}\xi_t^X, \tag{6.56}$$

where ξ_t^α ($\alpha = S, X$) is a zero-mean white Gaussian noise that satisfies $\langle \xi_t^\alpha \xi_{t'}^{\alpha'} \rangle = \delta_{\alpha\alpha'}\delta(t - t')$, and D^α denotes the noise intensity. Here, s_t can be regarded as the input signal, which relaxes exponentially with decay rate $\omega^S > 0$ and is affected by the fluctuation of the output signal x_t with rate ω^{SX}. The output signal x_t also relaxes exponentially with rate $\omega^X > 0$ and detects the input s_t with the differential gain ω^{XS}. We assume that

$$\omega^X \omega^S - \omega^{XS}\omega^{SX} > 0 \tag{6.57}$$

to ensure that the system reaches a steady state [198]. The corresponding Fokker-Planck equation reads

$$\partial_t p_t(s,x) = -\partial_s J_t^S(s,x) - \partial_x J_t^X(s,x), \tag{6.58}$$

where

$$J_t^S(s,x) := (-\omega^S s + \omega^{SX} x)p_t(s,x) - D^S \partial_s p_t(s,x), \tag{6.59}$$
$$J_t^X(s,x) := (\omega^{XS} s - \omega^X x)p_t(s,x) - D^X \partial_x p_t(s,x). \tag{6.60}$$

Fast relaxation limit of S

Hereafter, we focus on the typical case where the input signal s_t is a fast variable and regulates the output x_t. In other words, we assume a time-scale separation, $\epsilon := \omega^X/\omega^S \ll 1$. In this case, we can derive the effective dynamics for X, e.g., by using the singular perturbation technique [231]. We introduce a dimensionless time $\tau := \omega^S t$ and noise intensity $\bar{D}^S := D^S/\omega^S$ and $\bar{D}^X := D^X/\omega^X$. We also write $\bar{\omega}^{XS} := \omega^{XS}/\omega^X$ and $\bar{\omega}^{SX} := \omega^{SX}/\omega^S$. Then, the Fokker-Planck equation can be expressed as

$$\begin{aligned}\partial_\tau p_\tau(s,x) &= -\partial_s \left[\left(-s + \bar{\omega}^{SX} x\right) p_\tau(s,x) - \bar{D}^S \partial_s p_\tau(s,x)\right] \\ &\quad - \epsilon \partial_x \left[\left(\bar{\omega}^{XS} s - x\right) p_\tau(s,x) - \bar{D}^X \partial_x p_\tau(s,x)\right] \\ &=: (\mathcal{L}^S + \epsilon \mathcal{L}^X) p_\tau(s,x).\end{aligned} \tag{6.61}$$

The form of this equation implies that the system first relaxes toward the slow manifold characterized by $\mathcal{L}^S$ on the fast time scale $\tau \sim 1$ and then evolves slowly on the slow manifold. The motion on the slow manifold is characterized by the following equation for the reduced probability $p_\tau^X(x) = \int ds p_\tau(s,x)$:

$$\partial_\tau p_\tau^X(x) = -\epsilon \partial_x \left[\bar{\omega}^{XS} \int ds s p_\tau(s,x) - x p_\tau^X(x) - \bar{D}^X \partial_x p_\tau^X(x)\right]. \tag{6.62}$$

Because p_τ^X evolves slowly, secular terms arise in the naive perturbation expansion $p_\tau = p_\tau^{(0)} + \epsilon p_\tau^{(1)} + \cdots$. Therefore, to describe the dynamics on the slow manifold, we assume that the τ-dependence of p_τ is expressed in terms of the τ-dependent operator M_τ that acts on p_τ^X:

$$M_\tau[p_\tau^X](s,x) := p_\tau(s,x). \tag{6.63}$$

From this functional ansatz, we can decompose the τ-dependence of p_τ into its explicit and implicit part through p_τ^X. Correspondingly, we introduce Ω_τ as the τ-dependent operator that represent the slow dynamics:

$$\Omega_\tau[p_\tau^X](x) := -\epsilon \partial_x \left[\bar{\omega}^{XS} \int ds s M_\tau[p_\tau^X](s,x) - x p_\tau^X(x) - \bar{D}^X \partial_x p_\tau^X(x)\right]. \tag{6.64}$$

In terms of M_τ and Ω_τ, (6.61) can be expressed as

$$\partial_\tau M_\tau[p_\tau^X](s,x) + \int dx' \frac{\delta M_\tau[p_\tau^X]}{\delta p_\tau^X(x')} \Omega_\tau[p_\tau^X](x') = (\mathcal{L}^S + \epsilon \mathcal{L}^X) M_\tau[p_\tau^X](s,x). \tag{6.65}$$

We now assume that M_τ and Ω_τ have asymptotic expansions in terms of the asymptotic sequences $\{\epsilon^n\}_{n=0}^\infty$ as $\epsilon \to 0$:

$$M_\tau = M_\tau^{(0)} + \epsilon M_\tau^{(1)} + \cdots, \tag{6.66}$$

$$\Omega_\tau = \epsilon \Omega_\tau^{(1)} + \epsilon^2 \Omega_\tau^{(2)} + \cdots. \tag{6.67}$$

The leading order of (6.65) gives

$$\partial_\tau M_\tau^{(0)}[p_\tau^X] = \mathcal{L}^S[M_\tau^{(0)}[p_\tau^X]]. \tag{6.68}$$

From this equation, it follows that

$$M_\tau^{(0)}[p_\tau^X](s,x) \simeq p_\tau^X(x)\pi_{\rm ss}(s|x) \quad \text{for} \quad \tau \gg 1, \tag{6.69}$$

where $\pi_{\rm ss}(s|x)$ denotes the stationary distribution that satisfies $\mathcal{L}^S[\pi_{\rm ss}(s|x)] = 0$, i.e.,

$$\pi_{\rm ss}(s|x) = \frac{1}{\sqrt{2\pi \bar{D}^S}} \exp\left[-\frac{1}{2\bar{D}^S}\left(s - \bar{\omega}^{SX}x\right)^2\right]. \tag{6.70}$$

Here, we have imposed the condition $p_\tau^X(x) = \int ds M_\tau^{(0)}[p_\tau^X](s,x)$. By substituting (6.69) into (6.64), we obtain

$$\Omega_\tau^{(1)}[p_\tau^X](x) \simeq -\partial_x\left[\left(\bar{\omega}^{XS}\bar{\omega}^{SX} - 1\right)xp_\tau^X(x) - \bar{D}^X\partial_x p_\tau^X(x)\right]. \tag{6.71}$$

Therefore, the effective dynamics for X is given by

$$\partial_\tau p_\tau^X(x) \simeq -\epsilon\partial_x\left[\left(\bar{\omega}^{XS}\bar{\omega}^{SX} - 1\right)xp_\tau^X(x) - \bar{D}^X\partial_x p_\tau^X(x)\right]. \tag{6.72}$$

Then, the stationary distribution for X reads

$$p_{\rm ss}^X(x) = \sqrt{\frac{1 - \bar{\omega}^{XS}\bar{\omega}^{SX}}{2\pi\bar{D}^X}} \exp\left[-\frac{1}{2\bar{D}^X}\left(1 - \bar{\omega}^{XS}\bar{\omega}^{SX}\right)x^2\right]. \tag{6.73}$$

From the stationary distributions (6.70) and (6.73), we find that $\langle x_t\rangle_{\rm ss} = \langle s_t\rangle_{\rm ss} = 0$ and

$$\langle s_t^2\rangle_{\rm ss} = \left(\bar{\omega}^{SX}\right)^2\frac{\bar{D}^X}{1 - \bar{\omega}^{XS}\bar{\omega}^{SX}} + \bar{D}^S, \tag{6.74}$$

$$\langle x_t^2\rangle_{\rm ss} = \frac{\bar{D}^X}{1 - \bar{\omega}^{XS}\bar{\omega}^{SX}}, \tag{6.75}$$

$$\langle s_t x_t\rangle_{\rm ss} = \bar{\omega}^{SX}\frac{\bar{D}^X}{1 - \bar{\omega}^{XS}\bar{\omega}^{SX}}. \tag{6.76}$$

Information thermodynamic efficiency

Here, we investigate the information-thermodynamic efficiency for this system. We note that the externally applied work $\hat{\dot{W}}^S$ and $\hat{\dot{W}}^X$ are zero in this model. Therefore, we only consider the efficiency defined by (6.49) and (6.50). We first calculate the medium entropy production rate in the steady state. From (6.74)-(6.76), we obtain[5]

$$\begin{aligned}\dot{S}_{\rm env}^X &= \frac{1}{D^X}\langle(\omega^{XS}s_t - \omega^X x_t)\circ\dot{x}_t\rangle_{\rm ss} \\ &= \frac{\omega^{XS}\omega^{SX}}{\omega^S}\left(\frac{\omega^{XS}D^S}{\omega^{SX}D^X} - 1\right).\end{aligned} \tag{6.77}$$

[5]We note that $\dot{S}_{\rm env}^X$ is induced by the fast variable s_t, which does not appear in the effective dynamics (6.72). Indeed, the (coarse-grained) medium entropy production rate corresponding to the effective dynamics is zero. Thus, $\dot{S}_{\rm env}^X$ is an entropy production invisible from the effective dynamics, which is called *hidden entropy* [240, 241].

Thus, $\dot{S}^X_{\rm env}$ becomes negative when $\omega^{XS}D^S < \omega^{SX}D^X$. Note that the detailed balance condition is satisfied when $\omega^{XS}D^S = \omega^{SX}D^X$.

We next calculate the learning rate in the steady state. By noting that $p_{\rm ss}(s,x) \simeq p^X_{\rm ss}(x)\pi_{\rm ss}(s|x)$ in the fast relaxation limit of S, we obtain

$$\begin{aligned} l^X &= \int dsdx J^X_{\rm ss}(s,x)\partial_x \ln \frac{p_{\rm ss}(s,x)}{p^X_{\rm ss}(x)p^S_{\rm ss}(s)} \\ &= \int dsdx \left[(\omega^{XS}s - \omega^X x)p_{\rm ss}(s,x) - D^X\partial_x p_{\rm ss}(s,x)\right]\partial_x \ln \pi_{\rm ss}(s|x) \\ &= \frac{\omega^{SX}}{\omega^S \bar{D}^S}\left[\left\langle (\omega^{XS}s - \omega^X x)\left(s - \frac{\omega^{SX}}{\omega^S}x\right)\right\rangle_{\rm ss} - \frac{\omega^{SX}D^X}{\omega^S}\right] \\ &= \frac{(\omega^{SX})^2 D^X}{\omega^S D^S}\left(\frac{\omega^{XS}D^S}{\omega^{SX}D^X} - 1\right) \\ &= \frac{\omega^{SX}D^X}{\omega^{XS}D^S}\dot{S}^X_{\rm env}. \end{aligned} \tag{6.78}$$

Thus, the learning rate is proportional to $\dot{S}^X_{\rm env}$, and the tight-coupling condition is satisfied.

We now consider the case where $\omega^{XS}D^S \leq \omega^{SX}D^X$. In this case, both $\dot{S}^X_{\rm env}$ and l^X are negative. By combining (6.77) and (6.78), the information-thermodynamic efficiency can be expressed as

$$\begin{aligned} \eta^X &= \frac{|\dot{S}^X_{\rm env}|}{|l^X|} \\ &= \frac{\omega^{XS}D^S}{\omega^{SX}D^X} \leq 1. \end{aligned} \tag{6.79}$$

Thus, $\eta^X = 1$ is achieved when $\omega^{XS}D^S = \omega^{SX}D^X$. Note that both $\dot{S}^X_{\rm env}$ and l^X vanish in this case. Indeed, we can show that there are trade-offs between the information-thermodynamic efficiency and $\dot{S}^X_{\rm env}$ or l^X [242]. On the contrary, if $\omega^{XS}D^S \geq \omega^{SX}D^X$, then both $\dot{S}^X_{\rm env}$ and l^X are positive. The corresponding information-thermodynamic efficiency reads

$$\begin{aligned} \eta^X &= \frac{l^X}{\dot{S}^X_{\rm env}} \\ &= \frac{\omega^{SX}D^X}{\omega^{XS}D^S}. \end{aligned} \tag{6.80}$$

6.4 Appendix: Stochastic calculus

In this section, we provide a brief introduction to stochastic differential equations. For more exhaustive and pedagogical reviews, see, e.g., [198, 243, 244].

First, we consider a Langevin equation of the form

$$\dot{x}_t = f_t(x_t) + \sigma_t(x_t)\xi_t, \tag{6.81}$$

where ξ_t is the zero-mean white Gaussian noise that satisfies $\langle \xi_t \xi_s \rangle = \delta(t-s)$. We note that ξ_t is formally interpreted as the "derivative" of the Wiener process W_t, which is not differentiable anywhere with probability one. In other words, (6.81) is mathematically the following *stochastic differential equation* (SDE):

$$dx_t = f_t(x_t)dt + \sigma_t(x_t)dW_t, \tag{6.82}$$

which is a shorthand notation of the stochastic integral equation

$$x_t = x_0 + \int_0^t f_s(x_s)ds + \int_0^t \sigma_s(x_s)dW_s. \tag{6.83}$$

The important point here is that the last term on the right-hand side of (6.83) cannot be defined as a Riemann-Stieltjes integral, because W_t is not of bounded variation.[6] Thus, different Riemann-Stieltjes sums lead to different values.

Now, we define stochastic integrals of the form

$$\int_0^t G_s(x_s)dW_s, \tag{6.87}$$

where $G_s(x_s)$ is an arbitrary sufficiently regular function. Let $0 = t_0 < t_1 < t_2 < \cdots < t_N = t$ be a partition of the interval $[0, t]$. We introduce a parameter $\alpha \in [0, 1]$ such that

$$\bar{t}_n := \alpha t_{n+1} + (1 - \alpha)t_n \tag{6.88}$$

for $n = 0, 1, \cdots, N - 1$. We define the stochastic integral as the mean square limit of the Riemann-Stieltjes sum

$$\int_0^t G_s(x_s) \overset{\alpha}{\otimes} dW_s := \lim_{\|\Delta\|\to 0} \sum_{n=0}^{N-1} G_{\bar{t}_n}(\bar{x}_n)\, \Delta W_n, \tag{6.89}$$

where $\|\Delta\| := \max |t_{n+1} - t_n|$, $\bar{x}_n := \alpha x_{t_{n+1}} + (1-\alpha)x_{t_n}$, and $\Delta W_n := W_{t_{n+1}} - W_{t_n}$. Here, the symbol $\overset{\alpha}{\otimes}$ is used to indicate that this integral depends on the choice of α. When $\alpha = 0$, the integral is called the Ito integral

$$\int_0^t G_s(x_s) \cdot dW_s := \int_0^t G_s(x_s) \overset{\alpha=0}{\otimes} dW_s. \tag{6.90}$$

Importantly, for *nonanticipating function* $G_s(x_s)$, where $G_s(x_s)$ is statistically independent of the increment $W_t - W_s$ for $t > s$, we have $\langle G_s(x_s) \cdot dW_s \rangle = \langle G_s(x_s) \rangle \langle dW_s \rangle = 0$. When $\alpha = 1/2$, the integral is called the Stratonovich integral

$$\int_0^t G_s(x_s) \circ dW_s := \int_0^t G_s(x_s) \overset{\alpha=1/2}{\otimes} dW_s. \tag{6.91}$$

[6](Riemann-Stieltjes integral). Let f and g be two functions on $[0, t]$, where g is of bounded variation, i.e., the total variation of g is finite:

$$V_0^t(g) := \sup \sum_{n=0}^{N-1} |g(t_{n+1}) - g(t_n)| < \infty, \tag{6.84}$$

where $0 = t_0 < t_1 < t_2 < \cdots < t_N = t$ is a partition of the interval $[0, t]$, and the supremum is taken over all partitions of the interval. We consider the Riemann-Stieltjes sum

$$\sum_{n=0}^{N-1} f(\bar{t}_n)[g(t_{n+1}) - g(t_n)], \tag{6.85}$$

where $\bar{t}_n \in [t_n, t_{n+1}]$. If the sum approaches a limit independent of the choice of the partition $\{t_n\}$ and $\bar{t}_n$ as $\|\Delta\| := \max |t_{n+1} - t_n| \to 0$, this limit is called the Riemann-Stieltjes integral of f with respect to g, which is denoted by

$$\int_0^t f(s)dg(s) := \lim_{\|\Delta\|\to 0} \sum_{n=0}^{N-1} f(\bar{t}_n)[g(t_{n+1}) - g(t_n)]. \tag{6.86}$$

For more details, see, e.g., [115].

In contrast to the Ito integral, we have $\langle G_s(x_s) \circ dW_s \rangle \neq 0$ in general. Furthermore, the Stratonovich integral satisfies ordinary calculus, such as $dG(x_t) = \partial_x G(x_t) \circ dx_t$. If the integrand $G_s(x_s)$ depends on W_s through x_s that is a solution of the SDE (6.83), there is a relation between Ito and Stratonovich integrals:

$$\int_0^t G_s(x_s) \circ dW_s = \int_0^t G_s(x_s) \cdot dW_s + \frac{1}{2} \int_0^t \sigma_s(x_s) \partial_x G_s(x_s) ds, \tag{6.92}$$

where we have used the rule $(dW_t)^2 = dt$ and $dt dW_t = 0$, which is valid in the mean square limit. Thus, the SDE interpreted in the Stratonovich sense

$$dx_t = f_t(x_t)dt + \sigma_t(x_t) \circ dW_t \tag{6.93}$$

is equivalent to the following SDE in the Ito sense

$$dx_t = \left(f_t(x_t) + \frac{1}{2} \sigma_t(x_t) \partial_x \sigma_t(x_t) \right) dt + \sigma_t(x_t) \cdot dW_t. \tag{6.94}$$

Chapter 7

Information flow in turbulence

As we emphasized in Chapter 5, turbulence can be regarded as a nonequilibrium cooperative phenomenon that emerges from extremely complicated nonlinear interactions. The most prominent property that distinguishes fluid turbulence from other nonequilibrium cooperative phenomena is its extremely strong fluctuations observed over a wide range of scales, as exemplified by intermittency. While the existence of universality seems to suggest that small-scale turbulent fluctuations behave independently of large-scale fluctuations, it is known that they exhibit some cooperative behavior. Specifically, along with the energy cascade, fluctuations of small-scale quantities (e.g., the energy dissipation rate) follow those of large-scale quantities (e.g., the energy injection rate) with a time delay that corresponds to the large-eddy turnover time [71–73]. Moreover, the energy cascade induces chaos synchronization of small-scale motions, where small-scale velocity field is slaved to the chaotic dynamics of large-scale velocity field [74–78]. These phenomena suggest that information of large-scale turbulent fluctuations is transferred to small scales.

These observations motivate us to explore the nature of the information transfer across scales associated with turbulent cascade. Revealing the details of the information transfer process in turbulence may not only provide insights into the generation mechanism of turbulent fluctuations leading to intermittency, but also allow comparative studies with other information processing systems. While turbulence has been studied in various contexts from such an information-theoretic viewpoint over recent decades [213, 245–255], no previous studies have theoretically shown that information flows across scales along with turbulent cascade.

Here, we aim to elucidate the nature of information flow in fully developed three-dimensional fluid turbulence. To this end, we employ information thermodynamics, introduced in Chapter 6, by explicitly accounting for the thermal fluctuations inherent in fluid. From the second law of information thermodynamics, we can obtain universal constraints on information flow. Furthermore, this approach enables us to investigate the effects of thermal fluctuations on information transfer, which can affect the turbulence dynamics significantly [20, 256–261]. While our approach can be applied to various turbulence models, here we use the stochastic Sabra shell model, which is a simplified caricature of the fluctuating Navier–Stokes equation in wave number space [23, 187]. This model has recently been used to investigate the effects of thermal fluctuations on turbulence [20, 258].

In this chapter, we prove that information of turbulent fluctuations is transferred from large to small scales along with the energy cascade. Our main result, (7.12) and (7.13), can be regarded as one of the few exact and universal results in the field of turbulence research. We numerically illustrate our findings and show that the rate of information

transfer is characterized by the large-eddy turnover time. Furthermore, our numerical simulations suggest that the corresponding information-thermodynamic efficiency is quite low compared to other typical information processing systems such as Maxwell's demon. This implies that transferring information from large to small scales involves enormous thermodynamic costs, indicating the poor performance of turbulence as an information processing system.

This chapter is organized as follows. In the next section, we introduce the Sabra shell model with thermal noise. Its basic properties are described in Section 7.2. In Section 7.3, we introduce important information-theoretic quantities that quantify the directional information flow across scales. In Section 7.4, we describe our main result and its derivation. We also introduce the information-thermodynamic efficiency for the shell model. In Section 7.5, we numerically illustrate the main result. We further show that the information-thermodynamic efficiency is quite low and that the information transfer is characterized by the large-eddy turnover time. Concluding remarks are provided in Section 7.6.

7.1 Setup

We consider the Sabra shell model with thermal noise [20, 258, 262]. Let $u_n(t) \in \mathbb{C}$ be the "velocity" at time t with the wave number $k_n = k_0 2^n$ $(n = 0, 1, \cdots, N)$. The time evolution of the complex shell variables $u := \{u_n\}$ is given by the following Langevin equation:

$$\dot{u}_n = B_n(u, u^*) - \nu k_n^2 u_n + \sqrt{\frac{2\nu k_n^2 k_{\rm B} T}{\rho}} \xi_n + f_n \tag{7.1}$$

with the scale-local nonlinear interactions given by

$$B_n(u, u^*) := i\left(k_{n+1} u_{n+2} u_{n+1}^* - \frac{1}{2} k_n u_{n+1} u_{n-1}^* + \frac{1}{2} k_{n-1} u_{n-1} u_{n-2} \right). \tag{7.2}$$

Here, $\nu > 0$ represents the kinematic viscosity, and $f_n \in \mathbb{C}$ denotes the external body force that acts only at large scales, i.e., $f_n = 0$ for $n > n_f$. The third term on the right-hand side of (7.1), $\xi_n \in \mathbb{C}$ is the zero-mean white Gaussian noise that satisfies $\langle \xi_n(t) \xi_{n'}^*(t') \rangle = 2\delta_{nn'}\delta(t - t')$. The specific form of the thermal noise term satisfies the fluctuation-dissipation relation of the second kind, where T denotes the absolute temperature, $k_{\rm B}$ the Boltzmann constant, and ρ the mass "density".[1]

7.2 Basic properties

The nonlinear term $B_n(u, u^*)$ satisfies the following relation:

$$\sum_{n=0}^{N} (B_n(u, u^*) u_n^* + B_n^*(u, u^*) u_n) = 0. \tag{7.3}$$

Hence, the energy balance equation reads

$$\frac{d}{dt} \sum_{n=0}^{N} \frac{1}{2} \langle |u_n|^2 \rangle = -\sum_{n=0}^{N} \nu k_n^2 \langle |u_n|^2 \rangle + \sum_{n=0}^{N} \frac{2\nu k_n^2 k_{\rm B} T}{\rho} + \varepsilon, \tag{7.4}$$

[1] Note that the mass "density" ρ has units of mass.

where $\varepsilon := \sum_{n=0}^{n_f} \langle u_n f_n^* + u_n^* f_n \rangle / 2$ denotes the energy injection rate. In the steady state, the energy injection rate balances the dissipation rate as follows:

$$\varepsilon \simeq \sum_{n=0}^{N} \nu k_n^2 \langle |u_n|^2 \rangle_{\rm ss}. \tag{7.5}$$

Here, we have ignored the energy injection due to the thermal noise by noting that the kinetic energy is much larger than the thermal energy over a wide range of scales in turbulence [20, 258].

Shell models are known to exhibit rich temporal and multiscale statistics that are similar to those observed in real turbulent flow [263]. Most importantly, the model exhibits energy cascade. To see this, we consider the time evolution of the large-scale energy at the scales $k_n \le K := k_{n_K}$ with $n_K \in \{n_f, \cdots, N\}$,

$$\frac{d}{dt} \sum_{n=0}^{n_K} \frac{1}{2} \langle |u_n|^2 \rangle = -\langle \Pi_K \rangle + \varepsilon - \sum_{n=0}^{n_K} \nu k_n^2 \langle |u_n|^2 \rangle + \sum_{n=0}^{n_K} \frac{2\nu k_n^2 k_{\rm B} T}{\rho}, \tag{7.6}$$

where Π_K denotes the scale-to-scale energy flux from the large scales $k_n \le K$ to the small scales $k_n > K$:

$$\Pi_K := -\frac{1}{2} \sum_{n=0}^{n_K} (B_n(u, u^*) u_n^* + B_n^*(u, u^*) u_n). \tag{7.7}$$

Because the viscous dissipation is negligible at scales much larger than the Kolmogorov dissipation scale $\eta \equiv k_\nu^{-1} := \nu^{3/4} \varepsilon^{-1/4}$, the last two terms on the right-hand side of (7.6) can be ignored within the inertial range $k_f \ll K \ll k_\nu$, where $k_f := k_{n_f}$. Hence, in the steady state, we obtain

$$\langle \Pi_K \rangle_{\rm ss} = \varepsilon \quad \text{for} \quad k_f \ll K \ll k_\nu. \tag{7.8}$$

The energy is thus transferred conservatively from large to small scales within the inertial range. Note that while the condition $k_f < K$ instead of $k_f \ll K$ is sufficient, we use the conventional definition for the inertial range.

7.3 Information-theoretic quantities

To quantify the information transfer among the shell variables, we use the information-theoretic quantities introduced in the previous chapter. We first define the large-scale and small-scale shell variables as $\boldsymbol{U}_K^< := \{u_n, u_n^* | n \le n_K\}$ and $\boldsymbol{U}_K^> := \{u, u^*\} \backslash \boldsymbol{U}_K^<$, respectively (see Fig. 7.1). The strength of the correlation between $\boldsymbol{U}_K^<$ and $\boldsymbol{U}_K^>$ is quantified by the mutual information (MI) [227]:

$$I[\boldsymbol{U}_K^< : \boldsymbol{U}_K^>] := \left\langle \ln \frac{p_t(\boldsymbol{U}_K^<, \boldsymbol{U}_K^>)}{p_t^<(\boldsymbol{U}_K^<) p_t^>(\boldsymbol{U}_K^>)} \right\rangle, \tag{7.9}$$

where $\langle \cdot \rangle$ denotes the average with respect to the joint probability distribution $p_t(\boldsymbol{U}_K^<, \boldsymbol{U}_K^>)$, and $p_t^<(\boldsymbol{U}_K^<)$ and $p_t^>(\boldsymbol{U}_K^>)$ are the marginal distributions. Note that the MI is nonnegative and is equal to zero if and only if $\boldsymbol{U}_K^<$ and $\boldsymbol{U}_K^>$ are independent.

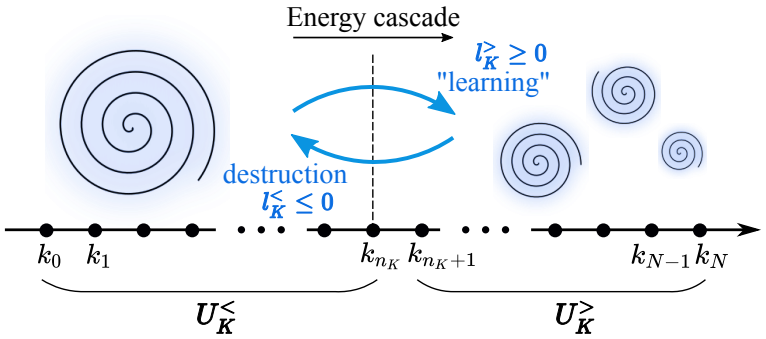

Fig. 7.1: Schematic of information flow in the energy cascade.

We quantify the directional information flow across scales by using learning rate (LR) [221, 224, 228, 264]. The LR that characterizes the rate at which $\boldsymbol{U}_K^<$ acquires information about $\boldsymbol{U}_K^>$ is defined as

$$l_K^< := \lim_{dt\to 0^+} \frac{I[\boldsymbol{U}_K^<(t+dt):\boldsymbol{U}_K^>(t)] - I[\boldsymbol{U}_K^<(t):\boldsymbol{U}_K^>(t)]}{dt}. \tag{7.10}$$

Similarly, the LR associated with $\boldsymbol{U}_K^>$ is defined by

$$l_K^> := \lim_{dt\to 0^+} \frac{I[\boldsymbol{U}_K^<(t):\boldsymbol{U}_K^>(t+dt)] - I[\boldsymbol{U}_K^<(t):\boldsymbol{U}_K^>(t)]}{dt}. \tag{7.11}$$

Note that, since $d_t I[\boldsymbol{U}_K^<:\boldsymbol{U}_K^>] = l_K^< + l_K^>$, the two LRs have opposite signs in the steady state $l_K^< = -l_K^>$. If $l_K^< > 0$ at time t, for example, then $\boldsymbol{U}_K^<$ acquires information about the instantaneous state $\boldsymbol{U}_K^>(t)$. In this sense, $\boldsymbol{U}_K^<$ is "learning" about or measuring $\boldsymbol{U}_K^>$. In contrast, if $l_K^< < 0$, then the correlation between $\boldsymbol{U}_K^<(t)$ and $\boldsymbol{U}_K^>(t)$ is destroyed or consumed.

7.4 Main result

7.4.1 Main result

In the steady state, for any K within the inertial range $k_f \ll K \ll k_\nu$, the LRs $l_K^<$ and $l_K^>$ satisfy the following inequalities:

$$0 \geq l_K^< \geq -\frac{\rho\varepsilon}{k_{\mathrm{B}}T}, \tag{7.12}$$

$$\frac{\rho\varepsilon}{k_{\mathrm{B}}T} \geq l_K^> \geq 0. \tag{7.13}$$

These inequalities are the main result of this chapter, which will be derived below. The inequality (7.12) implies that the large-scale shell variables $\boldsymbol{U}_K^<$ are destroying information about the small-scale variables $\boldsymbol{U}_K^>$ while transferring kinetic energy to small scales. In contrast, (7.13) states that the small-scale shell variables $\boldsymbol{U}_K^>$ are "learning" about $\boldsymbol{U}_K^<$ while receiving the kinetic energy from large scales (see Fig. 7.1). In particular, the maximum LR is given by $\rho\varepsilon/k_{\mathrm{B}}T$.

7.4.2 Derivation of the main result

The main result is a direct consequence of the second law of information thermodynamics for bipartite systems [218]. Specifically, we first formulate the second law of information thermodynamics for (7.1) by dividing the shell variables $\{u, u^*\}$ into the two groups $\boldsymbol{U}_K^<$ and $\boldsymbol{U}_K^>$, and then we take the inviscid limit $\nu \to 0$.

Let $S[\boldsymbol{U}_K^<]$ be the Shannon entropy of the large-scale shell variables, which is defined by $S[\boldsymbol{U}_K^<] := -\int d\boldsymbol{U}_K^< p_t^<(\boldsymbol{U}_K^<) \ln p_t^<(\boldsymbol{U}_K^<)$. The entropy increase in the heat bath associated with $\boldsymbol{U}_K^<$ is given by the sum of the contributions of each shell [219, 265]:

$$\begin{aligned}\dot{S}_{\rm env}^< &= -\sum_{n=0}^{n_K} \frac{\rho}{2k_{\rm B}T} \left\langle u_n^* \circ \left(-\nu k_n^2 u_n + \sqrt{\frac{2\nu k_n^2 k_{\rm B}T}{\rho}} \xi_n \right) + \text{c.c.} \right\rangle \\ &= \sum_{n=0}^{n_K} \frac{\rho}{2k_{\rm B}T} \langle u_n^* \circ (B_n(u, u^*) + f_n - \dot{u}_n) + \text{c.c.} \rangle, \end{aligned} \tag{7.14}$$

where c.c. denotes the complex conjugate, and $\circ$ denotes the multiplication in the sense of Stratonovich [198]. Similarly, let $S[\boldsymbol{U}_K^>]$ and $\dot{S}_{\rm env}^>$ be the Shannon entropy and entropy increase in the heat bath associated with the small-scale shell variables $\boldsymbol{U}_K^>$, respectively. The second law of information thermodynamics is then given by

$$\frac{d}{dt} S[\boldsymbol{U}_K^<] + \dot{S}_{\rm env}^< \geq I_K^<, \tag{7.15}$$

$$\frac{d}{dt} S[\boldsymbol{U}_K^>] + \dot{S}_{\rm env}^> \geq I_K^>. \tag{7.16}$$

See Appendix 7.7.1 for the derivation of the second law of information thermodynamics for the shell model. If $\boldsymbol{U}_K^<$ and $\boldsymbol{U}_K^>$ are independent, then $I_K^< = I_K^> = 0$ and the standard second law of thermodynamics follows. In contrast, if they are correlated, then $I_K^<$ and $I_K^>$ can be either positive or negative.

We now assume that the system is in the steady state and set K to be within the inertial range $k_f \ll K \ll k_\nu$. Then, $\dot{S}_{\rm env}^<$ and $\dot{S}_{\rm env}^>$ can be expressed in terms of the energy flux (7.7) as

$$\dot{S}_{\rm env}^< = \frac{\rho}{k_{\rm B}T} \left(\varepsilon - \langle \Pi_K \rangle_{\rm ss} \right), \tag{7.17}$$

$$\dot{S}_{\rm env}^> = \frac{\rho}{k_{\rm B}T} \langle \Pi_K \rangle_{\rm ss}, \tag{7.18}$$

where we have used $\Pi_{k_N} = 0$, which follows from the property of the nonlinear term $B_n(u, u^*)$ (7.3). By substituting these expressions into (7.15) and (7.16) and by noting that $\langle \Pi_K \rangle_{\rm ss} \to \varepsilon$ as $K/k_\nu \to 0$ and $I_K^< + I_K^> = 0$ in the steady state, we arrive at the main result (7.12) and (7.13).

7.4.3 Remark: information-thermodynamic efficiency

Here, we introduce the information-thermodynamic efficiency associated with the energy cascade. We consider the steady state and suppose that K is within the inertial range. Since $I_K^> \geq 0$ from the main result (7.13), we can introduce the following information-

thermodynamic efficiency for the small-scale shell variables (see Section 6.3.3):

$$\eta_K^> := \frac{l_K^>}{\dot{S}_{\rm env}^>} = \frac{l_K^>}{\rho\varepsilon/k_{\rm B}T}. \tag{7.19}$$

This efficiency quantifies how efficiently the small-scale eddies gain information about the large-scale eddies relative to the energy dissipation. We note that the information-thermodynamic efficiency for the large-scale shell variables defined as $\eta_K^< := |\dot{S}_{\rm env}^<|/|l_K^<|$ is zero if $l_K^< < 0$ because $\dot{S}_{\rm env}^< = 0$ in the inertial range (7.17). This is obvious because the shell model does not act as an information engine that converts information into output work. We remark that we can define another type of information-thermodynamic efficiencies by formulating the first law of information thermodynamics for the shell model, as in the previous chapter (see Appendix 7.7.2).

7.5 Numerical simulation

7.5.1 Setup

We here numerically illustrate the main result by estimating the LR. We set $N = 22$ and $n_f = 1$ to ensure that the external force acts only on 0th and 1st shells of the total 23 shells. The values of the external force and the other parameters are chosen following [20, 258] so that the achieved Reynolds number (Re) and the ratio of the thermal energy to the kinetic energy at the Kolmogorov dissipation scale are both comparable to the typical values in the atmospheric boundary layer, i.e., Re $\sim 10^6$ with $k_{\rm B}T/\rho u_\eta^2 \sim 10^{-8}$, where $u_\eta := (\varepsilon\nu)^{1/4}$ denotes the characteristic velocity at the Kolmogorov dissipation scale. To investigate the Reynolds number dependence of the LR, we have also performed a simulation for a low Reynolds number, Re $\sim 10^5$, by setting $N = 19$. For both $N = 19$ and 22 cases, we have used $N_{\rm samp} = 3 \times 10^5$ samples in the following averaging and estimation. Further details of the numerical simulation are given in Appendix 7.7.3.

7.5.2 Energy spectrum

Figure 7.2(a) shows the energy spectrum $E_n := \langle |u_n|^2 \rangle_{\rm ss}/2$ in the steady state. The achieved Reynolds numbers are Re $\simeq 9.25 \times 10^4$ and 1.46×10^6 for the two cases $N = 19$ and 22, respectively. From this figure, we can see that the spectrum is consistent with the Kolmogorov spectrum in the inertial range, $E_n \propto k_n^{-2/3}$, while it exhibits the equipartition of energy in the dissipation range, $E_n = k_{\rm B}T/\rho$.

7.5.3 Mutual information

We now estimate the LR defined by (7.10) and (7.11). To this end, we first estimate the MI. Note that the naive binning approach is not feasible in this case because it requires estimation of the $2(N+1)$-dimensional probability density $p_t(\boldsymbol{U}_K^<, \boldsymbol{U}_K^>)$. Instead, we use the so-called Kraskov-Stögbauer-Grassberger (KSG) estimator [266–268] (for the details of the KSG estimator, see Appendix 7.7.3), which has the advantage that it does not require estimation of the underlying probability density. The KSG estimator uses the distances to the k-th nearest neighbors of the sample points in the data to detect the structures of the

underlying probability distribution. While we set $k = 4$ here, following [266], essentially the same result can be obtained for other values of k. Because the KSG estimator is based on the local uniformity assumption of the probability density, the estimated value approaches the true value as $N_{\mathrm{samp}} \to \infty$ when this assumption is satisfied.

Figure 7.2(b) shows the estimated MI $\hat{I}^{(k)}_{\mathrm{KSG}}[\boldsymbol{U}^{<}_K(t):\boldsymbol{U}^{>}_K(t)]$. Its standard deviation is also estimated to be $\sim 10^{-3}$ by subsampling [268], which lies within the marker size. Notably, the MI is almost independent of K in the inertial range, while it takes relatively large and small values in the injection and dissipation scales, respectively. This result reflects the dynamics that is scale-invariant in the inertial range while affected by external forces and thermal fluctuations in the injection and dissipation scales.

7.5.4 Learning rate

The LR can be estimated by substituting $\hat{I}^{(k)}_{\mathrm{KSG}}$ into (7.10) or (7.11). Note that this procedure requires high accuracy in the estimation of the MI because the LR is defined through increments in the MI. Because it is not feasible to increase the number of samples, we instead take the approach of using the largest possible time increment Δt. Correspondingly, we focus only on $l^{<}_K$, because $l^{>}_K$ is defined through increments in the small-scale shell variables $\boldsymbol{U}^{>}_K$, which are fast variables relative to $\boldsymbol{U}^{<}_K$. We therefore estimate $l^{<}_K$, as defined by (7.10), using

$$\hat{l}^{<}_K := \frac{\hat{I}^{(k)}_{\mathrm{KSG}}[\boldsymbol{U}^{<}_K(t+\Delta t):\boldsymbol{U}^{>}_K(t)] - \hat{I}^{(k)}_{\mathrm{KSG}}[\boldsymbol{U}^{<}_K(t):\boldsymbol{U}^{>}_K(t)]}{\Delta t}. \tag{7.20}$$

Because we are interested in K within the inertial range, we choose Δt such that it is smaller than the smallest time scale in the inertial range. Therefore, we set $\Delta t = 0.1\tau_\eta$, where $\tau_\eta := \eta/u_\eta$ denotes the typical time scale at the Kolmogorov dissipation scale. Note that Δt is different from the time step $\delta t := 10^{-5}\tau_\eta$ used in solving (7.1) numerically.

In Fig. 7.2(c), we show the estimated LR $\hat{l}^{<}_K$ in units of the inverse of the large-eddy turnover time $\tau_L := 1/k_0 u_{\mathrm{rms}}$, where $u^2_{\mathrm{rms}} := \sum_{n=0}^{N}\langle|u_n|^2\rangle_{\mathrm{ss}}$. For $\mathrm{Re} \simeq 10^5$, we find that $\tau_L \simeq 181\tau_\eta$, while for $\mathrm{Re} \simeq 10^6$, we find that $\tau_L \simeq 734\tau_\eta$. From this figure, we can see that the LR takes negative values for K within the inertial range. Because $(\rho\varepsilon/k_{\mathrm{B}}T)\tau_L \simeq 7.79 \times 10^9$ for $\mathrm{Re} \simeq 10^5$ and 3.15×10^{10} for $\mathrm{Re} \simeq 10^6$, (7.12) is indeed satisfied. Interestingly, the lower bound of (7.12) is a loose bound. By noting that $l^{<}_K = -l^{>}_K$ in the steady state, this result states that the information-thermodynamic efficiency $\eta^{>}_K$ is quite low [218]. In other words, the small-scale eddies acquire information about the large-scale eddies at a relatively high thermodynamic cost. This property is in contrast to other typical information processing systems such as Maxwell's demon [218, 224, 228] and thus characterizes turbulence dynamics.

Furthermore, Fig. 7.2(c) suggests that the LR can be scaled as $l^{<}_K \sim C/\tau_L$ in the inertial range, where C denotes a Re-independent dimensionless constant. By noting that τ_L can be interpreted as the characteristic time scale for the largest eddies to be stretched into smaller eddies, this result implies that the information of large-scale eddies is transferred to small scales by this stretching process.

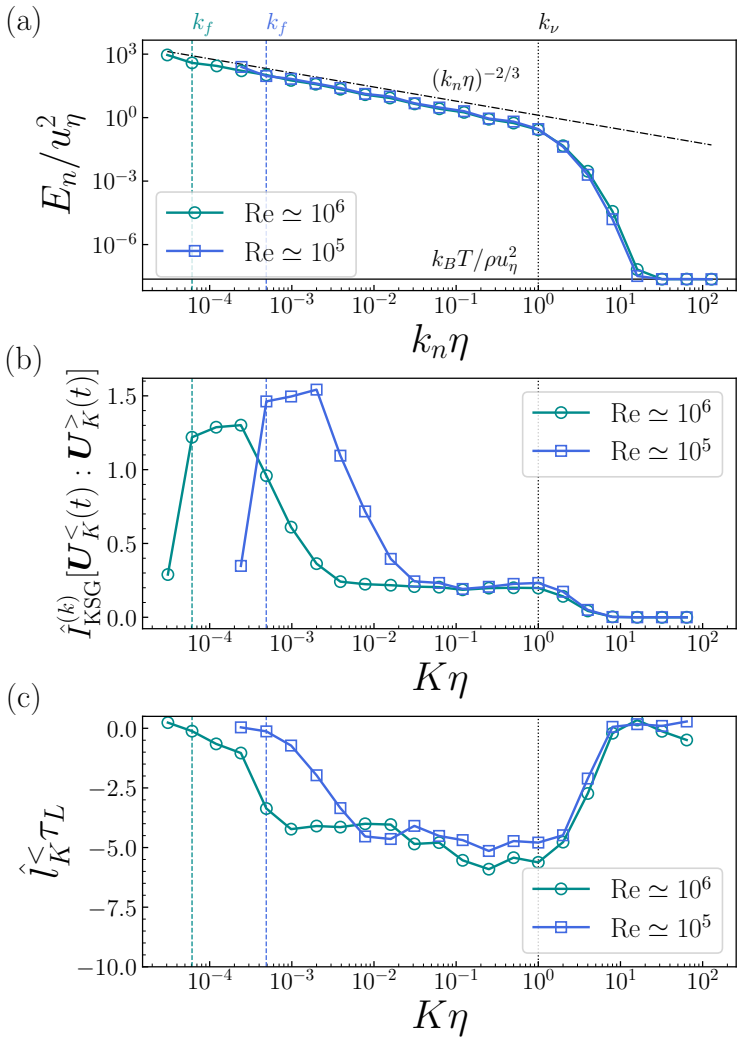

Fig. 7.2: (a) Scale dependence of the energy spectrum $E_n = \langle |u_n|^2 \rangle_{\mathrm{ss}}/2$. The dash-dotted line represents $\varepsilon^{2/3} k_n^{-2/3}$. The solid line represents the thermal equipartition value $k_{\mathrm{B}}T/\rho$. (b) Scale dependence of the estimated MI $\hat{I}^{(k)}_{\mathrm{KSG}}[\boldsymbol{U}^<_K(t):\boldsymbol{U}^>_K(t)]$ with $k = 4$. The error bars are within the marker size. (c) Scale dependence of the estimated LR $\hat{l}^<_K$. Note that it is plotted in units of the inverse of τ_L. In all panels, the dotted and dashed lines represent the Kolmogorov dissipation scale $k_\nu = 1/\eta$ and injection scale k_f, respectively.

7.6 Concluding remarks

We have investigated the nature of information flow in turbulence from an information-thermodynamic viewpoint. Thermal fluctuations are crucial in deriving the universal relation (7.12) and (7.13) for information flow. On the other hand, it should be noted that the information flow itself is mainly governed by the large-scale dynamics rather than by the thermal fluctuations. In fact, the LR in the deterministic case ($T = 0$) is found to be almost the same as in the noisy case ($T > 0$) in the inertial range (see Appendix 7.7.3). This result is consistent with the fact that the LR can be scaled as $l_K^< \sim C/\tau_L$ in the inertial range.

We now provide some technical remarks on estimation of the LR. Although the KSG estimator used here is asymptotically unbiased for $N_{\rm samp} \to \infty$, there are a sample-size-dependent bias and a k-dependent bias for a finite $N_{\rm samp}$ in general [268]. In our case, as shown in Appendix 7.7.3, we have found that the magnitude of $\hat{I}^{(k)}_{\rm KSG}[\boldsymbol{U}_K^< : \boldsymbol{U}_K^>]$ depends on k. This may be because the probability distribution $p_t(\boldsymbol{U}_K^<, \boldsymbol{U}_K^>)$ is skewed and has heavy tails, thus violating the local uniformity condition [268]. Nevertheless, we have also confirmed that the sign of $\hat{l}_K^<$ does not depend on the choice of k. It should also be noted that the number of samples $N_{\rm samp}$ used here is not sufficient for high accurate estimation of the LR because the standard deviation of the estimated MI is comparable to its increment. In other words, if we naively estimate the error bar of the LR $\hat{l}_K^<$ by using the estimated standard deviation of the MI, it is of the same order as $\hat{l}_K^<$ itself. It is therefore desirable to perform the numerical calculations with higher accuracy while taking the bias into account.

Although we have focused on the Sabra shell model, similar results to those presented here would hold for other turbulence models, including the fluctuating Navier–Stokes equation [23, 187]. Because turbulent cascade is a ubiquitous phenomenon as shown in the previous chapters, it would be interesting to investigate the nature of the information flow in these various systems.

7.7 Appendix

Here, we first provide the detailed derivation of the second law of information thermodynamics (Section 7.7.1). We then formulate the first law of information thermodynamics for the shell model and investigate another type of information-thermodynamic efficiency (Section 7.7.2). Finally, we describe the details of the numerical simulation (Section 7.7.3). In particular, we provide the result for the deterministic case at the end of this section.

7.7.1 Derivation of the second law of information thermodynamics

In this section, we explain the derivation of the second law of information thermodynamics for the stochastic Sabra shell model.

Formulation of the second law of thermodynamics

First, we formulate the standard second law of thermodynamics. Let $S[u, u^*]$ be the system entropy defined by

$$S[u, u^*] := -\int du du^* p_t(u, u^*) \ln p_t(u, u^*), \tag{7.21}$$

where $dudu^* := \prod_n d\mathrm{Re}[u_n] d\mathrm{Im}[u_n]$, and $p_t(u, u^*)$ denotes the probability distribution function. Here, we use the notation $S[u, u^*]$ to indicate the relevant random variables (u, u^*) although $S[u, u^*]$ is not a function of (u, u^*). The time evolution of $p_t(u, u^*)$ is governed by the following Fokker-Planck equation [269]:

$$\begin{aligned}\partial_t p_t(u,u^*) &= \sum_{n=0}^{N}\left[-\frac{\partial}{\partial u_n}\left(A_n(u,u^*)p_t(u,u^*)\right) - \frac{\partial}{\partial u_n^*}\left(A_n^*(u,u^*)p_t(u,u^*)\right)\right.\\ &\qquad \left. + \frac{4\nu k_n^2 k_{\mathrm{B}}T}{\rho}\frac{\partial^2}{\partial u_n \partial u_n^*}p_t(u,u^*)\right]\\ &= \sum_{n=0}^{N}\left[-\frac{\partial}{\partial u_n}J_n(u,u^*) - \frac{\partial}{\partial u_n^*}J_n^*(u,u^*)\right], \end{aligned} \tag{7.22}$$

where

$$A_n(u,u^*) := B_n(u,u^*) - \nu k_n^2 u_n + f_n, \tag{7.23}$$

and $J_n(u, u^*)$ denotes the probability current,

$$J_n(u,u^*) := A_n(u,u^*)p_t(u,u^*) - \frac{2\nu k_n^2 k_{\mathrm{B}}T}{\rho}\frac{\partial}{\partial u_n^*}p_t(u,u^*). \tag{7.24}$$

Therefore, the average rate of change of the system entropy is given by

$$\begin{aligned}\frac{d}{dt}S[u,u^*] &= -\frac{d}{dt}\int dudu^* p_t(u,u^*)\ln p_t(u,u^*)\\ &= -\int dudu^*(\partial_t p_t(u,u^*))\ln p_t(u,u^*) - \int dudu^*\partial_t p_t(u,u^*)\\ &= \int dudu^*\sum_{n=0}^{N}\left[\frac{\partial}{\partial u_n}J_n(u,u^*) + \frac{\partial}{\partial u_n^*}J_n^*(u,u^*)\right]\ln p_t(u,u^*) - \frac{d}{dt}\int dudu^* p_t(u,u^*)\\ &= \sum_{n=0}^{N}\dot{S}_n[u,u^*]. \end{aligned} \tag{7.25}$$

In the last line, we have introduced $\dot{S}_n[u, u^*]$, which is given by

$$\dot{S}_n[u,u^*] := -\int dudu^*\left[J_n(u,u^*)\frac{\partial}{\partial u_n}\ln p_t(u,u^*) + J_n^*(u,u^*)\frac{\partial}{\partial u_n^*}\ln p_t(u,u^*)\right], \tag{7.26}$$

where the over-dot denotes the rates of change of observables that are not a time derivative of a state function.

Let Δs^{env} be the stochastic medium entropy production in an infinitesimal time interval $[t, t + dt]$. To identify Δs^{env}, we impose the local detailed balance condition [234, 270]:

$$\Delta s^{\mathrm{env}} = \ln\frac{p(u', u'^*, t+dt|u, u^*, t)}{p(-u, -u^*, t+dt|-u', -u'^*, t)}. \tag{7.27}$$

Here, the transition probability density $p(u', u'^*, t + dt|u, u^*, t)$ is given by, in the Ito scheme, [269]

$$p(u', u'^*, t+dt|u, u^*, t) = \prod_{n=0}^{N}\frac{\rho}{4\pi\nu k_n^2 k_{\mathrm{B}}T dt}\exp\left(-\frac{\rho}{4\nu k_n^2 k_{\mathrm{B}}T dt}|du_n - A_n(u,u^*)dt|^2\right), \tag{7.28}$$

where $du := u' - u$ with $u(t) = u$ and $u(t+dt) = u'$. Similarly, $p(-u, -u^*, t+dt|-u', -u'^*, t)$ is given by

$$\begin{aligned} &p(-u, -u^*, t+dt| - u', -u'^*, t) \\ &= \prod_{n=0}^{N} \frac{\rho}{4\pi\nu k_n^2 k_{\mathrm{B}} T dt} \exp\left(-\frac{\rho}{4\nu k_n^2 k_{\mathrm{B}} T dt} \left| du_n - \left[-A_n^{\mathrm{ir}}(u,u^*) + A_n^{\mathrm{rev}}(u,u^*) \right] dt \right|^2 \right. \\ &\quad \left. - \left[\frac{\partial}{\partial u_n} A_n^{\mathrm{ir}}(u,u^*) + \frac{\partial}{\partial u_n^*} A_n^{\mathrm{ir}*}(u,u^*) - \frac{\partial}{\partial u_n} A_n^{\mathrm{rev}}(u,u^*) - \frac{\partial}{\partial u_n^*} A_n^{\mathrm{rev}*}(u,u^*) \right] dt \right), \end{aligned} \tag{7.29}$$

where $A_n^{\mathrm{ir}}(u,u^*)$ and $A_n^{\mathrm{rev}}(u,u^*)$ denote the irreversible and reversible parts of $A_n(u,u^*)$, respectively:

$$\begin{aligned} A_n^{\mathrm{ir}}(u,u^*) &:= \frac{1}{2}\left[A_n(u,u^*) - A_n(-u,-u^*) \right] \\ &= -\nu k_n^2 u_n, \end{aligned} \tag{7.30}$$

$$\begin{aligned} A_n^{\mathrm{rev}}(u,u^*) &:= \frac{1}{2}\left[A_n(u,u^*) + A_n(-u,-u^*) \right] \\ &= B_n(u,u^*) + f_n. \end{aligned} \tag{7.31}$$

By substituting (7.28) and (7.29) into (7.27), we obtain

$$\Delta s^{\mathrm{env}} = \sum_{n=0}^{N} \Delta s_n^{\mathrm{env}}, \tag{7.32}$$

where

$$\begin{aligned} \Delta s_n^{\mathrm{env}} := &\frac{\rho}{2\nu k_n^2 k_{\mathrm{B}} T} \left[A_n^{\mathrm{ir}}(u,u^*) du_n^* - A_n^{\mathrm{ir}}(u,u^*) A_n^{\mathrm{rev}*}(u,u^*) dt \right] \\ &+ \left[\frac{\partial}{\partial u_n} A_n^{\mathrm{ir}}(u,u^*) - \frac{\partial}{\partial u_n} A_n^{\mathrm{rev}}(u,u^*) \right] dt + \text{c.c.}. \end{aligned} \tag{7.33}$$

Note that, by using the Stratonovich product [198], this expression can be simply rewritten as

$$\Delta s_n^{\mathrm{env}} = \frac{\rho}{2k_{\mathrm{B}}T} \left\{ u_n^* \circ \left[(B_n(u,u^*) + f_n) dt - du_n \right] + u_n \circ \left[(B_n^*(u,u^*) + f_n^*) dt - du_n^* \right] \right\}. \tag{7.34}$$

The average medium entropy production can be calculated as

$$\langle \Delta s^{\mathrm{env}} \rangle = \int du du^* p_t(u,u^*) \langle \Delta s^{\mathrm{env}} | u, u^* \rangle, \tag{7.35}$$

where the conditional average $\langle \Delta s^{\mathrm{env}} | u, u^* \rangle$ can be evaluated by replacing du_n (resp. du_n^*) with $A_n(u,u^*)dt$ (resp. $A_n^*(u,u^*)dt$) in Δs^{env}. Then, the medium entropy production rate reads

$$\frac{\langle \Delta s^{\mathrm{env}} \rangle}{dt} = \sum_{n=0}^{N} \dot{S}_n^{\mathrm{env}}, \tag{7.36}$$

where $\dot{S}_n^{\rm env}$ denotes the contribution from the n-th shell:

$$\begin{aligned}\dot{S}_n^{\rm env} &:= \frac{\langle \Delta s_n^{\rm env}\rangle}{dt} \\ &= \int dudu^* p_t(u,u^*)\left\{\frac{\rho}{\nu k_n^2 k_{\rm B}T}|A_n^{\rm ir}(u,u^*)|^2 + \left[\frac{\partial}{\partial u_n}A_n^{\rm ir}(u,u^*) - \frac{\partial}{\partial u_n}A_n^{\rm rev}(u,u^*) + {\rm c.c.}\right]\right\}\end{aligned} \tag{7.37}$$

By combining (7.25) and (7.36), the second law of thermodynamics can be expressed as

$$\begin{aligned}\frac{d}{dt}S[u,u^*] + \frac{\langle \Delta s^{\rm env}\rangle}{dt} &= \sum_{n=0}^{N}\int dudu^* \frac{\rho}{\nu k_n^2 k_{\rm B}T}\frac{|J_n^{\rm ir}(u,u^*)|^2}{p_t(u,u^*)} \\ &\geq 0,\end{aligned} \tag{7.38}$$

where $J_n^{\rm ir}(u,u^*)$ denotes the irreversible current given by

$$\begin{aligned}J_n^{\rm ir}(u,u^*) &= \frac{1}{2}\left[J_n(u,u^*) - J_n(-u,-u^*)\right] \\ &= A_n^{\rm ir}(u,u^*)p_t(u,u^*) - \frac{2\nu k_n^2 k_{\rm B}T}{\rho}\frac{\partial}{\partial u_n^*}p_t(u,u^*).\end{aligned} \tag{7.39}$$

Furthermore, since the total system $\{u,u^*\}$ can be considered as a $N+1$ multipartite systems, i.e., each shell variable (u_n,u_n^*) experiences independent noise, it follows that the second law holds for each shell variable individually [265]:

$$\begin{aligned}\dot{S}_n[u,u^*] + \dot{S}_n^{\rm env} &= \int dudu^* \frac{\rho}{\nu k_n^2 k_{\rm B}T}\frac{|J_n^{\rm ir}(u,u^*)|^2}{p_t(u,u^*)} \\ &\geq 0.\end{aligned} \tag{7.40}$$

Derivation of the second law of information thermodynamics

We now derive the second law of information thermodynamics for the bipartite systems $\boldsymbol{U}_K^<$ and $\boldsymbol{U}_K^>$ [218, 265]. First, we rewrite $\dot{S}_n[u,u^*]$ for $n \leq n_K$ as

$$\begin{aligned}\dot{S}_n[u,u^*] &= -\int dudu^*\left[J_n(u,u^*)\frac{\partial}{\partial u_n}\ln p_t(\boldsymbol{U}_K^<|\boldsymbol{U}_K^>) + J_n^*(u,u^*)\frac{\partial}{\partial u_n^*}\ln p_t(\boldsymbol{U}_K^<|\boldsymbol{U}_K^>)\right] \\ &= \dot{S}_n[\boldsymbol{U}_K^<|\boldsymbol{U}_K^>],\end{aligned} \tag{7.41}$$

where we have used $p_t(u,u^*) = p_t(\boldsymbol{U}_K^<,\boldsymbol{U}_K^>)$ and $\partial p_t(\boldsymbol{U}_K^>)/\partial u_n = \partial p_t(\boldsymbol{U}_K^>)/\partial u_n^* = 0$ for $n \leq n_K$. Note that $\dot{S}_n[\boldsymbol{U}_K^<|\boldsymbol{U}_K^>]$ is related to the learning rate through the following relation:

$$\begin{aligned}l_K^< &:= \frac{I[\boldsymbol{U}_K^<(t+dt):\boldsymbol{U}_K^>(t)] - I[\boldsymbol{U}_K^<(t):\boldsymbol{U}_K^>(t)]}{dt} \\ &= \frac{1}{dt}\Big(S[\boldsymbol{U}_K^<(t+dt)] - S[\boldsymbol{U}_K^<(t+dt)|\boldsymbol{U}_K^>(t)] - S[\boldsymbol{U}_K^<(t)] + S[\boldsymbol{U}_K^<(t)|\boldsymbol{U}_K^>(t)]\Big) \\ &= \frac{d}{dt}S[\boldsymbol{U}_K^<] - \sum_{n=0}^{n_K}\dot{S}_n[\boldsymbol{U}_K^<|\boldsymbol{U}_K^>].\end{aligned} \tag{7.42}$$

From (7.40)-(7.42), we obtain the second law of information thermodynamics for $\boldsymbol{U}_K^<$,

$$\frac{d}{dt}S[\boldsymbol{U}_K^<] + \dot{S}_{\rm env}^< \geq l_K^<, \tag{7.43}$$

where

$$\dot{S}_{\rm env}^< := \sum_{n=0}^{n_K} \dot{S}_n^{\rm env}. \tag{7.44}$$

Similarly, we can derive the second law of information thermodynamics for $\boldsymbol{U}_K^>$:

$$\frac{d}{dt}S[\boldsymbol{U}_K^>] + \dot{S}_{\rm env}^> \geq l_K^>, \tag{7.45}$$

where

$$\dot{S}_{\rm env}^> := \sum_{n=n_K+1}^{N} \dot{S}_n^{\rm env}. \tag{7.46}$$

7.7.2 First law of information thermodynamics

Here, we formulate the first law of information thermodynamics, following Chapter 6. We identify heat absorbed by the large-scale shell variables as

$$\begin{aligned}\hat{\dot{Q}}_K^< &= \sum_{n=0}^{n_K} \frac{\rho}{2}\left[u_n^* \circ \left(-\nu k_n^2 u_n + \sqrt{\frac{2\nu k_n^2 k_{\rm B}T}{\rho}}\xi_n\right) + \text{c.c.}\right] \\ &= -\sum_{n=0}^{n_K} \frac{\rho}{2}\left[u_n^* \circ (B_n(u,u^*) + f_n - \dot{u}_n) + \text{c.c.}\right], \end{aligned} \tag{7.47}$$

which is consistent with the medium entropy production rate (7.14). Similarly, externally applied work to the large-scale shell variables is identified with

$$\hat{\dot{W}}_K^< = \sum_{n=0}^{n_K} \frac{\rho}{2}\left[u_n^* f_n + \text{c.c.}\right]. \tag{7.48}$$

By combining these two expressions, we obtain

$$\frac{d}{dt}\left(\sum_{n=0}^{n_K}\frac{1}{2}\rho|u_n|^2\right) + \rho\Pi_K = \hat{\dot{W}}_K^< + \hat{\dot{Q}}_K^<. \tag{7.49}$$

Similarly, for the small-scale shell variables, we obtain

$$\frac{d}{dt}\left(\sum_{n=n_K+1}^{N}\frac{1}{2}\rho|u_n|^2\right) - \rho\Pi_K = \hat{\dot{W}}_K^> + \hat{\dot{Q}}_K^>. \tag{7.50}$$

By comparing (7.49) and (7.50) with (6.36) and (6.37) for the overdamped Langevin case, the term $\rho\Pi_K$ can be interpreted as work from the large-scale to small-scale shell variables.

As in Section 6.3.3, we can also introduce another type of information-thermodynamic efficiencies by using the first law of information thermodynamics. We first note that in

the steady state, the second law of information thermodynamics (7.15) and (7.16) can be expressed in terms of $\dot{W}_K^< := \langle \hat{\dot{W}}_K^< \rangle$ and $\dot{W}_K^> := \langle \hat{\dot{W}}_K^> \rangle$ as

$$\beta \dot{W}_K^< - \beta\rho \langle \Pi_K \rangle_{\rm ss} - l_K^< \geq 0, \tag{7.51}$$

$$\beta \dot{W}_K^> + \beta\rho \langle \Pi_K \rangle_{\rm ss} - l_K^> \geq 0. \tag{7.52}$$

Since $\dot{W}_K^< = \rho\varepsilon$ and $\dot{W}_K^> = 0$ in the inertial range, the transduced capacity $\beta\rho\langle \Pi_K \rangle_{\rm ss} - l_K^>$ is nonnegative. Then, as in Section 6.3.3, we can introduce the following information-thermodynamic efficiency:

$$\begin{aligned} \tilde{\eta}_K^< &:= \frac{\beta\rho\langle \Pi_K \rangle_{\rm ss} + l_K^<}{\beta \dot{W}_K^<} \\ &= 1 - \frac{|l_K^<|}{\rho\varepsilon / k_{\rm B}T} \\ &= 1 - \eta_K^>, \end{aligned} \tag{7.53}$$

where we have used $\langle \Pi_K \rangle_{\rm ss} = \varepsilon$ and the main result (7.12), and

$$\tilde{\eta}_K^> := \frac{|\beta \dot{W}_K^>|}{\beta\rho\langle \Pi_K \rangle_{\rm ss} - l_K^>}, \tag{7.54}$$

which is zero if $\beta\rho\langle \Pi_K \rangle_{\rm ss} - l_K^> \neq 0$. The efficiency (7.53) quantifies how efficiently the large-scale eddies converts applied work into transduced capacity. Interestingly, there is a trade-off between $\eta_K^>$ and $\tilde{\eta}_K^<$. For example, if $\tilde{\eta}_K^<$ approaches 1, then $\eta_K^>$ must go to zero. Note that this result is specific to turbulence because it is based on the relation $\langle \Pi_K \rangle_{\rm ss} = \varepsilon$.

The numerical estimation of the LR described in Section 7.5.4 implies that $\tilde{\eta}_K^< \simeq 1$. That is, the large-scale eddies operate with high efficiency, while almost all the externally applied work is converted into work from large-scale to small-scale eddies rather than information transfer.

7.7.3 Details of the numerical simulation

In this section, we explain the details of the numerical simulation. After describing the setup, the details of the KSG estimator are explained. In particular, we provide a detailed explanation of the method used to estimate the variance and bias of the KSG estimator. We also present the result in the deterministic case ($T = 0$).

Setup

To evaluate the inertial range straightforwardly, we first nondimensionalize the equation (7.1) with the Kolmogorov dissipation scale η and the velocity scale $u_\eta := (\varepsilon\nu)^{1/4}$ by setting

$$\hat{u}_n := u_n/u_\eta, \quad \hat{k}_n := \eta k_n, \quad \hat{t} := t/\tau_\eta, \quad \hat{\xi}_n := (u_\eta/\eta)^{-1/2}\xi_n, \quad \hat{f}_n := f_n/F, \tag{7.55}$$

where $\tau_\eta := \eta/u_\eta$ denotes the typical time scale at the Kolmogorov dissipation scale, and F denotes the typical magnitude of the force per mass. The nondimensionalized equation (7.1) reads

$$\dot{\hat{u}}_n = \hat{B}_n(\hat{u}, \hat{u}^*) - \hat{k}_n^2 \hat{u}_n + (2\theta_\eta)^{1/2}\hat{k}_n\hat{\xi}_n + \mathcal{F}_\eta \hat{f}_n, \tag{7.56}$$

where

$$\hat{B}_n(\hat{u},\hat{u}^*) := i\left(\hat{k}_{n+1}\hat{u}_{n+2}\hat{u}^*_{n+1} - \frac{1}{2}\hat{k}_n\hat{u}_{n+1}\hat{u}^*_{n-1} + \frac{1}{2}\hat{k}_{n-1}\hat{u}_{n-1}\hat{u}_{n-2}\right). \tag{7.57}$$

Here, $\theta_\eta := k_{\rm B}T/\rho u_\eta^2$ denotes the ratio of the thermal energy to the kinetic energy at the Kolmogorov dissipation scale, and $\mathcal{F}_\eta := F\eta/u_\eta^2$ denotes the nondimensionalized magnitude of the force. Correspondingly, we set the shell index to be $n = M, \cdots, R$ with $M = -[(3/4)\log_2(\mathrm{Re})]$ and $R = N - M$, so that $k_0 = 1$ corresponds to the Kolmogorov dissipation scale.

We use a slaved 3/2-strong-order Ito-Taylor scheme [271] with the time-step $\delta\hat{t} := 10^{-5}$, which is smaller than the viscous time scale at the highest wavenumber $\hat{\tau}_{\rm vis} := 1/\hat{k}_R^2 \sim 10^{-4}$. The parameter values are set to the same values used in [20,258], which are consistent with the typical values in the atmospheric boundary layer (ABL). Specifically, the range of shell numbers is chosen as $n = -15, \cdots, 7$ so that the achieved Reynolds number is comparable to the typical value in the ABL of $\mathrm{Re} \sim 10^6$. To investigate the Re dependence of the LR, we also perform the numerical simulation for $\mathrm{Re} \sim 10^5$ by setting $n = -12, \cdots, 7$. In both cases, the dimensionless temperature is chosen as $\theta_\eta := 2.328 \times 10^{-8}$, and the external force acts only on the first two shells, i.e., $n_f = -14$ for $\mathrm{Re} \sim 10^6$ and -11 for $\mathrm{Re} \sim 10^5$. The values of the external forces are adjusted such that $\hat{u}_{\rm rms} := \sqrt{\sum_{n=M}^R \langle|\hat{u}_n|^2\rangle} \sim 10^2$ and $\hat{\varepsilon} := \sum_{n=M}^R \hat{k}_n^2\langle|\hat{u}_n|^2\rangle \simeq 1$ [20,258]: for $\mathrm{Re} \sim 10^6$,

$$\begin{aligned}
\mathcal{F}_\eta\hat{f}_{-15} &= -0.008900918232183095 - 0.0305497603210104i,\\
\mathcal{F}_\eta\hat{f}_{-14} &= 0.005116337459331228 - 0.018175040700335127i,
\end{aligned} \tag{7.58}$$

while for $\mathrm{Re} \sim 10^5$,

$$\begin{aligned}
\mathcal{F}_\eta\hat{f}_{-12} &= -0.017415685046854878 - 0.05977417049893835i,\\
\mathcal{F}_\eta\hat{f}_{-11} &= 0.010010711194151034 - 0.03556158772544649i.
\end{aligned} \tag{7.59}$$

In the averaging of the energy spectrum and the estimation of the MI, we use $N_{\rm samp} = 3 \times 10^5$ samples. For the case of $\mathrm{Re} \sim 10^6$, these samples are obtained by sampling 100 snapshots at time $\hat{t} = 1000i$ $(i = 1, 2, \cdots, 100)$ for each of the 3000 noise realizations. That is, for each of the 3000 independent runs, we sample 100 snapshots. Here, the time interval of the sampling, 1000, is chosen to be larger than one large-eddy turnover time $\tau_L/\tau_\eta \simeq 734 < 1000$. Similarly, for the case of $\mathrm{Re} \sim 10^5$, $N_{\rm samp} = 3 \times 10^5$ samples are obtained by sampling 100 snapshots at time $\hat{t} = 500i$ $(i = 1, 2, \cdots, 100)$ for each of the 3000 noise realizations, where the time interval, 500, is chosen to be larger than one large-eddy turnover time $\tau_L/\tau_\eta \simeq 181 < 500$.

The KSG estimator

The KSG estimator for the mutual information $I[X:Y]$ (either or both of the random variables X and Y can be multidimensional) is defined as follows [266]:

$$\hat{I}^{(k)}_{\rm KSG}[X:Y] := \psi(k) - 1/k + \psi(N_{\rm samp}) - \frac{1}{N_{\rm samp}}\sum_{i=1}^{N_{\rm samp}}\left[\psi(n_x(i)) + \psi(n_y(i))\right], \tag{7.60}$$

where $k \in \mathbb{N}$ denotes the parameter of the KSG estimator, ψ is the digamma function, $N_{\rm samp}$ denotes the total number of samples, and $n_\alpha^{(k)}(i)$ $(\alpha = x, y)$ is the number of samples

such that $\|\alpha_j - \alpha_i\| \leq \varepsilon_\alpha^{(k)}(i)/2$. Here, $\varepsilon_\alpha^{(k)}(i)$ denotes the α extent of the smallest hyper-rectangle in the (x, y) space centered at the i-th sample (x_i, y_i) that contains k of its neighboring samples. While any norms can be used for $\|\alpha_j - \alpha_i\|$, we use the standard Euclidean norm here.

Note that k is the only free parameter of the KSG estimator. By varying k, we can detect the structure of the underlying probability distribution in different spatial resolutions. To choose the optimal k (if it exists), we must estimate both the standard deviation and the bias of the KSG estimator [268].

Estimation of the variance of the KSG estimator

In this section, we explain the method used to estimate of the variance of the KSG estimator based on the subsampling approach proposed by Holmes and Nemenman [268]. This method is based on the fact that the variance of any function that is an average of N i.i.d. random variables scales as $1/N$. Therefore, we write the variance of the KSG estimator as

$$\mathrm{Var}_{N_{\mathrm{samp}}}[\hat{I}^{(k)}_{\mathrm{KSG}}] = \frac{B^{(k)}}{N_{\mathrm{samp}}}. \tag{7.61}$$

We estimate $B^{(k)}$ via a subsampling approach. Specifically, we first partition the $N_{\mathrm{samp}} = N$ samples into n nonoverlapping subsets of equal size as much as possible. Let $\hat{I}^{(k)}_{\mathrm{KSG},i}(N/n)$ be the i-th realization of $\hat{I}^{(k)}_{\mathrm{KSG}}[X:Y]$ with $N_{\mathrm{samp}} = N/n$ $(i = 1, 2, \cdots, n)$. Then, we calculate the unbiased sample variance of these n values of $\hat{I}^{(k)}_{\mathrm{KSG},i}(N/n)$:

$$\sigma^2_{k,N/n} := \frac{1}{n-1}\sum_{i=1}^{n}\left(\hat{I}^{(k)}_{\mathrm{KSG},i}(N/n) - \frac{1}{n}\sum_{i=1}^{n}\hat{I}^{(k)}_{\mathrm{KSG},i}(N/n)\right)^2. \tag{7.62}$$

This is our estimate of $\mathrm{Var}_{N/n}[\hat{I}^{(k)}_{\mathrm{KSG}}] = nB^{(k)}/N$. Finally, we estimate $B^{(k)}$ by using maximum likelihood estimation. In doing so, we first calculate $\sigma^2_{k,N/n_\ell}$ for various n_ℓ $(\ell = 1, 2, \cdots, L)$. Then, from Cochran's theorem, $(n_\ell - 1)\sigma^2_{k,N/n_\ell}/\mathrm{Var}_{N/n_\ell}[\hat{I}^{(k)}_{\mathrm{KSG}}]$ follows the χ^2-distribution with $n_\ell - 1$ degrees of freedom:

$$P^{(\chi^2)}_{n_\ell-1}(x) := \frac{1}{2^{(n_\ell-1)/2}\Gamma(\frac{n_\ell-1}{2})}x^{\frac{n_\ell-1}{2}-1}e^{-x/2}. \tag{7.63}$$

By assuming independence of $\{\sigma^2_{k,N/n_\ell}\}_{\ell=1}^{L}$, a likelihood function for $B^{(k)}$ is

$$\prod_{\ell=1}^{L} P^{(\chi^2)}_{n_\ell-1}\left(\frac{N(n_\ell-1)\sigma^2_{k,N/n_\ell}}{B^{(k)}n_\ell}\right). \tag{7.64}$$

We then obtain the maximum likelihood estimator:

$$\begin{aligned}\hat{B}^{(k)} &:= \arg\max_{B^{(k)}}\prod_{\ell=1}^{L} P^{(\chi^2)}_{n_\ell-1}\left(\frac{N(n_\ell-1)\sigma^2_{k,N/n_\ell}}{B^{(k)}n_\ell}\right)\\ &= \frac{\sum_{\ell=1}^{L}\frac{n_\ell-1}{n_\ell}N\sigma^2_{k,N/n_\ell}}{\sum_{\ell=1}^{L}(n_\ell-3)}.\end{aligned} \tag{7.65}$$

By combining (7.61) and (7.65), we can estimate the variance of the KSG estimator to be $\hat{B}^{(k)}/N_{\mathrm{samp}}$.

Estimation bias of the KSG estimator

Although the KSG estimator is asymptotically unbiased for sufficiently regular probability distributions as $N_{\mathrm{samp}} \to \infty$, both sample-size-dependent bias and k-dependent bias generally exist for a finite N_{samp} [268]. The sample-size-dependent (resp. k-dependent) bias can be detected by comparing the sample-size-dependence (resp. k-dependence) of the estimated MI with its standard deviation. If the sample-size-dependence (resp. k-dependence) of the estimated MI is much larger than its standard deviation, then a sample-size-dependent (resp. k-dependent) bias may be present.

Note that k is related to the spatial resolution in detecting the structure of the underlying probability distribution. For large k, because the fine structure of the probability distribution cannot be detected, we would expect the MI to be underestimated. At the same time, because $n_x(i)$ and $n_y(i)$ both increase with increasing k, the standard deviation of the estimated MI will be smaller for large k. If there is no k-dependent bias, we can choose the optimal k such that there is no sample-size-dependence compared to the standard deviation and the standard deviation is the smallest.

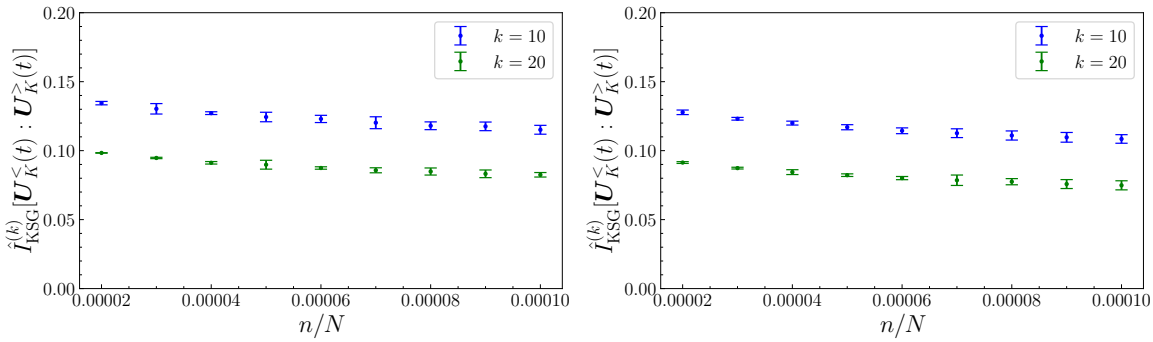

Fig. 7.3: Bias of the KSG estimator $\hat{I}^{(k)}_{\mathrm{KSG}}[\boldsymbol{U}^{<}_{K}(t):\boldsymbol{U}^{>}_{K}(t)]$ as a function of $1/N_{\mathrm{samp}} = n/N$ with $n = 2, 3, \cdots, 10$ and $N = 10^5$. $K = k_{10}$ (left) and $K = k_{15}$ (right).

Figure 7.3 shows bias of the KSG estimator $\hat{I}^{(k)}_{\mathrm{KSG}}[\boldsymbol{U}^{<}_{K}(t):\boldsymbol{U}^{>}_{K}(t)]$ as a function of $1/N_{\mathrm{samp}} = n/N$ with $N = 10^5$ in the case of $\mathrm{Re} \sim 10^6$. Here, we use $n = 2, 3, \cdots, 10$, following [268]. The wave number K is within the inertial range, $K = k_{10}$ (left), and at the Kolmogorov dissipation scale, $K = k_{15}$ (right). The error bars are estimated by using the unbiased sample variance (7.62). From (7.61) and (7.65), the standard deviation of $\hat{I}^{(k)}_{\mathrm{KSG}}[\boldsymbol{U}^{<}_{K}(t):\boldsymbol{U}^{>}_{K}(t)]$ is estimated to be $\sim 10^{-3}$ for $N_{\mathrm{samp}} \sim 10^5$. It can be seen from Fig. 7.3 that, while there is no significant sample-size-dependent bias, a k-dependent bias does exist. In particular, the estimated MI is underestimated as k is increased.

Figure 7.4 shows the scale dependences of the estimated MI and LR for $k = 4, 10, 20, 50$ with $N_{\mathrm{samp}} = 2 \times 10^5$ in the case of $\mathrm{Re} \sim 10^6$. Here, $k = 4$ is chosen because $k = 2, 3, 4$ are recommended in [266]. This results clearly show that the estimated MI and LR are underestimated as k is increased. Therefore, it is difficult to choose the optimal k in this case. The important point here is that the estimated LR is negative for K within the inertial range for all k. As mentioned in the main text, we remark that the error bar of the LR $\hat{l}^{<}_{K}$ is of the same order as $\hat{l}^{<}_{K}$ itself if we naively estimate it by using the estimated standard deviation of the MI.

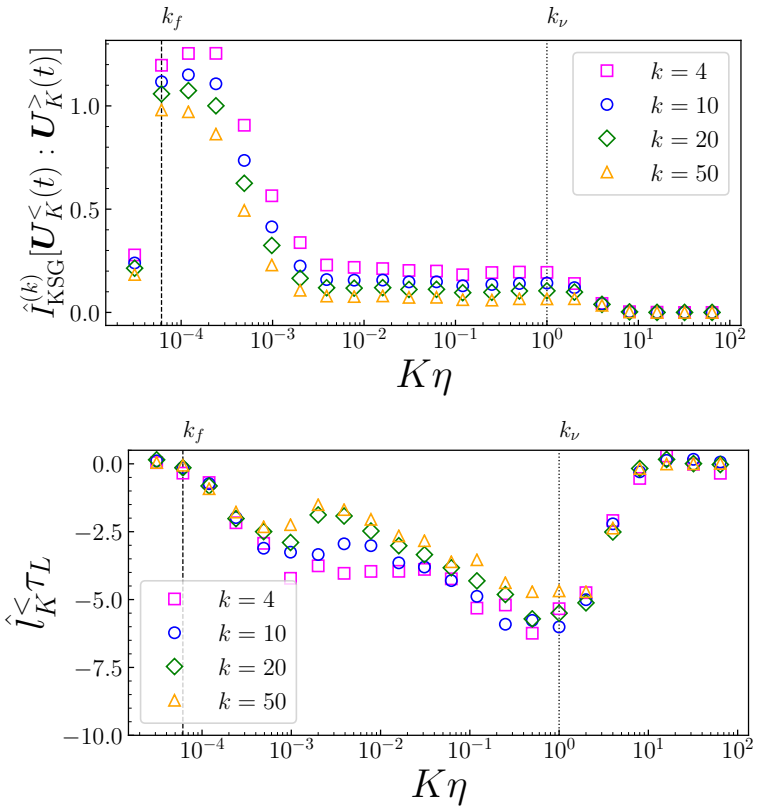

Fig. 7.4: Scale dependences of the estimated MI $\hat{I}^{(k)}_{\mathrm{KSG}}[\boldsymbol{U}^{<}_K(t) : \boldsymbol{U}^{>}_K(t)]$ (top) and LR $\hat{l}^{<}_K$ (bottom). Note that the LR is plotted in units of the inverse of τ_L.

Deterministic case

Here, we present the result in the deterministic case ($T = 0$). We calculate the deterministic case by setting $\theta_\eta = 0$ in the Ito-Taylor scheme. Other parameters are the same as in the noisy case with $N = 22$. As independent initial-data, we use the snapshots in the noisy case at time $\hat{t} = 10^5$. We have used $N_{\mathrm{samp}} = 2 \times 10^5$ samples in the following averaging and estimation. These samples are obtained by sampling 100 snapshots at time $\hat{t} = 1000i$ ($i = 1, 2, \cdots, 100$) for each of the 2000 independent runs.

Figure 7.5(a) shows the energy spectrum $E_n := \langle |u_n|^2 \rangle_{\mathrm{ss}}/2$ in the steady state. The achieved Reynolds number in the deterministic case is $\mathrm{Re} \simeq 1.46 \times 10^6$. In the inertial range, both the deterministic and noisy cases exhibit the Kolmogorov spectrum. In the dissipation range, in contrast, the deterministic case shows a rapid exponential decay.

Figure 7.5(b) shows the estimated MI $\hat{I}^{(k)}_{\mathrm{KSG}}[\boldsymbol{U}^{<}_K(t) : \boldsymbol{U}^{>}_K(t)]$ with $k = 4$. Its standard deviation is also estimated to be $\sim 10^{-3}$ by subsampling, which lies within the marker size. While the deterministic case is almost the same as the noisy case in the inertial range, it takes a finite value even in the dissipation range. In other words, the correlation between large and small scales is not destroyed because of the absence of thermal fluctuations.

In Fig. 7.5(c), we show the estimated LR $\hat{l}^{<}_K$ in units of the inverse of the large-eddy turnover time τ_L. In the deterministic case, we find that $\tau_L \simeq 732\tau_\eta$. From this figure, we can see that the LR in the deterministic case takes almost the same value as in the noisy case in the inertial range. This result implies that the information flow itself is mainly governed by the large-scale dynamics rather than by the thermal fluctuations. In contrast,

it takes finite negative value in the dissipation range. In other words, in the absence of thermal fluctuations, the information flow reaches the far dissipation range.

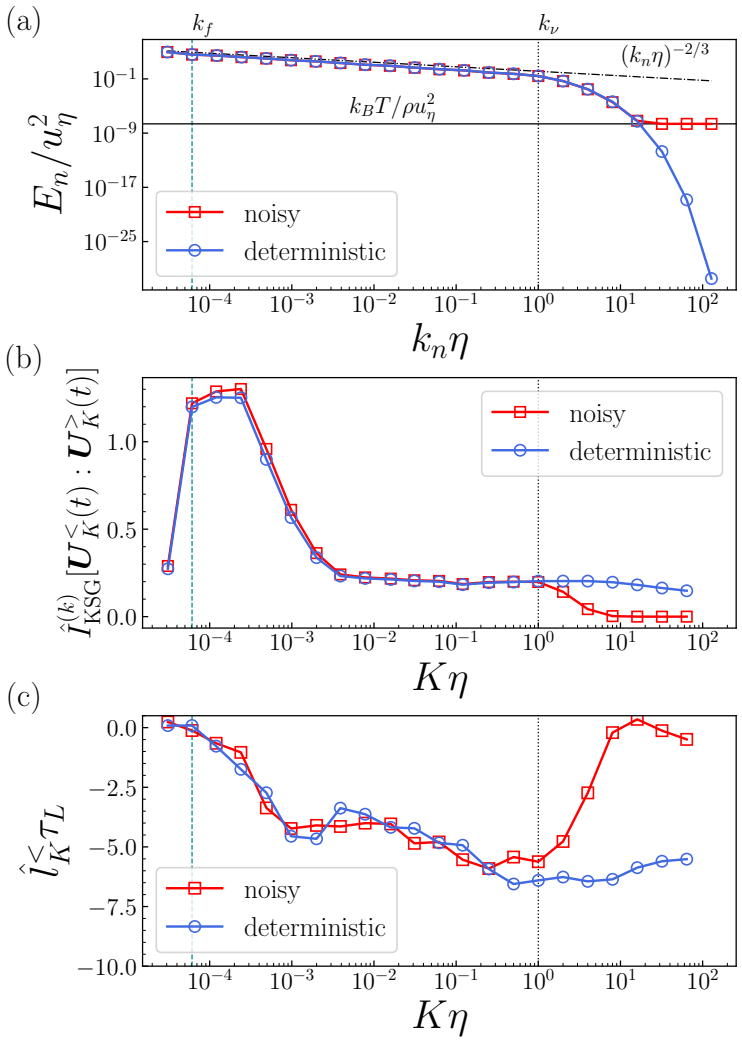

Fig. 7.5: (a) Scale dependence of the energy spectrum $E_n = \langle |u_n|^2 \rangle_{\mathrm{ss}}/2$. The dash-dotted line represents $\varepsilon^{2/3}k_n^{-2/3}$. The solid line represents the thermal equipartition value $k_{\mathrm{B}}T/\rho$. (b) Scale dependence of the estimated MI $\hat{I}^{(k)}_{\mathrm{KSG}}[\boldsymbol{U}^<_K(t):\boldsymbol{U}^>_K(t)]$ with $k = 4$. The error bars are within the marker size. (c) Scale dependence of the estimated LR $\hat{l}^<_K$. Note that it is plotted in units of the inverse of τ_L. In all panels, the dotted and dashed lines represent the Kolmogorov dissipation scale $k_\nu = 1/\eta$ and injection scale k_f, respectively. The noisy case is the same as the one presented in the main text (cyan line in Fig. 7.2).

Chapter 8

Conclusions and future perspectives

Cascade transfer lies at the core of turbulence. It is widely observed in various systems, not limited to ordinary fluids, and underlies the universality in those systems. In this thesis, we have investigated such universal aspects of cascade transfer from the viewpoint of statistical physics. Specifically, in Part I, we aim to establish the concept of "universality class" for cascade transfer. As a first step toward this end, we have explored novel types of cascade phenomena by considering (i) fluid quite different from ordinary fluid, (ii) ordinary fluid under extreme conditions, and (iii) a simple model different from a fluid model:

(i) We have investigated the similarity and difference between quantum and classical turbulence in Chapter 3. By using a phenomenological argument based on the Onsager "ideal turbulence" theory, we have shown that the compressibility effects can induce a novel energy cascade, which we call quantum stress cascade, at scales smaller than the mean intervortex distance.

(ii) We have explored a novel type of energy cascade by focusing on supercritical turbulence near a gas-liquid critical point in Chapter 4. By using a similar argument developed in Chapter 3, we have shown that it exhibits a novel type of energy cascade, which we call van der Waals cascade, at "microscopic length scales" smaller than the correlation length of equilibrium density fluctuations. Interestingly, the mechanism of this novel cascade is analogous to that of the quantum stress cascade in quantum turbulence.

(iii) In Chapter 5, we have proposed a simple model representing one universality class for cascade transfer without paying much attention to its relevance to real systems. The constructed model can be regarded as a modified XY model where the amplitude fluctuates. We have shown that an inverse energy cascade with a non-Kolmogorov energy spectrum $E(k) \propto k^{-3}$ emerges from spatially local interactions. Interestingly, the behavior of this model is similar to that observed in spin turbulence and atmospheric turbulence.

To summarize, we have found various types of cascade transfer in systems quite different from ordinary fluids. From these results, we propose a tentative and naive classification of various cascade transfer phenomena, which is summarized in Fig. 8.1. While these results are still far from our ultimate goal of establishing the concept of "universality class," the author believes that these findings provide a novel phenomenological perspective on turbulence.

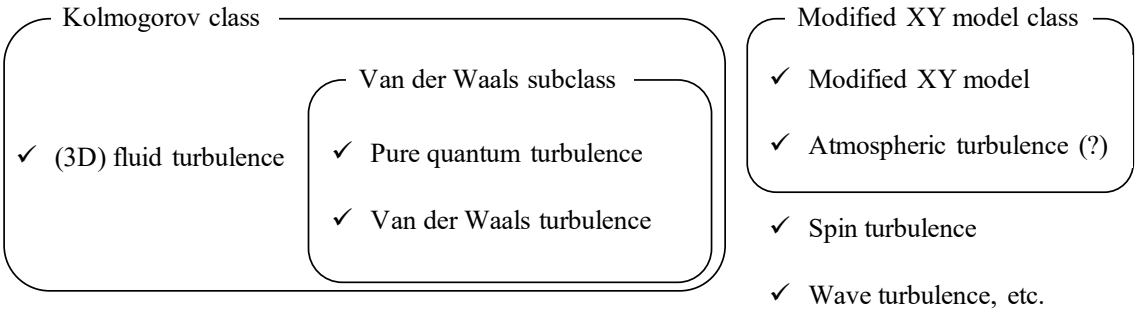

Fig. 8.1: Naive classification of various cascade transfer phenomena.

In Part II, we aim to elucidate the nature of information flow associated with cascade transfer in ordinary fluid turbulence. Specifically, we have investigated how information flows in the shell model with thermal noise from an information-thermodynamic viewpoint. We have shown that information of turbulent fluctuations flows from large to small scales along with the energy cascade. Furthermore, our numerical simulations suggest that transferring information from large to small scales involves enormous thermodynamic costs. While turbulence has been studied in various contexts from an information-theoretic viewpoint over recent decades, this is the first theoretical study to show the unidirectional information transfer across scales. Because this study is in the early-stage research, there are still many unsettled issues concerning information flow in turbulence. In the following, we list some topics for future work.

- **Universality and information flow**
  At the end of Section 1.3, we mentioned a common intuitive picture of the origin of universality that small-scale turbulent fluctuations "forget" the details of large scales because of the chaotic nature of the stepwise cascade process. This picture is somewhat contrary to the fact that information of turbulent fluctuations is transferred from large to small scales. However, the coexistence of information transfer and universality is not logically inconsistent. We conjecture that the coexistence can be explained by the stepwise "information cascade" process where "irrelevant information" is "deamplified" as the cascade develops. This cascade picture is analogous to that proposed by Wilson in the context of critical phenomena [272]. As a first step to establish this picture, simple models in information and communication theory would provide a useful starting point.

- **Tighter bound on information flow**
  In Chapter 7, we have found that the information-thermodynamic efficiency $\eta_K^>$ is quite low compared to other typical information processing systems. In other words, the bound on information flow based on the second law of information thermodynamics, $\frac{\rho\varepsilon}{k_{\rm B}T} \geq l_K^>$, is a loose bound. In recent years, the *thermodynamic uncertainty relation* (TUR) has been intensively investigated, which gives a lower bound on the entropy production via experimentally accessible quantities [273, 274]. In systems with time-reversal symmetry, this relation can be extended to bipartite systems and gives a bound on learning rate [242]. Thus, we conjecture that even in turbulence, where time-reversal symmetry is broken, there are tighter bounds on the learning rate than the second law of information thermodynamics.

- **Intermittency and information flow**

Intermittency remains the central enigma of turbulence. As we mentioned in Section 1.1, intermittency implies that the statistical property of the small-scale turbulent fluctuations depends on the injection scale L. In other words, the small-scale turbulent fluctuations "remember" the number of "cascade steps." From this observation, we naively expect that intermittency can be understood from the viewpoint of information flow. For example, by exploring universal relations that connect information flow with the higher-order longitudinal structure function, it would become possible to obtain universal bounds on the scaling exponent ζ_p.

- **Information flow in other systems**
  As we briefly mentioned at the end of Section 7.6, we conjecture that, even in other cascade transfer phenomena, information is transferred across scales along with the cascade transfer. Indeed, for two-dimensional fluid turbulence, we can show that information of turbulent fluctuations is transferred from small to large scales along with the inverse energy cascade. It would be interesting to investigate the nature of information flow in various systems, such as quantum fluids, supercritical fluids near a gas-liquid critical point, spin systems, and elastic bodies. Furthermore, such an information-theoretic viewpoint may provide a fresh perspective on the mechanism of the laminar-turbulence transition. It is known that the two characteristic collective modes, called *zonal flow* and *turbulent puffs*, govern the laminar-turbulence transition. Interestingly, their dynamics can be mapped to the stochastic predator-prey model, and fluctuations of zonal flows follow those of turbulent puffs with a time delay [275–277]. Thus, we conjecture that there is an information flow from turbulent puffs to zonal flows.

We hope that these studies open up a new research area, "information hydrodynamics," which would provide a theoretical framework to elucidate and control the dynamics of complicated systems, such as the Earth system and biochemical reaction networks.

Acknowledgment

I first would like to thank my supervisor, Shin-ichi Sasa, for his enlightening discussion and encouragement during my doctoral studies. His passion for science, pursuit of clarity, and many exciting scientific ideas have inspired me greatly.

Throughout my research life, I have benefited from discussions with a lot of people. I first thank my collaborator, Ryo Araki. His work on minimal modeling of quasi-cyclic phenomena inspired me to investigate information flow in turbulence. His dedicated support, especially on numerical simulations, was very helpful. He also read this manuscript critically and provided useful comments. I would like to thank Takeshi Matsumoto for fruitful discussions of almost all the topics contained in this thesis and for reading this manuscript. In particular, the discussion with him on the Onsager theory was very informative and interesting. I am very grateful to Gregory L. Eyink. He not only gave me kind and helpful comments on my research, especially on the Onsager theory and thermal noise effects, but also encouraged me greatly. I also thank Dmytro Bandak for his helpful comments on the numerical simulation for the stochastic shell model. I would like to thank Michikazu Kobayashi, Makoto Tsubota, and Kazuya Fujimoto for useful discussions on quantum turbulence and modified XY model. I express my appreciation to Susumu Goto and Masanobu Inubushi for their fruitful comments on the modified XY model and information flow in turbulence. I would also like to thank Keiji Saito and Tan Van Vu for useful discussions on quantum turbulence and ongoing collaborations on information thermodynamics. I also thank Rory T. Cerbus, Yoshiki Hiruta, Masaru Hongo, Takashi Sakajo, Shintaro Sato, Shota Shigetomi, and Akira Yoshida for useful comments or various discussions on my research.

I am also grateful to the past and present members of the Nonlinear Dynamics Group: Andreas Dechant, Hiroki Ohta, Yuki Minami, Masato Itami, Taiki Haga, Hiroyoshi Nakano, Akito Inoue, Shuhei Taniguchi, Mutsumi Minoguchi, Mao Hiraizumi, Ken Hiura, Kazuma Nishimura, Yuya Watanabe, Takaya Taguchi, Kanta Nunotani, Ikumi Kobayashi, Yusuke Yanagisawa, Kazuma Yokota, Yutaro Kado, Kenshin Matsumoto. They have helped me many times in my research and daily life.

Finally, I thank my family for their continuous support and encouragement.

References

[1] Schmitt, F. G. Turbulence from 1870 to 1920: The birth of a noun and of a concept. *Compt. Rend. Mécanique* **345**, 620–626 (2017).

[2] Ruelle, D. *Chance and Chaos*, vol. 110 (Princeton University Press, 1993). (邦訳：D. ルエール, 青木薫訳, 「偶然とカオス」, 岩波書店, (1993)).

[3] Eyink, G. L. & Sreenivasan, K. R. Onsager and the theory of hydrodynamic turbulence. *Rev. Mod. Phys.* **78**, 87 (2006).

[4] Tennekes, H. & Lumley, J. L. *A First Course in Turbulence* (MIT press, 1972).

[5] Frisch, U. *Turbulence* (Cambridge University Press, 1995).

[6] Bohr, T., Jensen, M. H., Paladin, G. & Vulpiani, A. *Dynamical Systems Approach to Turbulence* (1998).

[7] Pope, S. B. *Turbulent Flows* (Cambridge University Press, 2000).

[8] Davidson, P. A. *Turbulence: An Introduction for Scientists and Engineers* (Oxford University Press, 2015), 2nd edn.

[9] Dubrulle, B. Beyond Kolmogorov cascades. *J. Fluid Mech.* **867** (2019).

[10] Eyink, G. L. Turbulence Theory, Course Notes. http://www.ams.jhu.edu/~eyink/Turbulence/notes/.

[11] Dryden, H. L. A review of the statistical theory of turbulence. *Q. Appl. Math.* **1**, 7–42 (1943).

[12] Sreenivasan, K. R. On the scaling of the turbulence energy dissipation rate. *Phys. fluids* **27**, 1048–1051 (1984).

[13] Sreenivasan, K. R. An update on the energy dissipation rate in isotropic turbulence. *Phys. Fluids* **10**, 528–529 (1998).

[14] Cadot, O., Couder, Y., Daerr, A., Douady, S. & Tsinober, A. Energy injection in closed turbulent flows: Stirring through boundary layers versus inertial stirring. *Phys. Rev. E* **56**, 427 (1997).

[15] Pearson, B. R., Krogstad, P.-Å. & van de Water, W. Measurements of the turbulent energy dissipation rate. *Phys. fluids* **14**, 1288–1290 (2002).

[16] Kaneda, Y., Ishihara, T., Yokokawa, M., Itakura, K. & Uno, A. Energy dissipation rate and energy spectrum in high resolution direct numerical simulations of turbulence in a periodic box. *Phys. Fluids* **15**, L21–L24 (2003).

[17] Debue, P. *Experimental approach to the problem of the Navier-Stokes singularities.* Ph.D. thesis, Université Paris-Saclay (2019).

[18] Onsager, L. Statistical Hydrodynamics. *Nuovo Cimento Suppl.* **6**, 279 (1949).

[19] Garratt, J. R. *The Atmospheric Boundary Layer* (Cambridge University Press, 1994).

[20] Bandak, D., Goldenfeld, N., Mailybaev, A. A. & Eyink, G. Dissipation-range fluid turbulence and thermal noise. *Phys. Rev. E* **105**, 065113 (2022).

[21] Kolmogorov, A. N. Dissipation of energy in locally isotropic turbulence. *Dokl. Akad. Nauk SSSR* **32**, 16 (1941).

[22] Kolmogorov, A. N. The local structure of turbulence in incompressible viscous fluid for very large Reynolds numbers. *Dokl. Akad. Nauk SSSR* **30**, 9 (1941).

[23] Landau, L. D. & Lifshitz, E. M. *Fluid Mechanics*, vol. 6 (Addision-Wesley, Reading, MA, 1959).

[24] Oboukhov, A. M. On the distribution of energy in the spectrum of turbulent flow. *Dokl. Akad. Nauk SSSR* **32**, 22–24 (1941).

[25] Obukhov, A. M. Spectral energy distribution in a turbulent flow. *Izv. Akad. Nauk. SSSR, Ser. Geogr. Geofiz* **5**, 453–466 (1941).

[26] Onsager, L. The distribution of energy in turbulence. *Phys. Rev.* **68**, 286–286 (1945).

[27] von Weizsäcker, C. F. Das Spektrum der Turbulenz bei grossen Reynoldsschen Zahlen. *Zeit. f. Phys.* **124**, 614–627 (1948).

[28] Heisenberg, W. Zur statistischen Theorie der Turbulenz. *Zeit. f. Phys.* **124**, 628 (1948).

[29] Anselmet, F., Gagne, Y. l., Hopfinger, E. J. & Antonia, R. A. High-order velocity structure functions in turbulent shear flows. *J. Fluid Mech.* **140**, 63–89 (1984).

[30] Kolmogorov, A. N. A refinement of previous hypotheses concerning the local structure of turbulence in a viscous incompressible fluid at high Reynolds number. *J. Fluid Mech.* **13**, 82–85 (1962).

[31] Oboukhov, A. M. Some specific features of atmospheric tubulence. *J. Fluid Mech.* **13**, 77–81 (1962).

[32] She, Z.-S. & Leveque, E. Universal scaling laws in fully developed turbulence. *Phys. Rev. Lett.* **72**, 336 (1994).

[33] She, Z.-S. & Waymire, E. C. Quantized energy cascade and log-Poisson statistics in fully developed turbulence. *Phys. Rev. Lett.* **74**, 262 (1995).

[34] Dubrulle, B. Intermittency in fully developed turbulence: Log-Poisson statistics and generalized scale covariance. *Phys. Rev. Lett.* **73**, 959 (1994).

[35] Ruelle, D. Hydrodynamic turbulence as a problem in nonequilibrium statistical mechanics. *Proc. Natl. Acad. Sci. U. S. A.* **109**, 20344–20346 (2012).

[36] Ruelle, D. Non-equilibrium statistical mechanics of turbulence. *J. Stat. Phys.* **157**, 205–218 (2014).

[37] Ruelle, D. A Theory of Hydrodynamic Turbulence Based on Non-equilibrium Statistical Mechanics. *J. Stat. Phys.* **169**, 1039–1044 (2017).

[38] Oono, Y. & Puri, S. Study of phase-separation dynamics by use of cell dynamical systems. I. Modeling. *Phys. Rev. A* **38**, 434 (1988).

[39] Ladyzhenskaya, O. A. Sixth problem of the millennium: Navier-Stokes equations, existence and smoothness. *Russ. Math. Surv.* **58**, 251 (2003).

[40] Grad, H. Asymptotic theory of the Boltzmann equation. *Phys. Fluids* **6**, 147–181 (1963).

[41] Quastel, J. & Yau, H.-T. Lattice gases, large deviations, and the incompressible Navier-Stokes equations. *Ann. Math.* 51–108 (1998).

[42] Sasa, S.-i. Derivation of hydrodynamics from the Hamiltonian description of particle systems. *Phys. Rev. Lett.* **112**, 100602 (2014).

[43] Sreenivasan, K. R. *et al.* Asymmetry of velocity increments in fully developed turbulence and the scaling of low-order moments. *Phys. Rev. Lett.* **77**, 1488 (1996).

[44] Gotoh, T., Fukayama, D. & Nakano, T. Velocity field statistics in homogeneous steady turbulence obtained using a high-resolution direct numerical simulation. *Phys. Fluids* **14**, 1065–1081 (2002).

[45] Taylor, M. A., Kurien, S. & Eyink, G. L. Recovering isotropic statistics in turbulence simulations: The Kolmogorov 4/5th law. *Phys. Rev. E* **68**, 026310 (2003).

[46] Taylor, G. I. Statistical theory of turbulence. *Proc. R. Soc. Lond. A Math. Phys. Sci.* **151**, 421–444 (1935).

[47] Tsubota, M., Kobayashi, M. & Takeuchi, H. Quantum hydrodynamics. *Phys. Rep.* **522**, 191–238 (2013).

[48] Madeira, L., Caracanhas, M., Dos Santos, F. & Bagnato, V. Quantum Turbulence in Quantum Gases. *Annu. Rev. Condens. Matter Phys.* **11**, 37–56 (2020).

[49] Tsubota, M. Quantum Turbulence. *J. Phys. Soc. Jpn* **77**, 111006–111006 (2008).

[50] Barenghi, C. F., Skrbek, L. & Sreenivasan, K. R. Introduction to quantum turbulence. *Proc. Natl. Acad. Sci. U. S. A.* **111**, 4647–4652 (2014).

[51] Tsatsos, M. C. *et al.* Quantum turbulence in trapped atomic Bose–Einstein condensates. *Phys. Rep.* **622**, 1–52 (2016).

[52] Zakharov, V. E., L'vov, V. S. & Falkovich, G. *Kolmogorov Spectra of Turbulence I: Wave turbulence* (Springer, Berlin, 1992).

[53] Nazarenko, S. *Wave Turbulence*, vol. 825 (Springer Science & Business Media, 2011).

[54] Fujimoto, K. & Tsubota, M. Counterflow instability and turbulence in a spin-1 spinor Bose-Einstein condensate. *Phys. Rev. A* **85**, 033642 (2012).

[55] Fujimoto, K. & Tsubota, M. Spin turbulence in a trapped spin-1 spinor Bose-Einstein condensate. *Phys. Rev. A* **85**, 053641 (2012).

[56] Fujimoto, K. & Tsubota, M. Spin turbulence with small spin magnitude in spin-1 spinor Bose-Einstein condensates. *Phys. Rev. A* **88**, 063628 (2013).

[57] Tsubota, M., Aoki, Y. & Fujimoto, K. Spin-glass-like behavior in the spin turbulence of spinor Bose-Einstein condensates. *Phys. Rev. A* **88**, 061601(R) (2013).

[58] Fujimoto, K. & Tsubota, M. Direct and inverse cascades of spin-wave turbulence in spin-1 ferromagnetic spinor Bose-Einstein condensates. *Phys. Rev. A* **93**, 033620 (2016).

[59] Rodriguez-Nieva, J. F. Turbulent relaxation after a quench in the Heisenberg model. *Phys. Rev. B* **104**, L060302 (2021).

[60] Tanogami, T. Theoretical analysis of quantum turbulence using the Onsager ideal turbulence theory. *Phys. Rev. E* **103**, 023106 (2021).

[61] Tanogami, T. Reply to "Comment on 'Theoretical analysis of quantum turbulence using the Onsager ideal turbulence theory' ". *Phys. Rev. E* **105**, 027102 (2022).

[62] Tanogami, T. & Sasa, S.-i. Van der Waals cascade in supercritical turbulence near a critical point. *Phys. Rev. Research* **3**, L032027 (2021).

[63] Tanogami, T. & Sasa, S.-i. XY model for cascade transfer. *Phys. Rev. Research* **4**, L022015 (2022).

[64] Feynman, R. P. Application of quantum mechanics to liquid helium. In *Progress in Low Temperature Physics*, vol. 1, 17–53 (Elsevier, 1955).

[65] Goldenfeld, N. *Lectures on Phase Transitions and the Renormalization Group* (CRC Press, 2018).

[66] Oono, Y. & Puri, S. Computationally efficient modeling of ordering of quenched phases. *Phys. Rev. Lett.* **58**, 836 (1987).

[67] Hinrichsen, H. Non-equilibrium critical phenomena and phase transitions into absorbing states. *Adv. Phys.* **49**, 815–958 (2000).

[68] Barabási, A.-L. & Stanley, H. E. *Fractal Concepts in Surface Growth* (Cambridge University Press, 1995).

[69] Takeuchi, K. A. An appetizer to modern developments on the Kardar–Parisi–Zhang universality class. *Physica A* **504**, 77–105 (2018).

[70] Ramaswamy, S. The mechanics and statistics of active matter. *Annu. Rev. Condens. Matter Phys.* **1**, 323–345 (2010).

[71] Yasuda, T., Goto, S. & Kawahara, G. Quasi-cyclic evolution of turbulence driven by a steady force in a periodic cube. *Fluid Dyn. Res.* **46**, 061413 (2014).

[72] Goto, S., Saito, Y. & Kawahara, G. Hierarchy of antiparallel vortex tubes in spatially periodic turbulence at high Reynolds numbers. *Phys. Rev. Fluids* **2**, 064603 (2017).

[73] Araki, R., Bos, W. J. T. & Goto, S. Minimal modeling of the intrinsic cycle of turbulence driven by steady forcing. *arXiv preprint arXiv:2112.03417* (2021).

[74] Pecora, L. M. & Carroll, T. L. Synchronization in chaotic systems. *Phys. Rev. Lett.* **64**, 821 (1990).

[75] Boccaletti, S., Kurths, J., Osipov, G., Valladares, D. & Zhou, C. The synchronization of chaotic systems. *Phys. Rep.* **366**, 1–101 (2002).

[76] Yoshida, K., Yamaguchi, J. & Kaneda, Y. Regeneration of small eddies by data assimilation in turbulence. *Phys. Rev. Lett.* **94**, 014501 (2005).

[77] Lalescu, C. C., Meneveau, C. & Eyink, G. L. Synchronization of chaos in fully developed turbulence. *Phys. Rev. Lett.* **110**, 084102 (2013).

[78] Vela-Martín, A. The synchronisation of intense vorticity in isotropic turbulence. *J. Fluid Mech.* **913** (2021).

[79] Parrondo, J. M., Horowitz, J. M. & Sagawa, T. Thermodynamics of information. *Nat. Phys.* **11**, 131–139 (2015).

[80] Seifert, U. Stochastic thermodynamics, fluctuation theorems and molecular machines. *Rep. Prog. Phys.* **75**, 126001 (2012).

[81] Peliti, L. & Pigolotti, S. *Stochastic Thermodynamics: An Introduction* (Princeton University Press, 2021).

[82] Eyink, G. L. Review of the Onsager "Ideal Turbulence" Theory. *arXiv preprint arXiv:1803.02223* (2018).

[83] Eyink, G. L. Exact Results on Scaling Exponents in the 2D Enstrophy Cascade. *Phys. Rev. Lett.* **74**, 3800 (1995).

[84] Eyink, G. L. Dissipation in turbulent solutions of 2D Euler equations. *Nonlinearity* **14**, 787 (2001).

[85] Chae, D. Remarks on the Helicity of the 3-D Incompressible Euler Equations. *Commun. Math. Phys.* **240**, 501–507 (2003).

[86] Chen, Q., Chen, S. & Eyink, G. L. The Joint Cascade of Energy and Helicity in Three-Dimensional Turbulence. *Phys. Fluids* **15**, 361–374 (2003).

[87] Caflisch, R. E., Klapper, I. & Steele, G. Remarks on Singularities, Dimension and Energy Dissipation for Ideal Hydrodynamics and MHD. *Commun. Math. Phys.* **184**, 443–455 (1997).

[88] Aluie, H. & Eyink, G. L. Scale Locality of Magnetohydrodynamic Turbulence. *Phys. Rev. Lett.* **104**, 081101 (2010).

[89] Aluie, H. Coarse-grained incompressible magnetohydrodynamics: analyzing the turbulent cascades. *New J. Phys.* **19**, 025008 (2017).

[90] Feireisl, E., Gwiazda, P., Świerczewska-Gwiazda, A. & Wiedemann, E. Regularity and Energy Conservation for the Compressible Euler Equations. *Arch. Ration. Mech. An.* **223**, 1375–1395 (2017).

[91] Eyink, G. L. & Drivas, T. D. Cascades and Dissipative Anomalies in Compressible Fluid Turbulence. *Phys. Rev. X* **8**, 011022 (2018).

[92] Drivas, T. D. & Eyink, G. L. An Onsager Singularity Theorem for Turbulent Solutions of Compressible Euler Equations. *Commun. Math. Phys.* **359**, 733–763 (2018).

[93] Aluie, H. Compressible Turbulence: The Cascade and its Locality. *Phys. Rev. Lett.* **106**, 174502 (2011).

[94] Aluie, H. Scale locality and the inertial range in compressible turbulence. *arXiv preprint arXiv:1101.0150* (2010).

[95] Aluie, H. Scale decomposition in compressible turbulence. *Physica D* **247**, 54–65 (2013).

[96] Eyink, G. L. Cascades and Dissipative Anomalies in Nearly Collisionless Plasma Turbulence. *Phys. Rev. X* **8**, 041020 (2018).

[97] Eyink, G. L. & Drivas, T. D. Cascades and Dissipative Anomalies in Relativistic Fluid Turbulence. *Phys. Rev. X* **8**, 011023 (2018).

[98] Eyink, G. L. Energy dissipation without viscosity in ideal hydrodynamics I. Fourier analysis and local energy transfer. *Physica D* **78**, 222–240 (1994).

[99] von Neumann, J. Recent theories of turbulence. Unpublished report to the Office of Naval Research 1949, in Collected Works (Pergamon Press, New York, 1963), Vol. VI, p. 437. (邦訳：J. フォン ノイマン, 伊東恵一編訳, 「数理物理学の方法」, ちくま学芸文庫, (2013)).

[100] Constantin, P., Titi, E. S. & Weinan, E. Onsager's conjecture on the energy conservation for solutions of Euler's equation. *Commun. Math. Phys.* **165**, 207 (1994).

[101] Duchon, J. & Robert, R. Inertial energy dissipation for weak solutions of incompressible Euler and Navier-Stokes equations. *Nonlinearity* **13**, 249 (2000).

[102] Scheffer, V. An inviscid flow with compact support in space-time. *J. Geom. Anal.* **3**, 343–401 (1993).

[103] Shnirelman, A. On the nonuniqueness of weak solution of the Euler equation. *Comm. Pure Appl. Math.* **50**, 1261–1286 (1997).

[104] De Lellis, C. & Székelyhidi Jr, L. The Euler equations as a differential inclusion. *Ann. Math.* 1417–1436 (2009).

[105] De Lellis, C. & Székelyhidi, L. On admissibility criteria for weak solutions of the Euler equations. *Arch. Ration. Mech. Anal.* **195**, 225–260 (2010).

[106] De Lellis, C. & Székelyhidi, L. Dissipative continuous Euler flows. *Invent. Math.* **193**, 377–407 (2013).

[107] De Lellis, C. & Székelyhidi Jr, L. Dissipative Euler flows and Onsager's conjecture. *J. Eur. Math. Soc.* **16**, 1467–1505 (2014).

[108] Nash, J. C^1 isometric imbeddings. *Ann. Math.* **60**, 383–396 (1954).

[109] Kuiper, N. H. On C^1-isometric imbeddings. I **58**, 545–556 (1955).

[110] Kuiper, N. H. On C^1-isometric imbeddings. II **58**, 683–689 (1955).

[111] Gromov, M. A topological technique for the construction of solutions of differential equations and inequalities. *Intern. Congr. Math. (Nice 1970)* **2**, 221–225 (1971).

[112] Gromov, M. *Partial Differential Relations*, vol. 9 (Springer Science & Business Media, 1986).

[113] Isett, P. A proof of Onsager's conjecture. *Ann. of Math.* **188**, 871–963 (2018).

[114] Buckmaster, T., De Lellis, C., Székelyhidi, L. & Vicol, V. Onsager's conjecture for admissible weak solutions. *Comm. Pure Appl. Math.* **72**, 229–274 (2019).

[115] Kolmogorov, A. N. & Fomin, S. V. *Introductory Real Analysis* (Dover, New York, 1970). Trans. R. A. Silverman.

[116] Rudin, W. *Functional Analysis* (McGraw-Hill, 2006).

[117] Showalter, R. E. *Hilbert Space Methods in Partial Differential Equations* (Courier Corporation, 2010).

[118] Eyink, G. L. Besov Spaces and the Multifractal Hypothesis. *J. Stat. Phys.* **78**, 353–375 (1995).

[119] Triebel, H. *Theory of Function Spaces III* (Birkhäuser, Basel, 2006).

[120] Eyink, G. L. Local 4/5-law and energy dissipation anomaly in turbulence. *Nonlinearity* **16**, 137 (2002).

[121] De Lellis, C. & Székelyhidi Jr., L. On turbulence and geometry: from Nash to Onsager. *arXiv preprint arXiv:1901.02318* (2019).

[122] Buckmaster, T. & Vicol, V. Convex integration and phenomenologies in turbulence. *EMS Surv. Math. Sci.* **6**, 173–263 (2020).

[123] Spring, D. *Convex Integration Theory: Solutions to the h-principle in Geometry and Topology* (Springer Science & Business Media, 2010).

[124] Borrelli, V., Jabrane, S., Lazarus, F. & Thibert, B. Flat tori in three-dimensional space and convex integration. *Proc. Natl. Acad. Sci. U. S. A.* **109**, 7218–7223 (2012).

[125] Muzy, J.-F., Bacry, E. & Arneodo, A. Wavelets and multifractal formalism for singular signals: Application to turbulence data. *Phys. Rev. Lett.* **67**, 3515 (1991).

[126] Kestener, P. & Arneodo, A. Generalizing the wavelet-based multifractal formalism to random vector fields: application to three-dimensional turbulence velocity and vorticity data. *Phys. Rev. Lett.* **93**, 044501 (2004).

[127] Benzi, R., Ciliberto, S., Baudet, C. & Chavarria, G. R. On the scaling of three-dimensional homogeneous and isotropic turbulence. *Physica D* **80**, 385–398 (1995).

[128] Chen, S., Sreenivasan, K. R., Nelkin, M. & Cao, N. Refined similarity hypothesis for transverse structure functions in fluid turbulence. *Phys. Rev. Lett.* **79**, 2253 (1997).

[129] Nore, C., Abid, M. & Brachet, M. E. Decaying Kolmogorov turbulence in a model of superflow. *Phys. Fluids* **9**, 2644–2669 (1997).

[130] Nore, C., Abid, M. & Brachet, M. E. Kolmogorov Turbulence in Low-Temperature Superflows. *Phys. Rev. Lett.* **78**, 3896 (1997).

[131] Kobayashi, M. & Tsubota, M. Kolmogorov spectrum of quantum turbulence. *J. Phys. Soc. Japan* **74**, 3248–3258 (2005).

[132] Kobayashi, M. & Tsubota, M. Kolmogorov spectrum of superfluid turbulence: Numerical analysis of the Gross-Pitaevskii equation with a small-scale dissipation. *Phys. Rev. Lett.* **94**, 065302 (2005).

[133] Salort, J. *et al.* Turbulent velocity spectra in superfluid flows. *Physics of Fluids* **22**, 125102 (2010).

[134] Hänninen, R. & Baggaley, A. W. Vortex filament method as a tool for computational visualization of quantum turbulence. *Proc. Natl. Acad. Sci. U. S. A.* **111**, 4667–4674 (2014).

[135] Kozik, E. & Svistunov, B. Kelvin-wave cascade and decay of superfluid turbulence. *Phys. Rev. Lett.* **92**, 035301 (2004).

[136] L'vov, V. S. & Nazarenko, S. Spectrum of Kelvin-Wave Turbulence in Superfluids. *JETP Lett.* **91**, 428–434 (2010).

[137] Vinen, W. F. Classical character of turbulence in a quantum liquid. *Phys. Rev. B* **61**, 1410 (2000).

[138] Vinen, W. F. & Niemela, J. J. Quantum Turbulence. *J. Low Temp. Phys.* **128**, 167–231 (2002).

[139] Nemirovskii, S. K. Energy Spectrum of the 3D Velocity Field, Induced by Vortex Tangle. *J. Low Temp. Phys.* **171**, 504–510 (2013).

[140] Schwarz, K. W. Three-dimensional vortex dynamics in superfluid ^{4}He: Line-line and line-boundary interactions. *Phys. Rev. B* **31**, 5782 (1985).

[141] Kobayashi, M. & Tsubota, M. Quantum turbulence in a trapped Bose-Einstein condensate. *Phys. Rev. A* **76**, 045603 (2007).

[142] Madelung, E. Eine anschauliche Deutung der Gleichung von Schrödinger. *NW* **14**, 1004–1004 (1926).

[143] Madelung, E. Quantentheorie in hydrodynamischer form. *Z. Phys* **40**, 322–326 (1927).

[144] Wallstrom, T. C. Inequivalence between the Schrödinger equation and the Madelung hydrodynamic equations. *Phys. Rev. A* **49**, 1613 (1994).

[145] di Leoni, P. C., Mininni, P. D. & Brachet, M. E. Dual cascade and dissipation mechanisms in helical quantum turbulence. *Phys. Rev. A* **95**, 053636 (2017).

[146] Fujimoto, K. & Tsubota, M. Bogoliubov-wave turbulence in Bose-Einstein condensates. *Phys. Rev. A* **91**, 053620 (2015).

[147] Villois, A., Proment, D. & Krstulovic, G. Universal and nonuniversal aspects of vortex reconnections in superfluids. *Phys. Rev. Fluids* **2**, 044701 (2017).

[148] Dunn, J. E. & Serrin, J. On the thermomechanics of interstitial working. *Arch. Rat. Mech. Anal.* **88**, 95 (1985).

[149] Benzoni-Gavage, S. Propagating phase boundaries and capillary fluids. Lecture notes of CIRM Summer School "Mathematical Fluid Dynamics" (2010), available at http://math.univ-lyon1.fr/~benzoni/Levico.pdf.

[150] Wang, J. *et al.* Cascade of Kinetic Energy in Three-Dimensional Compressible Turbulence. *Phys. Rev. Lett.* **110**, 214505 (2013).

[151] Hänninen, R., Tsubota, M. & Vinen, W. F. Generation of turbulence by oscillating structures in superfluid helium at very low temperatures. *Phys. Rev. B* **75**, 064502 (2007).

[152] Hänninen, R. & Schoepe, W. Universal onset of quantum turbulence in oscillating flows and crossover to steady flows. *J. Low Temp. Phys.* **158**, 410 (2010).

[153] Skrbek, L., Schmoranzer, D., Midlik, Š. & Sreenivasan, K. R. Phenomenology of quantum turbulence in superfluid helium. *Proc. Natl. Acad. Sci. U. S. A.* **118** (2021).

[154] Aluie, H., Li, S. & Li, H. Conservative cascade of kinetic energy in compressible turbulence. *Astrophys. J. Lett.* **751**, L29 (2012).

[155] Favre, A. Statistical equations of turbulent gases. *Problems of hydrodynamics and continuum mechanics* 231–266 (1969).

[156] Lees, A. & Aluie, H. Baropycnal work: A mechanism for energy transfer across scales. *Fluids* **4**, 92 (2019).

[157] Eyink, G. L. Locality of turbulent cascades. *Physica D* **207**, 91–116 (2005).

[158] Tsepelin, V. *et al.* Visualization of quantum turbulence in superfluid ^{3}He-B: Combined numerical and experimental study of Andreev reflection. *Phys. Rev. B* **96**, 054510 (2017).

[159] Leadbeater, M., Winiecki, T., Samuels, D. C., Barenghi, C. F. & Adams, C. S. Sound Emission due to Superfluid Vortex Reconnections. *Phys. Rev. Lett.* **86**, 1410 (2001).

[160] Zuccher, S., Caliari, M., Baggaley, A. W. & Barenghi, C. F. Quantum vortex reconnections. *Phys. Fluids* **24**, 125108 (2012).

[161] Kobayashi, M. & Tsubota, M. Thermal dissipation in quantum turbulence. *Phys. Rev. Lett.* **97**, 145301 (2006).

[162] Rusaouen, E., Chabaud, B., Salort, J. & Roche, P.-E. Intermittency of quantum turbulence with superfluid fractions from 0% to 96%. *Phys. Fluids* **29**, 105108 (2017).

[163] Kraichnan, R. H. Inertial ranges in two-dimensional turbulence. *Phys. Fluids* **10**, 1417–1423 (1967).

[164] Kraichnan, R. H. Inertial-range transfer in two-and three-dimensional turbulence. *J. Fluid Mech.* **47**, 525–535 (1971).

[165] Boldyrev, S. On the spectrum of magnetohydrodynamic turbulence. *Astrophys. J. Lett.* **626**, L37 (2005).

[166] Mason, J., Cattaneo, F. & Boldyrev, S. Dynamic alignment in driven magnetohydrodynamic turbulence. *Phys. Rev. Lett.* **97**, 255002 (2006).

[167] Kobayashi, M. & Ueda, M. Topologically protected pure helicity cascade in non-Abelian quantum turbulence. *arXiv preprint arXiv:1606.07190* (2016).

[168] Krstulovic, G. Grid superfluid turbulence and intermittency at very low temperature. *Phys. Rev. E* **93**, 063104 (2016).

[169] Shukla, V., Mininni, P. D., Krstulovic, G., di Leoni, P. C. & Brachet, M. E. Quantitative estimation of effective viscosity in quantum turbulence. *Phys. Rev. A* **99**, 043605 (2019).

[170] Aluie, H. & Eyink, G. L. Localness of energy cascade in hydrodynamic turbulence. II. Sharp spectral filter. *Phys. Fluids* **21**, 115108 (2009).

[171] Swinney, H. L. & Henry, D. L. Dynamics of Fluids near the Critical Point: Decay Rate of Order-Parameter Fluctuations. *Phys. Rev. A* **8**, 2586 (1973).

[172] Cannell, D. S. Measurement of the long-range correlation length of SF_6 very near the critical point. *Phys. Rev. A* **12**, 225 (1975).

[173] Assenheimer, M. & Steinberg, V. Rayleigh-Bénard Convection near the Gas-Liquid Critical Point. *Phys. Rev. Lett.* **70**, 3888 (1993).

[174] Ashkenazi, S. & Steinberg, V. High Rayleigh Number Turbulent Convection in a Gas near the Gas-Liquid Critical Point. *Phys. Rev. Lett.* **83**, 3641 (1999).

[175] Ashkenazi, S. & Steinberg, V. Spectra and Statistics of Velocity and Temperature Fluctuations in Turbulent Convection. *Phys. Rev. Lett.* **83**, 4760 (1999).

[176] Accary, G., Bontoux, P. & Zappoli, B. Turbulent Rayleigh-Bénard convection in a near-critical fluid by three-dimensional direct numerical simulation. *J. Fluid Mech.* **619**, 127 (2009).

[177] van der Waals, J. D. The thermodynamic theory of capillarity under the hypothesis of a continuous variation of density. *J. Stat. Phys.* **20**, 200–244 (1979). Original work published 1893; translated by J. S. Rowlinson.

[178] Ginzburg, V. L. & Landau, L. D. On the Theory of Superconductivity. *Zh. Eksp. Teor. Fiz.* **20**, 1064 (1950).

[179] Cahn, J. W. & Hilliard, J. E. Free Energy of a Nonuniform System. I. Interfacial Free Energy. *J. Chem. Phys* **28**, 258–267 (1958).

[180] Korteweg, D. J. Sur la forme que prennent les équations du mouvements des fluides si l'ons tient compte des forces capillaires causées par des variations de densité. *Archives Néerl. Sci. Exactes Nat. Ser. II* **6** (1901).

[181] Onuki, A. Dynamic van der Waals Theory of Two-Phase Fluids in Heat Flow. *Phys. Rev. Lett.* **94**, 054501 (2005).

[182] Onuki, A. Dynamic van der Waals theory. *Phys. Rev. E* **75**, 036304 (2007).

[183] Onuki, A. *Phase Transition Dynamics* (Cambridge University Press, 2002).

[184] Anderson, D. M., McFadden, G. B. & Wheeler, A. A. Diffuse-interface methods in fluid mechanics. *Ann. Rev. Fluid Mech.* **30**, 139–165 (1998).

[185] Dębiec, T., Gwiazda, P., Świerczewska-Gwiazda, A. & Tzavaras, A. Conservation of energy for the Euler–Korteweg equations. *Calc. Var. Partial Dif.* **57**, 160 (2018).

[186] Onuki, A. Dynamic equations and bulk viscosity near the gas-liquid critical point. *Phys. Rev. E* **55**, 403 (1997).

[187] De Zarate, J. M. O. & Sengers, J. V. *Hydrodynamic Fluctuations in Fluids and Fluid Mixtures* (Elsevier, 2006).

[188] Hily-Blant, P., Falgarone, E. & Pety, J. Dissipative structures of diffuse molecular gas-III. Small-scale intermittency of intense velocity-shears. *Astron. Astroph.* **481**, 367–380 (2008).

[189] Wang, J. *et al.* Scaling and statistics in three-dimensional compressible turbulence. *Phys. Rev. Lett.* **108**, 214505 (2012).

[190] Wang, J., Gotoh, T. & Watanabe, T. Scaling and intermittency in compressible isotropic turbulence. *Phys. Rev. Fluids* **2**, 053401 (2017).

[191] Nikolai, P., Rabiyat, B., Aslan, A. & Ilmutdin, A. Supercritical CO_2: Properties and Technological Applications-A review. *J. Therm. Sci.* **28**, 394–430 (2019).

[192] Carlès, P. A brief review of the thermophysical properties of supercritical fluids. *J. Supercrit. Fluids* **53**, 2–11 (2010).

[193] Vesovic, V. *et al.* The transport properties of carbon dioxide. *J. Phys. Chem. Ref. Data* **19**, 763–808 (1990).

[194] Fisher, M. E. Correlation functions and the critical region of simple fluids. *J. Math. Phys.* **5**, 944–962 (1964).

[195] Takayasu, H., Taguchi, Y. & Katsuyama, T. Stochastic Shell Model: a model of anomalous scaling and non-Gaussian distribution in turbulence. *arXiv preprint chao-dyn/9503004* (1995).

[196] Mailybaev, A. A. Continuous representation for shell models of turbulence. *Nonlinearity* **28**, 2497 (2015).

[197] Matsumoto, T. & Sakajo, T. One-dimensional hydrodynamic model generating a turbulent cascade. *Phys. Rev. E* **93**, 053101 (2016).

[198] Gardiner, C. W. *Handbook of Stochastic Methods* (Springer, Berlin, 2009), 4th edn.

[199] Berezinskii, V. L. Destruction of long-range order in one-dimensional and two-dimensional systems having a continuous symmetry group I. Classical systems. *Sov. Phys. JETP* **32**, 493–500 (1971).

[200] Kosterlitz, J. M. & Thouless, D. J. Ordering, metastability and phase transitions in two-dimensional systems. *J. Phys. C* **6**, 1181 (1973).

[201] Kosterlitz, J. M. The critical properties of the two-dimensional xy model. *J. Phys. C* **7**, 1046 (1974).

[202] Bernard, D. Three-point velocity correlation functions in two-dimensional forced turbulence. *Phys. Rev. E* **60**, 6184 (1999).

[203] Boffetta, G. & Musacchio, S. Evidence for the double cascade scenario in two-dimensional turbulence. *Phys. Rev. E* **82**, 016307 (2010).

[204] Boffetta, G. & Ecke, R. E. Two-dimensional turbulence. *Annu. Rev. Fluid Mech.* **44**, 427–451 (2012).

[205] Cerbus, R. T. & Chakraborty, P. The third-order structure function in two dimensions: The Rashomon effect. *Phys. Fluids* **29**, 111110 (2017).

[206] Eyink, G. L. & Aluie, H. Localness of energy cascade in hydrodynamic turbulence. I. Smooth coarse graining. *Phys. Fluids* **21**, 115107 (2009).

[207] Lilly, D. K. & Petersen, E. L. Aircraft measurements of atmospheric kinetic energy spectra. *Tellus A* **35**, 379–382 (1983).

[208] Nastrom, G. D., Gage, K. S. & Jasperson, W. H. Kinetic energy spectrum of large- and mesoscale atmospheric processes. *Nature* **310**, 36–38 (1984).

[209] Smithr, L. M. & Yakhot, V. Finite-size effects in forced two-dimensional turbulence. *J. Fluid Mech.* **274**, 115–138 (1994).

[210] Xia, H., Punzmann, H., Falkovich, G. & Shats, M. G. Turbulence-Condensate Interaction in Two Dimensions. *Phys. Rev. Lett.* **101**, 194504 (2008).

[211] Lindborg, E. Comment on "Turbulence-Condensate Interaction in Two Dimensions". *Phys. Rev. Lett.* **102**, 149401 (2009).

[212] Xia, H., Shats, M. G., Punzmann, H. & Falkovich, G. Xia et al. reply. *Phys. Rev. Lett.* **102**, 149402 (2009).

[213] Vladimirova, N., Shavit, M. & Falkovich, G. Fibonacci turbulence. *Phys. Rev. X* **11**, 021063 (2021).

[214] Steffen, W. *et al.* Trajectories of the Earth System in the Anthropocene. *Proc. Natl. Acad. Sci. U. S. A.* **115**, 8252–8259 (2018).

[215] Ghil, M. & Lucarini, V. The physics of climate variability and climate change. *Rev. Mod. Phys.* **92**, 035002 (2020).

[216] Fan, J. *et al.* Statistical physics approaches to the complex Earth system. *Phys. Rep.* **896**, 1–84 (2021).

[217] Feinberg, M. *Foundations of Chemical Reaction Network Theory* (Springer, 2019).

[218] Horowitz, J. M. & Esposito, M. Thermodynamics with continuous information flow. *Phys. Rev. X* **4**, 031015 (2014).

[219] Sekimoto, K. *Stochastic Energetics* (Springer, New York, 2010).

[220] Van den Broeck, C. & Esposito, M. Ensemble and trajectory thermodynamics: A brief introduction. *Physica A* **418**, 6–16 (2015).

[221] Barato, A. C., Hartich, D. & Seifert, U. Efficiency of cellular information processing. *New J. Phys.* **16**, 103024 (2014).

[222] Sartori, P., Granger, L., Lee, C. F. & Horowitz, J. M. Thermodynamic costs of information processing in sensory adaptation. *PLoS Comput. Biol.* **10**, e1003974 (2014).

[223] Ito, S. & Sagawa, T. Maxwell's demon in biochemical signal transduction with feedback loop. *Nat. Commun.* **6**, 1–6 (2015).

[224] Hartich, D., Barato, A. C. & Seifert, U. Sensory capacity: An information theoretical measure of the performance of a sensor. *Phys. Rev. E* **93**, 022116 (2016).

[225] Amano, S. *et al.* Insights from an information thermodynamics analysis of a synthetic molecular motor. *Nat. Chem.* **14**, 530–537 (2022).

[226] Penocchio, E., Avanzini, F. & Esposito, M. Information Thermodynamics for Deterministic Chemical Reaction Networks. *arXiv preprint arXiv:2204.02815* (2022).

[227] Cover, T. M. & Thomas, J. A. *Elements of Information Theory* (Wiley-Interscience, Hoboken, NJ, 2006), 2nd edn.

[228] Matsumoto, T. & Sagawa, T. Role of sufficient statistics in stochastic thermodynamics and its implication to sensory adaptation. *Phys. Rev. E* **97**, 042103 (2018).

[229] Chetrite, R., Rosinberg, M. L., Sagawa, T. & Tarjus, G. Information thermodynamics for interacting stochastic systems without bipartite structure. *J. Stat. Mech.* **2019**, 114002 (2019).

[230] Maes, C. On the Second Fluctuation–Dissipation Theorem for Nonequilibrium Baths. *J. Stat. Phys.* **154**, 705–722 (2014).

[231] Tanogami, T. Violation of the second fluctuation-dissipation relation and entropy production in nonequilibrium medium. *J. Stat. Phys.* **187**, 1–25 (2022).

[232] Hayashi, K. & Sasa, S.-i. Linear response theory in stochastic many-body systems revisited. *Phys. A* **370**, 407–429 (2006).

[233] Harada, T. & Sasa, S.-i. Energy dissipation and violation of the fluctuation-response relation in nonequilibrium Langevin systems. *Phys. Rev. E* **73**, 026131 (2006).

[234] Maes, C. Local detailed balance. *SciPost Phys. Lect. Notes* **32**, 1 (2021).

[235] Ehrich, J. & Sivak, D. A. Energy and information flows in autonomous systems. *arXiv preprint arXiv:2209.10644* (2022).

[236] Leighton, M. P. & Sivak, D. A. Inferring subsystem efficiencies in bipartite molecular machines. *arXiv preprint arXiv:2209.12084* (2022).

[237] Shiraishi, N. & Sagawa, T. Fluctuation theorem for partially masked nonequilibrium dynamics. *Phys. Rev. E* **91**, 012130 (2015).

[238] Lathouwers, E. & Sivak, D. A. Internal energy and information flows mediate input and output power in bipartite molecular machines. *Phys. Rev. E* **105**, 024136 (2022).

[239] Tănase-Nicola, S., Warren, P. B. & Ten Wolde, P. R. Signal detection, modularity, and the correlation between extrinsic and intrinsic noise in biochemical networks. *Phys. Rev. Lett.* **97**, 068102 (2006).

[240] Celani, A., Bo, S., Eichhorn, R. & Aurell, E. Anomalous thermodynamics at the microscale. *Phys. Rev. Lett.* **109**, 260603 (2012).

[241] Kawaguchi, K. & Nakayama, Y. Fluctuation theorem for hidden entropy production. *Phys. Rev. E* **88**, 022147 (2013).

[242] Tanogami, T., Van Vu, T. & Saito, K. *in preparation.*

[243] Brzeźniak, Z. & Zastawniak, T. *Basic Stochastic Processes: A Course Through Exercises* (Springer Science & Business Media, 2000).

[244] Pavliotis, G. A. *Stochastic Processes and Applications: Diffusion Processes, the Fokker-Planck and Langevin Equations*, vol. 60 (Springer, 2014).

[245] Betchov, R. Measure of the intricacy of turbulence. *Phys. Fluids* **7**, 1160–1162 (1964).

[246] Ikeda, K. & Matsumoto, K. Information theoretical characterization of turbulence. *Phys. Rev. Lett.* **62**, 2265 (1989).

[247] Cerbus, R. T. & Goldburg, W. I. Information content of turbulence. *Phys. Rev. E* **88**, 053012 (2013).

[248] Materassi, M., Consolini, G., Smith, N. & De Marco, R. Information theory analysis of cascading process in a synthetic model of fluid turbulence. *Entropy* **16**, 1272–1286 (2014).

[249] Cerbus, R. T. & Goldburg, W. I. Information theory demonstration of the Richardson cascade. *arXiv preprint arXiv:1602.02980* (2016).

[250] Goldburg, W. I. & Cerbus, R. T. Turbulence as information. *arXiv preprint arXiv:1609.00471* (2016).

[251] Granero-Belinchon, C., Roux, S. G. & Garnier, N. B. Scaling of information in turbulence. *Europhys. Lett.* **115**, 58003 (2016).

[252] Granero-Belinchón, C., Roux, S. G. & Garnier, N. B. Kullback-Leibler divergence measure of intermittency: Application to turbulence. *Phys. Rev. E* **97**, 013107 (2018).

[253] Lozano-Durán, A., Bae, H. J. & Encinar, M. P. Causality of energy-containing eddies in wall turbulence. *J. Fluid Mech.* **882** (2020).

[254] Shavit, M. & Falkovich, G. Singular measures and information capacity of turbulent cascades. *Phys. Rev. Lett.* **125**, 104501 (2020).

[255] Lozano-Durán, A. & Arranz, G. Information-theoretic formulation of dynamical systems: Causality, modeling, and control. *Phys. Rev. Research* **4**, 023195 (2022).

[256] Ruelle, D. Microscopic fluctuations and turbulence. *Phys. Lett. A* **72**, 81–82 (1979).

[257] Komatsu, T. S., Matsumoto, S., Shimada, T. & Ito, N. A glimpse of fluid turbulence from the molecular scale. *Int. J. Mod. Phys. C* **25**, 1450034 (2014).

[258] Bandak, D., Eyink, G. L., Mailybaev, A. & Goldenfeld, N. Thermal noise competes with turbulent fluctuations below millimeter scales. *arXiv preprint arXiv:2107.03184* (2021).

[259] Eyink, G. & Jafari, A. High schmidt-number turbulent advection and giant concentration fluctuations. *Phys. Rev. Research* **4**, 023246 (2022).

[260] McMullen, R. M., Krygier, M. C., Torczynski, J. R. & Gallis, M. A. Navier-Stokes Equations Do Not Describe the Smallest Scales of Turbulence in Gases. *Phys. Rev. Lett.* **128**, 114501 (2022).

[261] Bell, J. B., Nonaka, A., Garcia, A. L. & Eyink, G. Thermal fluctuations in the dissipation range of homogeneous isotropic turbulence. *J. Fluid Mech.* **939** (2022).

[262] L'vov, V. S., Podivilov, E., Pomyalov, A., Procaccia, I. & Vandembroucq, D. Improved shell model of turbulence. *Phys. Rev. E* **58**, 1811 (1998).

[263] Biferale, L. Shell models of energy cascade in turbulence. *Annu. Rev. Fluid Mech.* **35**, 441–468 (2003).

[264] Hartich, D., Barato, A. C. & Seifert, U. Stochastic thermodynamics of bipartite systems: transfer entropy inequalities and a Maxwell's demon interpretation. *J. Stat. Mech.* **2014**, P02016 (2014).

[265] Horowitz, J. M. Multipartite information flow for multiple Maxwell demons. *J. Stat. Mech.* P03006 (2015).

[266] Kraskov, A., Stögbauer, H. & Grassberger, P. Estimating mutual information. *Phys. Rev. E* **69**, 066138 (2004).

[267] Khan, S. *et al.* Relative performance of mutual information estimation methods for quantifying the dependence among short and noisy data. *Phys. Rev. E* **76**, 026209 (2007).

[268] Holmes, C. M. & Nemenman, I. Estimation of mutual information for real-valued data with error bars and controlled bias. *Phys. Rev. E* **100**, 022404 (2019).

[269] Risken, H. *The Fokker-Planck Equation* (Springer, 1996).

[270] Spinney, R. E. & Ford, I. J. Entropy production in full phase space for continuous stochastic dynamics. *Phys. Rev. E* **85**, 051113 (2012).

[271] Lord, G. J. & Rougemont, J. A numerical scheme for stochastic PDEs with Gevrey regularity. *IMA J. Numer. Anal.* **24**, 587–604 (2004).

[272] Wilson, K. G. The renormalization group: Critical phenomena and the Kondo problem. *Rev. Mod. Phys.* **47**, 773 (1975).

[273] Horowitz, J. M. & Gingrich, T. R. Thermodynamic uncertainty relations constrain non-equilibrium fluctuations. *Nat. Phys.* **16**, 15–20 (2020).

[274] Shiraishi, N. Optimal thermodynamic uncertainty relation in Markov jump processes. *J. Stat. Phys.* **185**, 1–15 (2021).

[275] Shih, H.-Y., Hsieh, T.-L. & Goldenfeld, N. Ecological collapse and the emergence of travelling waves at the onset of shear turbulence. *Nat. Phys.* **12**, 245–248 (2016).

[276] Goldenfeld, N. & Shih, H.-Y. Turbulence as a problem in non-equilibrium statistical mechanics. *J. Stat. Phys.* **167**, 575–594 (2017).

[277] Wang, X., Shih, H.-Y. & Goldenfeld, N. Stochastic model for quasi-one-dimensional transitional turbulence with streamwise shear interactions. *Phys. Rev. Lett.* **129**, 034501 (2022).